UNIVERSITÉ DU QUÉBEC À CHICOUTIMI

THÈSE PRÉSENTÉ À

L'UNIVERSITÉ DU QUÉBEC À CHICOUTIMI

COMME EXIGENCE PARTIELLE

DU DOCTORT EN INGÉNIERIE

PAR

ADEL MOHAMED

EFFET DES ADDITIFS SUR LA MICROSTRUCTURE ET LES PROPRIÉTÉS MÉCANIQUES DES ALLIAGES D'ALUMINIUM-SILICIUM

AVRIL 2008

Bibliothèque
Paul-Émile-Boulet

UQAC
Université du Québec
à Chicoutimi

Mise en garde/Advice

Afin de rendre accessible au plus grand nombre le résultat des travaux de recherche menés par ses étudiants gradués et dans l'esprit des règles qui régissent le dépôt et la diffusion des mémoires et thèses produits dans cette Institution, **l'Université du Québec à Chicoutimi (UQAC)** est fière de rendre accessible une version complète et gratuite de cette œuvre.

Motivated by a desire to make the results of its graduate students' research accessible to all, and in accordance with the rules governing the acceptation and diffusion of dissertations and theses in this Institution, the **Université du Québec à Chicoutimi (UQAC)** is proud to make a complete version of this work available at no cost to the reader.

L'auteur conserve néanmoins la propriété du droit d'auteur qui protège ce mémoire ou cette thèse. Ni le mémoire ou la thèse ni des extraits substantiels de ceux-ci ne peuvent être imprimés ou autrement reproduits sans son autorisation.

The author retains ownership of the copyright of this dissertation or thesis. Neither the dissertation or thesis, nor substantial extracts from it, may be printed or otherwise reproduced without the author's permission.

UNIVERSITÉ DU QUÉBEC À CHICOUTIMI

THESIS PRESENTED TO THE

UNIVERSITY OF QUEBEC AT CHICOUTIMI

IN PARTIAL FULFILLMENT OF

THE REQUIREMENT FOR THE DEGREE OF

DOCTOR OF PHILOSOPHY IN ENGINEERING

BY

ADEL MOHAMED

EFFECT OF ADDITIVES ON THE MICROSTRUCTURE AND MECHANICAL PROPERTIES OF ALUMINUM-SILICON ALLOYS

APRIL 2008

Dedicated to my parents,
Reham and my little Mahmoud

RÉSUMÉ

Les alliages aluminium-silicium, particulièrement à la composition eutectique, sont souvent employés dans l'industrie de l'automobile en raison de leur de faible densité relative à des matériaux traditionnels. Les propriétés mécaniques de tels alliages sont déterminées principalement par les constituants microstructuraux de leur structure après la coulée, les morphologies et les quantités de leurs phases intermétalliques. Dans l'état non modifié, les alliages Al-Si montrent un silicium eutectique ayant une forme aciculaire ou lamellaire, de ce fait, ces alliages ont tendance à montrer de faibles résistance et ductilité. Ainsi, les alliages avec une structure principalement eutectique doivent subir la modification afin d'assurer des propriétés mécaniques adéquates. La qualité de du produit coulé peut être améliorée par affinement des grains, ceci permet de réduire la taille des grains primaires de la phase α-aluminium qui solidifie autrement dans une structure de grain grossière. La production des alliages Al-Si avec une structure et des propriétés mécaniques améliorées implique l'application de deux processus principaux : (i) addition de tels éléments d'alliage comme Mg, Cu, Mn, et autres éléments semblables, pendant l'état liquide; et (ii) traitement thermique. Les éléments de microalliage ou éléments de trace utilisés dans les alliages commerciaux d'aluminium sont de 0.5 à 1.0 % en poids de Pb, Bi, Sn et In, qui ont peu ou pas de solubilité en aluminium, c.-à-d. ils ont des coefficients de distribution extrêmement bas.

L'influence du fer (0.5-1 % en poids), du manganèse (0.5-1 % en poids), du cuivre (2.25-3.25 % en poids), et du magnésium (0.3-0.5 % en poids), aussi bien que celle des éléments Pb, Bi, Sn, et In, sur la microstructure et les propriétés mécaniques de l'alliage préeutectique Al-10.8%Si modifié et raffiné a été étudiée dans deux conditions, à savoir, tel que coulé et application d'un traitement thermique. Les alliages en fusion ont été versés dans (a) un moule métallique graphite-enduit rectangulaire de forme L préchauffé à 450 °C pour des mesures métallographiques et de dureté ; et (b) un moule permanent de type ASTM B-108 et (c) un moule d'essai au choc d'acier doux pour produire les échantillons du test nécessaire. L'évaluation microstructurale a été effectuée en utilisant la microscopie optique en même temps que l'analyse d'image pour la quantification. L'identification de phase a été effectuée en utilisant la microsonde électronique (EPMA), couplé aux équipements d'EDX et de WDS. Les barreaux d'essai ont été divisés en sept jeux : un ensemble a été gardé dans la condition de tel que coulé, alors que les six autres ensembles étaient traités thermiquement, une mise en solution à 495°C pour 8 h, puis une trempe dans l'eau chaude à 65°C, suivi d'un vieillissement artificiel à 155 °C, 180 °C, 200 °C, 220 °C, et 240°C, respectivement, pendant 5 heures (c.-à-d. les traitements T6 et T7). Les propriétés mécaniques ont été évaluées à la température ambiante par la dureté, les propriétés de traction et d'impact pour les deux conditions, tel que coulé et application du traitement thermique. Les mesures de dureté ont été effectuées en utilisant un appareil de contrôle brinell de dureté. Des propriétés de traction ont été déterminées à l'aide d'une machine d'essai mécanique de Servohydraulic MTS. Les propriétés d'impact ont été évaluées à l'aide d'une machine de test d'impact Charpy.

En matière de l'addition des éléments d'alliage, les résultats prouvent que l'effet de modification du Sr diminue à mesure que la quantité de cuivre et de magnésium supplémentaires est augmentée, en raison des interactions entre ces éléments, ce qui cause une ségrégation grave des phases d'Al_2Cu dans les secteurs loin du silicium eutectique modifié et change la séquence de précipitation de la phase α-$Al_{15}(Fe,Mn)_3Si_2$ d'une réaction post-dendritique à pré-dendritique où l'intermétallique est observé pour se produire dans les dendrites d'α-Al. Dépendant de la teneur en Fe et en Mn dans l'alliage, une grande variation dans la phase α est observée sous forme de particules formées polyhédrales connues sous le nom de « sludge ». La phase d'Al_2Cu est vue pour se dissoudre presque totalement pendant le traitement thermique de mise en solution, alors que les phases $Al_5Cu_2Mg_8Si_6$ et les phases intermétalliques du fer α-$Al_{15}(Fe,Mn)_3Si_2$ s'avèrent pour persister pour tous les alliages étudiés, particulièrement ceux qui contiennent les niveaux élevés du Mg et du Fe. La phase intermétallique de fer de ß-$Al_5(Fe,Mn)_3Si$ se dissout partiellement dans les alliages modifiés par le Sr, et sa dissolution devient plus prononcée après traitement thermique de mise en solution.

Pour les alliages soumis à un traitement thermique, un vieillissement maximal est réalisé à 180 °C, bien que l'index de la plus haute qualité corresponde à la température du vieillissement 155 °C, et ce est pour tous les alliages étudiés. En conséquence, 155 °C peut être considéré comme traitement de vieillissement optimal. À 0.5% Mn, la phase β-Fe forme quand le contenu de Fe est au-dessus de 0.75%, entraînant une diminution massive au niveau des propriétés mécaniques. Le même résultat est obtenu quand les niveaux du Fe et du Mn sont augmentés au delà de 0.75%, en raison de la formation du résidu « sludge ». D'autre part, les propriétés mécaniques des alliages contenant du cuivre sont affectées légèrement aux niveaux élevés du magnésium en raison de la formation de la phase $Al_5Cu_2Mg_8Si_6$ qui diminue la quantité de magnésium libre disponible pour former la phase d'Al_2CuMg. Le contour courbé de la corrélation entre l'UTS (limite ultime) et l'allongement observé pour tous les alliages soumis au vieillissement reflète la transition d'une forte corrélation dans les conditions sous-vieillissement et vieillissement maximal liée à la faible corrélation associée avec la condition de survieillissement. L'énergie d'impact de Charpy de l'alliage Al-10.8%Si est influencée par sa microstructure qui dépend fortement de la composition d'alliage. La morphologie du silicium fibreux en alliages modifiés par le Sr augmente la dureté en raison de son effet fondamental sur le déclenchement des fissures et la résistance de propagation de fissure. Dans les alliages contenant ~1% de fer et 1% ou 0.5% Mn, l'addition du fer mène à une plus grande précipitation du résidu et des plaquettes β-Fe, respectivement; ces particules intermétalliques agissent en tant qu'emplacements de déclenchement de fissures et réduisent les propriétés d'impact considérablement. Dans les alliages contenant des niveaux élevés en cuivre, le niveau de Cu accru abaisse les propriétés d'impact de manière significative, puisque le comportement de rupture est maintenant également influencé par la phase d'Al_2Cu en plus des particules de silicium. Indépendamment de la composition d'alliage, le tracé combiné de l'énergie d'impact et le

pourcentage d'élongation montre des relations linéaires pour tous les alliages, que ce soit dans la condition tel que coulé ou traité thermiquement.

Des modèles de régression multiples ont été développés afin de prévoir l'influence des variations compositionnelles sur les propriétés mécaniques (L.U, L.É, %A, et E_T) de l'alliage Al-10.8%Si soumis à un traitement T6. Ces équations, sous forme de formules d'interpolation, fournissent des informations sur l'effet conjugué aussi bien que sur les effets conjugués de changer individuellement les additions d'élément d'alliage faites à l'alliage. Les équations montrent que l'augmentation de la teneur de Cu, de Mn et de Mg résulte de l'augmentation de la dureté et de la résistance à la traction. Le cuivre apporte la contribution la plus élevée de chacun des trois éléments à la résistance pour la gamme de composition étudiée, alors que le fer a des effets délétères sur les propriétés mécaniques de l'alliage. Chacun des quatre éléments réduit l'élongation et la dureté, avec du Cu ayant l'effet le plus intense. L'analyse détaillée indique que l'interaction des coefficients ne semble pas contribuer de manière significative aux propriétés mécaniques des alliages. L'exactitude des équations a été vérifiée contre les résultats expérimentaux dans les gammes de la variation des variables étudiées. Ces équations peuvent être employées pour prévoir les propriétés d'alliage dans ces marges de variation.

En ce qui concerne l'addition des éléments de trace, les résultats prouvent que l'addition individuelle du Pb n'a aucun effet significatif sur la microstructure et les propriétés mécaniques de l'alliage Al-10.8%Si dans les deux conditions, tel que coulé et traité thermiquement. L'addition du Bi contrecarre l'effet de modification du Sr, menant à un grossissement notable des particules eutectiques de silicium, tandis que des précipités en étain comme β-Sn sont observés dans le réseau d'Al_2Cu quand l'étain est ajouté individuellement à l'alliage. Une addition combinée de Pb et le Bi à l'alliage Al-10.8%Si entraîne une précipitation en tant que des cristaux primaires de Bi enveloppés par la phase Pb_3Bi et fournit de meilleures propriétés mécaniques dans l'alliage tel que coulé et vieilli artificiellement que l'addition combinée du Bi et du Sn.

Une étude séparée a été effectuée sur les alliages B319.2 et A356.2 modifiés et affinés afin d'étudier l'effet de l'ajout de Sn en faibles quantités (moins de 0.15 % en poids) sur la microstructure, et par conséquent sur la performance d'alliage sous différentes conditions de traitement thermique (T5 et T6), aussi bien que dans la condition de tel que coulé. Les barres d'essai ont été divisées en trois jeux : un ensemble a été maintenu dans la condition tel que coulé, le deuxième ensemble était soumis à un traitement thermique de mise en solution à 495 °C/8 h pour les alliages B319.2 et à 540 °C/8 h pour les alliages A356.2, puis les alliages ont été trempés dans l'eau chaude à 65 °C, suivi d'un vieillissement artificiel à 180 °C pendant 5 heures (c.-à-d. traitement thermique T6). Le troisième ensemble était soumis à un traitement thermique de type T5 à 175 °C pendant 10 heures. Les résultats expérimentaux prouvent que, dans l'alliage B319.2 l'alliage, les précipités de Sn sont de forme de particules de Sn (β-Sn) dans le réseau d'Al_2Cu, et ils sont comme des particules minuscules (300 ~ 500 nm) de type Mg_2Sn sur les particules eutectiques de silicium.

Cependant, dans l'alliage A356.2, Sn précipite principalement comme Mg_2Sn sous la forme d'écriture chinoise. La ductilité et la dureté des alliages B319.2 et A356 tel que coulés sont sensibles aux variations du contenu de Sn, alors que la limite d'élasticité demeure pratiquement inchangée. La ductilité et la dureté plus élevées des alliages contenants du Sn dans la condition tel que coulé peuvent être attribuées principalement à l'état de contrainte-tension dans la matrice associée à la finesse des phases de Sn. Il peut être également observé que la dureté et la résistance des alliages B319.2 et A356.2 tel que coulé et soumis à un traitement thermique sont réduites légèrement par Sn, un fait qu'on pense qui est dû au ramollissement des phases en étain.

ABSTRACT

Aluminum-silicon alloys, especially at the eutectic composition, are being used with increasing frequency in the automotive industry because of their low density relative to traditional materials. The mechanical properties of such alloys are determined mainly by the microstructural constituents of their cast structure and the morphologies and amounts of their intermetallic phases. In the unmodified state, Al-Si alloys exhibit an acicular or a lamellar form of eutectic silicon, due to which the alloys tend to display low strength and ductility. Thus, alloys with a predominantly eutectic structure must undergo modification in order to ensure adequate mechanical properties. The casting quality may be improved by grain refinement to reduce the size of the primary α-Al grains in the casting, which otherwise solidify in a coarse columnar grain structure. The production of Al-Si alloys with improved structure and mechanical properties involves the application of two major processes: (i) addition of such alloying elements as Mg, Cu, Mn, and the like, during the melting process; and (ii) heat-treatment. The microalloying, or trace, elements used in commercial Al alloys are 0.5 to 1.0 wt% Pb, Bi, Sn and In, which have little or no solubility in Al, *i.e.* they have extremely low distribution coefficients.

The influence of iron (0.5-1 wt%), Mn (0.5-1 wt%), Cu (2.25-3.25 wt%), and Mg (0.3-0.5 wt%) as well as of the trace elements Pb, Bi, Sn, and In, on the microstructure and mechanical properties of modified and grain-refined Al-10.8%Si near-eutectic alloy was investigated in both as-cast and heat-treated conditions. The alloy melts were poured into (a) a preheated (450°C) L-shaped rectangular graphite-coated metallic mold for metallographic and hardness measurements; and (b) an ASTM B-108 permanent mold and (c) a mild steel impact test mold to produce the necessary test samples. Microstructural assessment was carried out using optical microscopy in conjunction with image analysis for quantification purposes. Phase identification was carried out using an electron probe microanalyser (EPMA), coupled with EDX and WDS facilities. The test bars were divided into seven sets: one set was kept in the as-cast condition, while the other six sets were solution heat-treated at 495°C for 8 h, then quenched in warm water at 65°C, followed by artificial aging at 155°, 180°, 200°, 220°, and 240°C, respectively, for 5 hours (*i.e.* T6 and T7-tempered). Mechanical properties were evaluated at room temperature through hardness, tensile and impact properties for both as-cast and heat treated conditions. The hardness measurements were carried out using a Brinell hardness tester. Tensile properties were determined using a Servohydraulic MTS Mechanical testing machine. The impact properties were assessed using a Charpy instrumented impact testing machine.

In the matter of the addition of alloying elements, the results show that the modifying effect of Sr diminishes as the amount of added Cu and Mg is increased, due to the interactions between these elements, causes severe segregation of the Al_2Cu phases in areas away from the modified eutectic Si and alters the precipitation sequence of the α-$Al_{15}(Fe,Mn)_3Si_2$ iron intermetallic phase from a post-dendritic reaction to a pre-dendritic one where the

intermetallic is observed to occur within the α-Al dendrites. Depending upon the Fe and Mn content of the alloy, a coarser variation of the α-phase is observed in the form of polyhedral shaped particles known as "sludge". The Al_2Cu phase is seen to dissolve almost completely during solution heat treatment, while $Al_5Cu_2Mg_8Si_6$, sludge, and α-$Al_{12}(Fe,Mn)_3Si_2$ iron intermetallic phases are found to persist for all the alloys studied, especially those containing high levels of Mg and Fe. The β-$Al_5(Fe,Mn)Si$ iron intermetallic phase dissolves partially in the Sr-modified alloys, and its dissolution becomes more pronounced after solution heat treatment.

For the heat-treated alloys, peak aging is achieved at 180°C, although the highest quality index corresponds to 155°C aging temperature, for all the alloys investigated. Accordingly, 155°C may be considered as the optimal aging treatment. At 0.5% Mn, the β-Fe phase forms when the Fe content is above 0.75%, causing the mechanical properties to decrease drastically. The same result is obtained when the levels of both Fe and Mn are increased beyond 0.75%, due to the formation of sludge. On the other hand, the mechanical properties of the Cu-containing alloys are affected slightly at high levels of Mg as a result of the formation of $Al_5Cu_2Mg_8Si_6$ which decreases the amount of free Mg available to form the Al_2CuMg phase. The curved contour of the correlation between UTS and elongation observed for all aged alloys reflects the transition from a strong correlation in the underaged and peak-aged conditions to the weak correlation associated with the overaged condition. The Charpy impact energy of Al-10.8%Si alloy is influenced by its microstructure which depends strongly on alloy composition. The morphology of fibrous Si in Sr-modified alloys enhances toughness because of its underlying effect on crack initiation and crack propagation resistance. In alloys containing ~1% Fe and 1% or 0.5% Mn, the addition of iron leads to an increased precipitation of sludge and β-Fe platelets, respectively; these intermetallic particles act as crack initiation sites and reduce the impact properties considerably. In alloys containing high levels of copper, the increased copper level lowers the impact properties significantly, since the fracture behaviour is now also influenced by the Al_2Cu phase in addition to the Si particles. Regardless of alloy composition, the combined impact energy-percent elongation plots display linear relationships for all alloys for the as-cast and heat-treated conditions.

Multiple regression models were developed in order to predict the influence of compositional variations on the mechanical properties (UTS, YS, %El, and E_T) of T6-aged Al-10.8%Si alloy. These equations, in the form of interpolation formulae, provide information on the non-conjugated as well as conjugated effects of individually varying the alloying element additions made to the alloy. The equations show that increasing the content of Cu, Mn, and Mg results in an increase in hardness and tensile strength. Copper makes the highest contribution of all three elements to the strength for the composition range studied, while Fe has deleterious effects on the mechanical properties of the alloy. All four elements reduce the elongation and toughness, with Cu having the most intense effect. Detailed analysis indicates that the interaction of coefficients does not appear to contribute significantly to the mechanical properties of the alloys. The accuracy of the equations has

been verified against the experimental results in the ranges of variation of the variables studied. These equations may be used to predict the alloy properties within these ranges of variation.

As regards the addition of trace elements, the results show that individual addition of Pb has no significant effect on the microstructure and mechanical properties of Al-10.8%Si alloy in both as-cast and heat-treated conditions. The addition of Bi counteracts the modification effect of Sr, leading to a noticeable coarsening of the eutectic Si particles, whereas tin precipitates as β-Sn within the Al_2Cu network when added individually to the alloy. A combined addition of Pb and Bi to the Al-10.8%Si alloy precipitates as primary Bi crystals enveloped by the Pb_3Bi phase and provides better mechanical properties in the as-cast and artificially-aged conditions than does the combined addition of Bi and Sn.

In the context of this research study, where the main focus has been the development of the Al-10.8%Si alloys with a view to optimizing their machining characteristics and, hence, productivity, it was also thought worthwhile to investigate the microstructure and mechanical properties of the B319.2 and A356.2 alloys from this point of view. For this purpose, an examination of the microstructures of these alloys was thus undertaken after minor amounts of Sn had been added. The study was carried out on modified and grain-refined B319.2 and A356.2 alloys in order to investigate the effect that adding Sn in minimal amounts (less than 0.15 wt%) would have on the microstructure, and hence on the alloy performance under different heat treatment conditions (T5 and T6), as well as in the as-cast condition. The test bars were divided into three sets: one set was kept in the as-cast condition, the second set was solution heat-treated at 495°C/8 h for the B319.2 alloys and at 540°C/8 h for the A356.2 alloys, then quenched in warm water at 65°C, followed by artificial aging at 180°C for 5 hours (*i.e.* T6-tempered). The third set was T5 heat-treated at 175°C for 10 hours. Experimental results show that, in the B319.2 alloy, Sn precipitates in the form of tin particles (β-Sn) within the Al_2Cu network, and as miniscule (300-500 nm) Mg_2Sn particles on the eutectic Si particles. However, in A356.2 alloy, Sn precipitates mainly as Mg_2Sn in Chinese script form. Both the ductility and the toughness of as-cast B319.2 and A356.2 alloys are sensitive to variations in Sn content, while the yield strength remains practically unaffected. The higher ductility and toughness of Sn-containing alloys in the as-cast condition may be attributed mainly to the stress-strain state in the matrix material associated with the fineness of Sn-bearing phases. It may also be observed that the hardness and the strength of as-cast and heat-treated B319.2 and A356.2 alloys is reduced slightly by Sn, a fact which is believed to be due to softening of the tin-bearing phases.

ACKNOWLEDGMENTS

First of all, I would like to express my sincere gratitude towards my supervisor, Prof. Fawzy H. Samuel for motivating me to complete my Ph.D. Without his continuous guidance and support it would have been impossible for me to complete my Ph.D. I am truly indebted to him for helping me in every possible manner throughout the past three years. I admire his dedication and contribution to the field of science and he will be a constant inspiration to me throughout my life.

I would like to thank my co-supervisor, Dr. Agnes Marie Samuel who guided me and helped me so much. I learned many things from her and she was always very kind to me.

I would also like to thank the committee members for being in my committee and providing me helpful suggestions in improving the quality of my thesis.

Financial support in the form of scholarships received from the Natural Sciences and Engineering Research Council of Canada (NSERC), the Fondation de l'Université du Québec à Chicoutimi (FUQAC), General Motors Powertrain Group (U.S.A), and Corporativo Nemak (Mexico) is gratefully acknowledged.

I would like to extend my appreciation to Mr. Alain Bérubé of the TAMLA group, UQAC for his assistance with the castings and sample preparation, as also to Mr. Lang Shi of the Microanalysis Laboratory, Earth and Planetary Sciences, McGill University for carrying out the EPMA analysis.

An acknowledgment is specifically extended to Madame Marion Sinclair, for her patience and painstaking efforts in editing my thesis.

Behind every success of a married man, there is the shadow of a woman. I would like to thank my wife, Reham, for providing me with the best care at home, and creating a peaceful and loving environment. She and our little son, Mahmoud, are the most important motivation for completing my thesis. I have also to thank my parents. They have always supported me and allowed me to make up my own opinions.

PUBLICATIONS

Ten research articles have been prepared from this work for publication. Of these, six have been published. The details are provided below.

1. Precipitation of Tin in Cast 319 and 356 Aluminum Alloys
   A.M.A Mohamed, F.H. Samuel, A.M. Samuel, H.W. Doty, and S. Valtierra
   AFS Transactions, 2007, vol. 115, pp. 105-119.

2. Application of Experimental Design to Study and Control Properties and Behaviour of Cast Al-10.8%Si Eutectic Alloy.
   A.M.A Mohamed, F.H. Samuel, A.M. Samuel, H.W. Doty, and S. Valtierra
   International Journal of Cast Metals Research, 2007, vol. 20 (5), pp. 246-253.

3. Influence of Tin Addition on the Microstructure and Mechanical Properties of Al-Si-Cu-Mg and Al-Si-Mg Casting Alloys.
   A.M.A Mohamed, F.H. Samuel, A.M. Samuel, H.W. Doty, and S. Valtierra
   Metallurgical and Materials Transactions A, March 2008, vol. 39, pp. 490-501.

4. Influence of Alloying Elements Addition on the Microstructure and Hardness of Near-Eutectic Al-Si Alloys
   A.M.A Mohamed, F.H. Samuel, A.M. Samuel, H.W. Doty, and S. Valtierra
   Prepared for Submission to Materials Science and Engineering A, 2008.

5. Influence of Alloying Elements Addition on the Tensile and Impact Properties of Near-Eutectic Al-Si Alloys
   A.M.A Mohamed, F.H. Samuel, A.M. Samuel, H.W. Doty, and S. Valtierra
   Prepared for Submission to Materials Science and Engineering A, 2008.

6. Effect of Individual and Combined Additions of Pb, Bi, and Sn on the Microstructure and Mechanical Properties of Al-10.8%Si Eutectic Alloy.
   A.M.A Mohamed, F.H. Samuel, A.M. Samuel, H.W. Doty, and S. Valtierra
   Prepared for Submission to Metallurgical and Materials Transactions A, 2008.

7. Microstructure-Property Relationships in Al-10.8%Si Near-Eutectic Alloy.
   A.M.A Mohamed, F.H. Samuel, A.M. Samuel, H.W. Doty, and S. Valtierra
   Prepared for Submission to Metallurgical and Materials Transactions A, 2008.

Conferences & Presentations

8. Effect of Fe, Mn, Cu and Mg Additions on the Microstructure of Al-10.8 wt% Si Near-Eutectic Alloy.
   A.M.A Mohamed, F.H. Samuel, A.M. Samuel, H.W. Doty, and S. Valtierra

Proc. Int. Symp. On 'Aluminium: from Raw Materials to Applications', G. Dufour, F. Paray, J. Tessier (Eds), Conference of Metallurgists (CIM), Montreal, Quebec, October 2006, pp. 167-183.

9. Effect of Fe, Mn, Cu and Mg Additions on the Mechanical Properties of Al-10.8 wt% Si Near-Eutectic Alloy.
A.M.A Mohamed, F.H. Samuel, A.M. Samuel, H.W. Doty, and S. Valtierra
Proc. 18th Canadian Materials Science Conference (CMSC), Montreal, Quebec, June 2006, Session 10. Aluminum II, Paper 10.3.

10. Precipitation of Tin in Cast 319 and 356 Aluminum Alloys
A.M.A Mohamed, F.H. Samuel, A.M. Samuel, H.W. Doty, and S. Valtierra
111th Metalcasting Congress, Houston, Texas, USA, May 2007.

TABLE OF CONTENTS

LIST OF TABLES

LIST OF FIGURES

Chapter 2

Chapter 5

CHAPTER 1

DEFINITION OF THE PROBLEM

CHAPTER 1

DEFINITION OF THE PROBLEM

1.1 INTRODUCTION

Weight reduction in the manufacture of automobiles and trucks has become a key focus area because of the need to meet increased customer expectations for vehicle safety and performance while at the same time complying with regulations on fuel economy. This requirement has caused a decrease in the quantity of ferrous-based components in modern cars. These parts have been replaced to a great extent by light metals, most commonly by aluminum and plastics. Economic restrictions within the auto industry itself necessitate this type of replacement with a view to cost effectiveness. Aluminum alloys possess numerous technical advantages which make them one of the most useful alloy systems available. Such alloys may be separated into two major classes: cast alloys and wrought alloys. Cast-aluminum alloys are produced in hundreds of compositions by all commercially applied casting processes, including green-sand, dry-sand, composite-sand, plaster-mold, investment, permanent-mold and pressure-die casting. As cast alloys are poured into their final shape, they may be strengthened by heat-treatment but not by work-hardening. Cast aluminum has several advantages over cast iron, including increased thermal conductivity, an ability to be cast into more complex shapes, and lower density. Wrought alloys differ from cast alloys in that they can be shaped by deformation.

To date, cast aluminum components have been used primarily for engine parts, including blocks, cylinder heads, pistons, intake manifolds, brackets, and housings. With

the increase in the demand for reduced weight and lower mass, however, strong interest has been generated in using cast aluminum for chassis and suspension systems.[1] Aluminum in its pure form is not a metal that has good castability due to its poor fluid characteristics; alloying elements are thus usually added to overcome the problem and also to improve the mechanical properties of the castings. Since aluminum-silicon (Al-Si) alloys offer excellent casting characteristics as well as chemical, physical and mechanical properties, they constitute more than 80% of all aluminum alloy castings. The most significant use of these alloys is in the production of such automotive components as were listed previously, as well as in aeronautical and military applications. The mechanical properties of aluminum-silicon alloys, however, are different from those of cast iron and steel. Such a context creates a compelling need for detailed information on how the mechanical properties of aluminum alloys are affected by the processing parameters involved in casting. This information is especially pertinent with regard to the presence of microstructural features such as intermetallic phases and porosity, since such features can strongly affect the properties of the casting. In addition to reducing the amount of material capable of carrying the applied loads, these features often act as stress raisers and low-energy nucleation sites for cracks. As the majority of cast components have complex geometries, a variety of microstructures may arise within a single casting. Considering that mechanical properties are a function of the microstructure, they will tend to change as the microstructure changes, thus any study of the properties of cast aluminum must take into account all the factors which may influence the microstructure. The most significant microstructural features involved are second phase particles and grain structure; the second-phase particles of

concern here are: (i) coarse, insoluble particles formed during casting, or coarse particles of normally soluble phases formed during casting or subsequent processing; (ii) smaller intermediate particles formed during homogenization; and (iii) aging precipitates.

In the present study, Al-Si-Cu (319 alloys) and Al-Si-Mg (356 alloys) hypoeutectic, and Al-Si-Cu-Mg-Fe-Mn (an experimental Al-10.8%Si alloy) near-eutectic type cast Al-Si alloys were selected for investigation because of the high demand for these alloys in manufacturing structural components for the automotive industry, the largest consumer of Al-Si cast alloys.

Much attention has been turned towards near-eutectic Al-Si alloys because of their excellent castability. Strength and malleability are important reasons for increasing the practical application of this alloy system.[2] The addition of certain elements, such as calcium (Ca), antimony (Sb), sodium (Na), and strontium (Sr), to hypoeutectic and near-eutectic Al-Si alloys has the effect of altering or *modifying* the morphology of eutectic silicon from acicular plate-like form to fibrous form. This change in Si morphology enhances the mechanical properties of the alloy and, in particular, its ductility.[3] In recent years, the use of strontium as a modifier, instead of sodium and antimony, has become a widely accepted practice, although strontium has been reported to have an incubation-time problem.[4,5,6] It is worth noting, however, that at the same time when eutectic silicon particles change from acicular to fibrous, the amount, morphology and size of the dendritic α-Al phase are also affected. It was thought, in error, that it was enough to only modify the eutectic silicon phase in near-eutectic Al-Si alloys, and not necessary to refine the dendritic α-Al phase; but, in fact, at the same time that the morphology and size of the eutectic silicon phase is

transformed by the modification treatment, considerable changes to the amount, shape, and size of the α-Al phase also occur.[7] Previous investigations suggest that the addition of strontium to hypoeutectic and near-eutectic Al-Si alloys may promote the columnar growth of the dendrites, which are present in the form of fine slender highly-branched columnar grains; addition of Sr may also result in a noticeable increase in the amount of the dendritic α-Al phase.[2,3] Thus, with regard to such alloys, dendrite refinement is a necessary step. The master alloy Al-5Ti-1B, which is an effective grain refiner for pure aluminum and wrought aluminum alloys, is often used in Al-Si cast alloys to obtain fine equiaxed grains. Particles of TiB_2 and/or $TiAl_3$ from the Al-5Ti-1B master alloy are thought to be capable of acting as the nuclei for α-Al.[8,9,10] No final conclusion has yet been reached, however, on whether the transition of dendritic α-Al from a long columnar morphology to a fine equiaxed one results in improved mechanical properties in near-eutectic Al-Si alloys.[4]

In addition, in the production of hypoeutectic and near-eutectic Al-Si alloys, improving the quality in the form of better structure and mechanical properties involves the application of two major processes: (1) addition of alloying elements (Mg, Cu, Mn, and so forth) during the melting process; and (2) heat-treatment.

The percentage of alloying elements and impurities must be controlled carefully in all aluminum alloys. If it is not, properties such as strength, toughness, or corrosion resistance, may be affected adversely. Although certain mechanical properties may be improved, however, it is often at the expense of other properties. For example, tensile and yield strength can increase, although this may lead to lower elongation and fracture toughness values; consequently, heat treatments are designed with the intention of

optimizing the properties. The main strengthening elements in Al-Si cast alloys are Cu and Mg, where the age-hardening response is significantly influenced by a number of factors. An increase in Cu generally reduces ductility and changes the morphology of the Cu-containing phases, while the introduction of Mg into the alloy lowers the solidification temperature of the Cu-rich phase and leads to the formation of $Al_5Mg_8Si_6Cu_2$, as well.[11] On the other hand, the addition of Mg to Al-Si alloys also leads to the formation of the age-hardening compound Mg_2Si which increases strength and reduces ductility. The improvement in strength values observed with added Mg-content becomes more evident after heat treatment.

All elements which are not classified as alloying components are termed impurities, and they have a negative effect on the castability, mechanical properties and heat treatment of aluminum alloys. Among these elements, iron is considered to be the most deleterious impurity element. The high difference in the solubility of iron in molten and solid aluminum makes most of the iron appear as an intermetallic second phase. It has been reported that increased solidification rates, strontium additions and/or the presence of such transition elements as Mn promote the development of a more compact, less harmful α-Fe phase.[12,13]

Heat-treatment is of major importance since it is commonly used to alter the mechanical properties of cast aluminum alloys. Heat-treatment improves the strength of aluminum alloys through a process known as precipitation-hardening which occurs during the heating and cooling of an aluminum alloy and in which precipitates are formed in the aluminum matrix. These second-phase particles affect dislocation motion which in its turn

affects strength. The composition of a particular alloy determines the temperature of the heat treatment applied. When an alloy is heated above the solvus temperature of the secondary phases in the matrix, the alloying elements dissolve in the aluminum matrix to form a solid solution. Following a quench, or rapid cooling, the alloying elements precipitate out of solution. This step, known as aging, is called natural aging when it occurs at room temperature; an alloy can also be aged artificially at an elevated temperature in order to increase the kinetics of the process. The three heat-treatments to be examined here are the T5, the T6 (peak aging) and the T7 (overaging) treatments. The T7 heat-treatment is more commonly used in the automotive industry in that it provides a dimensionally stable microstructure; the T6 treatment, however, provides the maximum possible attainable tensile properties.

Tensile and impact properties are two important mechanical properties used routinely in design calculations. Both these properties are controlled by the microstructure, as well as the formation of porosity and intermetallics. In general, the relation between porosity and any of the mechanical properties is non-linear.[14] The shape of the non-linear graphs gives an indication of the pronounced influence of porosity on all the properties. Among the properties measured, ultimate tensile strength (UTS) appears to be the one most affected by porosity, followed by yield strength (YS) and then percentage elongation. An increase in the volume fraction and size of intermetallics also lead to a decrease in tensile and impact properties.

As machining is an important part of the production process, the machinability of cast components has been extensively studied. Chip formation is the same in most

machining processes, and it has been researched in order to determine closed-form solutions for speeds, feeds, and other parameters which have, in the past, been determined intuitively by the machinist.

The process of chip formation may be improved either by controlling the matrix properties or through the addition of low melting-point elements to the alloy; these include Pb, Bi, Sn, and In, or their eutectics. If the alloy matrix is rendered brittle, chips produced during a machining operation will be short and discontinuous. The addition of a low melting-point metal, on the other hand, provides a different scenario. Low melting-point additions tend to be fine and evenly dispersed throughout the alloy. The elements involved in these additions usually have very little or no solubility in the matrix, hence, their persistence as separate entities dispersed within it. During a typical machining operation, it is thought that the local rise in temperature is close to, equal to, or greater than the melting temperature of the dispersed entity. These conditions give rise to local loss of strength and ductility accompanied by the formation of short, discontinuous chips. In this respect, Pb-Bi, Bi-Sn, Sn, and In-Sn are suitable for forming low-melting inclusions in Al alloys.

This study will investigate the effects of the Al-insoluble elements Sn, Bi, Pb, and In (all of which have extremely low distribution coefficients in both Al and Si) on the microstructure and mechanical properties of an experimental Al-10.8% near-eutectic alloy, as well as the commercial Al alloys B319.2 and A356.2. Of significant interest in this entire context is the effect of these microalloying elements on the morphology and size of the eutectic Si particles, and whether or not their refinement translates into an increase in tensile strength, ductility and toughness values.

Selection of an alloy with certain specific properties is difficult since classical methods have not led to the development of quantitative relationships between the mechanical properties of alloys, on the one hand, and their composition or heat-treatment parameters, on the other. Thus, if two or more variables are varied together it becomes difficult to quantify what effect the interaction between them will have on the various properties, because the effect of such an interaction is not evident using the classical approach. Under these circumstances, physical metallurgists have used empirical methods to solve these problems. Experimentation is carried out to determine the effect of the independent variable (factor) on the dependent variable (response) and a relation between them is then illustrated by means of a regression model using the experimental data. Statistical design of experiments (DOE) is a widely-known and efficient experimentation technique which has been applied in a wide range of fields to produce high quality products, to implement operations more economically, and to ensure stable and reliable processes.[15,16]

In this study, the statistical design of experiments approach has been used to examine and control the properties and behaviour of the Al-10.8%Si near-eutectic alloy and also to develop regression equations between the percentage composition of alloying elements (factor) and the mechanical properties (response).

1. 2 OBJECTIVES

The research thesis was designed with the aim of understanding how alloying elements, trace elements, and heat treatment influence changes in the microstructure and,

consequently, the performance of hypoeutectic and near-eutectic Al-Si alloys. The importance of heat treatment lies in the fact that it is commonly used to alter the mechanical properties of cast aluminum alloys. Thus, the objectives of the proposed research are as follows:

1- Determine the effects of adding alloying elements, namely, Fe (0.5-1%), Mn (0.5-1%), Cu (2.25-3.25 %) and Mg (0.3-0.5%), trace elements, namely, Pb (0.5%), Sn (0.05-1%), Bi (0.5%), Zn (0.5%), and In (0.5%), and the relevant heat treatment parameters (solution treatment and aging conditions) on the microstructural characteristics, mechanical properties (hardness, tensile and impact properties), and precipitation of intermetallic phases in as-cast hypoeutectic and near-eutectic Al-Si alloys, with emphasis on the changes occurring in the microstructure as a result of solution heat treatment.

2- Establish a relationship between the tensile properties and impact energy.

3- Identify and quantify the new phases observed after addition of trace elements.

4- Carry out a mathematical analysis of the tensile and impact data obtained.

A thorough understanding of all the metallurgical parameters involved in the alloys studied would make it possible to select material and workpiece designs to obtain optimum machining combinations critical to maximum productivity.

1.3 THESIS LAYOUT

The research associated with this thesis is presented in the next seven chapters. These chapters are self-contained, with each chapter including a brief introduction, a review

of the pertinent technical literature, and a summary of the chapter contents. For completeness, the thesis contains a comprehensive literature review chapter, a thesis summary with conclusions chapter, and a complete set of references.

Chapter One of this thesis defines the objectives of undertaking this study. Chapter Two provides a detailed literature overview of the main aspects of modification, grain refinement, alloying and trace elements with special discussion of their effects on the microstructure and mechanical properties of commercial hypoeutectic and near eutectic Al-Si alloys. Experimental procedures and testing methods are given in Chapter Three. Analysis and discussion of experimental data results confirmed by statistical analysis are provided in Chapters Four, Five, and Six. Finally, concluding remarks and recommendations are presented in Chapter Seven.

The results presented in this thesis have been published in the form of several research articles in various international journals and conference proceedings. Complete details of these publications are provided in the Publications section on page ix.

CHAPTER 2

REVIEW OF THE LITERATURE

CHAPTER 2

REVIEW OF THE LITERATURE

2.1 INTRODUCTION

There are numerous reasons for the continuing popularity of aluminum alloys; these include low specific gravity, relatively low melting temperatures, negligible gas solubility with the exception of hydrogen, and good castability. Also, such properties as excellent strength-to-weight ratio, high thermal and electrical conductivity, good corrosion resistance, with good machinability and surface finish are some of the further advantages of using these alloys. The market for aluminum castings is expanding in increasingly varied fields of application. The largest production segment is to be found in the automotive industry with applications in the manufacture of engine blocks, cylinder heads, intake manifolds, pistons, wheels, and so forth. With an anticipated production of 50,000 cars per year, aluminum frame and body parts have become acceptable in mainstream automobiles.[17] Table 2.1 shows some annual numbers for aluminum consumption in specific automotive parts.

Table 2.1 Percentage of light vehicles produced in USA with various aluminum components[18]

Part	1998	2000	2006
Engine Blocks	25 %	35 %	55 %
Cylinder Heads	72 %	90 %	94 %
Intake Manifolds	70 %	60 %	40 %
Wheels	45 %	60 %	70 %
Transmission Cases	92 %	95 %	95 %
Brakes, Suspension Parts	1 %	8 %	15 %

According to the Aluminum Association (AA), a 10% reduction in vehicle mass results in a 6 to 8% improvement in fuel economy. The AA also points out that 85 to 90% of aluminum is already being reclaimed and recycled. Using aluminum sheet 1.5 times the thickness of steel provides 70% of the theoretical stiffness required with only 50% of the weight. Aluminum has proven to be one of the most cost-effective substitutions for more traditional materials like cast iron. Other areas of application include the civilian and military aircraft industries, and those requiring a wide variety of lower quality castings.[18,19,20,21,22,23]

2.2 ALUMINUM CASTING ALLOYS

Aluminum is relatively malleable compared to other materials, and it is well-suited to metal-forming applications. In its pure form, however, aluminum is possessed of low strength; for which reason it is typically alloyed with other elements for strengthening purposes. A number of metals may be alloyed with aluminum, but only a few are used as major alloying elements in commercial aluminum-based alloys; others are used as supplements to alloying additions for the improvement of alloy properties and characteristics. The effects of these alloying additives on the properties of aluminum depend on the individual elements and the specific amounts added, as well as on their interaction with aluminum and with each other. Major additions are primarily used for strengthening, while other elements are used to obtain specific microstructural characteristics which may include a finer grain size, higher critical recrystallization temperatures, or else to block the harmful effects of certain impurities.

Aluminum and its alloys are used in many aspects of modern life, from soda cans and household foil to the automobiles and aircraft in which people travel. The alloying elements in aluminum alloys may be present in the form of solid solution, dispersoids, precipitates within the grain, or intermetallic compounds at the grain boundaries. Due to the multiplicity of the alloying elements, many different phases precipitate during solidification and subsequent cooling.

Depending on their method of fabrication, aluminum alloys may be divided into two major groups: cast and wrought alloys. Cast aluminum alloys are classified on the basis of their chemical composition; there is, however, no internationally accepted system of nomenclature which has been adopted for identifying them. These alloys incorporate many advantages compared to other materials and processing methods, although continuous improvements will be necessary in the future for them to maintain their competitive advantage.

Aluminum casting alloys are the most versatile of all common foundry alloys. For large productions, the three main casting processes are sand casting, permanent mold casting and high pressure die casting. Aluminum is also castable by means of the lost foam process, as well as the plaster, centrifugal and shell mold processes. Wrought alloys differ from cast alloys in that they can be shaped by deformation. Both aluminum cast and wrought alloys may be separated into heat-treatable and non-heat-treatable alloys, where the alloys are strengthened using heat treatments in the first case, and work hardening in the second.

2.3 ALUMINUM-SILICON ALLOYS

Aluminum alloys containing silicon as the major alloying element are highly satisfactory from the point of view of castability, weldability, thermal conductivity, and excellent corrosion resistance; in particular, they also display good retention of physical and mechanical properties at elevated temperatures.[20,24] It is for this reason that Al-Si casting alloys have usually constituted 85 to 90% of the total of aluminum cast parts produced.[22]

The Al-Si system is a simple eutectic system, even though Al-Si alloys differ from standard eutectics. In the Al-Si system, the solid solubility of aluminum in solid silicon at any temperature is almost nil, with the maximum value being ~ 0.17 wt%,[25] as per the phase diagram shown in Figure 2.1. The maximum solubility of silicon in aluminum is 1.49 at.% at the eutectic temperature and is reduced to 0.05 at.% at 300°C and 0.01 at.% at 227°C.[26] There is no metastable intermetallic compound in this system. The eutectic reaction, $L \rightarrow Al + Si$, occurs at 577°C at a composition of about 11.8 at.% Si (12.0 wt%). An enlarged aluminum-rich portion of Figure 2.1 is shown in Figure 2.2 from which it is possible to conclude that there is no β terminal solid solution phase and thus, when considering dissolution, this secondary phase is pure silicon. Consequently, for Al-Si alloys, the eutectic composition is a structure of α + Si rather than $\alpha + \beta$, where the β phase or primary Si particles are cuboidal in form, whereas the eutectic is non-lamellar and appears to consist of separate flakes.[23] These coarse flakes of Si in the eutectic promote brittleness within the alloys. Most of the Al-Si alloys commonly used have a near-eutectic

composition since this gives a lower melting point and makes the alloys more economical to cast.[27]

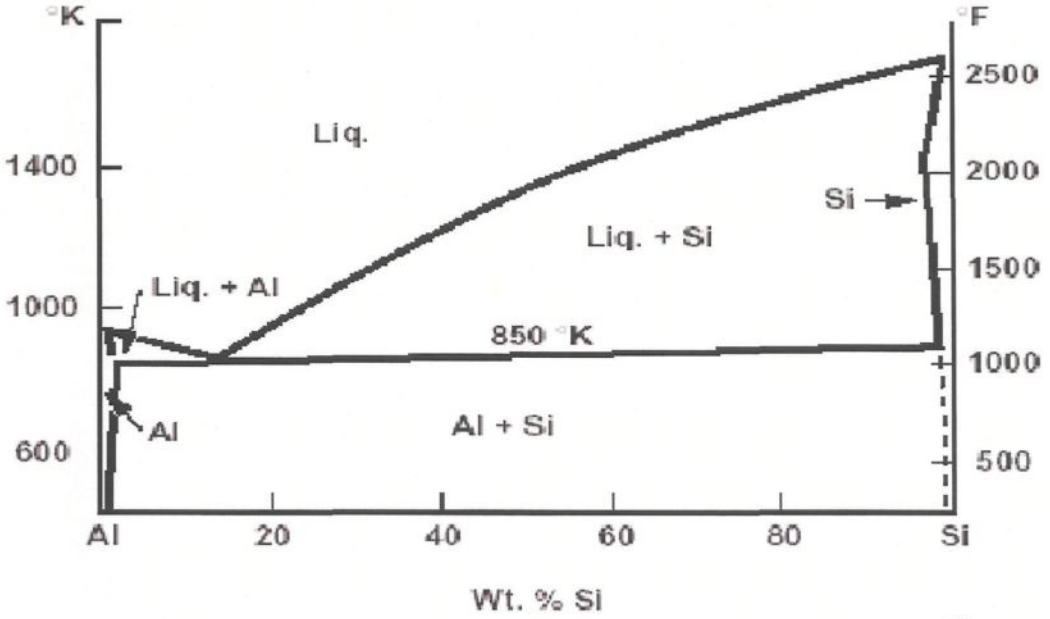

Figure 2.1 Aluminum-silicon phase diagram after Mondolfo.[22]

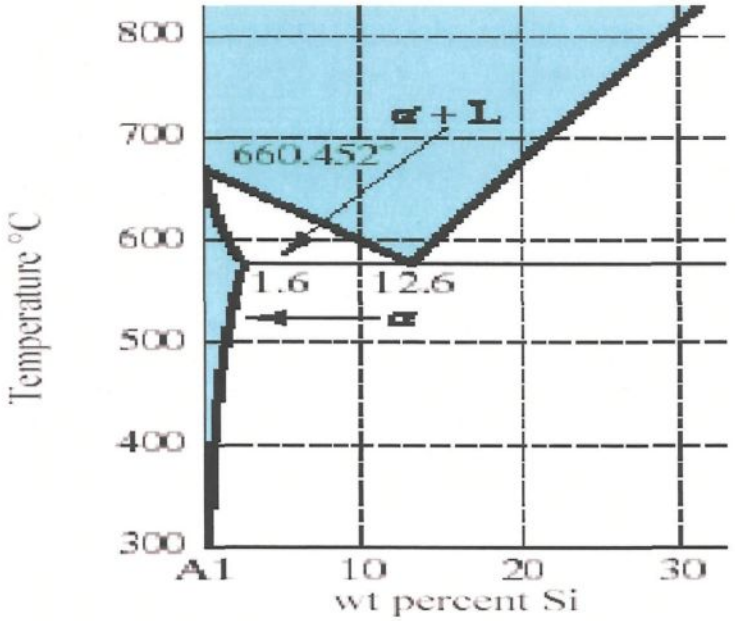

Figure 2.2 Aluminum-rich portion of the Aluminum-Silicon phase diagram.[23]

Depending on the amount of silicon, the alloys may be divided into three groups: hypoeutectic alloys with a Si content of 5-10%, eutectic alloys with 11-13% Si, and hypereutectic alloys with a normal Si content of 14-20%. A wide range of commercial compositions has thus far been developed in the Al-Si family, but the most preferred group is that of the hypoeutectic alloys, some of which are listed in Table 2.2.

Table 2.2 Chemical composition of typical hypoeutectic Al-Si casting alloys[20]

AA Alloy No.[a]	Chemical Composition, wt%[b]					
	Si	**Fe**	**Cu**	**Mg**	**Zn**	**other**
355	5.0	<0.6	1.25	<0.5	<0.35	
A355	5.0	<0.2	1.25	<0.5	<0.1	
356	7.0	<0.6	<0.25	<0.35	<0.35	
A356	7.0	<0.2	<0.2	<0.35	<0.1	
319	5.5-6.5	1.0	3.0-4.0	0.1	1.0	0.5 Mn
B319.1	5.5-6.5	0.9	3.0-4.0	0.15-0.5	1.0	0.8 Mn
357	7.0	<0.15	<0.05	0.55	<0.05	
A357	7.0	<0.20	<0.2	0.55	<0.10	0.05 Be
444	7.0	<0.6	<0.25	<1.0	<0.35	
A444	7.0	<0.6	<0.10	<0.05	<0.10	0.05 Be

a AA: Aluminum Association
b Remainder: Aluminum and unlisted impurities

The castability of near-eutectic and eutectic Al-Si alloys is known to be better than that of the hypoeutectic Al-Si alloys.[2] The applications of the near-eutectic and eutectic Al-Si alloys, however, are not as wide as those of hypoeutectic Al-Si alloys, such as A356 alloy, because of their poor strength and ductility. Concerted efforts are being made by researchers to improve the strength and ductility of these alloys in order to increase their overall range of application. The mechanical properties were found to depend less on the composition than on the distribution and shape of silicon particles. Small rounded, evenly

distributed particles, either eutectic or primary, result in high ductility with relatively high strength; faceted, acicular silicon crystals may produce slightly higher strengths, although with much lower ductility, impact and fatigue resistance.[23]

2.3.1 Al-Si-Cu-Mg Alloy System

The 319 (Al-Si-Cu-Mg) casting alloys represent the workhorse of aluminum foundry alloys. In this group, silicon provides good casting characteristics while copper provides high strength and machinability at the expense of somewhat reduced ductility and lower corrosion resistance.[28] Based on the Al-Si system, the alloy contains copper and magnesium as the main alloying elements. Its silicon content ranges from 5.5 to 6.5 wt%, and copper content varies from 3.0 to 4.0 wt%.

Addition of Cu leads to a slight increase in alloy fluidity, and a depression in the Si eutectic temperature of ~ 1.8°C for every 1 wt% Cu added. Also, a number of the mechanical properties, including YS and UTS, obviously benefit from the addition of Cu as an alloying element.[29] The presence of magnesium improves strain hardenability, while also enhancing the material strength by solid solution.[30] The as-cast structure of the 319 alloy includes α-Al, eutectic silicon particles, Mg_2Si, Al_2Cu, $Al_5Cu_2Mg_8Si_6$ and other complex intermetallic compounds.[23,31] At ~548°C, the amount of Cu in solid solution in Al is known to be about 5.7 wt%; this value decreases with decreasing temperatures, reaching 0.1-0.2 wt% at 250°C.[20] Copper forms an intermetallic phase with Al which precipitates during solidification either as block-like $CuAl_2$ or in its eutectic form as (Al + $CuAl_2$). In the 319 alloys, the copper intermetallic phase precipitates in both of these forms.[32]

2.3.2 Al-Si-Mg Alloy System

Another important group of alloys in the Al-Si system are Al-Si-Mg alloys, which are hardened by Mg_2Si, such as the 356 alloy. Magnesium is the basis for strength and hardness development in heat-treated Al-Si alloys. In the heat-treated condition, the hardening phase Mg_2Si has a solubility limit corresponding to approximately 0.7% Mg.[28] Beyond this limit, no further strengthening occurs nor does matrix softening take place. At room temperature, quantities of magnesium exceeding 0.3% Mg will be present as Mg_2Si. An increase of magnesium, within the alloy range, results in increased strength at the expense of ductility. Magnesium also has a beneficial effect on corrosion resistance. By including additional elements, it is possible to improve the mechanical properties of Al-Si-Mg alloys.

With regard to these alloys, iron is considered an impurity originating in the process of mining aluminum from the ore. It often appears in the form of AlFeSi intermetallics at the grain boundaries, causing a severe loss of ductility in the alloy; strength may also be noticeably affected. As a result, the iron-content is kept significantly low in premium quality alloys which are used for aircraft and aerospace castings requiring high-grade quality properties. Copper is present primarily as an impurity in Al-Si-Mg alloys and decreases the sensitivity of the alloy to quench rates. It also increases the stress-hardening effect as well as the strength in the T6 temper. Higher copper-content decreases ductility and resistance to corrosion, while additions of manganese, chromium, and zirconium inhibit recrystallization during solution treatment. Manganese additions increase creep and fatigue resistance and, to some extent, counteract copper in neutralizing the corrosion

susceptibility of the alloy. Manganese converts the crystallization of needle-like intermetallic phases to cubic or globular forms, such as Chinese script morphology, which have less harmful characteristics. This type of morphology improves tensile strength, elongation and ductility.[33,34,35] Furthermore, it should be noticed that small amounts of manganese (usually Mn:Fe = 1:2) play a positive role by breaking up the iron needles [35] When added in a higher ratio or in the presence of chromium, depending on the melt temperature, manganese produces a hard multi-component intermetallic compound, commonly referred to as sludge, which affects the mechanical properties of the casting. Lead and bismuth may be deemed useful additions for improving the machining characteristics of the alloy.[36,37]

2.4 MICROSTRUCTURE AND FEATURES OF Al-Si ALLOYS

The notable importance of Al-Si alloys to relevant industries has motivated several researchers to explore the microstructure of these alloys together with their properties. Two schools of thought exist, each with its distinct conception of the genesis of the Al-Si eutectic and the modification of its morphology.[38] One school believes that the mechanism underlying the nucleation of eutectic silicon in Al-Si alloys eventually determines the eutectic silicon morphology; the other attributes the morphology of the silicon eutectic to the kinetics of its growth.

The microstructure of Al-Si alloys depends on the chemical composition, casting process, and heat-treatment involved. The microstructure of Al-Si alloys is composed of two phases, *i.e.* Al and Si. These alloys are a combination of a high-strength brittle phase

(Si) and a low-strength ductile phase (Al), where the microstructure is typically composed of an aluminum matrix containing eutectic silicon. This silicon may be present in the form of acicular needles, blocklike plates, or a refined fibrous structure, depending upon the level of chemical modification and the cooling rate of the cast section. In general, the eutectic silicon is not uniformly distributed, but tends to be concentrated at the interdendritic boundaries. Figure 2.3 reveals some of the distinguishing features of typical alloy microstructures, in this case A319 alloy, as described below.

1- Eutectic Silicon

Eutectic silicon has a coarse, plate-like structure in which the coarse plates act as stress risers and provide planes of weakness; both may be combined to enhance crack initiation and propagation. The morphology of eutectic silicon may be modified by adding small amounts of Na or Sr to the melt, while solidification may also be obtained by increasing the solidification rate. Further details concerning the effect of Sr as a modifier will be presented in subsequent sections.

2- Intermetallic Phases

Two of the major intermetallic phases in the 319-type aluminum alloys are the Fe-based and Cu-based intermetallics. Iron-based intermetallics tend to form β-Fe and/or α-Fe phase particles. The β-Fe particles are acicular platelets which have a significant effect on the mechanical properties, while the α-Fe phase particles appear in a more compact, Chinese script form that is less harmful to the alloy properties. The Cu-based intermetallic is primarily Al_2Cu, which occurs either in the form of block-like particles or in a finer Al-Al_2Cu eutectic-like form.

3- Grain Size

Grain size in a casting typically ranges from several hundred microns to several millimetres in diameter.[39] In order to reduce the grain size, grain refiners such as Ti or TiB_2 may be added, or else the solidification rate may be increased.

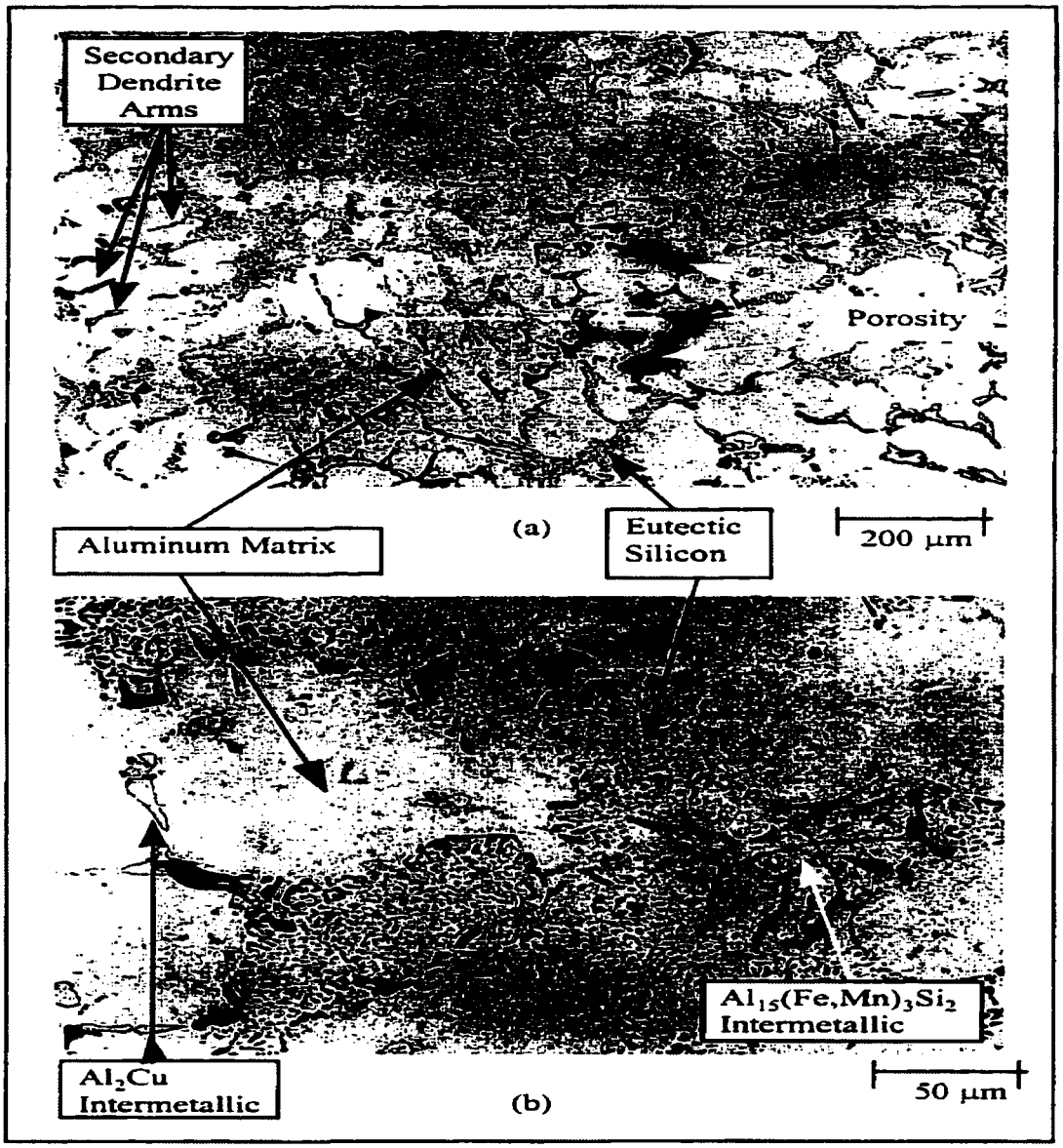

Figure 2.3 Typical features of A319 alloy microstructure.[40]

4- Secondary Dendrite Arm Spacing (SDAS)

Secondary Dendrite Arm Spacing (SDAS) is the linear distance between two of the secondary α-Al dendrites or arms.[41] As this SDAS is governed by the solidification conditions, it thus provides a direct measurement of the solidification rate in the local casting area. In general, the mechanical properties of aluminum castings tend to correlate better with the SDAS than with the grain size; all other things being equal, higher solidification rates yield finer spacing, which in turn provide better mechanical properties.[22]

5- Porosity

Porosity is a major defect in cast aluminum alloys; it may be observed in the form of pores, voids, or cavities which arise in the interior of a casting during solidification. In general, porosity has three sources. The first is poor casting design which prevents the casting from filling properly; this defect is commonly referred to as *macroshrinkage*. The next source of porosity is gas which is entrapped or dissolved in the liquid metal during casting; this is called *gas porosity* or *microporosity*. The third source of porosity develops from the natural volume contraction which occurs when a liquid solidifies; this is often referred to as *microshrinkage* porosity.[40] The presence of porosity is crucial in that it lowers the soundness of a casting and thereby its mechanical properties.

2.5 MECHANICAL PROPERTIES OF Al-Si ALLOYS

Strength, hardness, toughness, elasticity, brittleness, and ductility are mechanical properties used to determine how metals behave under load. These properties are described

in terms of the types of force or stress that the metal must withstand and the manner in which they are resisted.

Any improvement in mechanical properties is commonly evaluated through the tensile properties. Almost all of the steps in the processing of aluminum, from establishing a composition to heat-treatment, produce a variation in mechanical properties. The fact that tensile properties depend on several variables may go far to explain the confusion existing in connection with the properties of cast aluminum alloys. The following may be considered among the most important of the many variables which affect the mechanical properties of aluminum-silicon alloy castings.

(1) Alloy type and the variation of the chemical composition within the specified limits for that alloy.[42,43,44,45,46]

(2) Metal soundness, which may be affected by gas porosity, shrinkage porosity and non-metallic inclusions.[47,48]

(3) Metallurgical characteristics, examples of which are macro grain size and constituent distribution.[49]

(4) Solidification rate, which may be related directly to the dendrite arm spacing.[50, 51, 52]

(5) Heat-treatment, which brings about phase transformation in the solid state of the alloy.[53,54]

2.5.1 Hardness Test

In general, hardness implies resistance to deformation. Hardness has conventionally been defined as the resistance of a material to permanent penetration by another harder material with measurement being made after the applied force has been removed, such that elastic deformation is ignored. Currently, the indentation hardness test is used in practically every metalworking plant as a means of checking the quality and uniformity of metals and metal parts. Hardness measurements usually fall into three main categories: scratch hardness, static indentation hardness, and dynamic hardness.

A static indentation hardness method is widely used nowadays in determining the hardness of metals. The universally accepted and standardized indentation hardness test was proposed by Brinell in 1900. The Brinell hardness test consists of indenting a metal surface with a steel ball, 10 mm in diameter, at a load of 3000 kg mass.

For soft metals such as aluminum the load is reduced to 500 kg to avoid deep impression, while for very hard metals a tungsten carbide ball is used to minimize distortion of the indenter. The load is applied for a standard length of time, usually 30 seconds, and the diameter of the indentation is measured with a low-power microscope after removal of the load. The Brinell hardness number is calculated by dividing the load applied by the surface area of the indentation, as shown in Figure 2.4,[55] below.

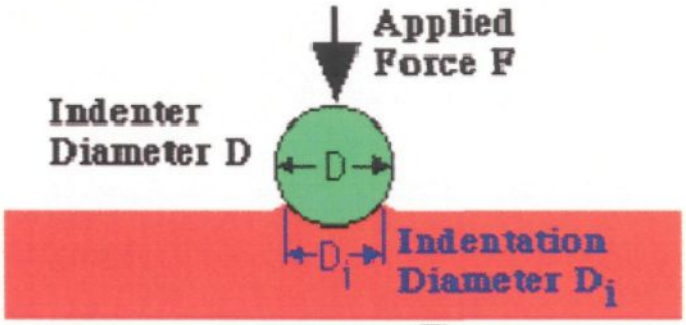

$$BHN = \frac{F}{\frac{\pi}{2} D \cdot (D - \sqrt{D^2 - D_i^2})}$$

Figure 2.4 Schematic diagram of Brinell hardness test.[56]

where BHN is the Brinell hardness number; F is the imposed load in kg; D is the diameter of the spherical indenter in mm; and D_i is the diameter of the resulting indenter impression in mm.

2.5.2 Tensile Testing

Tension tests provide information on the strength and ductility of materials under a uniaxial applied load. Standard analysis is based on an idealized physical situation, which in general may be thought of as being represented by a long, thin sample of material in which an applied load results in an elongation along its length. There are some basic assumptions which must be considered when analyzing the data obtained from such a test: firstly, that the loading must be entirely axial, and secondly, that the deformation should take place uniformly along the length and through the cross-section of the test specimen. The data recorded from load and elongation may be normalized by either the original specimen length or the instantaneous specimen length to produce either engineering stress-

strain plots or true stress-true strain plots, respectively. The American Society for Testing and Materials (ASTM) has produced standard test specimen geometries and guidelines for tension testing.[57,58]

Typical points of interest when testing a material include: ultimate tensile strength (UTS) or peak stress; offset yield strength (OYS) which represents a point just beyond the onset of permanent deformation; and the rupture (R) or fracture point where the specimen separates into pieces.

Engineering stress, S, is defined as

$$S = \frac{P}{A_o} \qquad \text{Eq. (1)}$$

where P is the load on the sample with an original zero (zero-stress) cross-sectional area, A_o. Sample cross-section refers to the region near the center of the length of the specimen. The engineering strain, e, is defined as

$$e = \frac{L - L_o}{L_o} = \frac{\Delta L}{L_o} \qquad \text{Eq. (2)}$$

where L is the sample gage length at a given load, and L_o is the original (zero-stress) length.

A stress-strain curve has two distinct regions: elastic deformation and plastic deformation. The curve shown in Figure 2.5 is typical of metallic behavior. Elastic deformation is temporary deformation, and displays full recovery when the load is removed. The elastic region of the stress-strain curve is the initial linear portion. Plastic deformation is permanent deformation. It does not recover when the load is removed, although a small elastic component may do so. The plastic region is the nonlinear portion

generated once the load-strain exceeds its elastic limit. There is some difficulty in specifying precisely the point at which the stress-strain curve deviates from linearity and enters the plastic region. The convention defines yield strength as the intersection of the deformation curve with a straight-line parallel to the elastic portion and offset 0.2% on the strain axis. The yield strength represents the stress necessary to generate this small amount of permanent deformation. The slope of the stress-strain curve in the elastic region is the modulus of elasticity, E.

$$S = E.e \qquad \text{Eq. (3)}$$

where S represents the stiffness of the material, i.e. its resistance to elastic strain.

In order to determine the true stress during a test, it is necessary to find the instantaneous cross-section area since

$$\sigma = \frac{P}{A} \qquad \text{Eq. (4)}$$

If the deformation in the gage section of the specimen is uniform, assuming that plastic deformation takes place at constant volume, then

$$V = V_o = A_o L_o = AL \qquad \text{Eq. (5)}$$

where L and A are the instantaneous values of the length and cross-sectional area, and L_o and A_o are the initial values.

The longitudinal strain is defined as

$$d\varepsilon = \frac{dL}{L} \qquad \text{Eq. (6)}$$

For extended deformation, integration is required:

$$\varepsilon = \int_{L_o}^{L} \frac{dL}{L} = \ln\left(\frac{L}{L_o}\right) = \ln\left(\frac{L_o + \Delta L}{L_o}\right) = \ln(1+e) \qquad \text{Eq. (7)}$$

Engineering stresses and strains are most frequently used in tensile tests with the objective of avoiding complications in the computation of σ and ϵ. Another indispensable objective is obtaining values which are clearly significant from an engineering point of view.

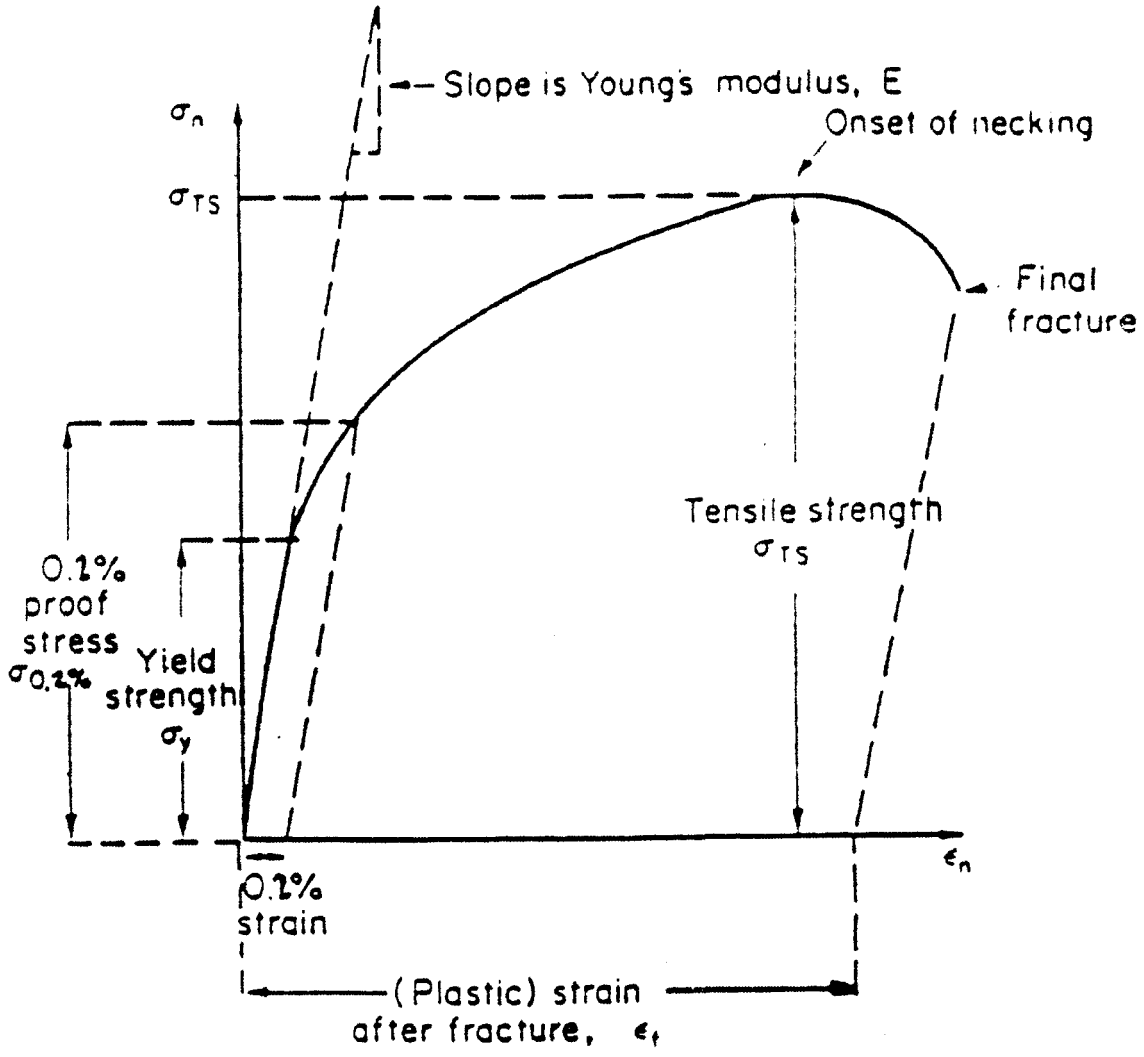

Figure 2.5 Characteristics of the engineering stress-strain curve.

The ductility of casting alloys is usually low, and changes to the casting process or changes in the chemical composition and/or heat treatment aimed at improving strength or other properties can render the material too brittle for structural applications. It is thus important to assess simultaneously what effect on material ductility and strength any changes to the microstructure would have. Hence castings are evaluated using strength-ductility diagrams known as quality index charts.[59]

Quality Index

For aluminum foundry alloys, the results of tensile tests are generally considered individually, whether for assessing the alloy quality or for investigating the influence of any given parameter such as composition, production process, cooling, or heat-treatment. High tensile strength and good tensile ductility are the most desirable properties in structural design, and if the quality index chart, shown in Figure 2.6, is used to plot the experimentally-determined tensile strength and tensile ductility for a particular alloy, the material of the best quality will be located near the upper right-hand corner. Different materials or processing conditions may thus be assessed on the basis of their locus on the chart. This is, in part, the logic behind the development of quality index charts.[60] Drouzy and co-workers[59] defined the quality index, Q, (in MPa) as:

$$Q = UTS + d \log (\%E) \qquad \text{Eq. (8)}$$

where UTS is the ultimate tensile strength (MPa) and E is the elongation (%); while the constant yield strength lines are as follows

$$YS = a*UTS - b*\log(\%E) - c \qquad \text{Eq. (9)}$$

where YS is the (0.2% offset) yield stress. The constants a, b, c, and d are empirically determined parameters whose values depend on the material.

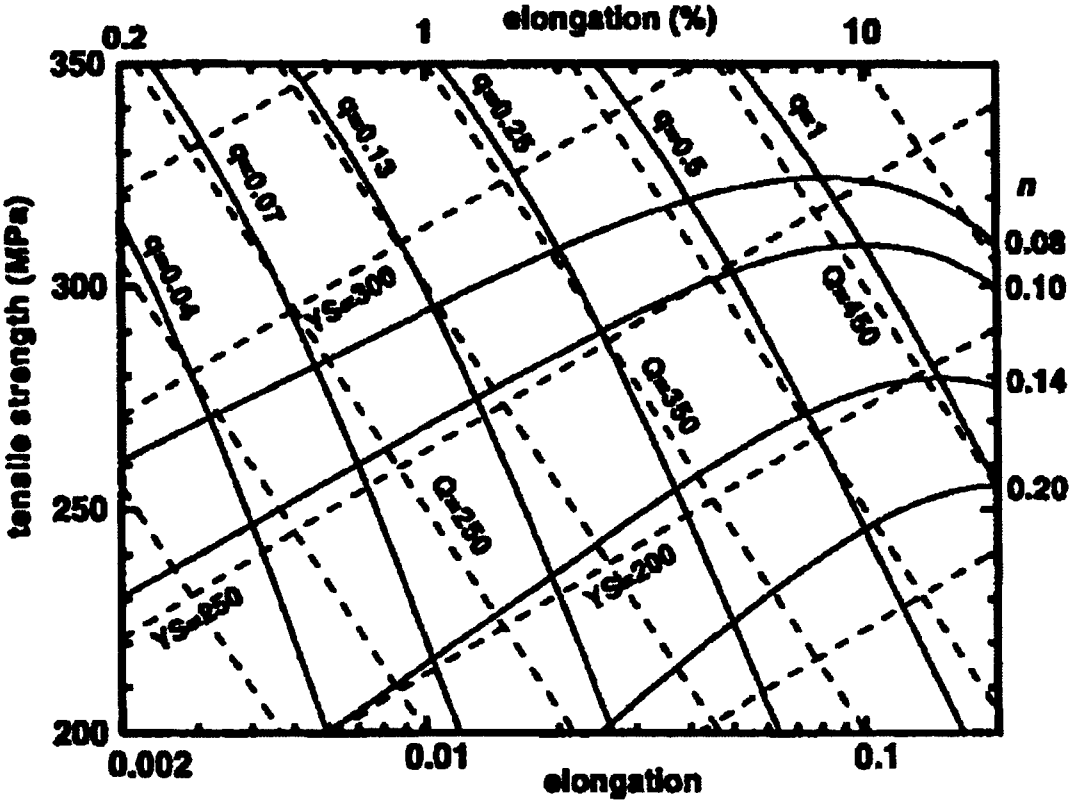

Figure 2.6 Quality index chart for alloy A356. The dashed lines represent the quality index charts as determined by Drouzy *et al.*[59] The solid lines are the flow curves (identified by n-value), and the iso-q lines (identified by q-value), calculated with Equations 4 and 6, respectively, assuming k = 430 MPa.[60]

Drouzy et *al.*,[59] observed that for a particular batch of cast alloy subjected to normal aging treatment, a graph of UTS versus log E is a straight line with a slope close to 150 in the case of A356 and A357 *i.e.* Al-7Si-Mg type alloys. The coefficient K, chosen to make Q practically independent of the tempering conditions, is most probably not the same for all aluminum alloy families. If steps are taken to improve the quality of the casting by reducing porosity, for instance, then a new parallel line is formed at higher levels of

strength and/or ductility.[59,61] In its most straightforward application, the Q-values allow for a comparison between different alloys, or between batches of samples of the same alloy. As stated previously, high Q-value lines are close to the upper right-hand corner of Figure 2.6 and they indicate that the material has both high UTS and high ductility, *i.e.* its mechanical quality is high.

It In general, a Q-value above 400 MPa is considered highly satisfactory for alloy A356.[62] It is normally assumed that the Q-value does not depend on the aging state or the Mg content, and that it thus measures not only the "quality" of the casting as determined by its content in Fe-rich intermetallics, but also the degree of the modification or process-related parameters such as porosity, dross and inclusions. Conversely, the yield strength characterizes the degree of hardening which depends primarily upon tempering treatment (magnesium content, tempering time and temperature). In a casting, the highest possible quality index should be targeted. This should be achieved by appropriate casting design (thickness and junctions), proper molding design (filling system, risers, chills) and careful processing (refining, modification, degassing).

The original quality index chart was developed for alloy A356, and thus its application to other materials conveys the implicit assumption that the parameters involved, particularly the slope, d, of the iso-Q lines in Equation 8, do not depend on the material. Drouzy *et al.*[59] included an explicit warning in this regard in their original publication; and indeed, it has been shown experimentally that the slope and position of the iso-Q lines in the quality index chart tend to change with both the chemical composition and temper in certain alloys.[61]

Although the quality index concept was developed for alloys 356/357, it has occasionally been applied to other alloy systems, including a particle-reinforced 359 alloy,[63] Cu-containing 319 alloys,[64,65] and Mg-base alloys.[66] The application of the quality index concept to alloys other than alloys 356/357 carries the implicit assumption of a similar response to aging, and that the empirical parameters in Equation 8 are the same. Recent studies on an Al-Cu-Mg-Ag alloy (alloy 201), however, show that in contrast with the linear behaviour of alloy 356, a plot of UTS vs. S_f (*i.e.* %El) for alloy 201 describes a circular contour when the material is aged. In addition, the parameters involved in Equation 8 have different numerical values and vary with the aging condition.[67] This shows that extending the quality index concept to systems other than Al-Si-Mg casting alloys requires determining, beforehand, the behaviour of the strength-ductility relationship as the materials are aged. Gauthier *et al.*[68] also observed a circular pattern in the strength-ductility relationship in Al-Si-Cu-Mg alloy 319.2 after aging at different temperatures. This observation suggests that the circular pattern in the quality index as the material is aged may be a characteristic of Cu-containing Al alloys.[69]

2.5.3 Instrumented Impact Testing

Most of the mechanical properties reported for cast Al-Si alloys are the outcome of tensile testing. Considerable scatter is usually observed in the results because this test is highly sensitive to additions of alloying and trace elements to the alloy sample. Furthermore, the test results are not a strong function of silicon morphology. In view of the fact that this thesis deals with variations in the alloying and trace element additions and

silicon morphology, a test much more sensitive to these parameters was used. Instrumented impact testing was thus used in our study since this test has been found to be extremely sensitive to the addition of alloying and trace elements and silicon morphology,[70] although data on impact properties is relatively scarce for these alloys.

The test apparatus consists of the standard hammer equipped with electronic components used to record load and energy as a function of time. The load acting on the impact specimen is recorded by a strain gage. The triggering system is used to turn on the recording system so as to coordinate the load-time and energy-time trace. The velocity system is used to measure the velocity of the hammer before, during, and after the impact which in turn provides information on the energy resulting from the change in kinetic energy of the hammer. Each of these two systems works by means of an opt-electronic device which is capable of measuring the load acting on the specimen on a timescale of milliseconds.

A typical load, energy, and time curve obtained from this test is shown in Figure 2.7. The y-axis represents load (upper curve) and energy (lower curve), while the x-axis records time. The load-time curve shows different stages of deformation. The initial rise corresponds to the elastic regime, P_o-P_y. At higher loads, prior to P_{max}, the specimen deforms plastically while beyond P_{max}, the load decay indicates the presence of controlled crack propagation.

The energy curve shows the amount of apparent energy, E_a, which is a direct integration of the load-time signal based on the assumed constant velocity, as a function of

recording time, while the more accurate energy value, E_t, may be obtained using the expression

$$E_t = E_a\left(1-\frac{E_a}{4E_0}\right) \qquad \text{Eq. (10)}$$

The absorbed energy may be separated into two stages. The first stage is the one where energy is required for crack initiation, E_i, which is the energy at T_{max}. The second stage is that of crack propagation energy, E_p, which is the difference between the total energy and the crack initiation energy.

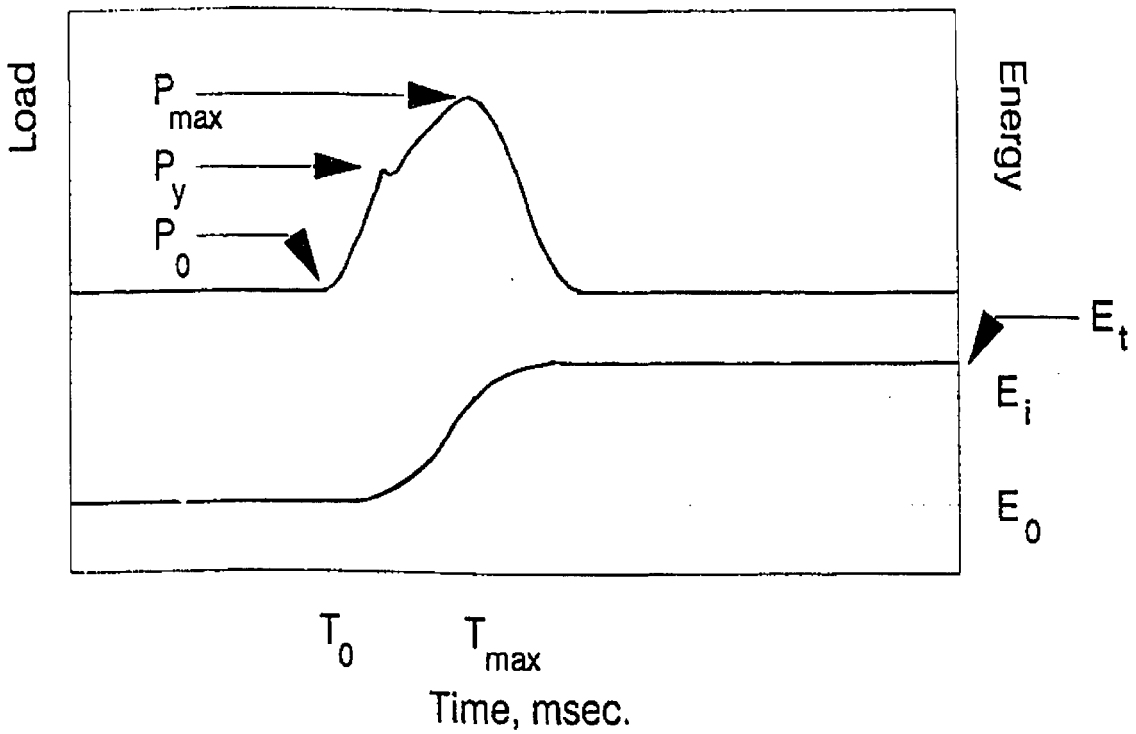

Figure 2.7 Typical load-time and energy-time curves as obtained from instrumented impact testing.

The production of hypoeutectic/eutectic Al-Si alloys displaying improved quality, *i.e.* better structure and mechanical properties, involves the application of two main

processes: (i) the addition of alloying elements during melting and melt treatment of the liquid alloy through grain refining and modification, and/or (ii) heat-treatment.

2.6 EFFECTS OF MELT TREATMENT

Melt treatments such as eutectic modification and grain refinement are frequently applied to Al-Si alloys; which goes far to explain why the effects of these processes on the microstructure and mechanical properties of Al-Si alloys have attracted so much attention. A divorced eutectic has already been observed in the Al-Si system involving areas of aluminum with silicon in solid solution mixed with discrete silicon particles. The mechanical properties of castings are also affected appreciably by the morphology of the silicon particles in the eutectic.

2.6.1 Modification of Al-Si Alloys

Although varying the cooling rate may also modify the eutectic structure,[71,72] it is not always possible to change the cooling rate of the cast components. Over the years, therefore, studies have been carried out to find improved methods of implementing eutectic modification, since modification techniques have advanced from the addition of alkali fluorides to the use of elemental sodium. Davies and West[73] provide an excellent starting point for studies into aluminium-silicon eutectic modification. The main characteristics of alloys modified by addition of elemental sodium or otherwise are:

1- Facetted silicon crystals are reduced in size and become rounder.

2- The freezing point of the eutectic becomes lowered while the melting-point remains unchanged, as shown in Figure 2.8. As the temperature does not rise after the onset of solidification, this alteration in temperature cannot be attributed to supercooling.

3- The eutectic composition moves to higher values of silicon with increased degrees of modification.

4- Primary α and β may both be found in hypereutectic alloys.

5- Overmodification causes bands of larger intermetallic crystals often accompanied by gas pores.

6- Modification causes an increase in viscosity accompanied by a decrease in fluidity and the rate of diffusion.

7- A modified eutectic structure may also be obtained through rapid chilling of the melt.

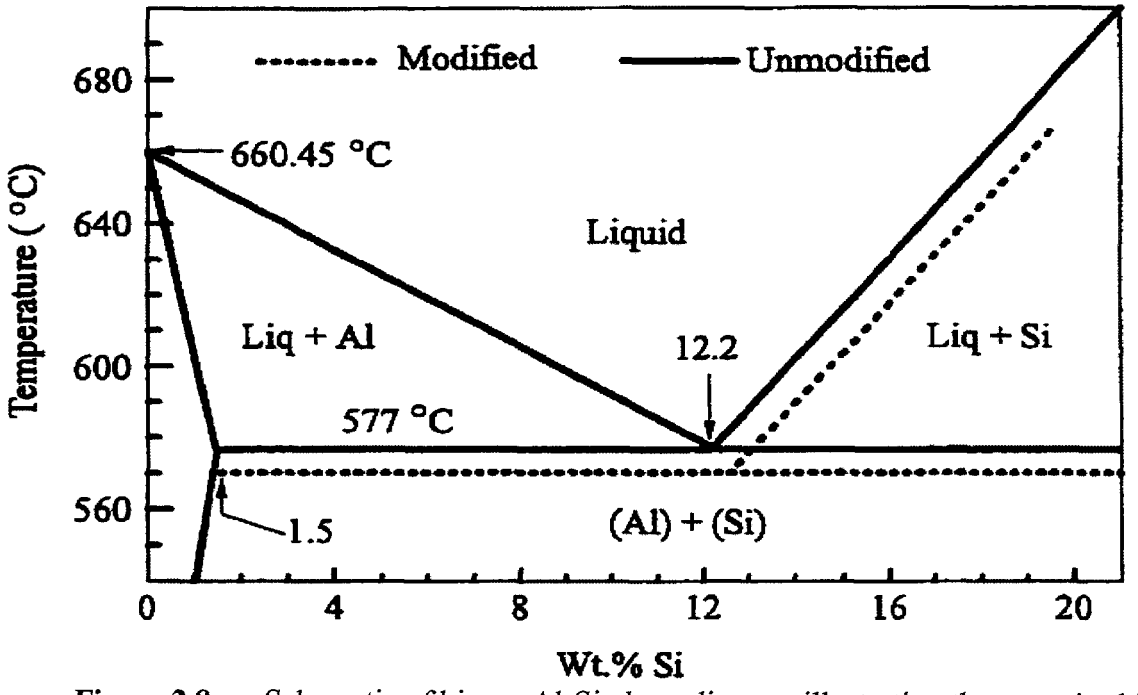

Figure 2.8 Schematic of binary Al-Si phase diagram illustrating the eutectic shift.[74]

2.6.1.1 Types of Chemical Modifier

Strontium, sodium, antimony, and calcium are well-known modifiers and change the morphology of eutectic silicon particles from an acicular to a lamellar or fibrous shape, resulting in improved properties of the alloys.[27,72,75,76,77] Antimony, used primarily in Japan and Europe, has the disadvantage of being toxic, and thus has the potential to form deadly stibine gas (SbH_3) when it combines with the hydrogen in the melt. This is one of the main reasons why antimony is generally not used in foundries[78], although pre-treated ingots may be obtained from primary aluminium suppliers.

In North America, it is mainly either sodium or strontium which is used to modify the aluminium silicon eutectic.[22,79] Both sodium and strontium have their advantages and disadvantages. These modifiers have been found to produce the most twins in eutectic silicon at the lowest concentrations. Lu and Hellawell [80,81] have demonstrated that substantial incorporation of foreign atoms of a certain size into the silicon lattice enhances the formation of twins. A study of the incorporated atom-to-silicon radius ratio for elements that are known to act as modifiers indicates that they all have a radius ratio in the vicinity of the ideal value; some of these modifiers are presented in Table 2.3. It is worthy of note that the size of the sodium atoms is closer to the ideal value than that of the strontium atoms. Values range from 0.005-0.01 wt% for sodium [22,82,83] while levels of 0.01-0.04 wt.% strontium [22,84,85] are required to produce similar levels of modification.

Table 2.3 Some properties of possible modifiers[75]

Element	Atomic radius (°A)	r/r_{Si}	Melting point	Vapour pressure (atm)	-ΔG oxide ($kJmol^{-1}$)	$K_{oxidation}$
Ba	2.18	1.85	725	$5*10^{-5}$	482	20
Sr	2.16	1.84	796	$1*10^{-3}$	480	15
Eu	2.02	1.72	822	$1.8*10^{-4}$	500	-
Ca	1.97	1.68	839	$2.6*10^{-4}$	509	400
Na	1.86	1.58	98	0.2	367	$2.7*10^{-5}$
Ce	1.83	1.56	798	10^{-16}	497	-

Of significant importance to the foundryman in choice of modifier for Al-Si alloys are such characteristics as:

- Ease of handling (reactivity with air, water, and so forth);
- Ease of dissolution (temperature/time requirements);
- Recovery (loss of modifier due to evaporation, reactions);
- Fading (time before losses become significant).

The melting-point is also of importance because elements which melt at lower temperatures will presumably dissolve more readily in Al-Si melts that are typically held at higher temperatures. The vapor pressure is of significant relevance since elements with high vapor pressure tend to boil off the melt. In addition to vaporization, effective modifiers may be lost through oxidation. The $K_{oxidation}$ values in Table 2.3 are the equilibrium constants for the following reaction:

$$XAl_2O_3 + Y\ Modifier \rightarrow 2x\ Al + 3\ Modifier_XO_Y \qquad \text{Eq. (11)}$$

High values of this parameter are indicative of an increased tendency to oxidation.[75]

Table 2.4 compares the corresponding eutectic Si morphology obtained as a result of treatment with each modifier, and then summarizes the beneficial and negative effects accompanying the addition of each modifier.[86] Typical examples of the microstructure of unmodified, Sr-modified, and Sb-modified alloys are shown in Figure 2.9.

Table 2.4 Effects of different modifying elements on Si morphology[22,83,86,87]

Modifying element	Si morphology achieved	Advantages	Disadvantages
Na	Fine Fibers	No incubation period. Mild sensitivity to cooling rate.	Rapid fade due to evaporation. Low recovery rate and difficult to add and control. Porosity redistribution. Over-modification.
Sb	Fine lamellae	Durable and modification effect remains even after remelting.	Generation of a harmful gas during addition and remelting. Only refined lamellar structure achieved.
Sr	Fine Fibers	Melts not easy to over-modify. Durable effect, easy addition and good recovery.	Incubation period. Relatively high cooling rates favoured. Porosity redistribution.

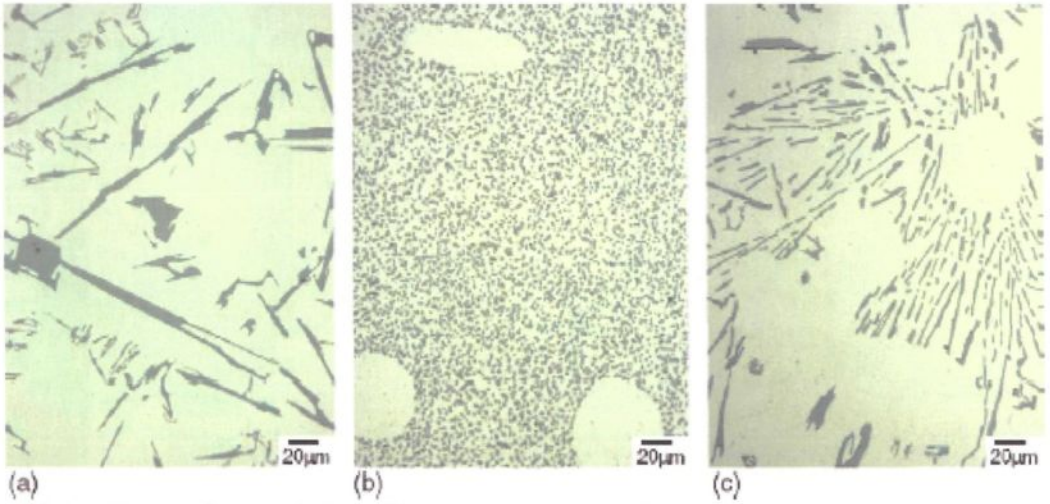

Figure 2.9 Comparison of the silicon morphology in: (a) unmodified; (b) Sr-modified (300 ppm Sr); and (c) Sb-modified (2400 ppm Sb), hypoeutectic aluminum-silicon alloys.[76]

Dahle *et al.*[76] compared the development of the cast structure on macroscopic scales in both unmodified and modified alloys with strontium, see Figure 2.10. In all alloys, co-zonal twinning is present in the silicon fibres with twins lying parallel to the apparent growth direction of the fibres. As shown in Figure 2.10(a), it was possible to find silicon crystals which were free of twinning in the unmodified alloys. In unmodified alloys, the vast majority of eutectic aluminum has an orientation identical to that of the surrounding dendrites, while in Sr-modified alloys the eutectic aluminum displays multiple orientations unrelated to the surrounding dendrites, see Figure 2.10(b). There was a dramatic difference to be observed in the size of the eutectic grains as shown in Figure 2.10(c).

The eutectic grains in the unmodified alloy are, at most, a few hundred microns in diameter and consist of relatively few coarse silicon plates. In the Sr-modified alloys, the eutectic grains are roughly circular in cross-section and are typically much larger than the unmodified alloys. Each eutectic grain in the Sr-modified alloys contains a high density of silicon fibres, see Figure 2.10(d).

The difference in eutectic grain size between the unmodified and Sr-modified alloys is further apparent in the macrographs of samples quenched early during eutectic solidification, as shown in Figure 2.10(e). The eutectic grain size in the unmodified sample is so small that no grains are resolvable in the macrograph; whereas there is a layer of coalesced eutectic grains lining the wall of the sample in the Sr-modified alloy, and several large grains may be seen independently distributed throughout the centre of the casting.[76]

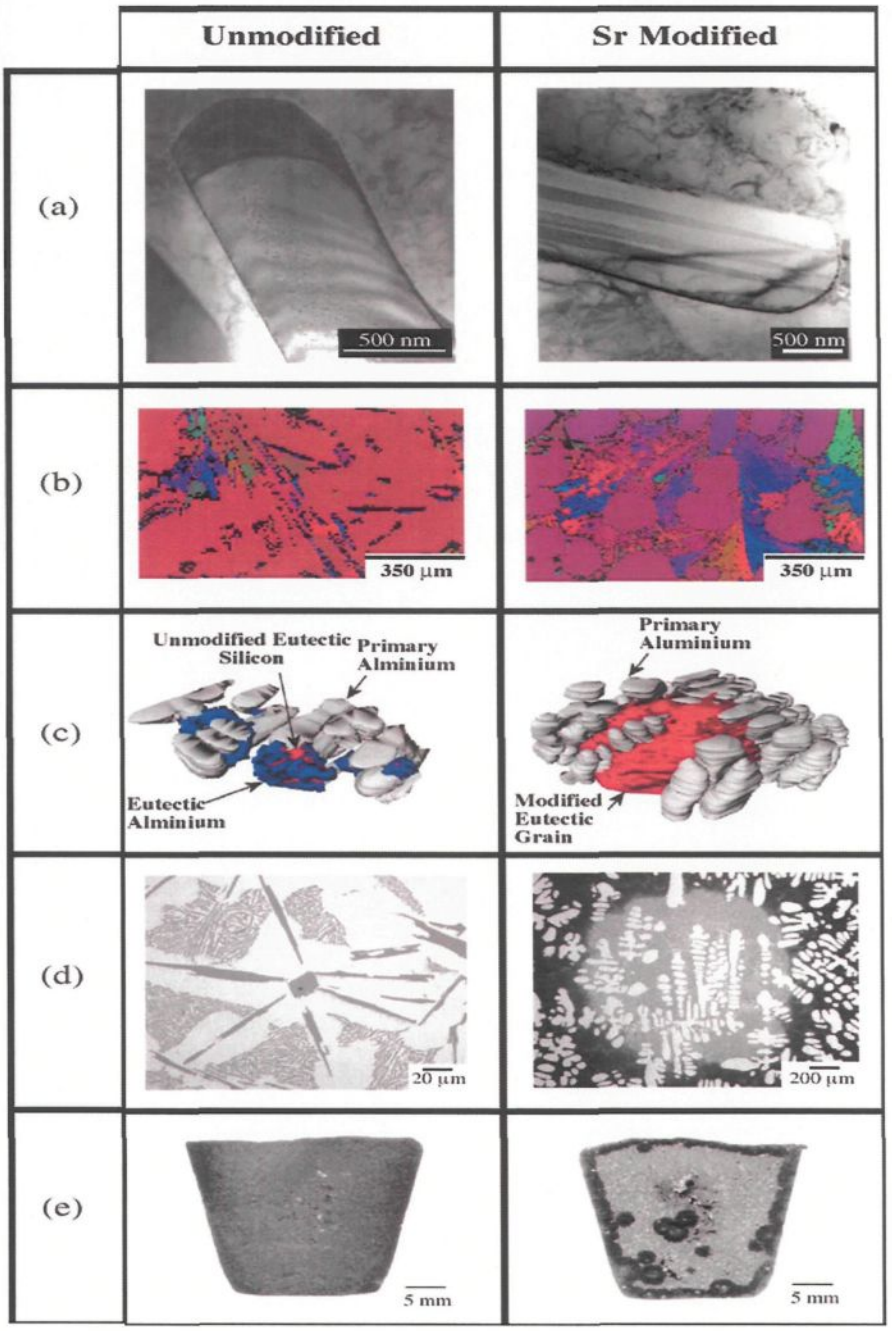

Figure 2.10 Comparison of unmodified and Sr-modified structures: (a) TEM images of silicon crystals; (b) EBSD maps illustrating the orientation of the eutectic aluminum relative to the primary aluminum dendrites; (c) 3D reconstruction of eutectic grains derived from serial sectioning of quenched samples (the unmodified sample is 85 μm deep, the modified one is 117 μm deep); (d) Optical micrographs of quenched samples; and (e) macrographs of quenched samples.[76]

In most applications, strontium is the recommended choice as a eutectic modifier. The ability to use strontium in master alloy form is a significant advantage over sodium for two reasons. First, the problem of reactivity with air and water is eliminated (master alloys containing less than 45% Sr). Second, using master alloys allows the foundryman to weigh out larger quantities of modifier, especially when preparing smaller quantities of melt, as opposed to the case of pure sodium, for instance, thereby making the process easier and allowing for greater accuracy in modifier content.

The addition of strontium to near-eutectic Al-Si alloys can promote the columnar growth of the dendrites which are observable as highly branched fine and slender columnar grains; addition of Sr can also result in a remarkable increase in the amount of the dendritic α-Al phase.[4] The addition of such modifiers to Al-Si cast alloys has been found to improve mechanical properties considerably, especially ductility.[88] In the 319 alloy, the strontium modifier can cause changes in the morphology of the copper-rich phases.

As shown in Figure 2.11, strontium promotes blocky Al_2Cu and fine $Al_5Mg_8Cu_2Si_6$ phases over the eutectic Al_2Cu phase because of the increased number of silicon particles present as nucleation sites in the interdendritic spaces.[89]

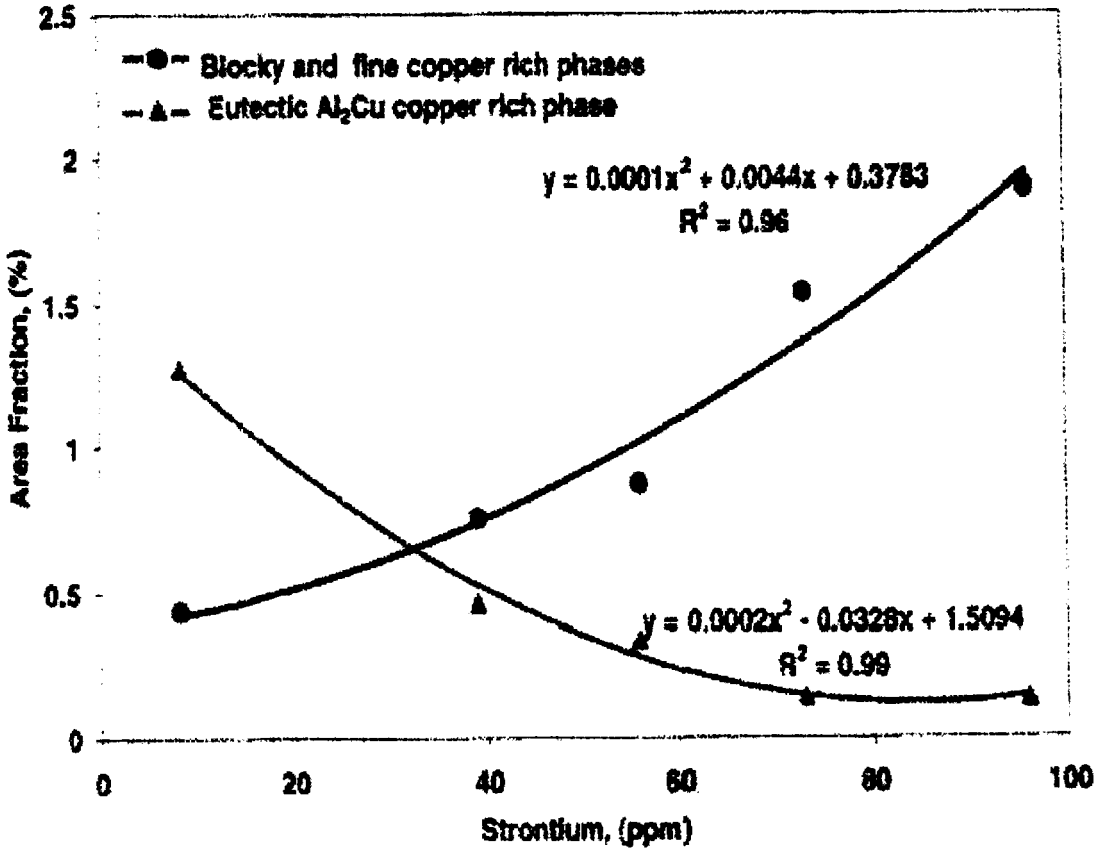

Figure 2.11 Change of area fraction of Cu phases as a function of strontium content.[90]

2.6.1.2 Effect of Modification on Mechanical Properties

The improvement in mechanical properties has generally been attributed to variations in the morphology and size of the eutectic silicon particles.[91] Silicon content and its morphology in the structure have a significant influence on the mechanical properties of the alloys as shown by the curves in Figure 2.12. As the silicon content increases, the tensile strength of the alloy is enhanced; however, at the same time, the brittle nature and flake morphology of the unmodified silicon phase will affect the alloy ductility adversely. After modification, both tensile strength and elongation are improved with the greatest improvement being observed in the elongation.

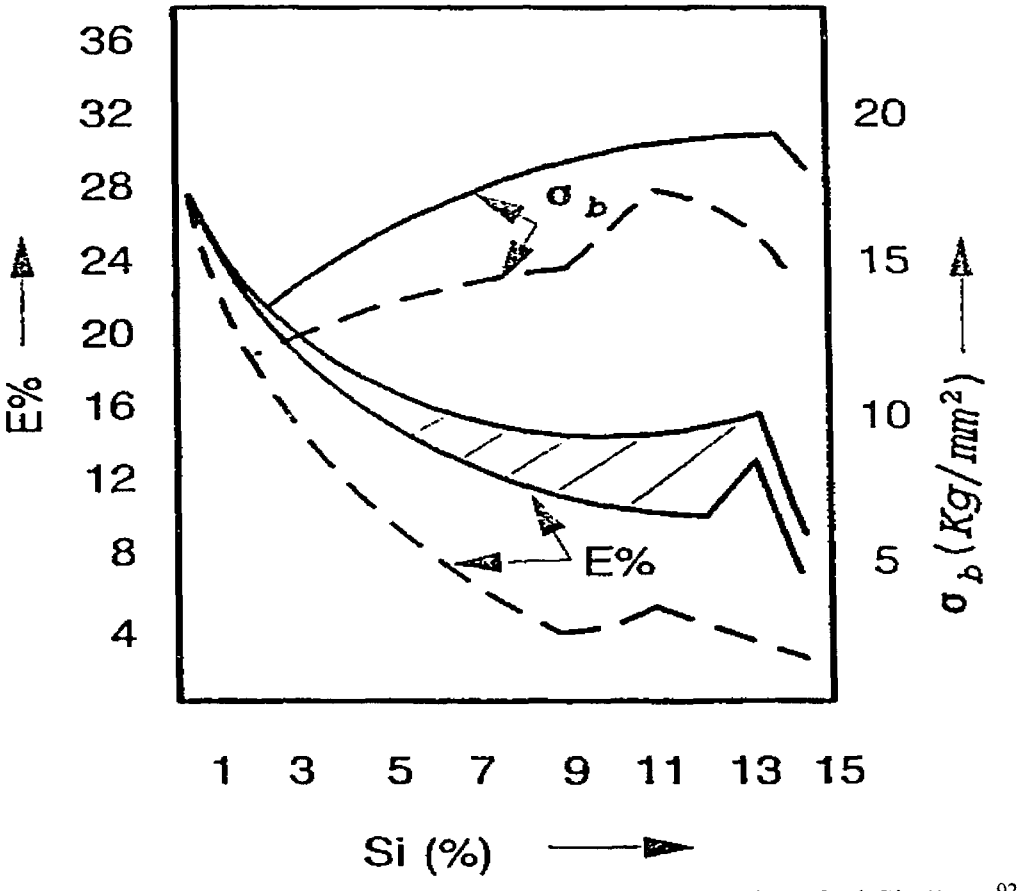

Figure 2.12 Influence of Si-content on the mechanical properties of Al-Si alloys.[92] (Full lines: modified alloys; and dashed lines: unmodified alloys.)

The tensile properties obtained for alloys treated with either sodium or strontium are more or less the same, although elongation is slightly higher for the Sr-modified alloy. It is believed that strontium modification produces better mechanical properties than does sodium modification.[93,94] Figure 2.13 shows the variation in the elongation with differing strontium levels for three different cooling rates in a 356 Al-Si alloy. At all cooling rates, the elongation due to strontium modification was observed to have been improved. The detrimental effect due to overmodification at higher Sr levels is also evident from these

graphs.[45] A comparison of the mechanical properties for modified and unmodified alloys is given in Table 2.5 for some commonly used Al-Si alloys.

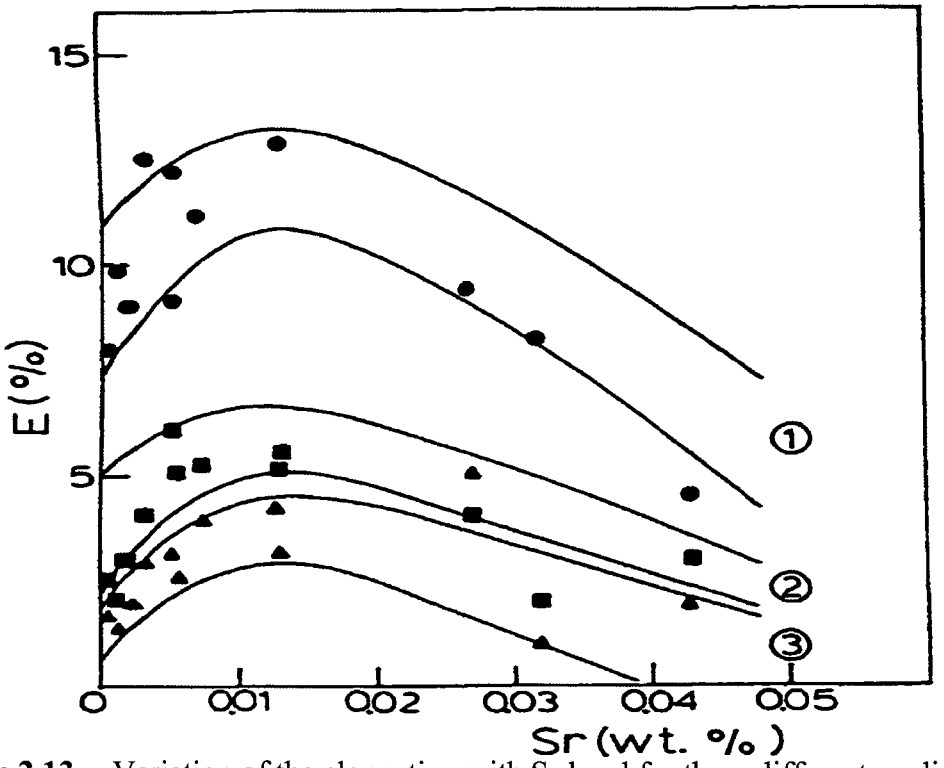

Figure 2.13 Variation of the elongation with Sr level for three different cooling rates.[45] Band 1: cooling rate 1.5°C/s. Band 2: cooling rate 0.5°C/s. Band 3: cooling rate 0.08°C/s.

Table 2.5 Typical mechanical properties of as-cast and modified aluminum casting alloys.[95]

Alloy and temper	Modification	UTS, MPa	Elongation %
356.0-T6	None	288.9	2.0
	0.07% Sr	293.0	3.0
A356.0-T6	None	275.8	4.8
	0.07% Sr	296.5	8
A413.2	None	136.5	1.8
	0.05-0.08 % Sr	191.0	12.0
A413.2	None	124.1	2.0
	Na modified	193.1	13.0

In tensile testing of commercial Al-Si alloys, the elongation is dependent on the silicon phase in the alloy to a greater degree than are the yield strength or tensile strength. It must be pointed out that porosity in alloy specimens is of great importance in determining the mechanical behaviour of the alloy and could be considered a more significant factor than the structure of the silicon. Hafiz *et al.*[96] pointed out that for steel-mold cast Al-Si alloy, the UTS improved from 177.2 MPa for the non-modified alloy to 225.6 MPa for the one which had been modified with 0.024 wt% Sr. In addition, percent elongation increased dramatically from 8.03% in the non-modified state, to 18.2% with 0.012 wt% Sr addition, and 22.2% at a strontium level of 0.024 wt%. Fat-Halla[97] also reported that the addition of 0.02% strontium to Al-13%Si type alloys increases the % elongation and the ultimate tensile strength values without significantly changing the yield strength.

It was also found that in the 413 alloy, addition of strontium leads to fragmentation of the β-Al_5FeSi intermetallic phase and increases the amount of the α-Fe intermetallic phase.[90] Kulunk and Zuliani[98] also studied the effect of strontium on the 380 high-pressure die casting alloy. They showed that the reduction in both size and number of iron intermetallic phase particles through the addition of strontium would lead to an increase in the tolerance of these alloys to higher iron concentrations without altering the mechanical properties.

According to previous studies,[42] it was observed that impact strength is the most sensitive of all the mechanical properties to silicon content for alloy compositions containing 3-15% Si. Modification causes a significant improvement in the impact strength of both as-cast and heat-treated alloys. Impact strength is imparted to the material through

the ductile aluminum matrix which separates the brittle silicon phase. Any process which reduces the size of brittle phase particles or increases their separation, will improve impact properties. Modification fulfils the former propose, while the coarsening process, which takes place during solution treatment, accomplishes the latter.[22] As Figure 2.14 shows, impact properties are much more sensitive to modification than tensile properties, where the impact strength of the modified alloy is seen to increase to three times its value, the elongation value is doubled, although both yield and strength remain virtually unaffected.

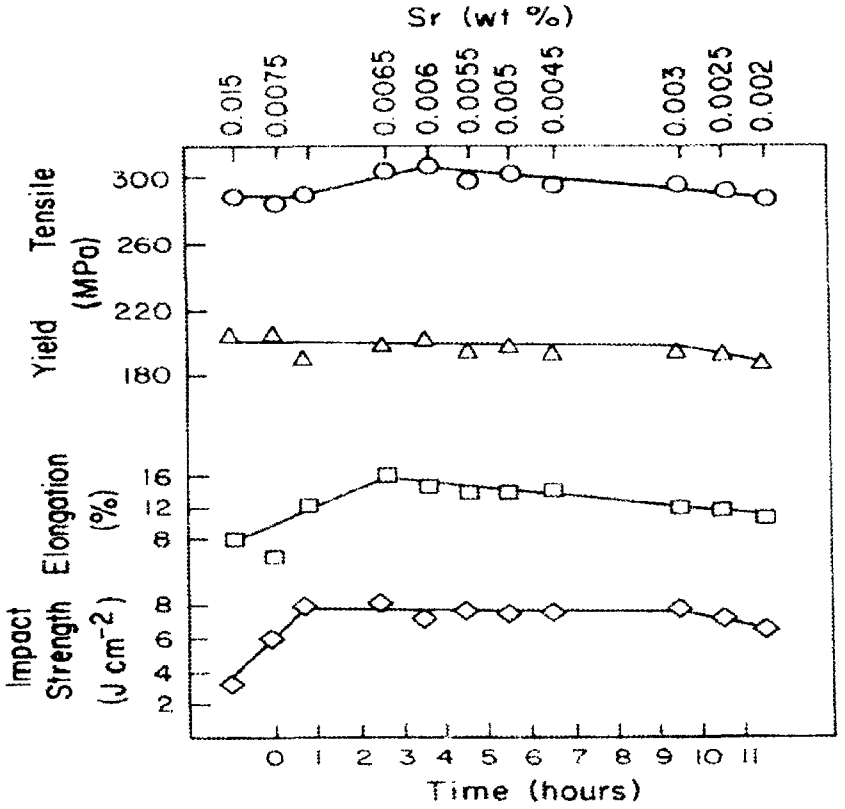

Figure 2.14 Mechanical properties of A356.0 alloy modified with strontium.[22]

Closset[99] investigated the modification and quality of low pressure aluminum alloy castings, and found that Sr-modification substantially improves elongation and, to a lesser extent, the tensile strength of Al-Si eutectic type 413 alloy. The impact strength of the alloy

was found to be highly sensitive to microstructure and was greatly improved by Sr-modification of the eutectic. Similar research results were also reported by Komatsu *et al.*[70] who applied instrumented impact testing to Na-modified and unmodified alloys after different stages of heat-treatment. They found that it was not only the impact strength which was significantly affected by silicon morphology, but the maximum load and propagation energy were as well. The fracture surfaces after tensile testing of unmodified alloys showed a lustrous, dark grey, well-faceted brittle appearance which resembled the appearance of silicon, whereas the modified alloys had a "lighter, silky fracture" which suggests that the fracture occurred largely through the ductile aluminum matrix.[50]

It is worth noting, however, that at the same time as eutectic silicon particles change from acicular to fibrous, the amount, morphology and size of the dendritic α-Al phase are also affected. It was thought, in error, that it would be sufficient to modify the eutectic silicon phase in near eutectic Al-Si alloys, and that it would not be necessary to refine the dendritic α-Al phase. In fact, however, at the same time as the morphology and size of the eutectic silicon phase is transformed by the modification treatment, considerable changes to the amount, shape, and size of the α-Al phase also occur.[86]

2.6.1.3 Effect of Modification on Melt Quality

The greatest problem associated with the modification of Al-Si casting alloys is the fact that modified castings are often more porous than their unmodified counterparts. It has also been reported that modification may reduce surface tension of the melt. Fang and Granger [100] used their porosity model to predict the porosity in a modified alloy; they found

that surface tension in such an alloy must be reduced by 50% in order to match both their calculated and experimental results.

Denton and Spittle[101] suggested that modification aggravates the porosity problem by increasing the hydrogen content or the rate of regassing of the melt; they also observed that melts containing Sr are more susceptible to hydrogen absorption than those containing sodium. They further suggested that the oxidation of Sr during melting causes the structure of the oxide layer on the surface to undergo changes thereby becoming more pervious to hydrogen. Some authors have suggested that strontium helps pore formation by increasing both the inclusion content of the melt and the amount of hydrogen absorbed into oxides.[100,102] Argo and Gruzleski[103] indicate that the increased porosity in modified castings is due to the problems associated with interdendritic feeding. The reduction of the eutectic temperature in modified alloys increases the length of the mushy zone, and, therefore, large pockets of interdendritic liquid may become isolated. Solidification of this liquid may result in the formation of large pores.

At the present time, it appears that the increase in porosity observed with Sr-modification is due to a change in both the nucleation and growth mechanisms of the pore, and may thus not be due to a single factor alone, but rather to complex interactions between such factors as alloying elements, surface tension, feeding, and inclusions.[104,105]

2.6.2 Grain Refining

The quality of the castings may be improved by grain refinement which reduces the size of primary α-Al grains therein, and which would otherwise solidify into a coarse

columnar grain structure. The degree of coarseness or the length of the columnar crystals depends on solidification and casting parameters which include pouring temperature, the liquid thermal gradient in the mold, and alloying elements. It should be noted that all the common alloying elements added to aluminum tend to reduce the grain size somewhat. In general, the more soluble the elements are, the greater the refinement which follows.

Basically, grain refiner addition involves two different concepts:

- The addition of potent substrates to act as exogenous nucleants in the melt.
- The addition of certain elements which would react initially with specific elements within the molten alloy so as to produce potent indigenous nucleant particles.

There are three principal methods for achieving grain refinement in Al alloys:[106]

a) Rapid cooling during solidification (*i.e.* chill grain-refinement);

b) Agitation of the melt, *e.g.* as occurs during semi-solid metal processing;

c) Addition of a grain refiner to the melt.

In the first, a fine grain structure is formed by varying the solidification conditions such as cooling rate and temperature gradient in the casting. This is due to shortening of grain growth during the solidification process. In the second method, grain refinement is obtained by mechanical or electromagnetic agitation, by forced convection, and by breaking up the dendrites in the semi-solid state. The fragmented parts are thereupon transported into the bulk and become effective nucleants. This type of refinement mechanism is the one in which the required stirring is applied during the formation of the semi-solid structure. By far the most successful method of controlling grain size is to introduce particles into the melt which will nucleate new crystals during solidification.

Each grain contains a family of aluminum dendrites originated from the same nucleus. Dendrite arm spacing (DAS) is determined by the cooling rate through the mushy zone, with slower cooling which then results in larger DAS values. The grain size in aluminum foundry alloys varies between 1-10 mm, while DAS values vary from 10-150 μm and the eutectic silicon may be found in the form of plates of up to 2 mm in length or in rounded particles of less than 1 μm in diameter.[22,78,91]

Chemical grain refinement involves the addition of special substrates to act as nucleants or to react with other elements in the melt to form solid nucleant particles. A fine grain size is promoted by the presence of an enhanced number of nuclei, with solidification proceeding at minimal undercooling. Furthermore, chemical grain refinement is beneficial to mechanical properties, particularly to those which are sensitive to hot tearing and porosity. The chemical grain refinement of aluminum and its alloys has been practiced for over 60 years, mostly by primary producers in ingot casting; this has led the foundry industry to borrow the techniques developed by these primary producers to some extent, although research has revealed that the best grain refiners for wrought alloys are not necessarily the best for foundry alloys.[107]

Chemical grain refiners are added to the melt as salt fluxes or master alloys. Salt fluxes contain K_2TiF_6 and KBF_4 salts as the active ingredients which react with the molten aluminum releasing titanium and boron. Aluminides ($TiAl_3$) and borides (TiB_2) are formed in the melt, acting as heterogeneous nuclei for the formation of crystals. Despite their good refining power, salts are prone to generate gas in the melt and to produce corrosive fumes.

Salts can also react with elements like strontium and reduce the modification of the eutectic silicon structure.[108]

The master alloys produced by reacting salts with aluminum under controlled conditions are more effective. Aluminides and borides are embedded in an aluminum matrix, typically containing 100 million, or more, intermetallic particles per cubic centimeter, each particle being a potential nucleant when released into the melt. Master alloys are commonly produced as waffle ingots or extruded rods containing titanium (in the order of 2 to 10 wt%) or boron (up to 5 wt%), or a combination of both elements in aluminum. Master alloys have a Ti/B ratio of unity.[107,108]

2.6.2.1 Grain Refinement by Adding Titanium

According to the Al-Ti phase diagram shown in Figure 2.15, the peritectic reaction occurs at 1.2 wt% titanium and 665°C, with the limit of the peritectic horizontal placed at 0.15% Ti. According to research by Crossely and Mondolfo,[109] the grain refinement of aluminum is associated with the following reaction. When Ti is present in sufficient amounts (*i.e.* >0.15%), it forms primary crystals of $TiAl_3$ which react peritectically with liquid forming α(Al).

$$\text{Liquid} + TiAl_3 \rightarrow \alpha(Al) + \text{liquid} \qquad \text{Eq. (12)}$$

The α(Al) particles then act as nucleants for the remaining liquid, where the degree of refinement is dependent on the number of primary crystals formed, as illustrated in Figure 2.16. From a technical point of view, it is predictable that an Al-Ti alloy which contains many small $TiAl_3$ particles will be a better grain refiner than one which contains

fewer but larger $TiAl_3$ particles. In fact, this is one of the difficulties associated with the use of master alloys whose effectiveness depends on the microstructure of the alloy and may vary from batch to batch and from supplier to supplier; thus Al-Ti master alloys do not refine foundry alloys as efficiently as wrought alloys. Sigworth and Guzowski[107] suggested that the effectiveness of the $TiAl_3$ nuclei may be poisoned by a silicon titanium compound.

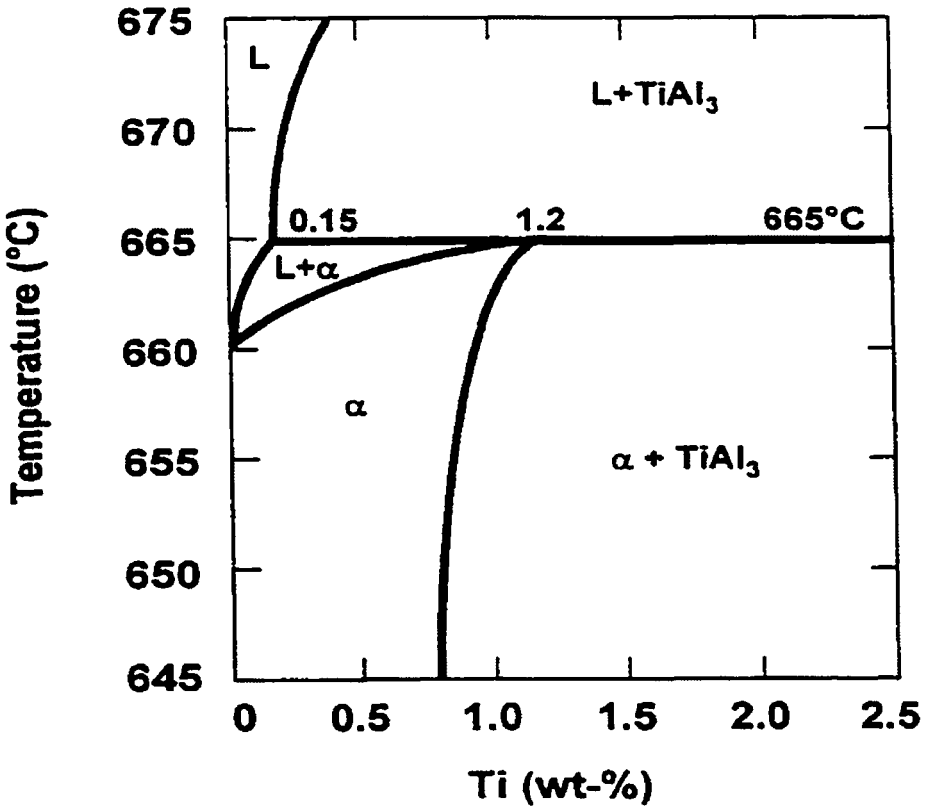

Figure 2.15 Al-Ti phase diagram.[110]

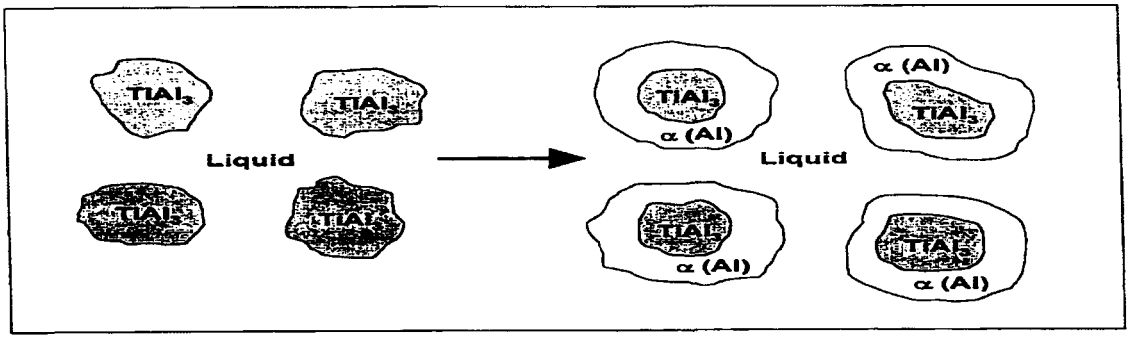

Figure 2.16 Nucleation of α-Al by the peritectic reaction in the Al-Ti system.[22]

2.6.2.2 Grain Refinement by Adding Boron

There are a number of grain refining manufacturers who have introduced a series of Ti-based grain refiners while neglecting Al-B alloys, although the effectiveness of Al-B master alloys as potential grain refiners was realized and reported as early as 1980.[111] Such results were reproduced by Sigworth and Guzowski[107] and Tondel *et al.*[112] The superior quality in this case may be ascribed to the dissolved Si in the foundry alloy to improve the refining efficiency of boron, since in the absence of Si, this element is unable to act as an efficient grain refiner. According to the Al-B binary phase diagram,[113] shown in Figure 2.17, a eutectic reaction exists at ~660°C and since the solubility of boron in the aluminum matrix is negligible (18 ppm), the eutectic reaction leads to the formation of primary α-Al on the AlB_2 particles. It has been proposed[114] that the effect of boron alone in the grain refinement of pure aluminum is virtually nil, but as regards the Al-Si alloys, it becomes most significant due to the eutectic reaction occurring at 0.02 wt% B, as represented by Equation 13 below. If a eutectic reaction does take place at this temperature, no nucleus for α-Al is formed above the freezing temperature of pure aluminum (660°C) since some undercooling will be necessary for the reaction shown in Eq. 14 to occur. For Al-Si alloys, the eutectic reaction takes place well above the liquidus temperature, which is 615°C for the 356 alloy, thus ensuring the presence of solid heterogeneous sites for nucleation.

$$\text{Liquid} \rightarrow \alpha(\text{Al}) + AlB_2 \qquad \text{Eq. (13)}$$

$$\text{Liquid} + Ti_xSi_yAl_{1-(x+y)} \rightarrow \alpha(\text{Al}) + AlB_2 \qquad \text{Eq. (14)}$$

Lu *et al.*[111] reported the effect of different master alloys on the grain size of small castings made from 356 and Al-5%Si alloys. Their results for 356 alloys, reproduced in

Figure 2.18, show the interesting fact that the Al-B master alloy is a more efficient grain refiner than both Al-Ti and Al-Ti-B alloys. As is evident, the addition of boron tripled grain refinement. The procedure of introducing boron into the alloy, however, is of significant importance from the point of view of the size and shape of the boron particles. A number of Al-B master alloys are composed of large particles and sometimes form large agglomerations of AlB_2 or AlB_{12} particles which cannot be dissolved rapidly in the melt because of the solubility limit. A further reason is the presence of impurities in the master alloy.

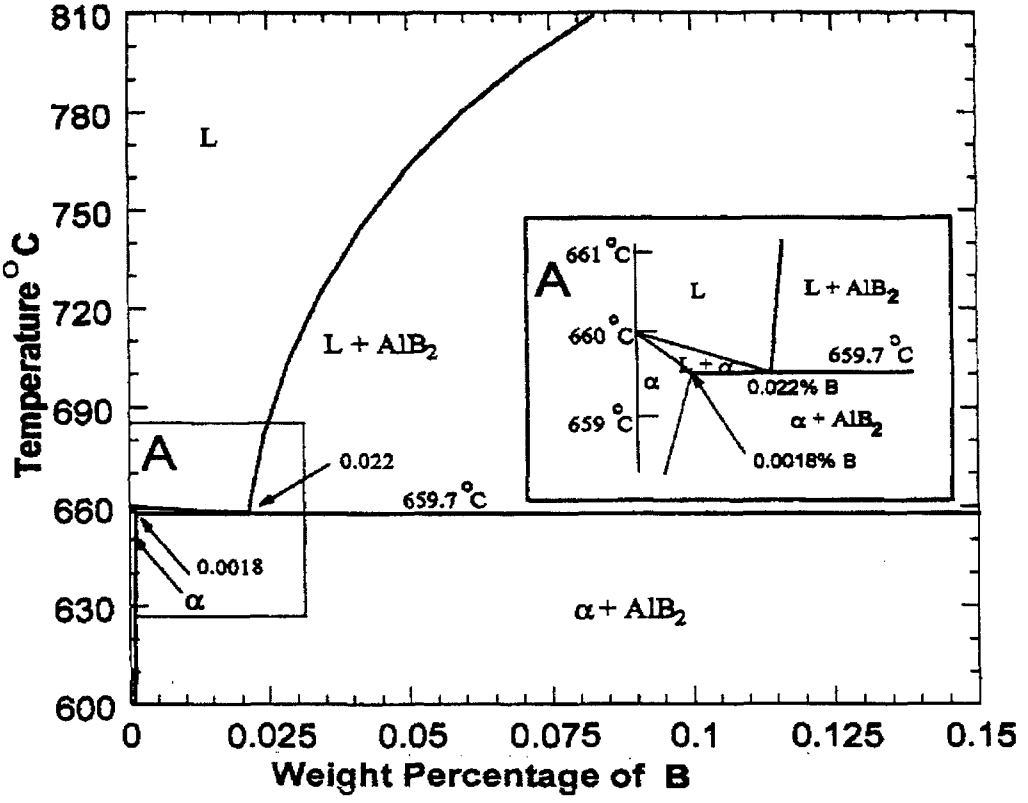

Figure 2.17 The Al-rich end of the Al-B phase diagram.[113]

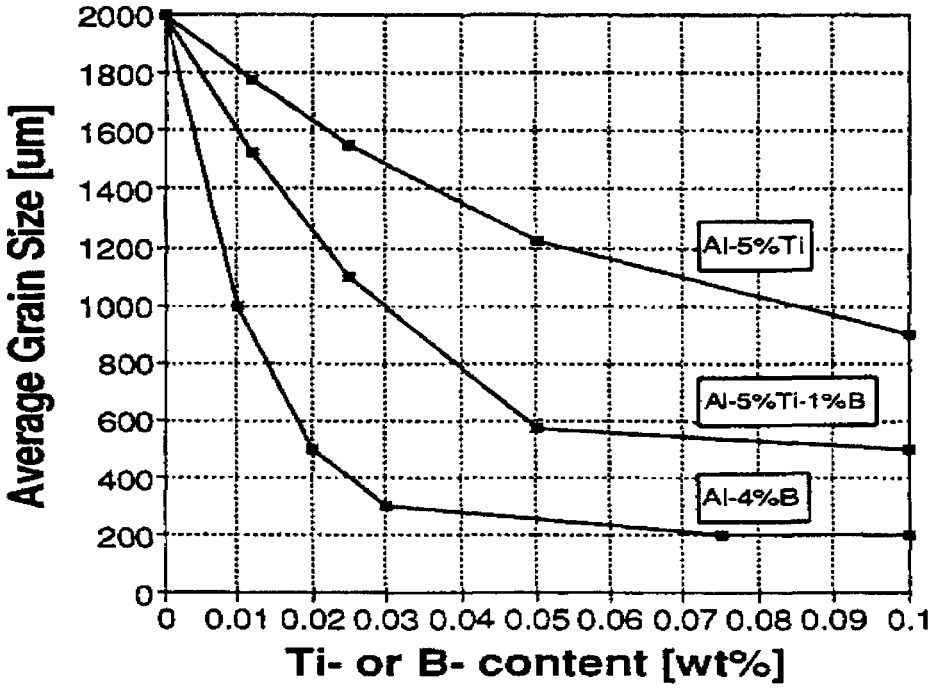

Figure 2.18 The grain refining of 356 Al-Si alloy with Al-Ti, Al-Ti-B, and Al-B.[111]

2.6.2.3 Grain Refinement by Adding of Titanium with Boron

The addition of boron to Al-Ti master alloys is widely known to produce a significant improvement in the effectiveness of grain refining in aluminum alloys. Mondolfo *et al.*[23,115] have suggested that Al-Ti-B master alloys perform better because the shift in the onset of the peritectic towards lower Ti in the Al-Ti phase diagram in the presence of boron (0.01%B), thereby ensuring the thermodynamic stability of $TiAl_3$ particles at low levels of titanium addition (0.05%Ti).

It has been observed[116] that Al-Ti-B master alloys contain a mixture of borides surrounding the aluminide phase, also sometimes found within the phase, which may improve protection against the dissolution of $TiAl_3$. The grain refining effect of these duplex particles seems to fade with time due to the complete dissolution of the aluminide

phase; [116,117] other authors,[118] however, claim that the loss of refining efficiency is a result of the settling of boride particles in the melt.

The importance of a combination of boron and titanium in grain refining was well established from the results obtained with the use of the LiMCA (Liquid Metal Cleanliness Analyzer) technique, as shown in Figure 2.19. It is evident from this figure that the highest and lowest particle counts apply to the addition of Al5Ti1B and Al6Ti master alloys, respectively. When Al6Ti is used as the additive, the inclusion content remains almost constant till the nominal Ti level reaches 0.12 wt%. An increase in Ti above this value changes the particle count drastically as a result of the thermodynamic stabilization of $TiAl_3$, which also causes a linear increase in the count with increasing Ti content.[110] It is important to note that by adding boron in the form of Al5Ti1B or Al5Ti0.6B, the critical titanium level shifts to a lower titanium level.

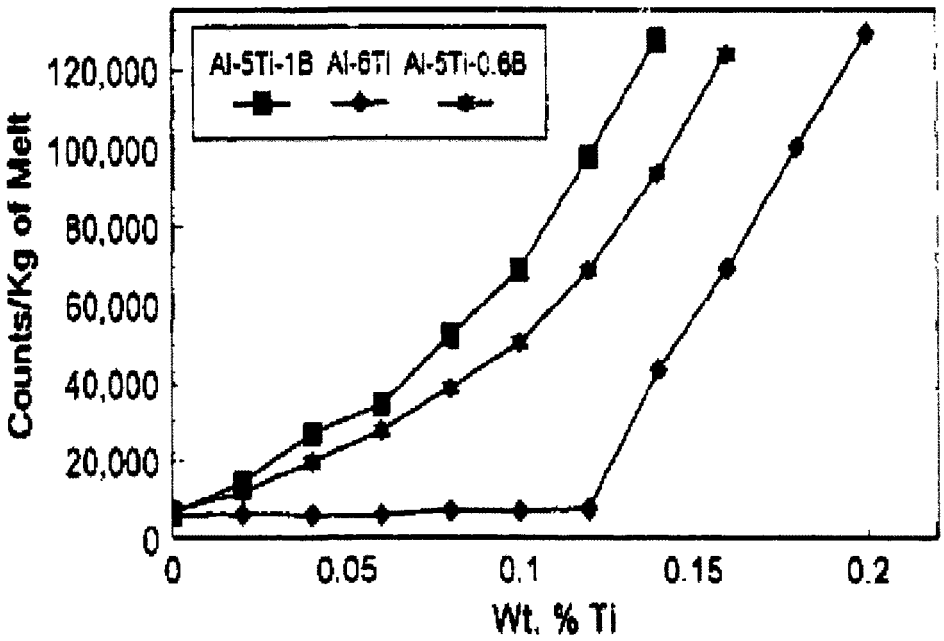

Figure 2.19 Particle counts *vs.* Ti content for different master alloys.[110]

2.6.2.4 Effect of Grain Refining on Properties

With the addition of grain refiners, which introduce large amounts of nucleants into the melt, a number of equiaxed grains are formed resulting in an improvement in the properties of cast solid solution type alloys.[119] Some of these enhanced properties include:

- Improved soundness. Fine grains promote the flow of molten metal which feeds shrinkage during the final stages of solidification, producing smaller and more uniformly dispersed shrinkage porosity.[120] A fine grain structure also promotes a finer distribution of gas porosity.[22,121]
- Better mechanical deformation characteristics. Fine equiaxed grains have a greater capacity for uniform deformation than columnar grains.[122]
- Improved mechanical properties, such as yield strength, toughness and fatigue life. Grain refinement also improves machinability, the deep drawability of products, and surface finishing.[123,124]

2.6.2.5 Effect of Grain Refinement on Melt Quality

Most experimental evidence indicates that grain refinement reduces porosity.[108,125] Grain refinement may therefore be considered to act in an opposite manner to modification. The presence of a grain refiner leads to a uniform redistribution of porosity.[22,126,127] In many cases, there is also an overall reduction in the amount of porosity upon grain refinement in alloys containing small or moderate amounts of gas.[126,127,128] Since the radius of the interdendritic liquid decreases with the addition of Ti as a grain refiner in Al-Si alloys, the average pore size is diminished. When the alloy is grain-refined, the dendritic network is broken down into small equiaxed grains. These fragmented dendrites are

transported within the casting and contribute significantly to the feeding during solidification. In order to enhance the strength and ductility of near eutectic Al-Si alloys, a combined melt treatment is necessary.

2.6.3 Mutual Poisoning Effect of Modification and Grain Refinement in Al-Si Casting Alloys

Researchers have frequently observed that certain alloying and impurity elements in Al alloys can adversely affect the grain refinement efficiency of Al-Ti-B master alloys, particularly the super-stoichiometric grain refiners, such as Al-5Ti-B, which contain both TiB_2 and $TiAl_3$. This deleterious effect is usually termed the poisoning effect. Silicon is a typical element which is capable of poisoning grain refinement through the addition of Al-5Ti-B master alloy.[2,107,111,114,129] During the grain refinement of Al-Si based casting alloys, it was observed that when the Si content exceeds ~2 wt%, a grain coarsening starts to occur and the extent of the poisoning effect worsens with increasing Si-content. In the high level Al-Si alloys, where the Si-content is greater than 7 wt%, the grain refining capacity of Al-5Ti-1B master alloy is less than that of Al-3B and Al-3Ti-3B master alloy.[2,107,111,114,129] Sigworth and Guzowski[107] proposed that a titanium silicide formed over the surface of the $TiAl_3$ particles in the melt and consequently poisoned their role as nuclei for the equiaxed dendrites; Kori *et al.*[123] pointed out that this poisoning effect could be neutralized by increasing the addition level of Al-5Ti-1B master alloy, although the presence of this compound has not been confirmed. Mohanty and Gruzleski[114] pointed out that Si might be dissolved in the $TiAl_3$, forming (Ti_{1-x},Si_x) and that high levels of Si (*i.e.* over 7%) resulted in a shift of the peritectic reaction temperature (liquid + $(Ti_{1-x}, Si_x)Al_3 \rightarrow \alpha$-Al) to a

temperature so low that the Al-5Ti-1B master alloy had no power to refine the dendritic α-Al.

Liao *et al.*[130] determined that the Al-5Ti-1B master alloy seemed to have only a slight influence on promoting the columnar-to-equiaxed transition in near-eutectic Al-Si alloy modified with Sr, and that a high addition level of the Al-5Ti-1B master alloy could result in reducing the modification effect of Sr on the Si particles considerably.

2.7 ALLOYING ELEMENTS

The alloying elements present in an alloy together with the cooling rate, determine which constituents will precipitate. These elements are added to increase the strength and companion properties of aluminum casting alloys.

2.7.1 Role of Copper and Magnesium in Al-Si Alloys

Based on the Al-Si system, the main alloying elements are Cu and Mg. Copper as an alloying element has been used since the beginning of the aluminum industry. In other words, the first and most widely used aluminum alloys for strength were aluminum-copper alloys, which contain 4 to 10% of Cu.[131,132] Copper has a capability of precipitation hardening, and its presence in aluminum alloys can thus improve strength and hardness in both the as-cast and heat-treated conditions.[23] The addition of copper also decreases the melting point and eutectic temperature of the alloy significantly, thereby increasing the solidification range of the alloy,[132] and facilitating the condition of porosity formation.

The increase in strength obtained with Mg-content becomes further evident after heat treatment, and this improvement is accompanied by a corresponding reduction in ductility. Dunn and Dickert[35] compared the effect of up to 0.55% Mg additions on the mechanical properties and hardness of A380 and 383 alloys. The presence of Mg was seen to increase the tensile strength, yield strength, and hardness at all temperatures. Elongation was observed to be reduced by the presence of Mg, although the minimum value appeared to be acceptable provided that Mg-content did not exceed 0.35%. Magnesium has a negative effect on Sr-modification, that is, it changes the microstructure from a well-modified to a partially modified. This effect is, most likely, due to the formation of a complex $Mg_2SrAl_4Si_3$ intermetallic compound, which is probably formed prior to the eutectic reaction.[34]

Al-Si-Cu-Mg cast alloys are usually heat-treated in order to obtain an optimum combination of strength and ductility. A comparative study of the mechanical properties of Al-Si-Cu-Mg alloys was carried out by Cáceres *et al.*[133] to investigate the effects of Si, Cu, Mg, Fe, and Mn, as well as solidification rate. The authors observed that increasing the Cu and Mg content generally resulted in an increase in strength and a decrease in ductility, whereas an increased Fe content (at an Fe/Mn ratio of 0.5) dramatically lowered the ductility and strength of low-Si alloys. They also reported that the Cu + Mg content of the alloys determines the precipitation strengthening and the volume fraction of the Cu-rich and Mg-rich intermetallics obtained.

2.7.2 Role of Iron and Manganese in Al-Si Alloys

Any element which is not classified as an alloying component is termed an impurity, and as such it is deemed to have a negative effect on the castability, mechanical properties and heat treatment of aluminum alloys. Among such elements, iron is a common impurity in aluminum alloys arising from a number of possible sources; it is usually considered detrimental in one or more ways, at least for Al-Si based casting alloys. Iron can enter the melt during further downstream melt activity through two basic mechanisms.

1- Liquid aluminum is capable of dissolving iron from unprotected steel tools and furnace equipment. Thus with long exposure times, Fe levels can reach 2 wt% at a normal melt temperature of ~700°C (an Al-Fe eutectic exists at 1.7 wt% Fe, 655°C, as shown in Figure 2.20). For a melt held at 800°C, the Fe level may reach up to 5%.

2- Iron may also enter an aluminum melt via the addition of low-purity alloying materials, such as Si, or via the addition of scrap that contains higher background iron than the primary metal.

Manganese is the most common alloying element used as an addition to neutralize the effect of iron and to modify the morphology and type of the intermetallic phases.[134] Manganese is added to many of the alloys for two main purposes: (i) to increase high-temperature strength and creep resistance through the formation of the high melting point compounds: $Cu_2Mn_3Al_{20}$, $MnCrAl_{12}$, and also $Al_{15}(FeMn)_3Si_2$; more complex compounds containing chromium and nickel may also involved; (ii) to correct the embrittling effect of Fe.

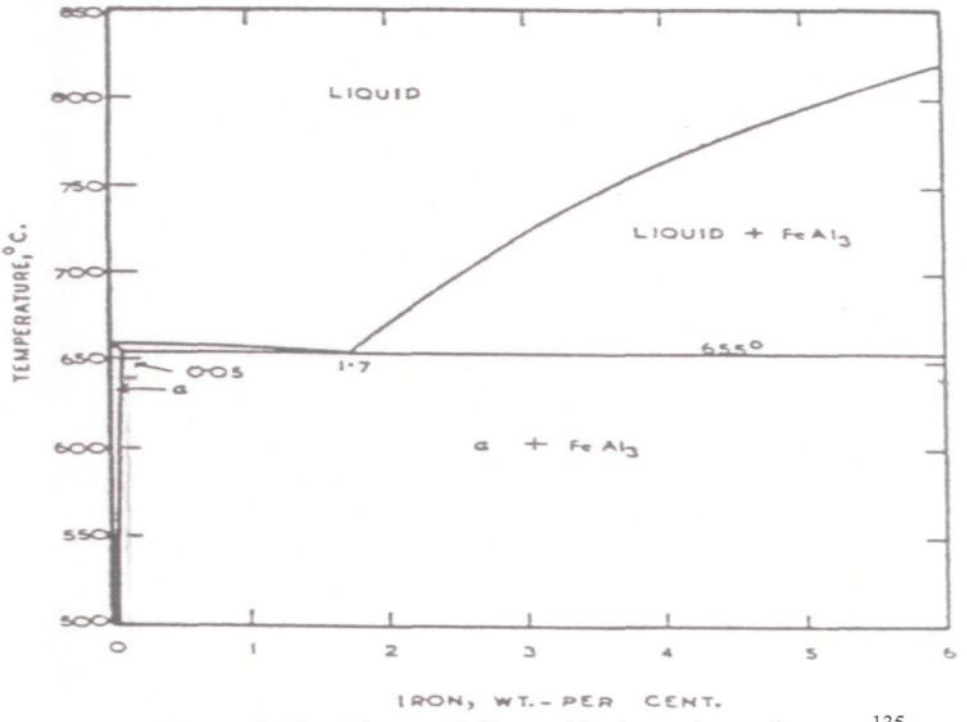

Figure 2.20 Binary Al-Fe equilibrium phase diagram.[135]

2.7.2.1 Formation of Iron-Intermetallics during Solidification

Although iron is highly soluble in liquid aluminum and its alloys, it has very little solubility in solid, and it thus tends to combine with other elements to form intermetallic phase particles of various types. When iron combines with Al and Si, it forms different intermetallics, of which the brittle, plate-like or needle-like β-Fe phase is deleterious to mechanical properties, see Figure 2.21(a). The composition of the β-Fe phase is Al_5FeSi (25.6% Fe, 12.8% Si), in a range of 25~30% Fe and 12~15% Si. This phase has a monoclinic structure with the parameters a = b = 6.12 Å; c = 41.5 Å; and $\alpha = 91°$; with a density of 3.30~3.35 g/cm^3, it appears in the form of thin platelets in the microstructure.

There are two types of β-Al_5FeSi platelets: pre-eutectic particles, characterized by their large size, and co-eutectic or post-eutectic particles, which are relatively thin. The difference in their sizes is directly related to the rates of diffusion of the iron atoms with respect to the temperatures at which the two particle types precipitate.

It has been proposed that increased solidification rates, strontium additions and/or the presence of transition elements such as Mn will promote the development of a more compact, less harmful α-Fe phase.[12,13,136,137,138] The composition of the α-Fe phase is Al_8Fe_2Si (31.6% Fe, 7.8% Si), often reported as $Al_{15}Fe_3Si_2$ (30.7% Fe, 10.2% Si), with a probable composition range of 30~33% Fe and 6~12% Si. The phase is reported to have a hexagonal structure with the parameters a = 12.3 Å; c = 26.3 Å; and a density of 3.58 g/cm^3; it appears in the form Chinese script particles as shown in Figure 2.21(b).[139] The α-phase exerts a less deleterious effect on the physical properties of the cast part due to its more compact shape and a more diffuse interface with the aluminum matrix, resulting in better cohesion.[140]

The α-AlFeSi phase shows an irregular, curved crystal growth which conforms to the complicated shape of the interdendritic spaces during solidification. It has a non-faceted interface with the aluminum matrix, and exhibits no growth twinning, which allows for a better bonding with the aluminium matrix. This type of growth occurs at high driving forces of solidification or rapid cooling, *i.e.* at a high degree of undercooling, ΔT. The β-AlFeSi phase, on the other hand, grows in a lateral or faceted mode which is poorly bonded to the aluminum matrix and contains multiple (001) growth twins parallel to the growth

direction. This type of growth occurs at low driving forces or at slow cooling, *i.e.* at a low degree of undercooling, ΔT.

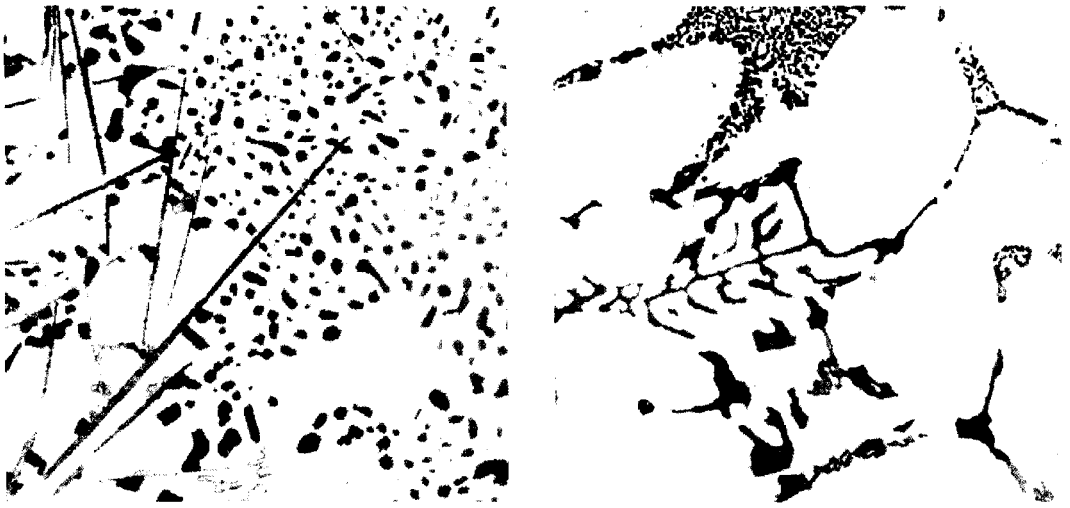

(a) (b)

Figure 2.21 Photomicrographs of common iron-containing intermetallics showing typical morphologies in Al-5%Si-1%Cu-0.5%Mg-(Fe) alloys: (a) β-Fe, (b) Chinese script-like α-Fe.[139]

2.7.2.2 Effect of β(AlFeSi) on the Properties of Al-Si Alloys

The detrimental effect of iron begins at a somewhat low primary Fe-level but becomes far more serious once a critical Fe-level (dependant on the alloy composition) is exceeded. The critical iron level is directly related to the silicon concentration of the alloy. Figure 2.22 shows a section of the Al-Si-Fe ternary phase diagram which draws attention to the reason for the existence of critical iron content. As the silicon content of the alloy increases, there is an increase in the amount of iron which can be tolerated before the β-phase starts to form prior to the Al-Si eutectic. At 5% silicon, the critical iron content is ~0.35%, at 7%Si it rises to ~0.5, at 9% it is ~0.6%, and by 11% it reaches ~ 0.75%. Also, the temperature (and therefore time) at which β-Fe can form prior to the Al-Si eutectic

decreases with increasing Si content for a given Fe content. The line AB between the β-phase field and the Al phase field is the period during which the larger and more detrimental intermetallic particles form.

The morphology of the β-phase allows it to act as a stress raiser, which may serve to explain the mechanical properties of the cast part. The threshold amount of iron, leading to the formation of primary Al_5FeSi capable of undermining the properties is > 0.7 wt%. When the phase forms in the eutectic structure (Fe < 0.7 wt%) it is believed to even enhance the tensile properties slightly.[43] It should be noted, however, that the percentage of iron quoted to form primary or secondary Al_5FeSi depends on the cooling rate and silicon content. The effect of increasing Fe is a gradual reduction in the elongation, impact strength, and tensile strength of aluminum-silicon alloys,[43,141] while Brinell hardness and yield strength are reported to increase gradually.[43]

Couture [142] reported that the addition of iron to Al-Si alloys is detrimental to the mechanical properties. Increasing the iron content from 0.5 to 1.2% in an Al-Si casting alloy dramatically reduces the mechanical properties, particularly the ductility, due to the formation of β-Fe platelets. Vorobev *et al.*[143] claimed that even a small addition of Fe to Al-Si alloys seriously diminishes tensile strength and elongation, because of the formation of the brittle β-Al_5FeSi at cooling rates normally employed in sand and permanent mold castings.[144] The volume percent and size of the β-phase formed depends to a high degree on the iron content, solidification rate and superheat temperature.[145]

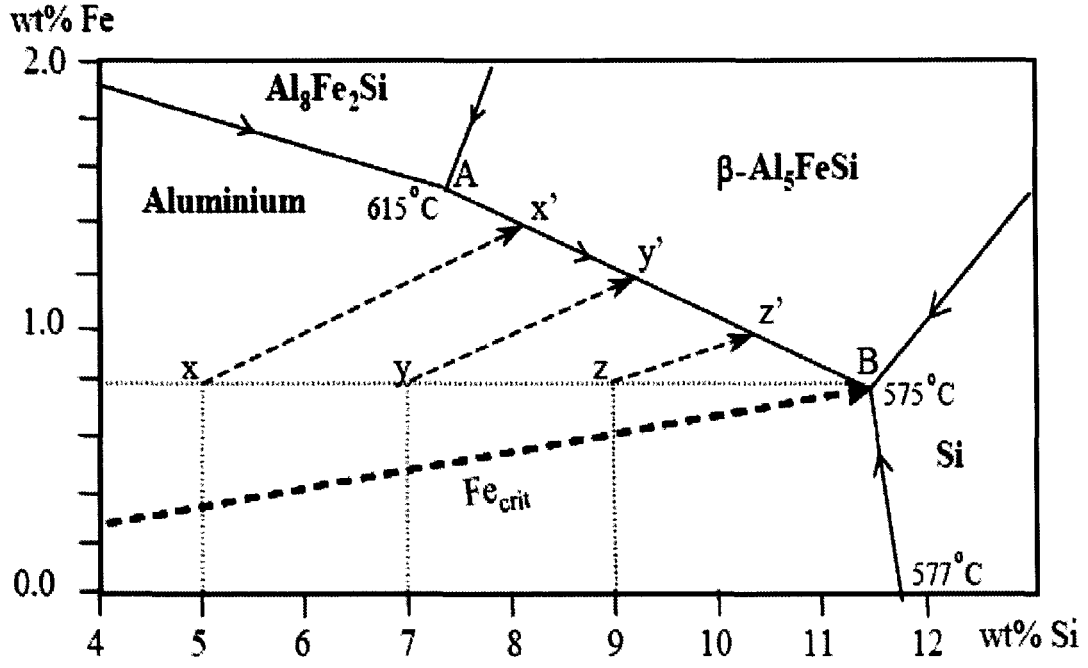

Figure 2.22 Ternary Al-Si-Fe phase diagram showing primary Al-solidification for alloys with Fe_{crit} iron levels.[137,142]

According to Bonsack[146] any amount of Fe over 0.5% will be present as Al-Fe-Si in large needles which, up to about 0.8% Fe, increases strength and hardness but reduces ductility slightly. Above 0.8% Fe, both strength and elongation deteriorate rapidly, and there is a deleterious effect on the machinability. Hajas[147] reported that the formation of Al_5FeSi causes stress cracking and void formation in Al-10%Si-Mg alloy castings. Iron contents of up to 0.2% improve the tensile strength, while higher levels reduce the tensile strength and elongation, and increase hardness. Komiyama *et al.*[148] observed that in Al-9.2%Si-4%Cu-0.5%Mg alloy, hardness increases, whereas tensile strength and elongation decrease with an increase in the iron content; the tensile strength decreases markedly when the iron content exceeds 0.5%. The Al_5FeSi phase has also been reported to impede fluidity and feeding, and to promote shrinkage porosity.[43,149] The resulting porosity in itself may

also contribute to the deterioration of mechanical properties. Fatigue strength may be affected by the formation of Al_5FeSi because the cohesion between the aluminum matrix and the intermetallic in question is poor.[140] One study for an Al-Si piston alloy found that room temperature tensile strength was reduced by the presence of the Al_5FeSi phase, although at elevated temperatures it was observed that the presence of these phases increased the tensile strength.

2.7.2.3 Effect of α-Fe on the Properties of Al-Si Alloys

Manganese has very little solubility in aluminum, and as a consequence the Mn in the remaining liquid will combine with Fe, Si, and Al to produce a different Fe-bearing intermetallic having the stoichiometry $Al_{15}(Mn,Fe)_3Si_2$.[149] The general morphology is the one known as Chinese script, although the phase has also been shown to have other morphologies such as blocky and dendritic.[150] The commonly accepted ratio of Mn to Fe required to form the α-phase rather than the β-phase is 1 to 2.[149,151,152] Overall, the α-phase, as it is usually called, is much more compact and less detrimental to the mechanical properties; it also improves feeding into interdendritic channels slightly. The reason for this formation, in the presence of Mn, may be illustrated by the phase diagram shown in Figure 2.23.[78]

Yaneva *et al.*[153] studied the appearance of iron intermetallic phases in Al-Si cast alloys at different Fe and Mn concentrations; they showed that the percentage of the β-phase rapidly increases with the iron concentration for a given concentration of Mn, as shown in Figure 2.24.

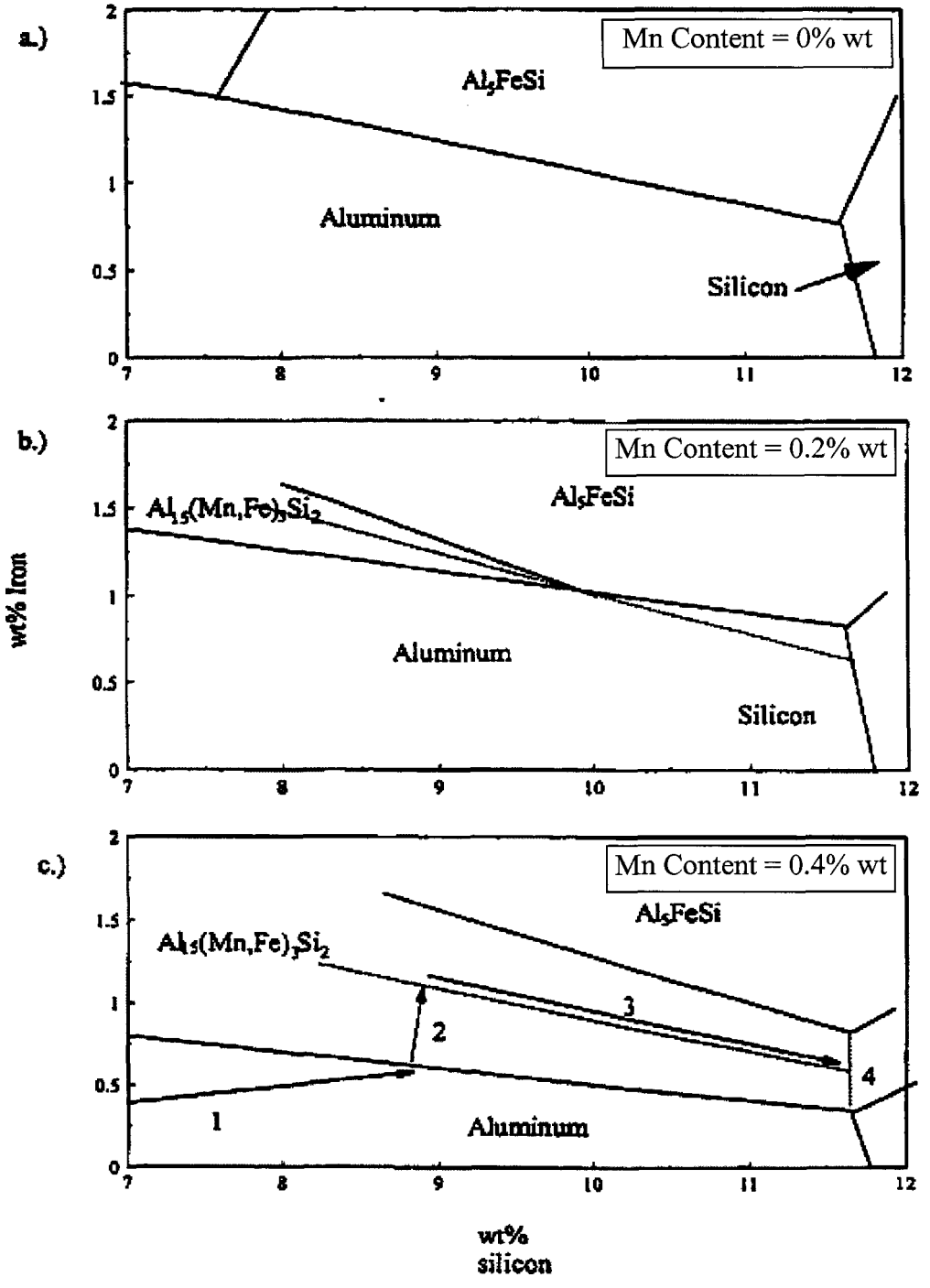

Figure 2.23 Simplified phase diagram of the Al-Fe-Si-Mn system at a constant Mn level.[78]

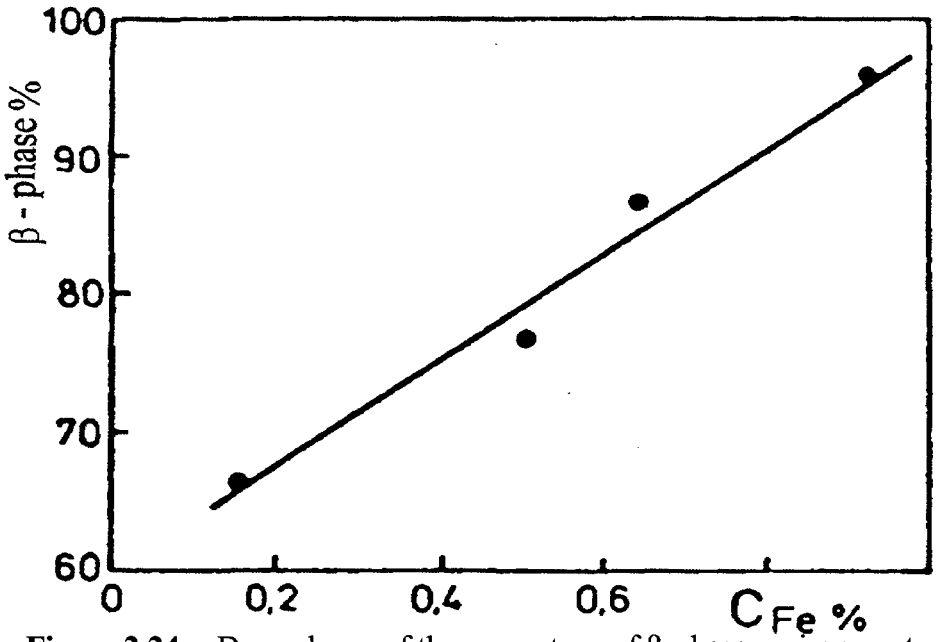

Figure 2.24 Dependence of the percentage of β-phase *vs.* iron content.[153]

According to ANSI/ASTM specifications, if the Fe-content exceeds 0.45%, the Mn content should be no less than half that of the Fe.[154] Colwell and Kissling[155] pointed out that when the Mn content is half that of iron, it breaks down the long needles of the β-Al_5FeSi phase thereby improving both the mechanical properties and castability of the alloy. Komiyama *et al.*[148] showed that Mn has a strong effect on the alloy tensile strength only at iron contents which are higher than 1%.When the Mn:Fe ratio exceeds a certain limit, however, then the addition of Mn is observed to have a harmful effect. According to Mondolfo,[144] $(Fe,Mn)Al_6$ is the first phase in the Al-Fe-Mn-Si system to form over a good part of the system where many of the commercial alloys are located. In many alloys, $(Fe,Mn)Al_6$ then reacts peritectically with the liquid to form $Al_{15}(Fe,Mn)_3Si_2$.[23] On the other hand, the quaternary phase Al(Fe,Mn)Si is very often the structural constituent in a wide group of commercial alloys. The α-iron phase may precipitate in the form of the Chinese

script-like $Al_{15}(Fe,Mn)_3Si_2$ phase, or else as compact polyhedral or star-like particles termed sludge with a composition close to the former, namely, Al_{12} to $Al_{15}(Fe,Mn)_3Si_2$,[136] depending upon the levels of Fe, Mn and Cr present in the alloy, and the processing parameters involved which include melt holding and pouring temperatures; melt additives such as Sr and Al-5Ti-1B grain refiner; and cooling conditions. The sludge compounds have high melting points and high specific gravity which causes them to settle to the floor of the melt. If they are stirred into the melt and incorporated into a casting, they act as hard spots and have a detrimental influence on the mechanical and physical properties of the cast parts.

An empirical formula called the "sludge factor" has been suggested by Gobrecht.[156] The sludge factor for Al-Si-Cu is used to determine how much Fe, Mn, and Cr can cause sludge to form; it also serves as a rough guide to avoid sludging. This factor is calculated as

$$\text{Sludge Factor} = (1* \text{ wt\% Fe}) + (2* \text{ wt\% Mn}) + (3* \text{ wt\% Cr}) \qquad \text{Eq. (15)}$$

The above formula is useful for predicting susceptibility to sludge formation, although metal temperature and the agitation of the molten metal, to some extent, also influences susceptibility to sludge formation. At higher holding temperatures, or with an agitated bath (as in induction furnaces), a sludge factor of 1.8 will normally result in sludge formation if a casting temperature of 650°C or more is maintained, despite this, for lower holding temperatures, a sludge factor of 1.4 or less may have to be applied. For alloys 319 and 413 the critical sludge factor is estimated to be 2.1.[157]

Dunn[158] reported on the chemical composition of sludge in A380 alloy. The material removed from the bottom of the melt produced an analysis which included 6.5% Fe, 3.03%

Mn and 1.44% Cr. The actual crystals of the sludge compound were analyzed using electron microprobe analysis, and had a composition which included, besides Al, 20% Fe, 10% Si, 6% Mn, 1% Cr and 1% Cu. Another analysis was made of the large crystals of sludge which had accumulated over a long period in a reverberatory furnace used for melting alloy A380. This sludge had a melting point of over 800°C and contained 9.4% Si, 11.4% Fe, 6.07% Mn, 2.16% Cu, 1.77% Cr and 0.4% Zn. The results recorded by Dunn for alloy A380 confirm that the factors 1, 2, and 3 for Fe, Mn, and Cr, respectively, in the sludge formula are reasonably correct and can be used as a melting control. The effects of Mn and Fe content on the formation of sludge is illustrated in Figure 2.25. Sludge tended to form at a high Fe-content, *e.g.* 1.2% Fe, or at high concentrations of Mn and Cr with a low Fe-content, *e.g.* 0.4% Fe. More than 0.2% Mn and 0.1% Cr were needed, however, to convert all Fe platelets to the star-like form.[159,160]

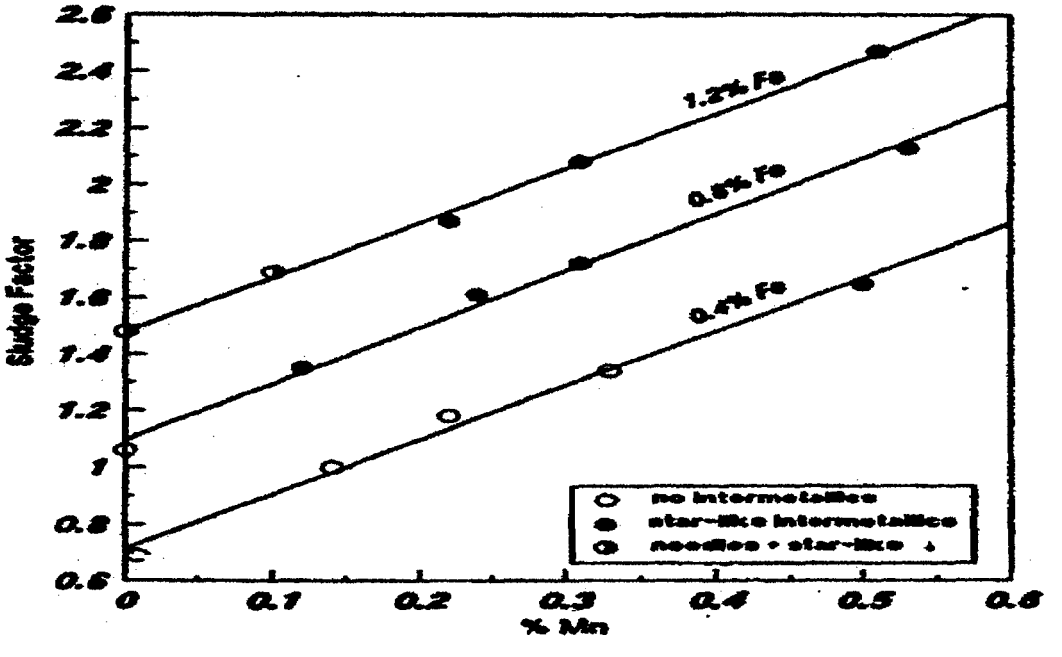

Figure 2.25 Effect of Mn and Fe on the sludge factor in the Al-12.7%Si-0.1%Cr alloy.[160]

More recently it was discovered that strontium has been linked to the formation of another α-phase having the stoichiometry Al_8Fe_2Si.[23,161] Phosphorus is an effective element in refining primary silicon grains of eutectic and hypereutectic Al-Si alloys. Apparently Sr reacts with P, preventing heterogeneous nucleation of Al_5FeSi on AlP.[152] As a result, Al_8Fe_2Si is formed during eutectic growth when the Si in the remaining liquid is nearly depleted. The method generally accepted to improve the properties of aluminum alloys containing Fe is through the addition of a master alloy containing Mn (*e.g.*, Al-25%Mn or Al-10%Mn-2%Ti), which would allow the Fe to crystallize in the more compact α-Fe form rather than the harmful β-Fe platelet-like form.[139] Other foundry researchers have found that master alloys containing Cr, Co, Be or Mo may have the same effect of converting the β-phase to α-phase.[149,151]

2.8 HEAT TREATMENT

Heat treatment is one of the major factors used to enhance the mechanical properties of heat-treatable Al-Si alloys, by means of an optimization of the solution and aging heat treatments applied to these alloys. The heat treatment is usually comprised of the following three stages: solutionizing, quenching, and aging. Table 2.6 details a few of the more commonly applied heat treatments.

2.8.1 Solution Heat Treatment

The solution treatment fulfils three roles[162,163]

- Homogenization of as-cast structure.

- Dissolution of certain intermetallic phases such as Al_2Cu and Mg_2Si
- Change of the morphology of eutectic silicon.

Table 2.6 Common aluminum heat treatment designations

Treatment	Solution	Quench	Aging
T4	Yes	Yes	Room Temperature only
T5	No	No	Elevated Temperatures
T6	Yes	Yes	Elevated (to yield increased strength)
T7	Yes	Yes	Elevated (to yield dimensional stability)

The segregation of solute elements resulting from dendritic solidification may have an adverse effect on mechanical properties. The time required for homogenization is determined by the solution temperature and by the dendrite arm spacing. Hardening alloying elements such as Cu and Mg display significant solid solubility in heat-treatable aluminum alloys at the solidus temperature; this solubility decreases noticeably as the temperature decreases.

The changes in the size and morphology of the silicon phase have a significant influence on the mechanical properties of the alloy. It has been proposed that the granulation or spheroidization process of silicon particles through heat treatment takes place in two stages: (i) fragmentation or dissolution of the eutectic silicon branches and (ii) spheroidization of the separated branches.[164] During solution treatment, the particles undergo changes in size and in shape. In the initial stages, the unmodified silicon particles undergo necking and separate into segments, which retain their original morphology. As a result of the separation, the average particle size decreases and the fragmented segments are

eventually spheroidized. The spheroidization and the coarsening of eutectic Si can occur concurrently during the second stage.

Modification facilitates fragmentation since it promotes eutectic silicon branching. The rate of spheroidization of the eutectic silicon phase is obviously faster in modified alloys than in unmodified alloys, due to the increased driving force provided by the finer as-cast structure of the modified eutectic silicon in the former. Tiryakioglu[165] studied the effects of solution treatment temperature time on the microstructure of a cast Al-7%Si-0.6%Mg alloy. The results showed that, with increasing solution treatment time, Si particles become gradually rounded and coarsened, see Figure 2.26.[137]

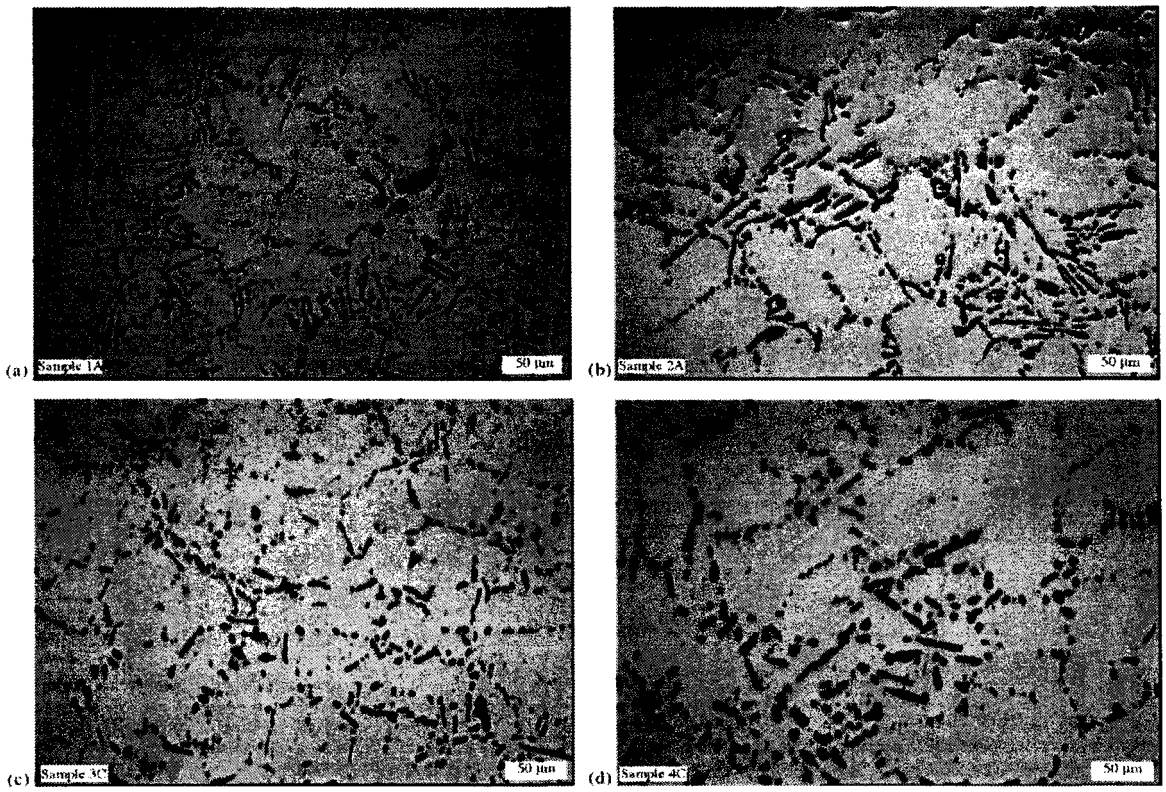

Figure 2.26 The effect of solution treatment time at 540°C on the microstructure of Al-7%Si-0.6%Mg alloy.[165] Castings were solution treated for: (a) 1 h; (b) 4 h; (c) 16 h; and (d) 64 h.

Based on conventional solution treatment rules, the solution temperature of Al-Si-Cu-Mg alloys is restricted to 495°C,[166,167] in order to avoid incipient melting of the copper-rich phase. The time at the nominal solution treatment temperature must be long enough to homogenize the alloy and to ensure a satisfactory degree of precipitate solution. In alloys containing high levels of copper, complete dissolution of the Al_2Cu phase is not usually possible. The solution time must then be chosen carefully to allow for the maximum dissolution of this intermetallic phase, bearing in mind nevertheless, that solutions treating the alloy for long times are expensive and may not be necessary to obtain the required alloy strength. Moreover, the coarsening of the microstructural constituents and the possible formation of secondary porosity which result after prolonged annealing at such temperatures can have a deleterious effect on the mechanical properties.[168]

Studies by Gauthier *et al.*[68,163] on the solution heat treatment of 319 alloy over a temperature range of 480°C to 540°C, for solution times of up to 24 hours, showed that the best combination of tensile strength and ductility was obtained when the as-cast material was solution heat-treated at 515°C for 8 to 16 hours, followed by quenching in warm water at 60°C. A higher solution temperature was seen to result in the partial melting of the copper phase, the formation of a structureless form of the phase and related porosity upon quenching, with a consequent deterioration of the tensile properties. A two-stage solution heat treatment suggested by Sokolowski *et al.*[169] is reported to reduce the amount of the copper-rich phase in the 319 alloys significantly, giving rise to better homogenization prior to aging and improving mechanical properties. Also, Crowell *et al.*[170] stated that the blocky

Cu phase in Al-Si-Cu alloys dissolves with increasing solution time at the recommended solution temperature of 495°C; also the rate of dissolution increases with Sr concentration.

Figure 2.27 shows that the solubility of Mg and Si in the Al-rich α-phase decreases with temperature. Therefore, in order to dissolve maximum Mg and Si into solid solution, the temperature of the solution heat treatment must approach eutectic temperature. At the same time, this temperature should never exceed the melting-point in order to avoid any local melting at the grain boundaries which can irreversibly reduce the mechanical properties. In most cases, with regard to A356 alloys, the temperature of solution heat treatment is controlled at 540 ± 5°C, to obtain a solubility of about 0.6% Mg in solid solution, followed by quenching and natural or artificial aging which allows for the formation of interdendritic non-equilibrium precipitates of Mg_2Si and also for changes in the characteristics of Si-particles.[142,143]

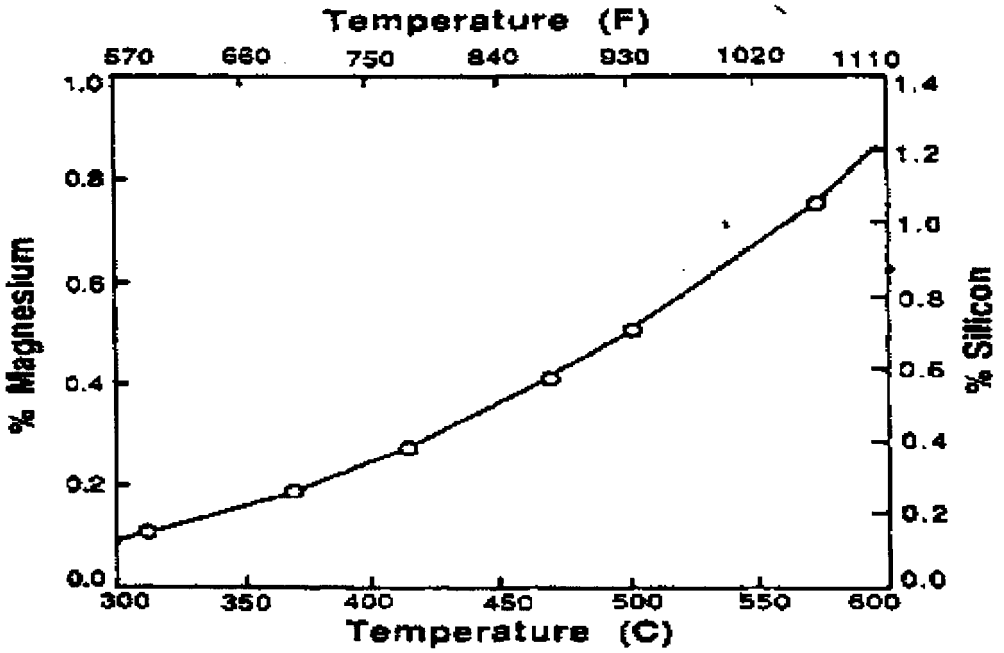

Figure 2.27 Equilibrium solubility of Mg and Si in solid aluminum when both Mg_2Si and Si are present.[142]

Yoshida and Arrowood[171] investigated the effects of variations from T6 Standard treatment on the hardness, ductility, and UTS of aluminum alloy A356 cast in a permanent mold with and without strontium modification. The main variables considered in the experiments were solutionizing time and temperature. The as-cast samples were solutionized for various periods of time (t = 2, 4, 8, 16, and 32 hours) at 520°C/540°C and aged at 160°C for 6.5 hours. The highest hardness was obtained at the shortest solutionizing time of 2 hours for both the unmodified and modified A356 alloy, while the highest ductility was not reached until the samples were solutionized for 8 hours at the same temperature, as shown in Figure 2.28. A slight change in solutionizing temperature did not cause much variation in hardness, ductility, or UTS. It may also be seen from Figure 2.28 that the strontium-modified samples exhibit higher elongation than the unmodified ones under all the heat treatment conditions reported in this study.[171]

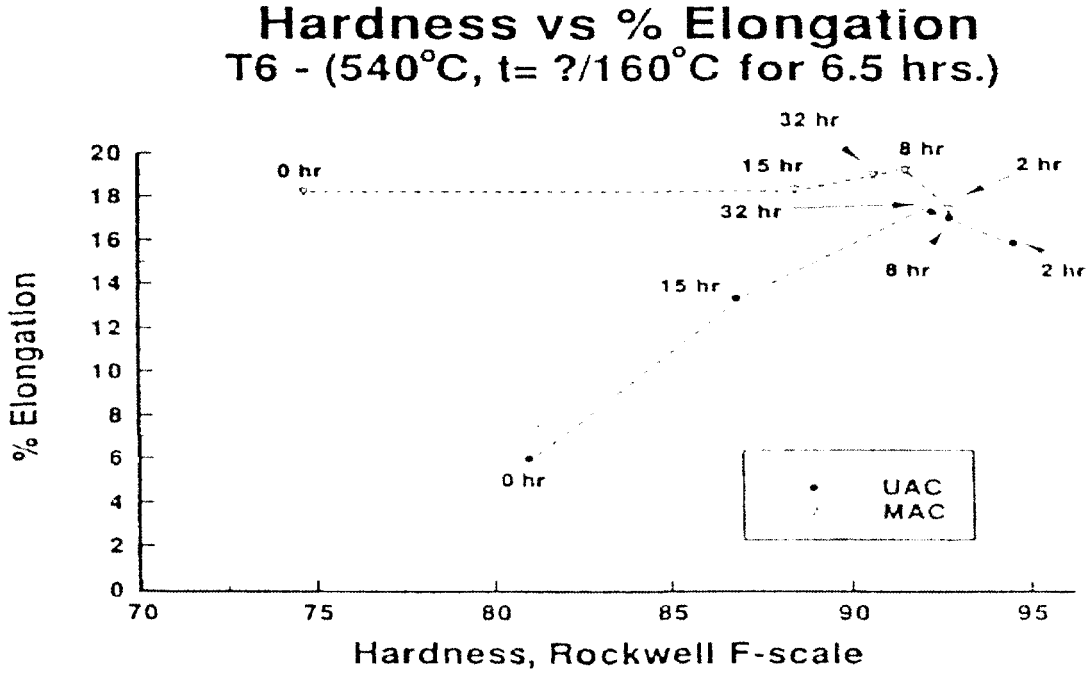

Figure 2.28 Hardness *vs.* elongation with respect to variations in solutionizing time.[171]

2.8.2 Quenching

Following solution heat treatment, quenching is the next important step in the heat-treatment cycle. The objectives of quenching are to suppress precipitation during quenching; to retain the maximum amount of the precipitation hardening elements in solution to form a supersaturated solid solution at low temperatures; and to trap as many vacancies as possible within the atomic lattice.[172,173] The best combination of strength and ductility is achieved from a rapid quenching. Cooling rates should be selected to obtain the desired microstructure and to reduce the duration time over certain critical temperature ranges during quenching in the regions where diffusion of smaller atoms can lead to the precipitation of potential defects.[174] The effectiveness of the quench is dependent upon the quench media (which controls the quench rate) and the quench interval. The media used for quenching aluminum alloys include water, brine solution and polymer solution.[175,176,177] Water used to be the dominant quenchant for aluminum alloys, but water quenching most often causes distortion, cracking, and residual stress problems.[175,176,178,179] It has been reported that the water temperature affects the properties of the cast aluminum alloy A356 subjected to T6 heat treatment once the water exceeds 60-70°C, with UTS and YS being significantly more sensitive than ductility.[174]

2.8.3 Aging

Age-hardening has been recognized as one of the most important methods for strengthening aluminum alloys, which involves strengthening the alloys by coherent precipitates which are capable of being sheared by dislocations.[180] By controlling the aging

time and temperature, a wide variety of mechanical properties may be obtained; tensile strengths can be increased, residual stresses can be reduced, and the microstructure can be stabilized. The precipitation process can occur at room temperature or may be accelerated by artificial aging at temperatures ranging from 90 to 260°C.

It was indicated that aging must be accomplished below a metastable miscibility gap called the Guinier-Preston (GP) zone solvus line.[181] Age-hardening can take place either at room temperature (natural, T4 temper) or at elevated temperatures (artificial, T6 temper).

The phenomenon of precipitation was originally discovered by Ardel in 1906.[182] He found that the hardness of aluminum alloys which contained magnesium, copper, and other trace elements increased with time at room temperature, which was later explained by precipitation hardening. Over the years, much research was carried out to understand the aging kinetics of T4 and T6 heat treatments and to study the effects of underaging, peak-aging, and overaging on hardness,[183,184,185] ultimate tensile strength,[185] crack propagation behavior,[186] and the cyclic stress-strain response of cast aluminum-silicon alloys.[187]

The precipitation sequence for an Al-Si-Cu alloy, such as 319, is based upon the formation of Al_2Cu-based precipitates. The Al_2Cu precipitation sequence is generally described as follows: [20,188,189,190]

$$\alpha_{ss} \rightarrow \text{GP Zones} \rightarrow \theta'' \rightarrow \theta' \rightarrow \theta\ (Al_2Cu)$$

The sequence begins with the decomposition of the solid solution and the clustering of Cu atoms; the clustering then leads to the formation of coherent, disk-shaped GP zones. At room temperature aging conditions, GP zones arise homogeneously; these zones manifest as two-dimensional, copper-rich disks with diameters of approximately 3-5 nm.[20]

As time increases, these GP zones increase in number while remaining approximately constant in size.

With regard to the Al-Cu alloys, as the aging temperature is increased above 100°C, the GP zones dissolve and are replaced by the θ'' precipitate. This precipitate is a three-dimensional disk-shaped plate having an ordered tetragonal arrangement of Al and Cu atoms; θ'' also appears to nucleate uniformly in the matrix, and is coherent with the matrix in binary Al-Cu alloys. The high degree of coherency causes extensive coherency-strain fields to arise, [188] giving peak strength to the material at this time.

As aging proceeds, the θ'' starts to dissolve, and θ' begins to form by nucleating on dislocations and/or cell walls;[188,189] θ' also has a plate-like shape and is composed of Al and Cu atoms in an ordered tetragonal structure; θ' loses coherency with the matrix, however, as it grows. Thus, since the long-range coherency-strain fields do not arise, a decrease in strength properties may be observed, while continued aging causes the equilibrium θ (Al_2Cu) precipitate to occur. Tetragonal in shape, the θ phase is completely incoherent with the matrix; this fact, combined with its relatively large size and coarse distribution, reduces the strength properties significantly.[20]

The effects of varying Mg-content on the mechanical properties of a 380 aluminum die-casting alloy as a function of aging time at 180°C was studied by Samuel *et al.*[191] They concluded that the tensile and yield strengths increased substantially with increasing Mg content when the alloys were subjected to artificial aging. The hardness (measured by Brinell) increased from 76 BHN to 96 BHN when 0.57 wt% Mg was added to the 380 alloy. Aging for 8 h at 180°C increased this value to 112 BHN. Increases in Cu were found

mainly to reduce ductility and change the morphology of the Cu-containing phases.[11] The strength of an age-hardenable alloy is governed by the interaction of moving dislocations and precipitates. The obstacles in precipitation-hardened alloys which hinder the motion of dislocations may be either the strain field around the GP zones resulting from their coherency with the matrix, or the zones and precipitates themselves, or both. The dislocations are then forced to cut through them or go around them forming loops. The preceding thus implies clearly that there are three sources for age hardening: strain field hardening, chemical hardening and dispersion hardening.

Gloria *et al.*[192] investigated the dimensional changes occurring during the heat treatment of an automotive 319 alloy by means of T6 and T7 tempers involving solution treatment, quenching and artificial aging. They observed that increasing the solution temperature has the greatest influence in the dimensional change of samples due to dissolution of the Al_2Cu phase. By increasing the aging temperatures, however, expansion is produced as a result of the transformation of the metastable phases into equilibrium phases.

Shivkumar *et al.*[193] have studied the parameters which control the tensile properties of A356 alloy in the T6 temper. The improvement in the alloy strength has been attributed to the precipitation of negligible phases from a supersaturated matrix. The sequence of precipitation in Al-Si-Mg alloys can be described as follows:

(i) Precipitation of GP zones, (needles about 10 nm long);

(ii) Intermediate phase β''-Mg_2Si, (homogeneous precipitation);

(iii) Intermetallic phase β'-Mg_2Si, (heterogeneous precipitation);

(iv) Equilibrium phase β-Mg_2Si, FCC structure (a = 0.639), rod or plate-shaped.

The maximum alloy strength (peak-aging) is achieved just before the precipitation of the incoherent β-platelets. Apelian *et al.*[172] studied the aging behaviour of Al-Si-Mg alloys and observed that the precipitation of very fine β'-Mg_2Si during aging leads to a pronounced improvement in strength properties. Both aging time and temperature determine the final properties. Their study also established that increasing the aging temperature by 10°C is equivalent to increasing the aging time by a factor of two.

2.9 EFFECTS OF TRACE ELEMENTS ON MATERIALS

The effect of the addition of trace elements on the properties of materials is a well-known phenomenon in materials. Under a number of specific conditions, the addition of trace amounts of certain elements has a disproportionate effect on properties. In order to produce such an effect, these elements must segregate to specific microstructural or crystallographic sites. Additions of Sr or Sb affect the nucleation of the eutectic Si in Al-Si castings, thereby promoting a finer Si phase and improved properties.[76,77] As little as 0.05% Sn, In or Cd suppresses natural aging and stimulates the artificial aging of Al-Cu alloys.[194] Doping of Si with a few parts per million of Ga changes its electrical conductivity characteristics which led to the semiconductor revolution.[195] The creep life of nickel-based superalloys may be increased by one order of magnitude through the addition of 0.01% Zr + 0.009% B.[196] During the vacuum brazing of Al, additions of Mg[197,198] as well as Ca, Sr, Li[197] Sb and Bi[199] improve joint properties. Additions of less than 1% Pb are used to modify the reactivity of Zn dust produced during atomisation.[200] These are all examples of trace

elements having a beneficial effect on properties, although this is not always the case. When the trace element causes a reduction in properties, it is generally regarded as an impurity and considerable efforts are made to keep such impurities to a minimum level. One such example is Pb in recycled Al alloys, caused by the addition of fishing weights to recycled Al cans, leading to a significant reduction in tensile ductility.[201]

2.9.1 Tin in Al-Si Alloys

Tin is a minor alloying element in aluminum alloys; in the past it was added to increase the fluidity of casting alloys and today it is added to the alloys used for bearings. According to the phase diagram shown in Figure 2.29, Al and Sn have mutual solid insolubility, with the maximum of Sn solubility in Al being about 0.1 wt% at approximately 627°C, and then decreasing to reach a probable value of 0.05-0.07% Sn at the eutectic temperature, and much smaller values at lower temperatures.[23] The eutectic point is at 228-229°C and 99.5% Sn, which is very close to the Sn end and melting-point.

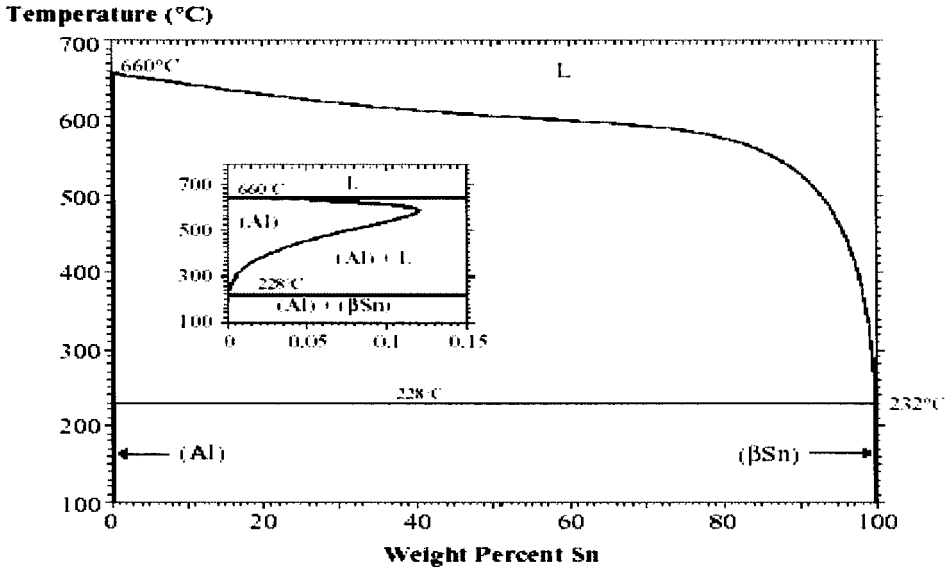

Figure 2.29 Aluminum-Tin phase diagram.[202]

The purpose of this thesis is to study the Al-Si-Cu-Mg and Al-Si-Mg system as a basis for understanding the role of Sn in more complex systems which may be employed for industrial applications. In particular, it was shown that it is possible to replace toxic lead by nontoxic tin in an Al-Cu-Bi-Pb alloy, which is one of the most common machinable Al-based alloys.[203] Nevertheless, contrary to Pb, the decomposition sequence of Al-Cu is substantially influenced by the presence of even a small amount of Sn.[204] Solid lubricants, such as graphite and Pb are dispersed in Al-Si alloys so as to increase their resistance to seizure. With the addition of graphite, however, the ductility, formability and thermal conductivity decrease.[205] The addition of Sn to Al-Si alloys can meet many of the above requirements and can also act as a solid lubricant to minimize the chances of seizure. The possibility of using tin in aluminum free-cutting alloys has been known for some time.[206,207] Tin was one of the first elements to be added to aluminum alloys in amounts up to 2 wt%.[208] At that time, its widespread use was not accepted in general practice because of a supposed worsening of the corrosion properties,[209] lower ductility of the alloys and the high costs incurred.[208] In Al-Cu alloys, trace element or microalloying additions of Sn, Cd, or In are known to increase the hardening response during elevated temperature aging (130°C and 190°C).[210,211] It was also observed that hardening of the Sn-containing alloy proceeds through a single stage at both temperatures. This fact is associated with the preferred nucleation of the θ′ phase at the expense of the Guinier-Preston (GP) zones and θ″.[210,212] The resulting effect, usually attributed to the high tin-vacancy binding energy, is due to a reduced solubility of copper in the presence of tin.[213] The β-tin phase was found in the Al-Cu-Sn alloy immediately after quenching, followed soon after by precipitation of Al_2Cu in

the early stages of aging.[214] Those tin particles which could be clearly identified as β-Sn phase shared a crystallographic relationship of the form (001)Sn‖(001)Al‖(001)θ′, [110]Sn‖[100]Al‖ [100]θ′ with the α-Al and θ′ phases with which they were simultaneously in contact.[215] These observations imply that, while tin may assist nucleation of θ′ platelets, the formation of θ′ also influences the crystallography of β-Sn which forms in association with θ′.

Murali *et al.*[216] investigated the effect of trace additions of tin, indium, and cadmium on the natural aging of Al-7%Si-Mg precipitation-hardened alloy. Delays of up to 24 hours in aging were observed to reduce the final UTS by 20 MPa, yield strength by 10 MPa, and hardness by 10-15 BHN, although elongation was improved by 50%. In Al-Si-Cu-Mg alloys, Sn prevented the formation of Mg_2Si, while Sn and Pb prevented the formation of the $Al_xMg_5Cu_4Si_4$ phase. Grebenkin *et al.*[217] also determined that tin is analogous to silicon electronically and replaces silicon in the magnesium compounds Mg_2Si and $Al_xMg_5Cu_4Si_4$. No free tin was found in Al-Si-Mg alloys when tin and magnesium levels were similar. The Mg_2Sn phase contained little silicon.

Sircar[218] also examined alternative alloying additions by focusing on the substitution of In+Sn for the Pb+Bi in the composition of 6262 base alloy. The results showed that these elements produce the desired low melting-point eutectic phases and somewhat improved machinability over that of the 6262 alloy. Alloy X6030 was registered in 1995 with In+Sn additions, although this alloy is at present in the process of being deactivated. The development of the alloy had originally aimed at producing one which maintained a good balance of machinability with high impact strength. No specific alloys

have thus far been registered as a result of this research. As mentioned earlier, the selection of these low melting-point elements was limited to binary systems. After a rigorous review of the various phase diagrams, the following system was considered. The Bi-Pb phase diagram shown in Figure 2.30 has the eutectic composition at 44.8 wt% Pb and a eutectic temperature of about 125.5°C. This displays great similarly to the Bi-Sn and In-Sn binary systems shown in Figures 2.31 and 2.32, which illustrate, respectively, a eutectic point at 43 wt% Sn and a eutectic temperature of 139°C, and a eutectic point at 49.1 wt% Sn at a eutectic temperature of 120°C.

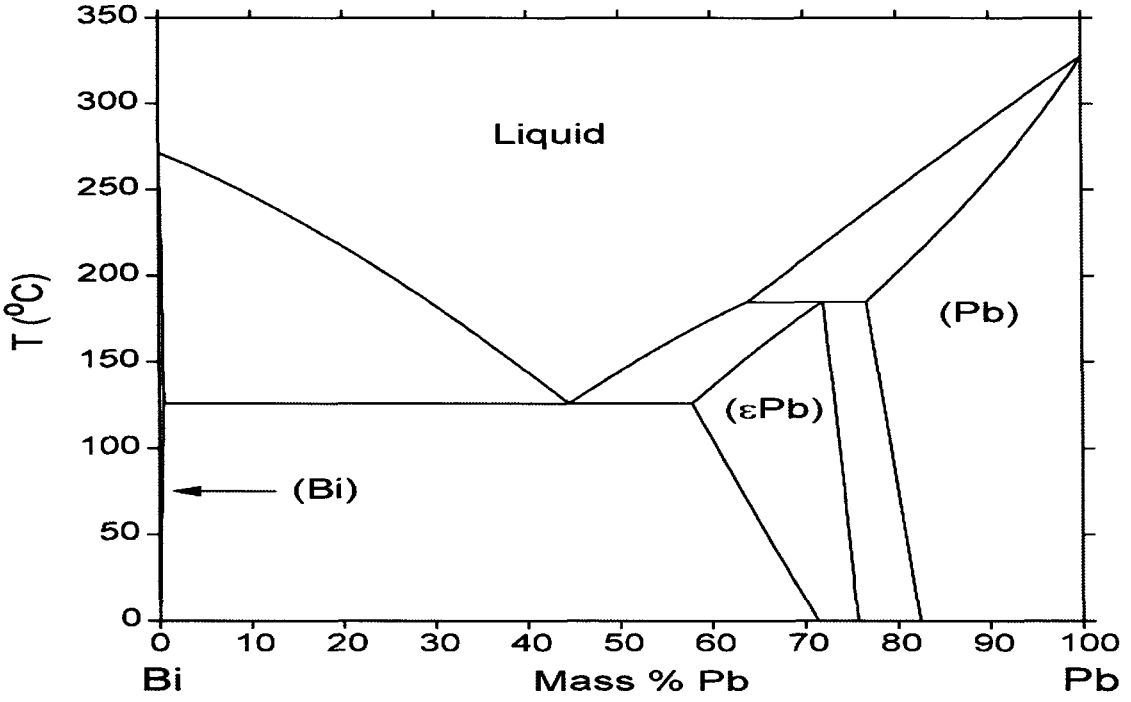

Figure 2.30 The Bi-Pb equilibrium binary phase diagram.[219]

Bismuth and Sn, and In and Sn, just like Pb and Bi, have very little solubility in aluminum in the solid state. The well-recognized problem with Pb-Bi system is that a large amount of Pb and Bi addition is needed to obtain the necessary volume percent in the alloy

for free machining. Since lead is extremely dense, large additions are required, thereby increasing the environmental unacceptability of this type of alloy. While Bi has a low affinity for Sn so that the two elements form only limited amounts of a low melting-point eutectic, the addition of indium, even in small amounts, has a surprising impact in that large amounts of a ternary low melting-point eutectic are formed. This ternary eutectic also has a substantially lower melting-point than the bismuth-tin eutectic. The Bi-Sn-In eutectic has a melting temperature of less than 100°C.

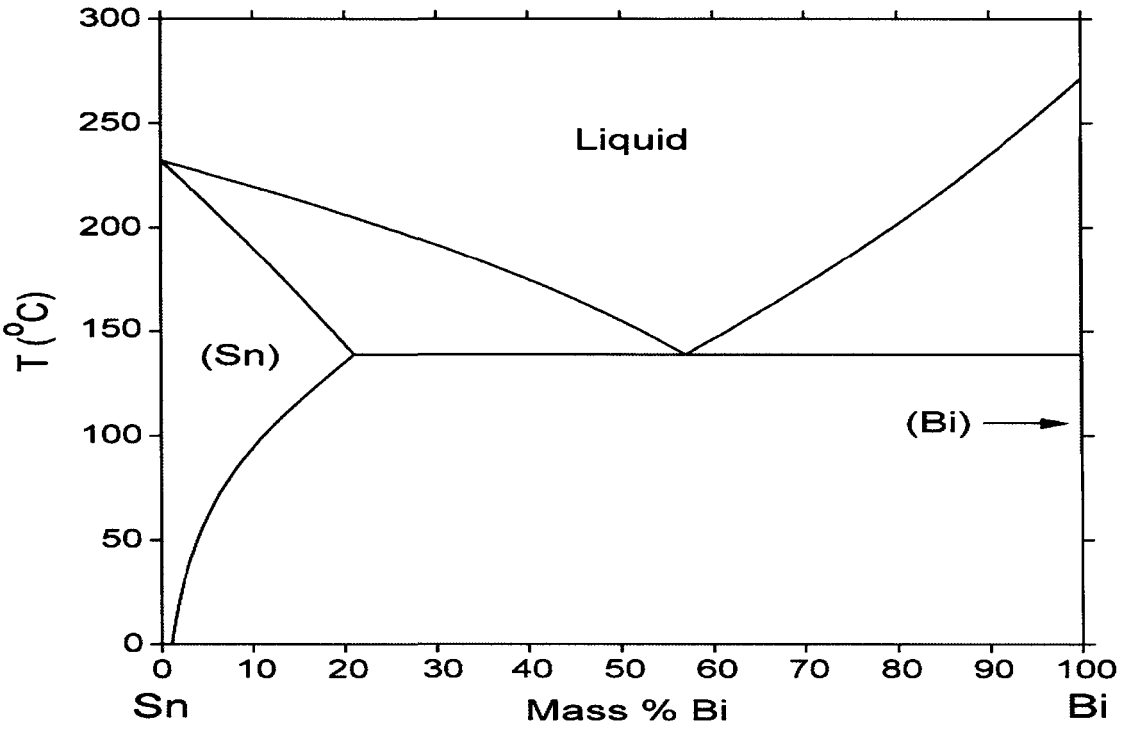

Figure 2.31 The Sn-Bi equilibrium binary phase diagram.[219]

In spite of the published literature, there is very little data describing the effect of lead, bismuth, tin, and indium additions on the microstructure and mechanical properties of Al-Si-Cu-Mg and Al-Si-Mg alloys. Thus, the study will focus on investigating the

precipitation of these elements and their influence on the mechanical properties of experimental Al-10.8% Si, B319.2 and A356.2 alloys.

For the purposes of this study, the effect of the Al-insoluble elements Sn, Bi, Pb, and In on the microstructure and mechanical properties of experimental Al-10.8% eutectic alloy are investigated taking into account that they all have extremely low distribution coefficients in both Al and Si. Of great interest here is the effect of these micro-alloying elements on the morphology and size of Si particles, and whether or not the refinement translates into an increase in tensile strength, ductility and toughness.

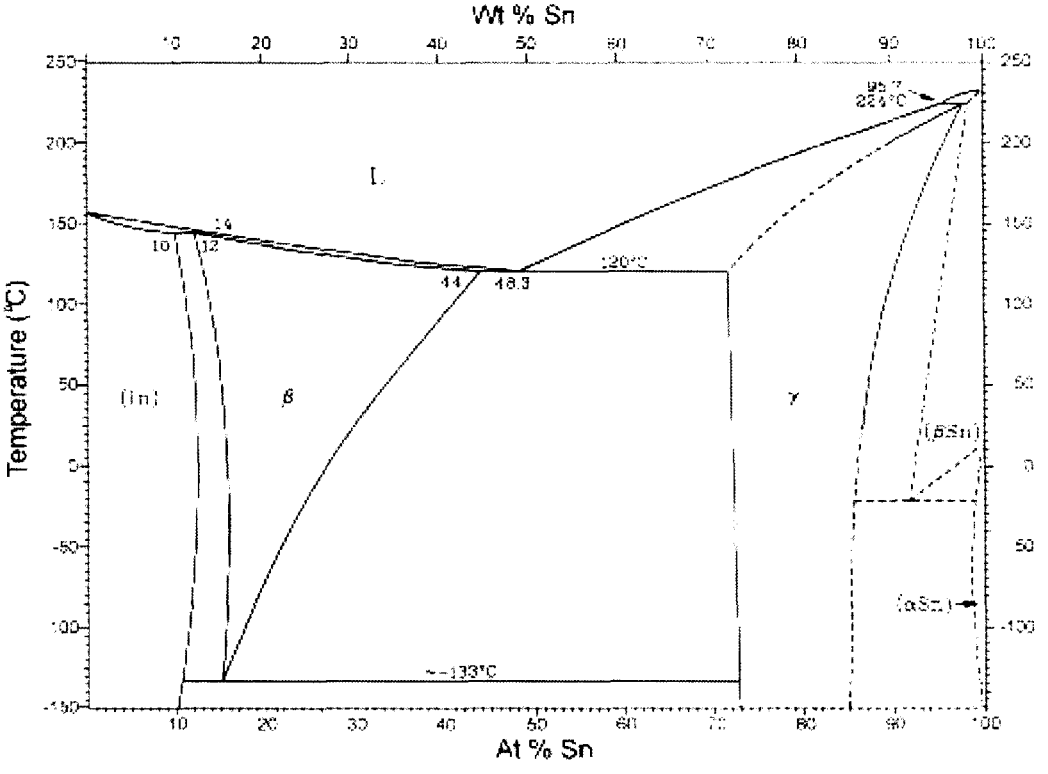

Figure 2.32 The In-Sn equilibrium binary phase diagram.[220]

CHAPTER 3

EXPERIMENTAL PROCEDURES

CHAPTER 3

EXPERIMENTAL PROCEDURES

3.1 INTRODUCTION

This chapter will provide all the relevant details concerning the alloys and additives used in this research, the general melting and casting procedures applied, the various techniques used for microstructural characterization and phase identification, namely optical microscopy, image analysis, and electron probe microanalysis (EPMA) including EDX and WDS techniques, as well as the tensile, hardness and impact testing methods used to determine the mechanical properties of the alloys investigated. It is worthwhile mentioning here that the number of samples which were cast for this study was considerable, giving an idea of the quantity of molten metal which was processed in the preparation of the corresponding castings.

Four kinds of test samples were produced: (i) hardness test bars; (ii) tensile test bars; (iii) impact test specimens; and (iv) samples for chemical analysis. The alloy codes for the various alloys that were prepared have been collectively listed in Table 3.1. Details of the experimental procedures which were adopted are provided in the following subsections.

3.2 EXPERIMENTAL PROCEDURES

The experimental Al-10.8%Si base alloy used in this research, and coded R, was received from the supplier in the form of 12.5-kg ingots. Using this base alloy, four main

groups of alloys were prepared, corresponding to Sr and Ti, Fe and Mn, Cu and Mg, and Pb, Sn and Bi additions, and coded R, RF, RC, and RT, respectively. The bulk of the experimental work was carried out using the Al-10.8%Si near-eutectic alloy.

In addition, B319.2 (coded N) and A356.2 (coded K) commercial Al-Si alloys were used to investigate the role played by the addition of tin with regard to the microstructure and mechanical properties of these alloys. Table 3.1 lists the chemical analyses of the various alloys studied and their respective codes, as obtained from samplings for chemical analysis taken from the corresponding melts.

3.2.1 Preparation of Alloys and Melting Procedures

The as-received Al-10.8%Si ingots were cut into smaller pieces, cleaned, dried and melted in charges of 34 kg each to prepare the required alloys. The melting process was carried out in a SiC crucible of 40-kg capacity, using an electrical resistance furnace. The melting temperature was maintained at 750 ± 5°C. All alloys were grain-refined by adding 0.25%Ti as Al-5%Ti-1%B in rod form and modified by adding Sr, in the form of an Al-10%Sr master alloy (150 ppm Sr), using a perforated graphite bell. Taking the grain-refined and modified alloy, coded RGM, as a reference, additions of Fe, Mn, Cu, and Mg were then made to the RGM alloy in order to study the effects of these alloying elements on the microstructure and mechanical properties of the grain-refined and modified alloy.

Table 3.1 Chemical composition of the various Al-10%Si alloys prepared for this research

Alloy code	Chemical Composition (wt %)														
	Si	Cu	Mg	Fe	Mn	Sr	Ti	Sn	Bi	Pb	Zn	In	Al	Mn/Fe	S.F [c]
	R Group - Sr and Ti addition														
R[a]	10.89	2.243	0.309	0.464	0.492	0.014	0.057	0.0	0.0	0.0	0.0	0.0	bal.	1.069	1.06
RM	10.93	2.221	0.370	0.449	0.494	**0.030**	0.077	0.0	0.0	0.0	0.0	0.0	bal.	1.099	1.44
RGM[b]	10.92	2.138	0.373	0.429	0.471	**0.030**	**0.22**	0.0	0.0	0.0	0.0	0.0	bal.	1.096	1.37
	RF Group - Fe and Mn addition														
RF1	10.82	2.099	0.276	**0.733**	**0.667**	0.03	0.22	0.0	0.0	0.0	0.0	0.0	bal.	0.909	2.07
RF2	10.87	2.092	0.325	**0.848**	**0.801**	0.03	0.20	0.0	0.0	0.0	0.0	0.0	bal.	0.944	2.45
RF3	10.90	2.132	0.275	**0.735**	0.481	0.03	0.26	0.0	0.0	0.0	0.0	0.0	bal.	0.654	1.69
RF4	10.93	2.128	0.333	**0.980**	0.482	0.03	0.26	0.0	0.0	0.0	0.0	0.0	bal.	0.492	1.95
	RC Group - Cu and Mg addition														
RC1	10.95	**2.726**	0.276	0.464	0.487	0.03	0.27	0.0	0.0	0.0	0.0	0.0	bal.	1.050	1.44
RC2	11.11	**3.308**	0.353	0.499	0.476	0.03	0.26	0.0	0.0	0.0	0.0	0.0	bal.	0.955	1.46
RC3	10.85	2.300	**0.491**	0.462	0.46	0.03	0.23	0.0	0.0	0.0	0.0	0.0	bal.	0.955	1.39
RC4	10.99	**2.743**	**0.552**	0.466	0.458	0.03	0.28	0.0	0.0	0.0	0.0	0.0	bal.	0.983	1.39
RC5	11.30	**3.128**	**0.604**	0.473	0.451	0.03	0.29	0.0	0.0	0.0	0.0	0.0	bal.	0.952	1.39
	RT Group - Trace Element additions														
RP	10.82	2.33	0.32	0.4	0.51	0.028	0.27	0.0	0.0	**0.43**	0.0	0.0	bal.	1.2	1.44
RB	10.89	2.21	0.34	0.38	0.49	0.027	0.25	0.0	**0.57**	0.0	0.0	0.0	bal.	1.28	1.37
RN	10.71	2.37	0.32	0.43	0.48	0.031	0.25	**> 0.48**	0.0	0.0	0.0	0.0	bal.	1.11	1.39
RPB	10.85	2.35	0.33	0.41	0.50	0.028	0.25	0.0	**0.55**	**0.46**	0.0	0.0	bal.	1.2	1.42
RBN	10.90	2.24	0.38	0.46	0.49	0.024	0.25	**> 0.48**	**0.57**	0.0	0.0	0.0	bal.	1.06	1.44
R2BN	10.62	2.21	0.33	0.42	0.49	0.023	0.26	**> 0.48**	**0.53**	0.0	0.0	0.0	bal.	1.16	1.40
RZ	10.91	2.33	0.45	0.42	0.49	0.028	0.24	**> 0.48**	**0.53**	0.0	**0.55**	0.0	bal.	1.20	1.41
RNN	10.91	2.20	0.33	0.41	0.51	0.028	0.25	**> 0.48**	0.0	0.0	0.0	**0.50**	bal.	1.2	1.43

Main additives are in bold;

a: an experimental Al-10.8%Si base alloy;

b: grain-refined and modified Al-10.8%Si alloy, used as a reference alloy;

c: sludge factor.

Iron and Mn were added in the form of Al-25%Fe and Al-25%Mn master alloys, respectively, whereas Cu and Mg were added in the form of the pure metal. These additions produced the alloys classified as groups RF and RC in Table 3.1. Finally, additions of the trace elements Sn, Bi Pb, Zn, and In (individually and in different combinations) to the RGM alloy produced the alloys corresponding to the group RT. These trace elements were added in the form of pure metals, in amounts calculated to obtain the desired compositions.

In a separate study, the standard commercial B319.2 and A356.2 aluminum cast alloys were used as a base-line in order to study the influence of tin on the microstructure and mechanical properties of these alloys. The alloys were grain-refined by adding 0.2%Ti in the form of Al-5%Ti-1%B rod and Sr-modified with an Al-10%Sr master alloy (200 ppm Sr), using a perforated graphite bell. The chemical compositions of the grain-refined modified B319.2 and A356.2 alloys, coded N and K, respectively, and the four Sn-containing alloys prepared from them and their respective codes are provided in Table 3.2.

Table 3.2 Chemical composition of B319.2 and A356.2 Alloys with Sn additions

Alloy code	Chemical Composition (wt%)											
	Si	**Cu**	**Mg**	**Fe**	**Mn**	**Sr**	**Ti**	**Sn**	**Zn**	**Al**	**Mn/Fe**	**S.F**
	B319.2 Alloys											
N (base)	7.16	3.32	0.29	0.29	0.27	0.019	0.27	0.0	0.14	bal.	0.95	0.87
NS	7.08	3.29	0.31	0.28	0.28	0.017	0.27	**0.05**	0.13	bal.	0.98	0.84
NSS	7.08	3.29	0.31	0.28	0.28	0.017	0.27	**0.17**	0.13	bal.	0.98	0.84
	A356.2 Alloys											
K (base)	6.76	0.01	0.36	0.08	0.28	0.017	0.27	0.0	0.01	bal.	3.30	0.64
KS	6.87	0.01	0.39	0.08	0.28	0.019	0.27	**0.05**	0.01	bal.	3.52	0.64
KSS	6.87	0.01	0.39	0.08	0.28	0.019	0.27	**0.15**	0.01	bal.	3.52	0.64

Main additives are in bold; S.F: sludge factor

All melts were degassed using pure, dry argon injected into the melt for ~15 min by means of a rotating graphite degassing impeller, at 125 rpm rotation, to ensure homogeneous mixing of the additives, and a melt hydrogen level of 0.1 mL/100g. The humidity varied between 11 and 15% when preparing these melts. The degassed melt was carefully poured into various preheated molds to prepare castings for obtaining samples for metallographic observations, hardness measurements, tensile testing, and impact testing. The pouring temperature was 730 ± 5°C.

3.2.2 Casting Procedures

The degassed melt was carefully poured into (a) two preheated (450°C) L-shaped rectangular graphite-coated metallic molds for preparing castings/samples for metallographic and hardness measurements; (b) an ASTM B-108 permanent mold to obtain castings for tensile testing; and (c) a mild steel impact test mold to obtain samples for impact testing. For each pouring/casting, a sampling for chemical analysis was also taken simultaneously to obtain the corresponding alloy melt composition.

The chemical analysis was carried out using arc spark spectroscopy at GM facilities in Milford, NH. The alloy compositions listed in Tables 3.1 and 3.2 represent average values taken over three spark measurements made on each chemical analysis sample. For each set of melt conditions, identical castings were prepared for metallographic observations, hardness measurements, tensile testing, and impact testing.

Samples for metallography and hardness testing purposes were obtained from castings obtained from the L-shaped metallic mold, as shown in Figure 3.1(a). The points A

and B in Figure 3.1(b) shows the location on the casting from which the hardness test bar was sectioned, while the inset shows the surface of such a bar with indentations, resulting from the hardness measurements.

In the case of the samples used for metallographic analysis, two samples were sectioned (25 mm x 25 mm each) from the L-shaped casting, as shown in the schematic diagram of Figure 3.2, to examine the alloy microstructure in the as-cast and solution heat-treated conditions.

Figure 3.3(a) shows the ASTM B-108 type permanent mold used for preparing the tensile test castings, while Figure 3.3(b) shows the actual casting obtained. As can be seen, each casting provides two tensile test bars.

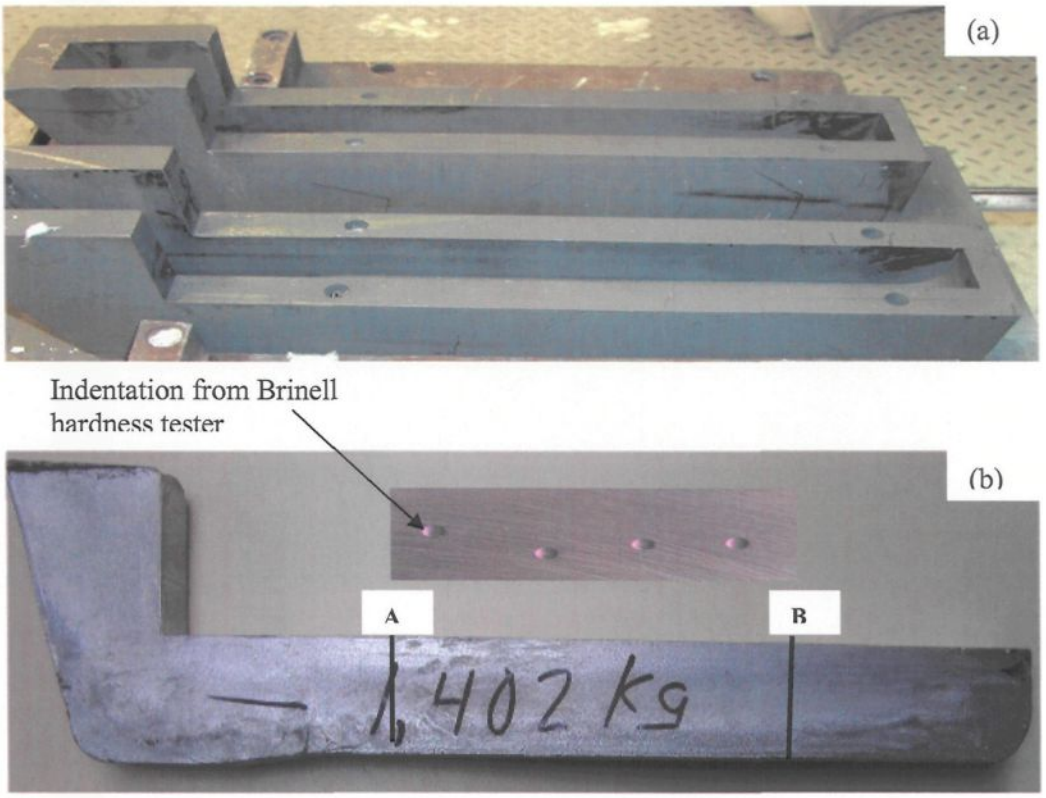

Figure 3.1 (a) Molds used to prepare the casting; (b) Alloy casting and hardness test bar (2.54 cm x 2.54 cm x7.62 cm) obtained from the casting.

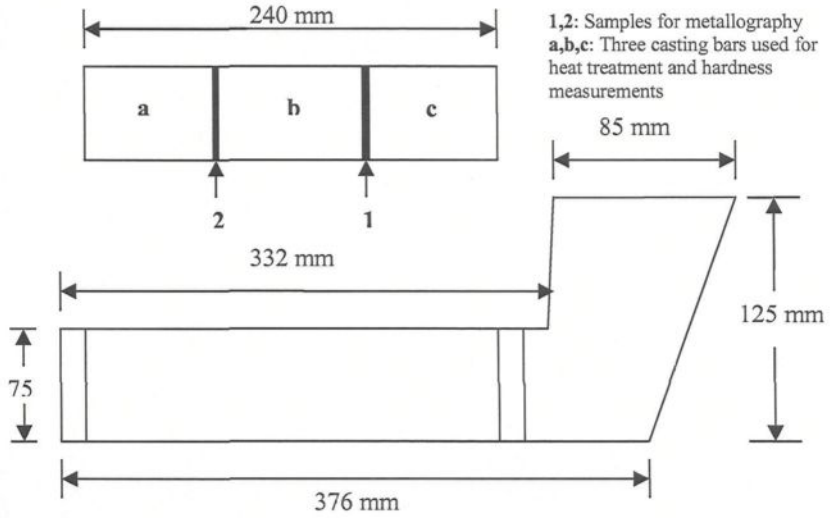

Figure 3.2 Schematic diagram of the L-shaped metallic mold casting showing sectioning of the two samples used for the metallography.

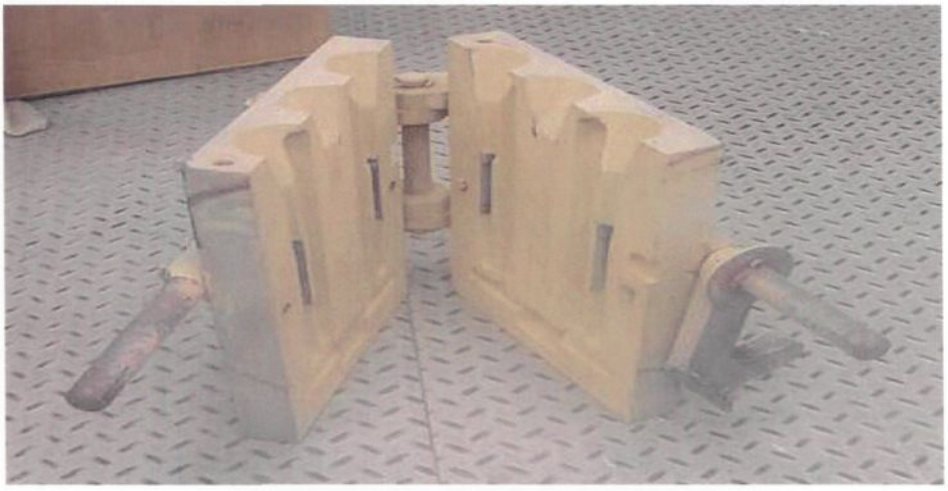

(a)

(b)

Figure 3.3 (a) ASTM B-108 permanent mold; (b) Actual tensile test specimen.

The test mold used to prepare the impact test bars is shown in Figure 3.4, with the casting still intact in the bottom half of the mold, and the open upper half behind the latter. Each casting provides ten impact bars, which are cut from the casting, and then machined to the required ASTM specifications for conducting Charpy impact tests thereafter.

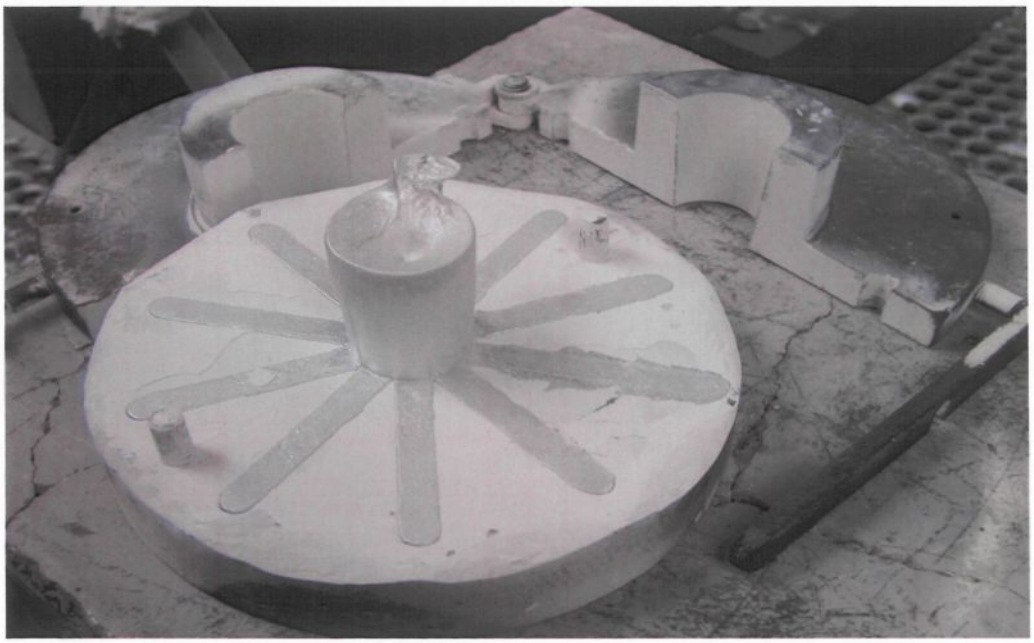

Figure 3.4 Metallic mold used to prepare impact test bars.

3.2.3 Metallography-Microstructural Examination

From each of the castings prepared for metallographic observations, two samples measuring 25 x 25 mm were sectioned off to represent each alloy condition. One sample was used in the as-cast condition, while the second sample was solution heat-treated at 495°C for 8 h, and then immediately quenched in warm water (~65°C). The samples were then mounted in bakelite using a Struers Labopress-3 Mounting Press (force of 30 N; heating time of 9 min, cooling time of 6 min) then polished using a Struers Tegrapol-35

Grinder-Polisher to obtain the desired fine finish (1 μm Mastermet). Details of the grinding and polishing procedures are provided in Table 3.3.

At each stage of the procedure, the coolant which was used also acted as a lubricant and ensured constant cleaning of the paper and the specimen simultaneously. Between the different stages, the samples were cleaned with water. Care was taken to see that the pressure exerted on the specimen was high enough to ensure proper cutting by the abrasive and a sufficient rate of abrasion, without the unwanted production of heat and premature wear and tear of the abrasive.

Table 3.3 Grinding and polishing procedures for metallographic samples

Stage	Abrasive	Particle Size (μm)	Coolant	Pressure (N)	Time (sec)	Speed (rpm)
1	SiC (120)	125	Running water	30	60	150
2	SiC (240)	52	Running water	30	60	150
3	SiC (320)	35	Running water	30	60	150
4	SiC (400)	22	Running water	30	60	150
5	SiC (600)	14	Running water	30	30	150
6	SiC (800)	10	Running water	30	30	150
7	Diamond	9	Special oil	30	360	150
8	Diamond	6	Special oil	30	360	150
9	Diamond	3	Special oil	30	360	150
10	Mastermet	1	Running water	30	180	80

Note: Special Oil indicates lubricant fluid

Microstructures of the polished sample surfaces were examined using an Olympus PMG3 optical microscope. The eutectic silicon particle characteristics, including area, length, aspect ratio, roundness and density, were measured and quantified using a Leco

2001 image analyzer system in conjunction with the optical microscope. For each sample, 50 fields at a magnification of 500x were examined, so as to cover the entire sample surface in a regular and systematic manner. In addition, porosity measurements were carried out, over 30 fields per sample, at a magnification of 50x. The porosity parameters measured were percentage porosity, pore area, and pore length. As a rule, the outer edges of a sample were avoided in taking these measurements so as to eliminate any distortions that might occur in the peripheral regions. Figure 3.5 shows the optical microscope-image analysis system used for these measurements.

Figure 3.5 The optical microscope-image analysis system used for microstructural analysis.

Phase identification was carried out using electron probe microanalysis (EPMA) coupled with energy dispersive X-ray (EDX) and wavelength dispersive spectroscopic (WDS) analyses, using a JEOL JXA-8900l WD/ED combined microanalyzer operating at

20 KV and 30 nA, where the electron beam size was ~2 μm. Mapping of certain specific areas of the polished sample surfaces was also carried out where required, to show the distribution of trace elements in the phases. Figure 3.6 shows the JEOL WD/ED combined microanalyzer which was employed for this purpose.

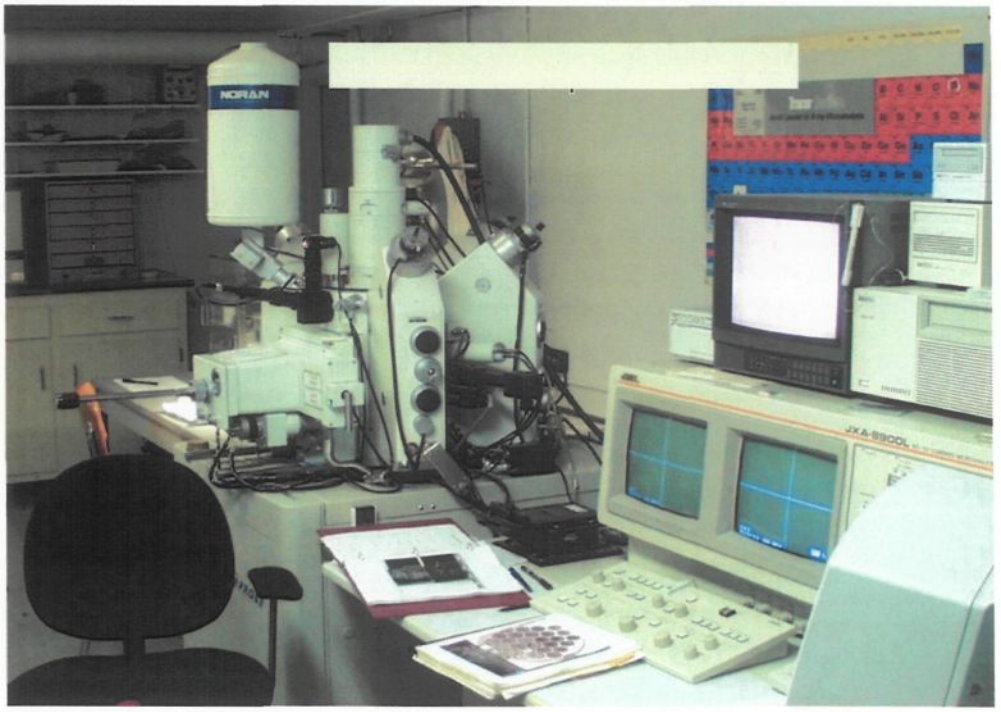

Figure 3.6 Electron probe microanalyzer used for this research.

3.2.4 Heat Treatment

For the Al-10%Si near-eutectic alloy, thirty-five bars were prepared for each alloy composition. The test bars were divided into seven sets: one set was kept in the as-cast condition, while the other six sets were solution heat-treated at 495°C for 8 h, then quenched in warm water at 65°C, followed by artificial aging at 155°, 180°, 200°, 220°, and 240°C for 5 hours (*i.e.* T6 and T7-tempered).

In the case of the B319.2 and A356.2 alloys, fifteen bars were prepared for each composition. The test bars in this case were divided into three sets: one set was kept in the as-cast condition, while the second set was solution heat-treated at 495°C/8 h in the case of the B319.2 alloys, and at 540°C/8 h for the A356.2 alloys, then quenched in warm water at 65°C, followed by artificial aging at 180°C for 5 hours (*i.e.* T6-tempered). The third set was T5 heat-treated at 175°C for 10 hours.

A summary of the heat treatment procedures is provided in Table 3.4. The solution and aging heat-treatments were carried out in a forced-air Blue M Electric Furnace equipped with a programmable temperature controller (± 2°C). The aging delay was less than 10 s. For each individual heat treatment, five test bars were used. These procedures were followed for the heat treatment of the tensile, hardness and impact test samples.

Table 3.4 Heat treatment procedures used

Alloy codes	Solution Heat Treatment	T5, T6, and T7- Temper	
		Temp. (°C)	Time (h)
Al-10.8%Si alloys			
1. Groups R, RF, RC, and RT	1. SHT[a] (495°C/8h) 2. Water quenching (65°C)	T6: 155 T6: 180 T6: 200 T7: 220 T7: 240	5 5 5 5 5
B319.2 alloys			
1. N, NS, and NSS	1. SHT[a] (495°C/8h) 2. Water quenching (65°C)	T6: 180	5
2. N, NS, and NSS		T5: 175	10
A356.2 alloys			
1. K, KS, and KSS	1. SHT[a] (540°C/8h) 2. Water quenching (65°C)	T6: 180	5
2. K, KS, and KSS		T5: 175	10

a: Solution heat-treatment

3.2.5 Mechanical Testing

The mechanical properties examined in this study were the tensile, hardness and impact properties. A description of the castings prepared for these tests and the details of test samples sectioned from the respective castings have been provided in subsection 3.2.2.

3.2.5.1 Tensile Testing

Tensile test bars were produced using the ASTM B-108 mold, shown in Figure 3.3 in subsection 3.2.2. Each mold casting provided two tensile bars, each with a gauge length of 50 mm and a cross-sectional diameter of 12.7 mm. Figure 3.7(a) shows an example of the actual test bar sectioned from the casting, while Figure 3.7(b) shows the dimensions of the test bar according to ASTM specifications.

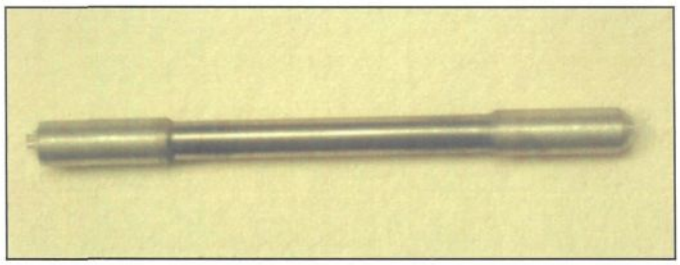

(a)

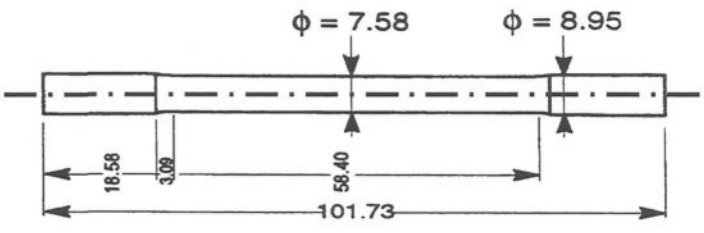

(b)

Figure 3.7 Shows (a) an example of the actual test bar sectioned from the casting, and (b) the dimensions of the test bar according to ASTM specifications.

For the Al-10%Si near-eutectic alloy, thirty-five bars were prepared for each alloy composition, and divided into seven sets corresponding to the heat-treatment conditions described in section 3.2.4. In the case of the B319.2 and A356.2 alloys, fifteen bars were prepared for each composition and divided into three sets corresponding to the heat-treatment conditions described in their case. For each individual heat treatment, at least 5 test bars were used.

The as-cast and heat-treated test bars were pulled to fracture at room temperature at a strain rate of 4 x 10^{-4}/s using a Servohydraulic MTS Mechanical Testing machine, as shown in Figure 3.8. A strain gauge extensometer was attached to the test bar to measure percentage elongation as the load was applied.

Figure 3.8 Servohydraulic MTS Mechanical Testing machine with data-acquisition system.

The yield strength (YS) was calculated according to the standard 0.2% offset strain, and the fracture elongation was calculated as the percent elongation (%El) over the 50 mm

gauge length. The ultimate tensile strength (UTS) was also obtained from the data acquisition system of the MTS machine. This machine was calibrated each time before any testing was carried out. The average %El, YS or UTS value obtained from the five samples tested was considered as the value representing a specified condition.

3.2.5.2 Hardness Testing

Hardness test bars measuring 2.54 cm x 2.54 cm x 7.62 cm were cut from the casting, as shown in Figure 3.1(b). All test samples were heat-treated in the same way as the tensile samples, and the specimen surfaces were polished with fine sandpaper to remove any machining marks. The hardness measurements were carried out on the as-cast and heat-treated samples using a Brinell hardness tester, employing a steel ball of 10 mm diameter and a load of 500 kgf applied for 30 seconds. Figure 3.9 shows the Brinell hardness tester used for these measurements. An average of eight readings obtained from two perpendicular surfaces was taken to represent the hardness value in each case.

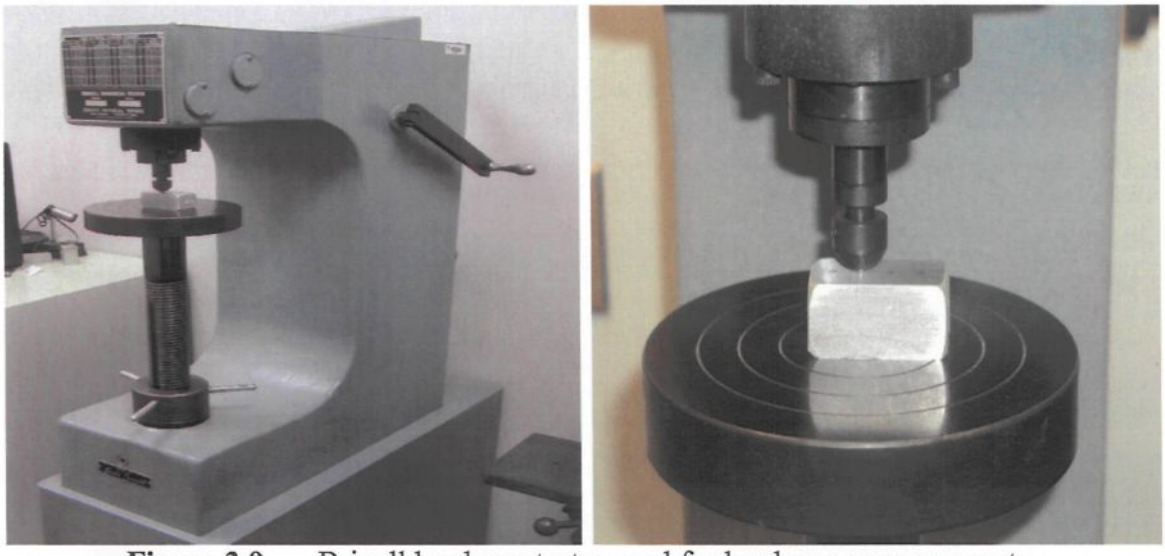

Figure 3.9 Brinell hardness tester used for hardness measurements.

3.2.5.3 Impact Testing

As mentioned in subsection 3.2.2 and shown in Figure 3.4, each impact mold-casting provided ten impact test bars. The samples were sectioned from the casting, and machined according to the dimensions shown in Figure 3.10. The specimen surfaces were polished with fine sandpaper to remove any machining marks. The impact tests were performed on unnotched samples.

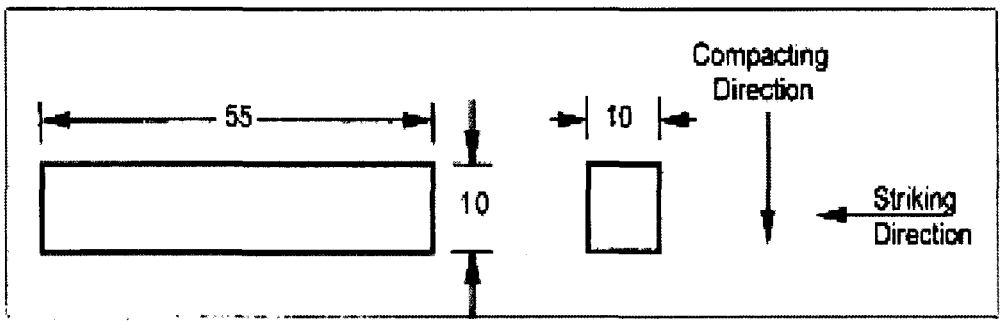

Figure 3.10 Charpy unnotched impact specimen (all dimensions in mm).

A computer-aided instrumented SATEC SI-1 Universal Impact Testing Machine (SATEC Systems Inc., Model SI-1D3) was used to carry out the impact tests, as shown in Figure 3.11. This machine is equipped with bolt-on weights in addition to the pendulum. The pendulum is capable of being latched in two separate modes, known as "high latch" and "low latch," providing a total of four operating capacities, namely, a capacity of 25 ft-lbs (33.9 J) on low latch and 60 ft-lbs (81.35 J) on high latch without the bolt-on weights attached, and a capacity of 50 ft-lbs (67.8 J) on low latch and 120 ft-lbs (162.7 J) on high latch with the additional weights attached. A data acquisition system connected to the impact machine monitored the dynamic behavior of the test specimen and measured the load and energy values as a function of time.

Figure 3.11 A computer-aided instrumented SATEC SI-1 universal impact testing machine, with a Dynatup IPM/PC impact testing system for data acquisition.

The total absorbed energy (E_t) during impact testing was determined, together with a number of specific parameters such as crack initiation and propagation energies, total time, and the maximum load required to break the specimens. The load-deflection curves and energies absorbed were obtained using a Dynatup IPM/PC Impact Testing System. The average values of the energies obtained from the five samples tested for each alloy condition were taken as the representative values for that particular condition.

CHAPTER 4

EFFECT OF ALLOYING ELEMENT-ADDITIONS ON THE MICROSTRUCTURE, HARDNESS, AND TENSILE PROPERTIES OF Al-10.8%Si NEAR-EUTECTIC ALLOY

CHAPTER 4

EFFECT OF ALLOYING ELEMENT-ADDITIONS ON THE MICROSTRUCTURE, HARDNESS, AND TENSILE PROPERTIES OF Al-10.8%Si NEAR-EUTECTIC ALLOY

4.1 INTRODUCTION

In keeping with the objectives of this thesis, the effects of the addition of the alloying elements Fe, Mn, Mg and Cu on the microstructural characteristics and on the mechanical properties of an experimental Al-10.8%Si near-eutectic alloy will be examined and discussed in both Chapters Four and Five.

Modification and grain refinement are commonly employed in producing aluminum castings in order to improve their mechanical properties. Aluminum-silicon alloys without modification treatment are characterized by relatively poor mechanical properties due to the presence of coarse acicular plates of eutectic silicon which act as internal stress raisers. Grain structure is also an important feature in aluminum alloy castings. Researchers have often noted that fine grain size is beneficial to castings since feeding characteristics, tear resistance, and mechanical properties are all observed to be improved by it. For this reason, grain refiners are often added to the melt before casting so as to obtain a fine equiaxed solidification structure. The addition of such alloying elements as copper and magnesium enhances the mechanical properties of aluminum-silicon casting alloys. In the light of the above, the subject of this chapter will thus be the effects of the addition of melt treatment and alloying elements on the microstructure, hardness, and tensile properties of an experimental Al-10.8%Si near-eutectic alloy.

4.2 CHARACTERIZATION OF MICROSTRUCTURE

A metallographic study was conducted to examine the specific changes resulting from melt treatment procedures (modification and grain refining), addition of alloying elements, and solution heat-treatment from the point of view of microstructure and chemical composition. In addition to observing the qualitative evolution of the morphology and size of the Si constituent, quantitative analysis was also employed using a Leco 2001 image analyzer in conjunction with an Olympus optical microscope. The results obtained will be discussed in the following subsections. Due to the very large number of samples and conditions investigated, only selected representative micrographs will be shown.

4.2.1 Characteristics of Silicon Particles

The morphology of eutectic Si plays a vital role in determining the mechanical properties of Al-Si alloys. Particle size, shape, and spacing are all factors which characterize the structure of silicon. Table 4.1 summarizes the silicon particle characteristics obtained for the alloys investigated.

As may be seen from this table and Figure 4.1(a), the Si particles are present in the form of coarse acicular plates with an aspect ratio of 2.41 in the as-cast condition for the base alloy (R). The silicon represents the hard phase of the alloy which causes a discontinuity of the soft and ductile matrix of aluminum. Because α-Al is the softer phase and Si is the harder and less ductile one, stresses cause anisotropic distribution of the plastic deformation, which is greater in the softer phase. The local plastic constraint in the softer phase leads to a rapid strengthening of the alloy, with dislocations piling up at the α-

Al/Si interfaces. This can lead to the formation of cleavage microcracks at these ductile-brittle sites. On such a basis, it is to be expected that differences between the mechanical properties of the five tensile bars will be higher for the unmodified alloy.

The addition of 150 ppm of Sr transforms the morphology of the Si particles from an acicular form to a fibrous one (RM alloy) with an aspect ratio of 1.98; it also increases the roundness ratio from 57% to 74%, as shown in Figure 4.2(a). The average Si-particle length decreases from 5.86 μm (R alloy) to 2.43 μm (RM alloy), and the average Si particle area decreases from 8.59 μm^2 to 2.39 μm^2, *i.e.* by about 58% and 72%, respectively. As a result of the decrease in the size of the particles, the density of the Si particles increases from 10096 to 45490 particles/mm^2; implying that, in the presence of Sr, the eutectic Si phase was fibrous and finely divided, as indicated in the micrograph shown in Figure 4.2(a). The modified structure is often improperly called globular[221] since the fibres appear to be small individual globules (particles) on a conventionally polished surface; they are, in fact, connected in a coral or seaweed-like structure. Figures 4.1(a) and 4.2(a) clearly show the structural differences between the unmodified and modified alloys, respectively. In the unmodified alloy, the Si phase was to be observed in the form of large plates with sharp sides and ends known as acicular silicon. The globules of the modified structure are the ends of silicon fibres which form an interconnected network. Such a structural transformation from acicular to fibrous silicon is responsible for the improvement in the mechanical properties of modified castings.

The variations existing between the particles were estimated by means of the standard deviation, although it was not used exactly as defined according to statistical

principles, which is to assess the accuracy of the measurements under the same experimental conditions. For the purposes of this examination of microstructures, the standard deviation was considered to assess the structural uniformity of the silicon phase within the microstructure. In the presence of strontium, the degree of modification was appreciable, and one of the aspects of this was reflected by a narrowing of the deviations. The standard deviation between the particles decreased from ± 14.11 to ± 7.82 thereby showing the increase in the uniformity of the microstructure associated with modification.

The micrograph shown in Figure 4.3(a) and Table 3 illustrate the combined effects of Sr and Ti additions on Si particles in the RGM alloy. The primary α-Al phase has a fully columnar (dendritic) structure in the untreated alloy, see Figure 4.1(a), but transforms to equiaxed morphology with the combined addition, as shown in Figure 4.3(a). Such an effect is believed to be due solely to the grain refiner segment of the combined treatment. The average Si-particle area, length, and aspect ratio of the RGM alloy in the as-cast condition decrease by 69%, 54%, and 12%, respectively, compared to the R alloy, whereas the average roundness and density increase by 24% and 304%, respectively. It should be noted that the average Si particle area, length, and aspect ratio of the RGM alloy in the as-cast condition increase by 12%, 11%, and 7%, respectively, compared to the RM alloy, whereas the average roundness and density decrease by 3% and 10%, respectively. It may thus be concluded that the addition of Ti has a slight poisoning effect on the effectiveness of Sr-addition as a modifier.

Table 4.1 Silicon-particle characteristics of the alloys investigated

Alloy code	Solution time (hr)	Particle area (μm^2)		Particle length (μm)		Roundness ratio (%)		Aspect ratio		Density (particles/ mm^2)
		Av	SD	Av	SD	Av	SD	Av	SD	
R	0[a]	8.59	14.11	5.86	6.37	57.34	29.46	2.41	1.23	10096
	8	7.25	13.1	5.58	6.02	62.0	20	2.21	1.27	14457
RM	0[a]	2.39	7.82	2.43	2.88	73.50	25.07	1.98	1.05	45490
	8	5.34	7.12	3.37	5.21	80.5	18.39	1.72	0.68	26766
RGM	0[a]	2.67	4.71	2.69	2.65	71.29	24.97	2.11	0.94	40807
	8	5.22	7.04	3.66	3.25	75.42	21.47	1.93	0.84	20903
RF1	0[a]	2.48	2.29	2.50	2.80	73.47	25.04	2.13	0.99	31218
	8	4.35	7.69	3.10	2.78	78.31	20.44	1.86	0.79	19405
RF2	0[a]	2.47	2.61	2.58	2.59	77.07	23.58	2.04	0.89	32064
	8	5.65	9.77	3.46	3.20	79.32	19.19	1.78	0.72	19257
RF3	0[a]	2.46	4.56	2.58	2.46	73.0	23.98	2.11	0.95	39816
	8	4.39	5.64	3.28	2.71	76.62	20.0	1.93	0.85	22567
RF4	0[a]	3.29	6.05	3.14	3.02	70.40	24.93	2.11	0.97	39298
	8	4.89	6.61	3.49	2.97	76.0	20.40	1.95	0.89	22022
RC1	0[a]	2.67	5.08	2.76	2.74	70.77	25.11	2.14	0.96	27438
	8	2.73	5.11	2.82	2.87	76.35	18.96	1.90	0.74	25282
RC2	0[a]	3.41	4.45	3.11	3.44	70.10	26.08	2.14	0.98	25142
	8	3.61	7.35	3.43	3.17	75.85	21.11	1.94	0.88	24449
RC3	0[a]	6.32	5.43	4.83	5.29	63.13	27.94	2.17	1.01	24966
	8	5.92	5.72	4.72	2.84	66.68	19.66	1.99	0.82	23973
RC4	0[a]	7.08	12.61	4.87	5.47	61.90	27.8	2.29	1.12	24704
	8	5.92	7.37	4.01	3.49	64.02	21.87	1.99	0.93	21218
RC5	0[a]	7.46	13.92	5.16	5.97	61.37	28.67	2.32	1.14	22018
	8	6.80	8.91	4.27	3.85	63.28	22.07	2.27	0.95	20762

a: as-cast; Av: average; SD: standard deviation.

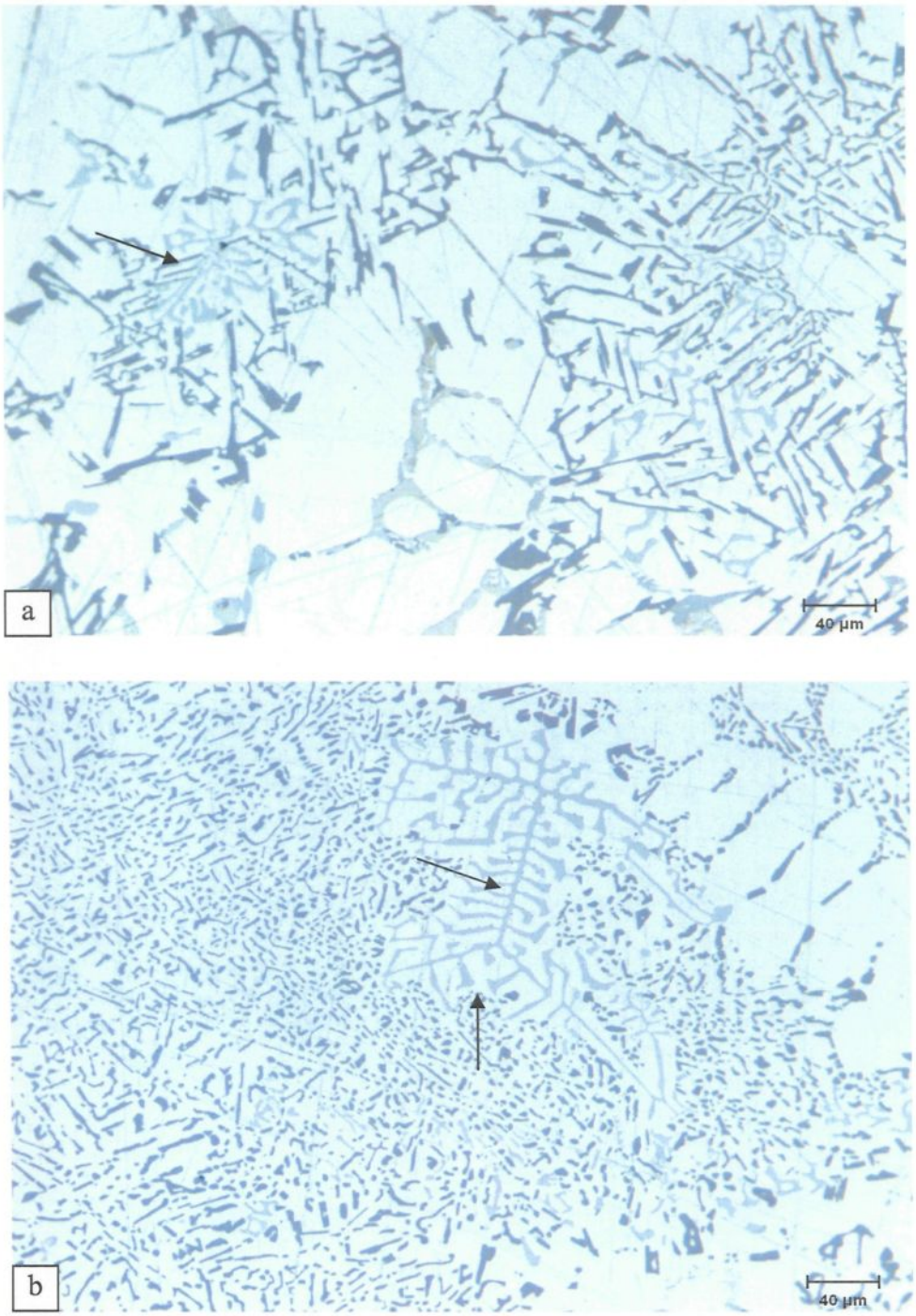

Figure 4.1 Optical micrographs showing the effect of solution treatment at 495°C on Si morphology in the base R alloy: (a) 0 h; and (b) 8 h.
Arrows point to α-Fe script particles.

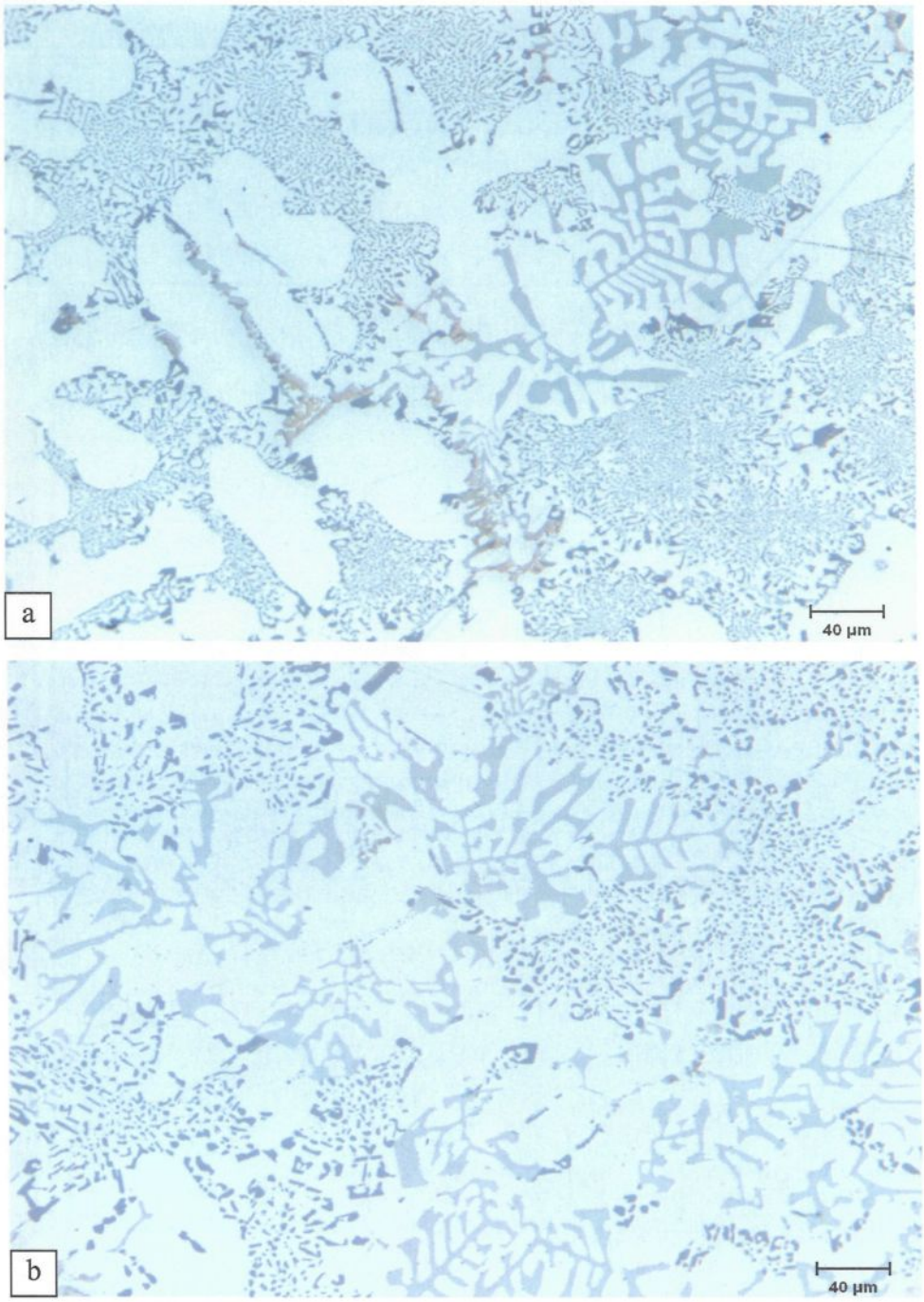

Figure 4.2 Optical micrographs showing the effect of solution treatment at 495°C on Si morphology in Sr-modified RM alloy: (a) 0 h; and (b) 8 h.

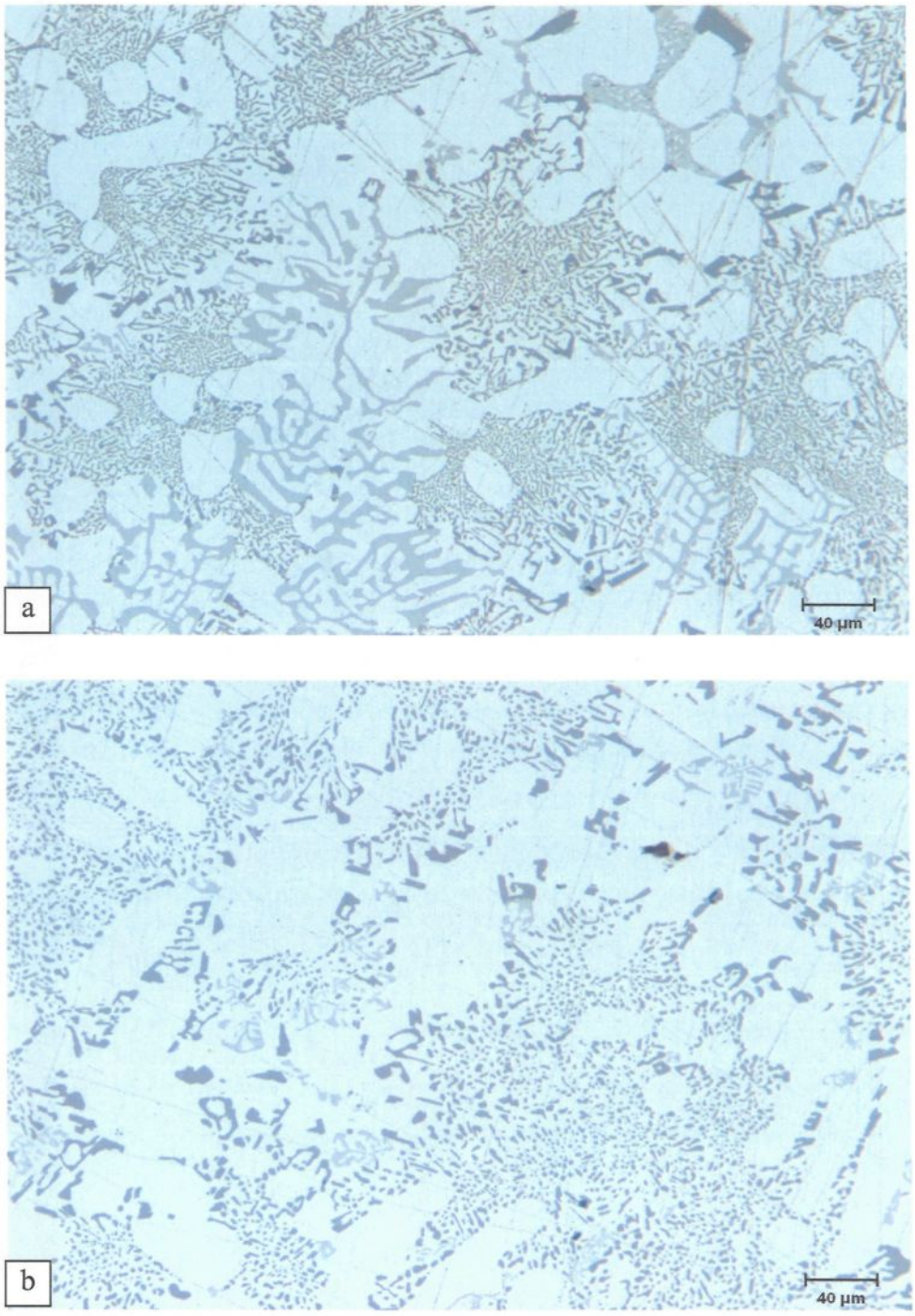

Figure 4.3 Optical micrographs showing the effect of solution treatment at 495°C on Si morphology in Sr-modified and grain-refined RGM alloy (a) 0 h; and (b) 8 h.

Under normal cooling conditions, eutectic silicon forms a network of interconnected irregular flakes. As was observed earlier, the eutectic Si may be chemically modified to a fine fibrous structure. High temperature treatments can also alter Si particle characteristics. In recent years, both chemical and thermal modification have been used in conjunction with each other to produce the desired properties of the casting. Several investigators have used quantitative metallographic techniques to monitor the changes in Si-particle morphology during solution heat-treatment.[172,222] One of the objectives of solution heat-treatment is to allow the soluble hardening elements of the alloy to dissolve into solid solution and to homogenize castings. Because solubility and diffusion rate both increase with temperatures, it is usually desirable to use the highest treatment temperature possible without causing melting. When castings are heat-treated at temperatures lower than the normal range, dissolution is incomplete and mechanical properties are not optimum.

A common feature of eutectic alloys is that there is a certain degree of solubility of the discontinuous phase in the matrix at temperatures below the eutectic point. The solubility of Si in the matrix of Al-Si alloys, however, is not constant because it is affected by the Si morphology. Eutectic Si is an imperfect crystal and according to the curvature of the surface, the lattice deformation energy will vary and hence the solubility of Si is affected. For example, the solubility of Si in the matrix is greater at locations such as the roots of branches (A), or the tips (B), than it is on the flat face of eutectic silicon (C), as shown in Figure 4.4. The energy state, *i.e.* the surface curvature and lattice deformation of the discontinuous eutectic phase is inhomogeneous. During high temperature treatment, a mass transport of the solute occurs from areas of high energy. The silicon atoms in the

matrix at locations A and B diffuse to location C, resulting in the dissolution of eutectic Si at A and B, and the precipitation of Si on the eutectic Si at C, as shown in Figure 4.4. This mass transport of silicon causes the fragmentation and spheroidization of eutectic silicon, both of which are dependent on the diffusion of both solute atoms and matrix atoms.

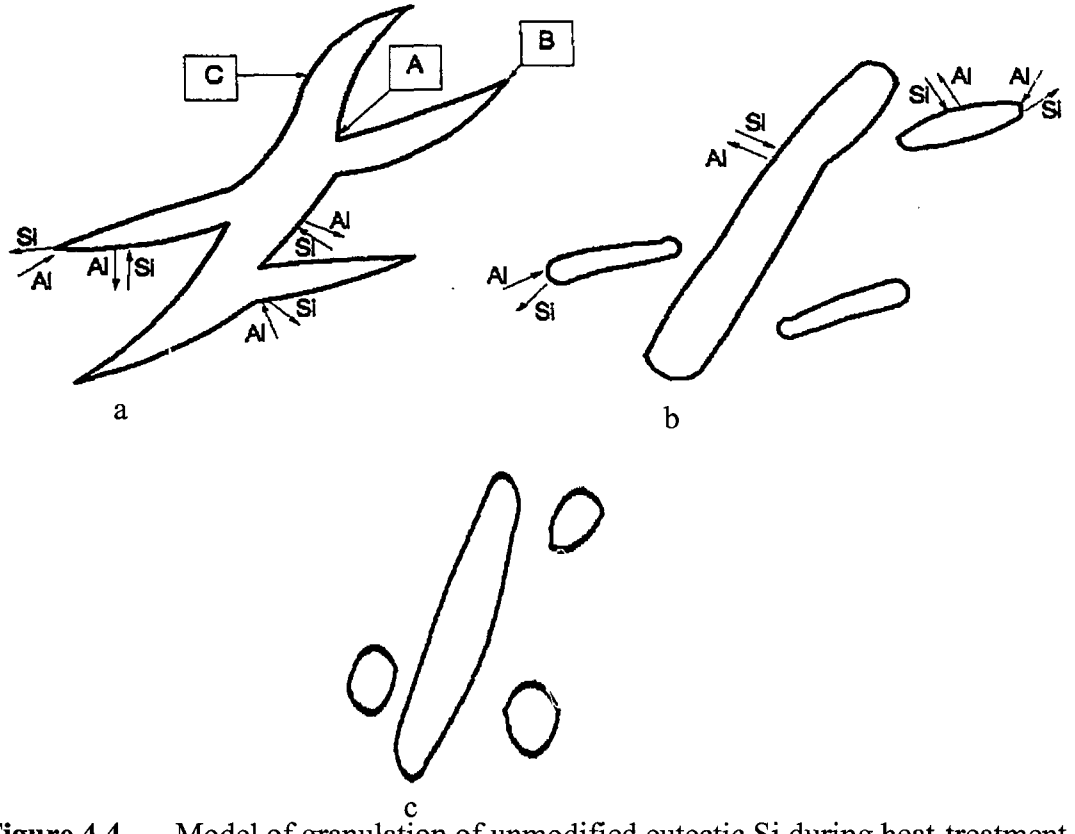

Figure 4.4 Model of granulation of unmodified eutectic Si during heat-treatment.[223]
(a) Transport of Si with cooperation of Al begins.
(b) Transport continues after fragmentation.
(c) Eutectic Si becomes spheroidized.

The microstructural changes occurring during solution heat-treatment of the as-received Al-10.8% Si alloy (R) are shown in Figure 4.1(b). Initially, the Si particles break down into smaller fragments and become gradually coarsened. From Figures 4.2(b) and 4.3(b), it may be observed clearly that modification has a profound influence on

spheroidization. In the modified alloys (RM and RGM), a high degree of spheroidization followed by coarsening occurs during solutionizing at 495°C. The microstructural changes resulting from solution heat-treatment originate from the instability of the interface between two phases. Plate-like eutectics are more resistant to interfacial instabilities and subsequent spheroidization than the fibrous kind. Thus, the rate of spheroidization is extremely rapid in modified alloys. Spheroidization and coarsening of the discontinuous phase occurs at elevated temperatures,[224] because the interfacial energy of a system decreases with the reduction in interfacial surface area per unit volume of the discontinuous phase. The reduction in interfacial energy is the driving force for the spheroidization and the coarsening processes which are also diffusion-controlled.[225,226] The degree of interconnection of the Si crystals is reduced as spherical and finely dispersed particles are obtained in the aluminum matrix. The changes in size and morphology of the discontinuous silicon phase are significant since they have a direct influence on the mechanical properties.

A number of researchers have proposed[223,227,228,229] that the spheroidization process of silicon through solution heat-treatment takes places in two stages: dissolution/separation of the eutectic branches and spheroidization of the separated branches. In the first stage, the Si particles are separated into segments at the corners of thin growth steps, but retain their flake-like morphology. In the second stage, the broken segments spheroidize and the aspect ratio decreases. The dissolution stage has the greatest effect on the time required to complete spheroidization and is strongly affected by the morphology of the Si particles; the smaller the flake length, the greater the spheroidization.[223,227] Any process which promotes eutectic branching, whether modification or higher cooling rate, will speed up the progress

of separation and spheroidization. Modification by addition of impurities tends to refine the eutectic Si greatly, to promote twin branching, to raise the energy state with its inhomogeneity, and consequently to promote the kinetics of the granulation of eutectic silicon. As Table 4.1 shows, after solution treatment of the RM and RGM alloys, the average Si-particle area, length, and roundness increase, while the aspect ratio and density decrease, compared to the as-cast condition, which may also be seen from Figures 4.2(b) and 4.3(b).

In the absence of a modifier, the density of the Si particles is seen to increase from 10096 to 14457 particles/mm^2 after solution heat-treatment. Due to the spheroidization process described previously, fragmentation of the eutectic Si takes place, and spheroidization of the separated branches begins. The rate of spheroidization is affected by the segment size; subsequently, the smaller particles eventually spheroidize and coarsen while other large ones continue to segment, thereby accounting for the smaller variations in particle density as obtained for the unmodified alloy compared to the modified specimens. The processes occurring during solution heat-treatment thus have an opposite effect on the number of particles per unit area in modified and unmodified eutectic structures. The combination of alloying elements and liquid alloy treatments is a satisfactory option for obtaining improved control of the microstructure during solidification and hence of improving the mechanical properties, and eliminating the need for heat treatment. Such an approach is likely to result in ultimately reducing production costs. In the course of this study, while investigating the effects of Fe-content on the microstructural aspects of an experimental Al-10.8%Si near-eutectic alloy, some very interesting observations

concerning the effect of the presence of Fe-based intermetallics on Si-modification in this alloy were noted. It can be observed that the average Si particle length, area, aspect ratio and roundness in the RF group of alloys are slightly affected by an increase in the level of Fe and Mn compared to the RGM alloy.

It is also clear that increasing the level of Cu and Mg leads to an increase in the average length and area of Si particles. In the as-cast condition, the Si-particle length increases from 2.69 μm (RGM alloy) to 3.11 μm (RC2 alloy, with 3.3% Cu and 0.35% Mg), and 5.16 μm (RC5 alloy, with 3.1% Cu and 0.6% Mg), while the average particle area increases from 2.67 μm^2 to 3.41 μm^2 and 7.46 μm^2, respectively. Moreover, the Si-particle aspect ratio increases from 2.11 (RGM) to 2.32 (RC5), *i.e.* by about 10%, due to the fact that both Mg and Cu react with the Si and Sr in the alloy to form $Mg_2Sr(Si,Al)$ and Al-Cu-Sr compounds, respectively. Thus, there is less Sr available to achieve the same level of modification in the eutectic Si particles than would be expected with the amount added (~150 ppm). The presence of Mg and Cu also affects the roundness ratio of the eutectic Si particles, as shown in Table 4.1. An increased Mg-content results in a clear reduction in the roundness ratio which is most pronounced at higher Cu contents (RC5 alloy). On the other hand, in the alloys containing low levels of Mg (~0.3%), increasing the level of Cu has a negligible influence on the roundness ratio. The effect becomes more significant as the Mg-content increases. Thus, from the point of view of these observations, the addition of Mg and Cu may be deemed to diminish the effect of Sr as a Si-particle modifier, and to decrease the particle density as a result. Figure 4.5 shows how the increase in the level of Mg and Cu hinders the modification effect of Sr when these elements are added to the

RGM alloy. The microstructures reveal that some Si areas are fully modified, whereas others are only partially modified.

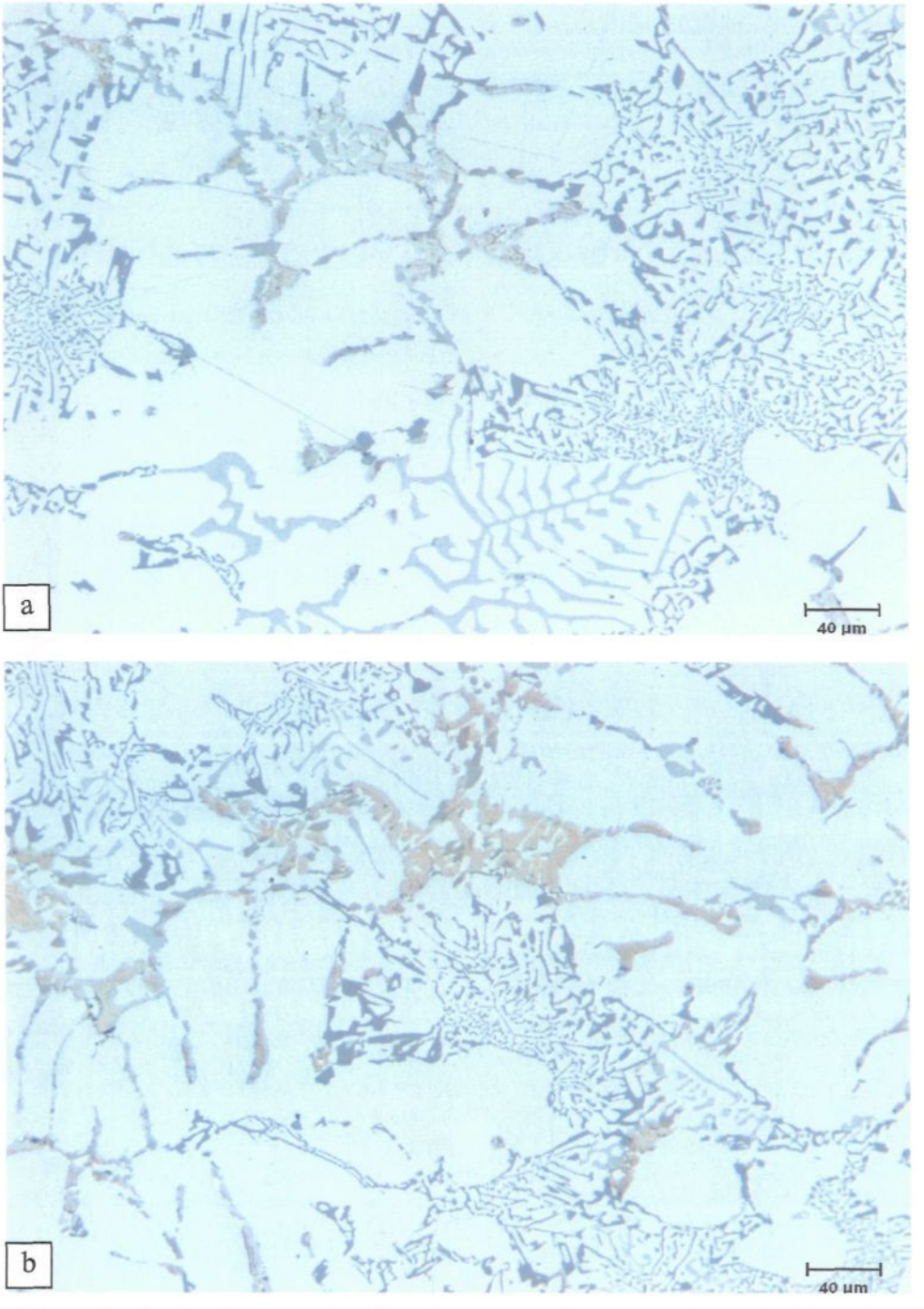

Figure 4.5 Optical micrographs showing the effects of Cu and Mg addition on Si morphology in as-cast (a) RC3, and (b) RC5 alloys.

After solution heat-treatment for 8 hours at 495°C, the Si particle area, length, roundness, aspect ratio and density remain more or less unchanged compared to the as-cast condition. If the experimental error and the standard deviation values listed in Table 4.1 are taken into account, it may be concluded that increasing the levels of Mg and Cu hinders the effect of solution heat treatment on the Si particles.

It is worthwhile noting that the R alloy exhibits the highest average values for particle area and length, whereas the RM alloy shows the lowest of all the alloys investigated. This implies that any further addition of alloying elements would decrease or weaken the effect of Sr as a modifier as a result of their interaction with Sr to form complex intermetallic compounds.

4.2.2 Intermetallic Phases

The separation of high melting-point intermetallic compounds from liquid metal may occur by means of precipitation and gravity segregation. These intermetallics are, in actual fact, solid solutions which have a substantial capacity for dissolving other elements. Although expressed by definite chemical formulae, these compounds exhibit a wide range of compositions and precipitation temperatures.[78]

Cáceres *et al.*[64] showed that an increased Si-content in Al-Si-Cu-Mg alloys does indeed have a size-refining effect on the β-Al_5FeSi platelets; this may be ascribed to the tendency in the alloys containing high levels of Si to form large particles of pre-eutectic β-Al_5FeSi and α-$Al_{15}(Mn,Fe)_3Si_2$ particles during solidification as a result of a reduction in the available growth period. The size-refining effect of a high Si-content is also evident in

other intermetallics such as α-$Al_{15}(Mn,Fe)_3Si_2$ and θ-Al_2Cu which form from the eutectic liquid in Al-Si-Cu-Mg alloys. Thus, the evidence suggests that an increased Si-content tends not only to refine the size of intermetallic particles but also to redistribute them into a more uniform dispersion within the intermetallic and intergranular regions compared with a lesser Si-content which promotes long clusters of intertwined particles along the grain boundaries. The growth and propagation of microcracks nucleated by the cracking of the intermetallics is therefore more difficult and involves greater local plasticity when the particles are further dispersed, increasing the tensile ductility for high Si-content alloys. It is known that the degree of Si-content may change the primary aluminum grain structure radically, from a globular morphology at Si-contents of less than ~6%, to an orthogonal dendritic structure at higher Si levels.[230] It has been suggested that these Si-induced morphological changes in the structure are responsible for the refining effect on the Cu- and Fe-rich intermetallic phases during solidification, in turn leading to the increase observed in tensile ductility.[133]

4.2.2.1 Iron-Rich Intermetallics

In addition to the silicon structure, another important consideration from the point of view of microstructure is controlling the Fe-content of the alloy. Accurate identification of the relatively coarse Fe-rich intermetallic phases commonly found in Al-Si casting alloys is also important, since some of these phases are associated with reduced mechanical properties. Figure 4.1(a) shows the microstructure of the R alloy in which the α-Fe phase appears in the form of small Chinese-script particles interspersed with Si particles; this

observation indicates that the α-Fe particles had precipitated in co-eutectic or post-eutectic reactions. When 150 ppm Sr is added to the base alloy (*i.e.* the RM and RGM alloys), the α-Fe phase precipitates in the form of a pre-dendritic phase, as shown in Figures 4.2(b) and 4.3(b).

The backscattered images shown in Figure 4.6 reveal the influence of iron concentrations, at each level of manganese, on the formation of different iron intermetallics. It is seen that when the Fe-content increases from ~0.5 wt% (RGM alloy) to 1 wt% (RF4 alloy), platelet-like β-Fe and Chinese-script α-Fe compounds form at low levels of manganese content. Upon increasing the manganese level (RF2 alloys), the Al(Fe,Mn)Si primary particles which precipitate directly from the liquid display a predominantly polyhedral shape; they are located within the α-Al dendrites, as shown in Figure 4.6(c), where the clear, sharp edges of the particle confirm that it has not been transformed into the α-script, as was reported elsewhere.[142,13] As mentioned previously, the presence of hard sludge particles within the soft α-Al dendrites should lead to a more uniform distribution of the stresses throughout the alloy matrix and, hence, to improved mechanical properties. This shows that the precipitation of sludge particles need not necessarily be harmful to the alloy, as is commonly perceived in the literature, where the sludge particles are usually observed in the interdendritic regions. This phenomenon of iron intermetallic precipitation within the α-Al dendrites proves very useful in the case of such Al-Si die-casting alloys as 380 alloy, containing 9% Si, where the proportion of α-Al dendrites is relatively higher.[191] The various phases shown in Figure 4.6 were analyzed

using wavelength dispersion spectroscopy (WDS) and the corresponding chemical compositions are listed in Tables 4.2 through 4.4, showing both the calculated formulae and the phases to which it is suggested that they correspond.

The polyhedral intermetallic compounds have the same chemical composition as the α-Fe phase and they remain unaffected by solution heat treatment, as shown in Figure 4.6(d). On the other hand, as shown in Figure 4.6(e), fragmentation of β-Fe due to the modification effect of Sr was observed, leading to a breakdown of the β needles into small thin fragments by means of two mechanisms: (i) splitting of the needle into two halves through the formation of longitudinal cracks, and (ii) fragmentation through Si rejection. These results are consistent with the research of Samuel *et al.*,[222] who reported that Sr has a poisoning effect on the nucleation sites for β-Fe needles. The partial dissolution of β needles becomes more pronounced after solution heat-treatment, as shown in Figure 4.6(f). These observations confirm the findings of Villeneuve and Samuel[231] on the fragmentation and dissolution of the β-Fe phase during solution heat-treatment of Al-13%Si-Fe alloys at 540°C.

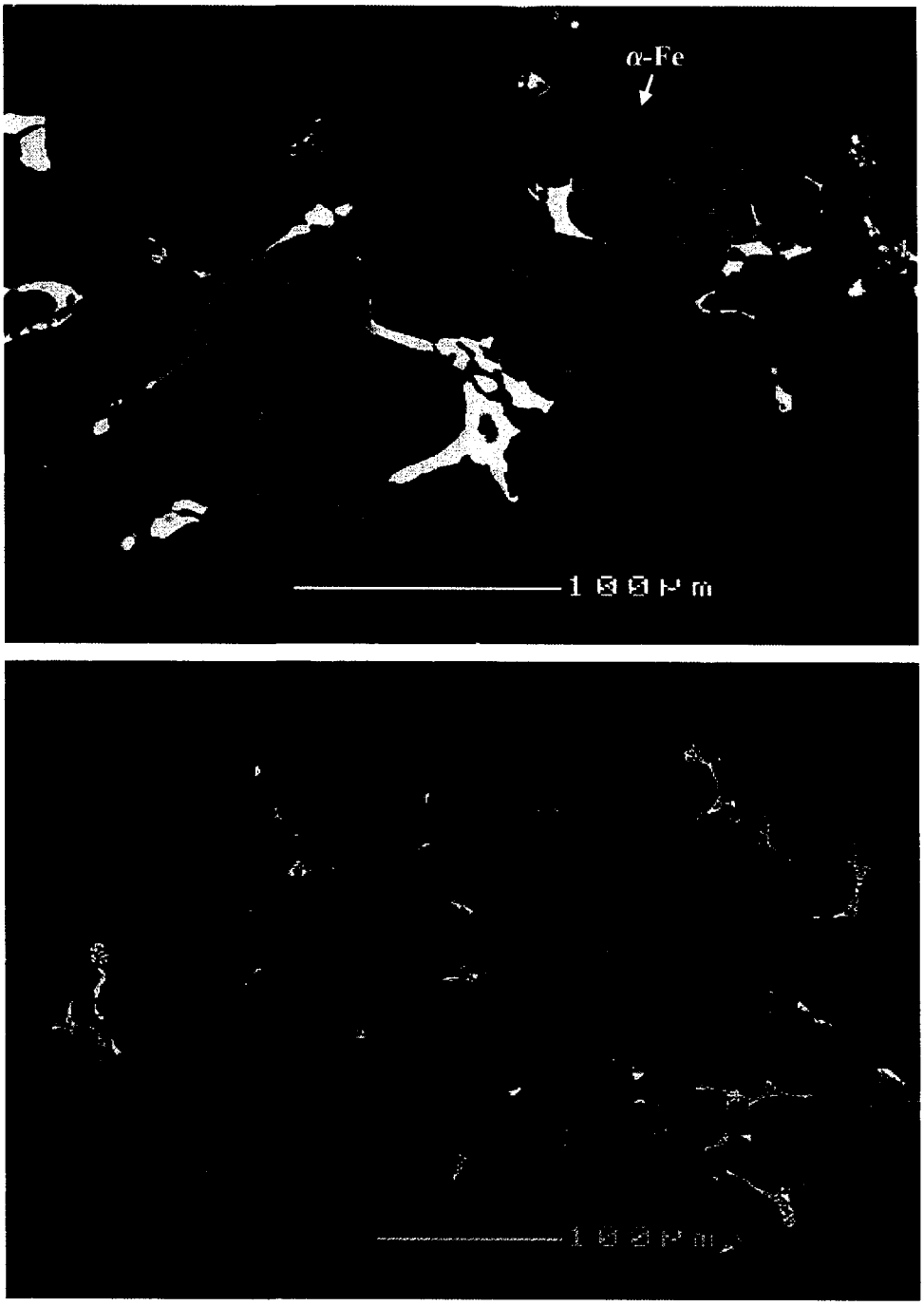

(b) Solution-treated RGM

Figure 4.6 ⟶ **Continued**

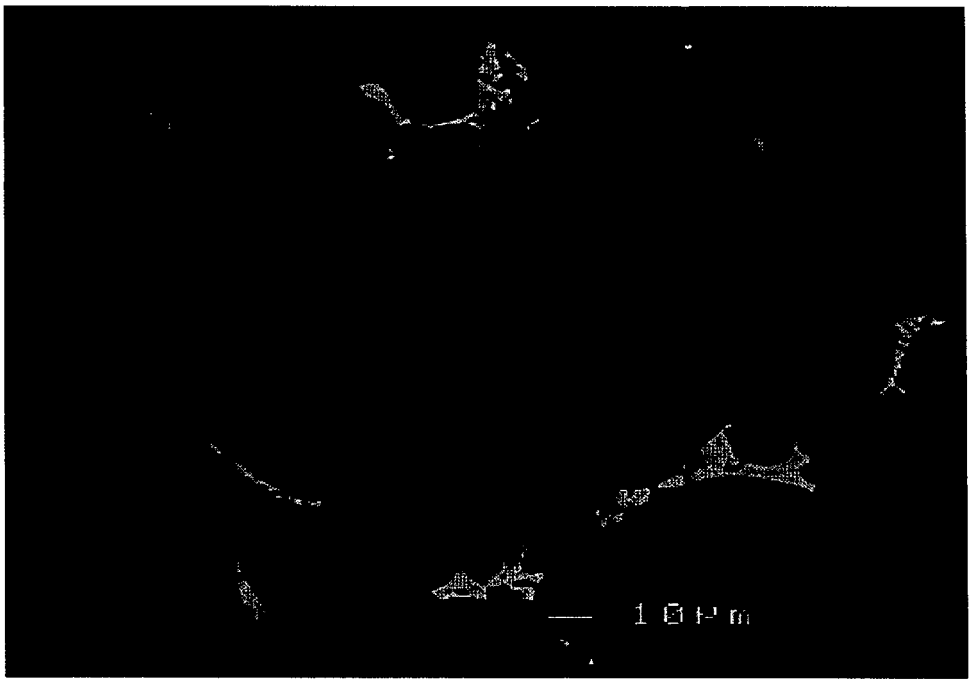

(c) As-cast RF2

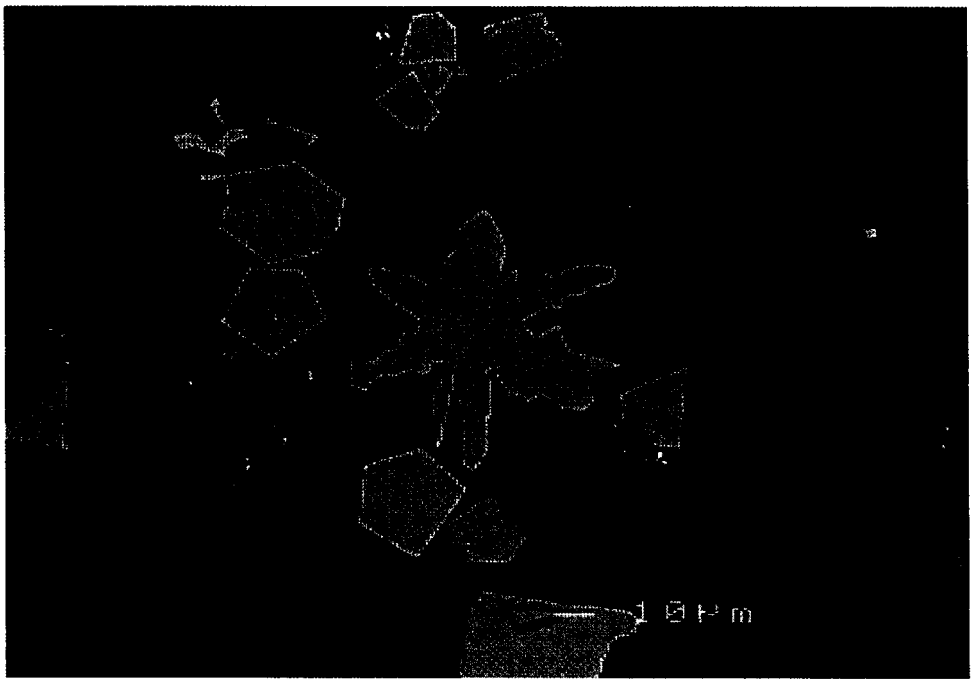

(d) Solution-treated RF2

Figure 4.6 ⟶ **Continued**

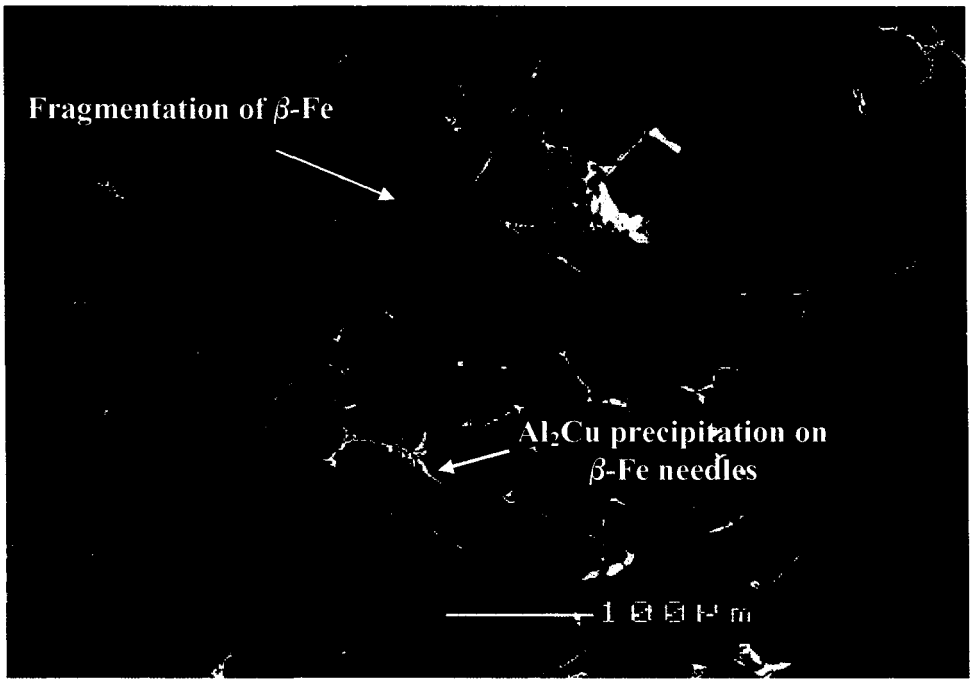

(e) As-cast RF4

(f) Solution-treated RF4

Figure 4.6 Backscattered images of Fe intermetallics observed in (a, b) RGM, (c, d) RF2, and (e, f) RF4 alloys in the (a, c, e) as-cast condition and (b, d, f) after solution treatment.

Table 4.2 Chemical composition of the intermetallics observed in as-cast RGM alloy

Phase	Element	Wt%	At%	Calculated formula	Shape & color	Suggested formula
α-Fe phase	Al	56.75	68.98	$Al_{12}Si_2(FeMnCu)_3$	Chinese-script, grey	$Al_{12}Si_2(FeMnCu)_3$
	Si	9.93	11.59			
	Fe	16.31	9.58			
	Mn	13.5	8.06			
	Cu	3.43	1.77			
	Total	99.92	99.98			
Cu phase	Al	48.17	67.16	$Al_{2.18}Cu$	Block-like, white	Al_2Cu
	Cu	52.03	30.80			
	Total	100.2	97.96			
AlSiCuMg phase	Al	15.83	16.78	$Al_{3.13}Cu_{1.74}Si_{5.7}Mg_8$	Small particles, grey	$Al_5Cu_2Si_6Mg_8$
	Si	29.96	30.51			
	Cu	20.74	9.33			
	Mg	36.42	42.84			
	Total	102.9	99.46			

Table 4.3 Chemical composition of the intermetallics observed in as-cast RF2 alloy

Phase	Element	Wt%	At%	Calculated formula	Shape & color	Suggested formula
α-Fe phase	Al	59.10	70.39	$Al_{12}Si_2(FeMnCu)_{3.1}$	Chinese-script, grey	$Al_{12}Si_2(FeMnCu)_3$
	Si	9.88	11.30			
	Fe	12.76	7.34			
	Mn	18.01	10.53			
	Cu	0.68	0.34			
	Total	100.43	99.90			
Sludge phase	Al	57.93	70.16	$Al_{12}Si_2(FeMnCu)_{3.1}$	Poly-hedral, grey	$Al_{12}Si_2(FeMnCu)_3$
	Si	9.70	11.28			
	Fe	12.51	7.32			
	Mn	18.18	10.81			
	Cu	0.66	0.34			
	Total	98.98	99.91			

Table 4.4 Chemical composition of the intermetallic observed in as-cast RF4 alloy

Phase	Element	Wt%	At%	Calculated formula	Shape & color	Suggested formula
α-Fe phase	Al	56.98	69.45	$Al_{12}Si_2(FeMnCu)_{3.2}$	Chinese-script, grey	$Al_{12}Si_2(FeMnCu)_3$
	Si	9.80	11.48			
	Fe	14.51	8.54			
	Mn	15.19	9.10			
	Cu	2.51	1.30			
	Total	98.99	99.87			
β-Fe phase	Al	55.89	64.89	$Al_5(FeMn)Si_{1.5}$	Needle-like, dark grey	$Al_5(FeMn)Si$
	Si	17.87	19.93			
	Fe	20.49	11.49			
	Mn	6.21	3.54			
	Total	100.4	99.85			

The volume fraction of iron intermetallics was plotted as a function of the amount of Fe and Mn added to the RGM alloy, as shown in Figure 4.7. It was found that this volume fraction increased with the addition of increasing levels of Fe and/or Mn addition. Also, the volume fraction of iron phases after solution heat-treatment came closer to their values in the as-cast condition for each Fe/Mn combination. These observations indicate that the α-Fe and sludge phases are not affected by solution heat-treatment. On the other hand, due to the partial dissolution and fragmentation of the β-Fe phase during solution heat-treatment, the volume fraction of iron phases decreased markedly at high levels of Fe and low levels of Mn (RF4 alloy) compared to the as-cast condition.

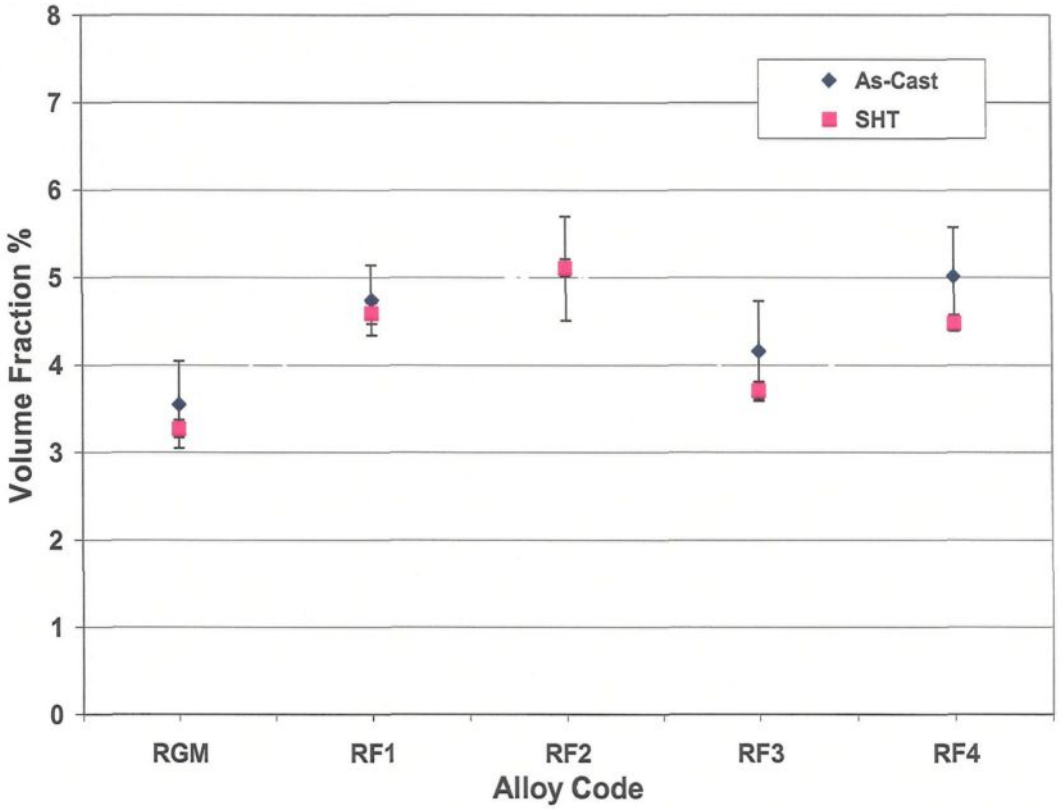

Figure 4.7 Volume fraction (%) of Fe intermetallics as a function of Fe and Mn additions to RGM alloy.

4.2.2.2. Copper-Rich Intermetallics

Copper forms the intermetallic phase Al_2Cu with aluminum which precipitates during solidification. Depending on the cooling rate and the local concentration of segregated Cu atoms, Al_2Cu may precipitate in a block-like form directly from the liquid, at a Cu concentration of ~53.5 wt%, especially in the presence of the β-Fe phase; or in the form of eutectic (Al + Al_2Cu); or, as in many cases, as a mixture of both.[232] Figure 4.1(a) shows the as-cast microstructure of the base R alloy, in which the copper phase is seen mainly as small pockets of the blocky Al_2Cu phase nucleating on pre-existing coarse Si particles. A similar observation was reported by Samuel *et al.*[11] The addition of Sr to the R alloy (RM and RGM alloys) leads to the segregation of the Al_2Cu particles in regions away from the growing Al-Si eutectic colonies, as shown in Figures 4.2(a), and 4.3(a). The backscattered image of the as-cast RF4 alloy (with ~1.0% Fe and 0.5% Mn), as seen in Figure 4.6(e), shows that the β-Fe needles and blocky Al_2Cu particles are connected to each other, indicating that the β-Fe needles act as nucleation sites for the copper phase particles.

In order to study the effects of solution heat-treatment, the volume fraction of the undissolved copper phase was measured for the various alloy samples/conditions. The amounts of the undissolved copper phase thus determined were plotted as a function of different alloying elements added to the RGM alloy and are presented in Figures 4.8 and 4.9. It can be observed that the quantity of the Al_2Cu phase after solution heat-treatment decreased abruptly for all alloys compared to other cases in the as-cast condition. About 78% of the total Al_2Cu phase was dissolved in the matrix of the RGM alloy; this observation was confirmed by subsequent examination of the microstructure.

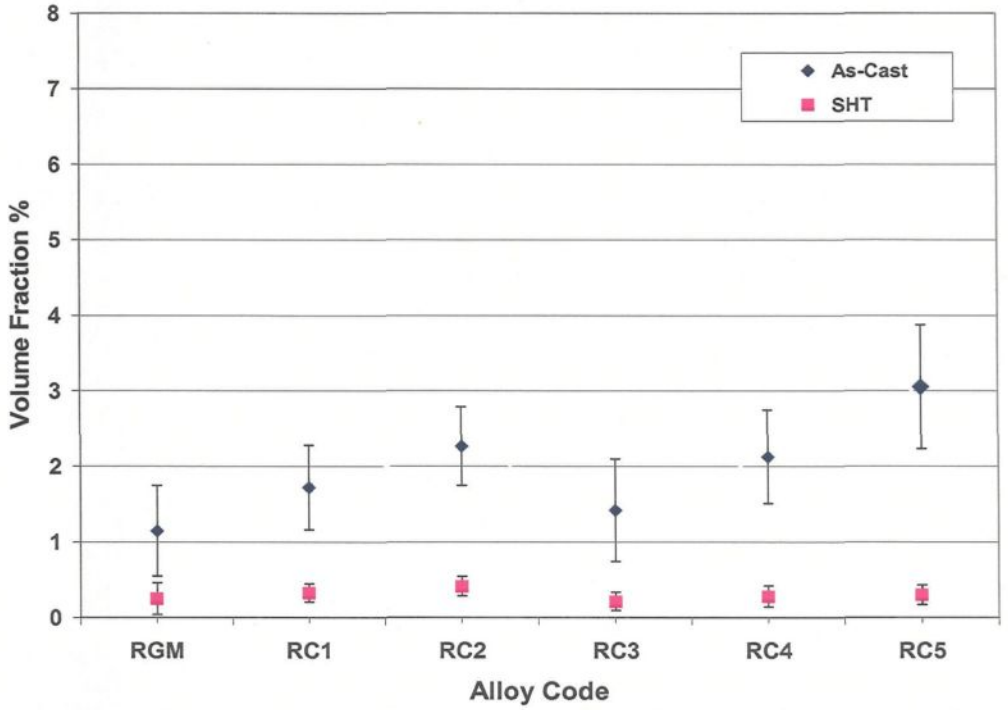

Figure 4.8 Volume fraction (%) of undissolved Cu intermetallics as a function of Cu and Mg additions to RGM alloy.

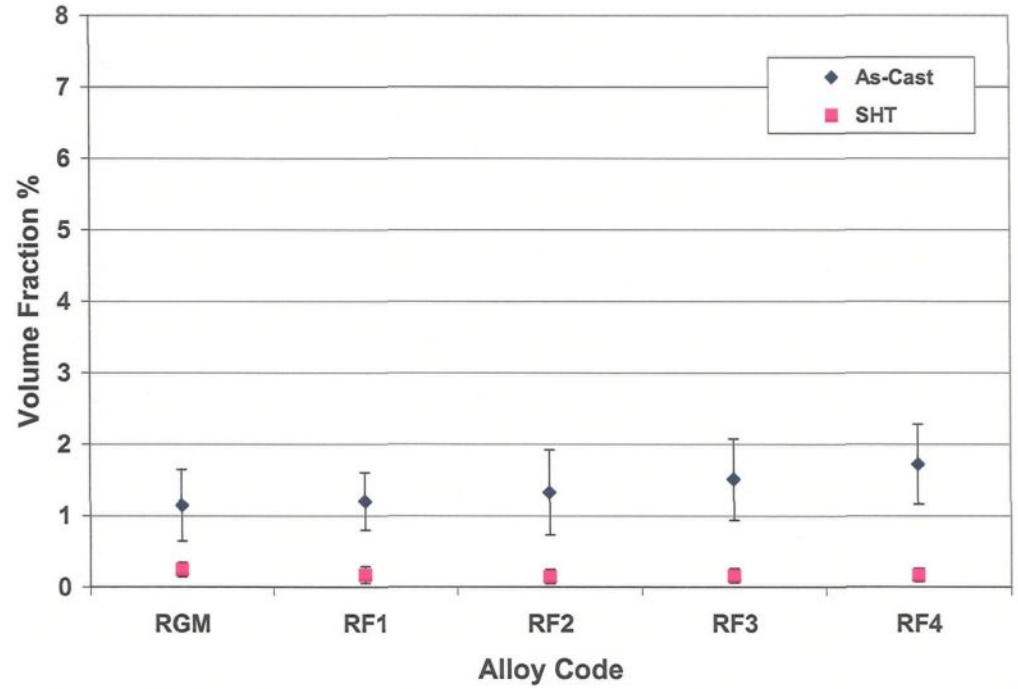

Figure 4.9 Volume fraction (%) of undissolved Cu intermetallics as a function of Fe and Mn additions to RGM alloy.

The highest dissolution of the Al_2Cu phase was observed in the solution-treated RF4 and RC5 alloys (90% in each case). As regards the RF4 alloy, the high level of iron (~1%) assisted in the dispersion of the Al_2Cu particles and the formation of the β-Fe phase which precipitated prior to the Cu-rich phase, thereby providing nucleation sites for the Al_2Cu particles, while also reducing both Al_2Cu phase segregation and, hence, the size of the Al_2Cu particles. Thus, during solution heat-treatment, these Al_2Cu particles would be much more easily dissolved as a result of the reduction in their size. The high degree of dissolution of the Al_2Cu phase in the RC5 alloy may be attributed to the presence of Mg (0.5 wt%) which lowers the temperature of eutectic Si and, consequently, that of all the subsequent reactions, leading to faster dissolution of Al_2Cu particles during solution heat-treatment. At the same time, it was also observed that during the process of dissolution, the Al and Cu concentrations in the Al_2Cu phase remain virtually stable. It may be concluded, therefore, that the dissolution of the Al_2Cu phase occurs by diffusion, into the surrounding matrix, of the Cu atoms located in the outer layer of the Al_2Cu phase particles, without changing the chemical composition of the remaining portion of the particles. Figure 4.10(a) shows a backscattered micrograph obtained of the RC3 alloy in the as-cast condition, whereas Figure 4.10(b) reveals almost complete dissolution of the phase after solution heat-treatment for 8 hours at 495°C. The white spots in Figure 4.10(b) point to traces of the undissolved Al_2Cu phase.

4.2.2.3 Al-Cu-Mg-Si Phases

In Al-Si-Cu-Mg systems, precipitation of $Al_5Cu_2Mg_8Si_6$ is reported to take place at the end of the Al-Al_2Cu eutectic reaction.[191] In most cases, this phase appears in the form of small grey particles growing out of the Al_2Cu phase particle clusters as shown in Figure 4.11 which represents a high magnification backscattered image of the RGM alloy. The distribution of Cu- and Mg-containing particles is shown in Figures 4.12(a) and (b), respectively. The amount of the phase is found to increase progressively with an increase in Mg-content, see Figure 4.10(a). It is interesting to observe the persistence of this phase after solution heat-treatment, as shown in Figure 4.10(b) and the WDS analysis of the phase is provided in Table 4.5. It should be mentioned that the WDS analysis of these particles revealed an unexpectedly higher concentration of aluminum, by 3 wt%, than that obtained for the as-cast condition. This observation may be an indirect indication of the sluggish dissolution of the $Al_5Cu_2Mg_8Si_6$ phase during solution heat-treatment.

Table 4.5 Chemical composition of the Cu-intermetallic phases in RC3 alloy

Phase	Element	Wt %	At. %	Calculated formula	Shape & color	Suggested formula
Cu phase (As-cast)	Al	48.57	67.30	$Al_{2.18}Cu$	Block-like, white	Al_2Cu
	Cu	52.25	30.74			
	Total	100.8	98.04			
AlCuMgSi phase (As-cast)	Al	16.12	17.20	$Al_{3.2}Cu_{1.7}Si_{5.7}Mn_8$	Small particles, grey	$Al_5Cu_2Si_6Mg_8$
	Si	29.73	30.45			
	Cu	20.09	9.10			
	Mg	36.16	42.79			
	Total	102.1	99.54			
AlCuMgSi phase (solution treated)	Al	16.61	17.72	$Al_{3.4}Cu_{1.7}Si_{5.8}Mn_8$	Small particles, grey	$Al_5Cu_2Si_6Mg_8$
	Si	29.78	30.52			
	Cu	20.09	9.10			
	Mg	35.40	41.93			
	Total	101.8	99.27			

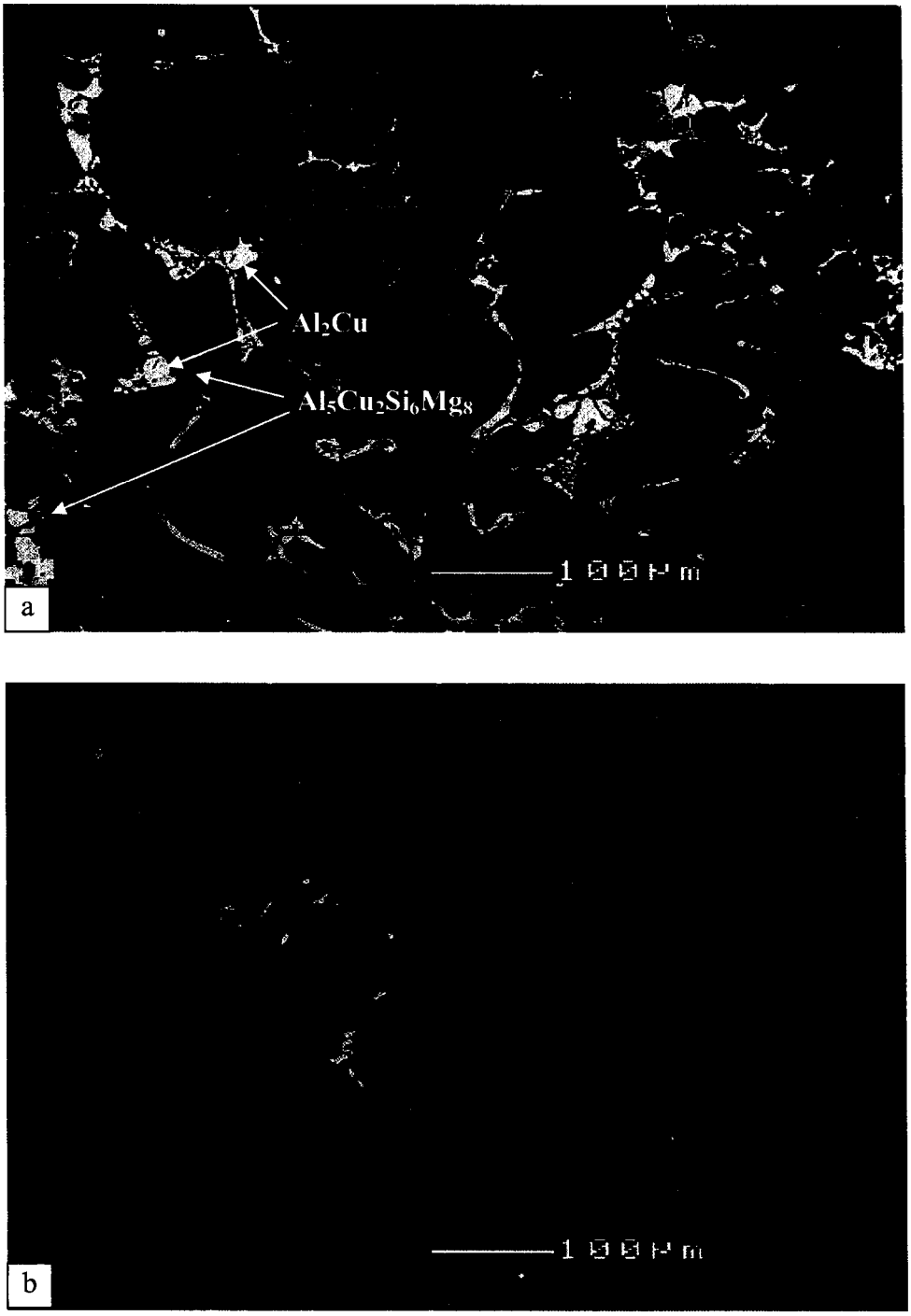

Figure 4.10 Backscattered images showing Al_2Cu and AlCuMgSi phase particles observed in: (a) as-cast; and (b) solution-treated RC3 alloy.

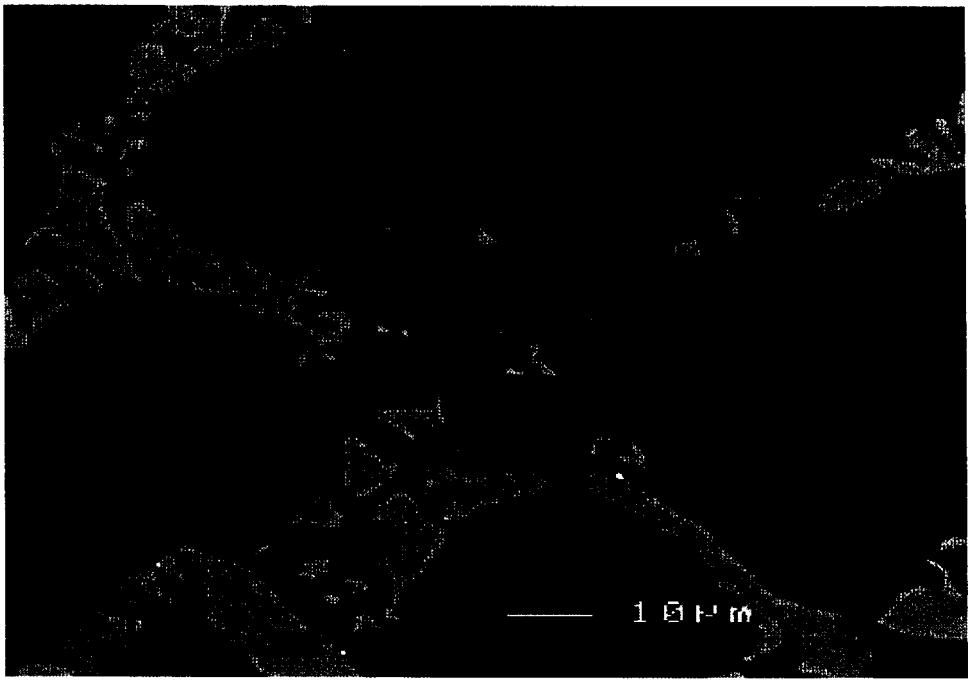

Figure 4.11 High magnification backscattered image taken of RGM alloy in as-cast condition showing Al_2Cu and AlCuMgSi phase particles.

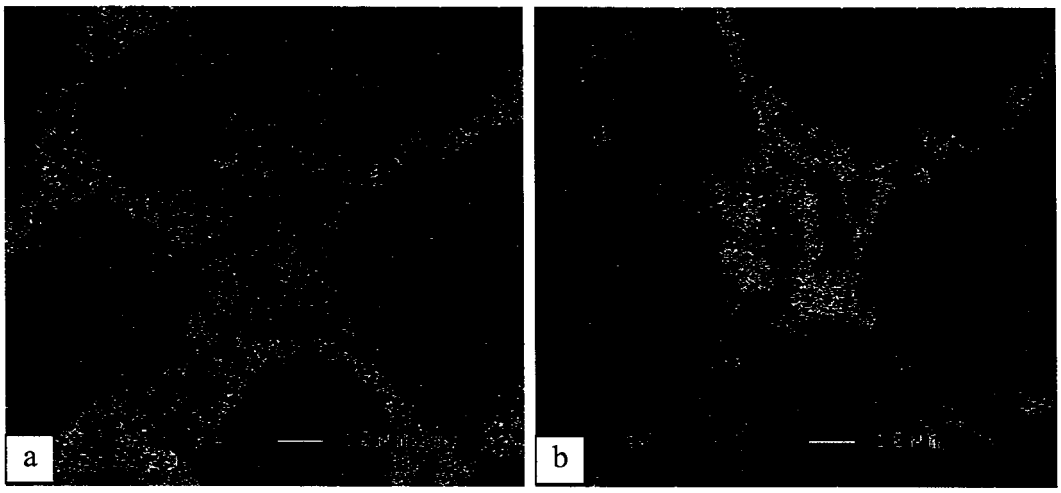

Figure 4.12 X-ray images of (a) Cu, and (b) Mg, corresponding to the backscattered image shown in Figure 4.11.

4.3 POROSITY MEASUREMENTS

There are several factors which affect porosity formation in Al-Si alloys. Alloying is a factor which can seriously complicate the study of porosity since alloying influences almost every aspect of the solidification process as well as a variety of metallurgical, physical and chemical properties. Changes from one alloy to another may cause considerable confusion in the study of porosity since the results are often not comparable. For the purposes of the current study, porosity characteristics were analyzed and quantified using a Leco 2001 image analyzer in conjunction with an optical microscope. Figure 4.13 and Table 4.6 provide pertinent data for various alloy samples in the as-cast condition with regard to the percentage surface porosity which may be defined as the area fraction of porosity observed on a measured sample surface area. It should be noted here that in all of the cases, the liquid metal was continuously degassed prior to casting in order to minimize the effects of gas- and inclusion-related porosity. The Sr-modified RM alloy is characterized by a higher porosity level than the unmodified R alloy (cf. 0.19% with 0.11%). It is worthy of note that the percentage surface porosity is, in fact, a multiple of the pore density and the average pore size. Thus, the increase in percent porosity observed in the Sr-modified RM alloy may be due to an increase in pore density and/or pore size. The increased porosity of the Sr-modified RM alloy can cause a reduction in the mechanical properties in contrast with the unmodified R alloy, even though the eutectic Si has been modified.

As mentioned previously in Chapter 2, grain refining has several advantages, including the redistribution and reduction of porosity. Grain refinement of a casting may

alter the amount and the morphology of pores in a casting; in many cases, there is also an overall reduction in the amount of porosity in alloys containing small or moderate amounts of gas.[126,127,128] The combined addition of grain refiner and modifier to the R alloy causes no significant variation observable in the percentage surface porosity, as shown in Figure 4.13.

The introduction of Mn to the RGM alloy results in the occurrence of fine pores from the precipitation of Fe in the form of the α-Chinese script phase. The contour of these script particles facilitates the filling up with liquid metal of the space in between the dendrite arms of the particles, as opposed to the blocking action of the β-phase platelets. In fact, Table 4.6 shows that the Mn-containing RGM alloy, *i.e.* RF1 and RF2 alloys, reveals porosity values comparable with those obtained from the base R alloy.

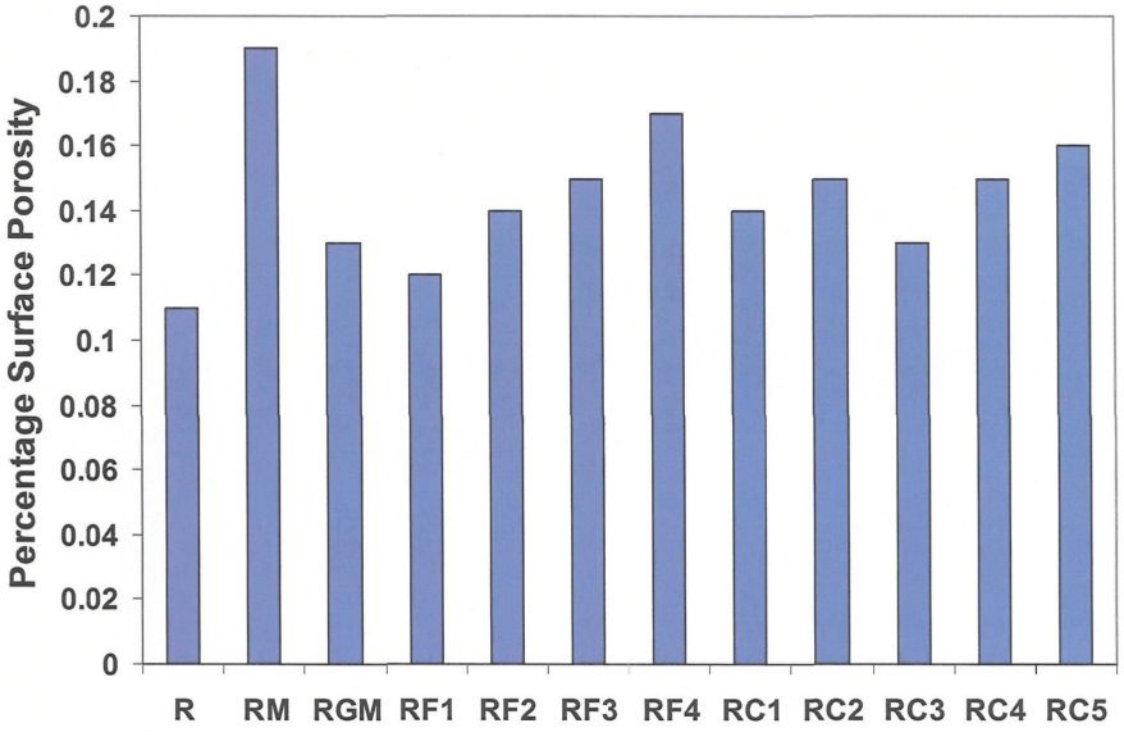

Figure 4.13 Percentage surface porosity as a function of the addition of alloying elements in as-cast conditions for an experimental Al-10.8%Si alloy.

Table 4.6 Percentage surface porosity in samples obtained from various alloys

Alloy Code	Addition	Surface Porosity (%)
R	No addition	0.11
RM	R alloy + 0.015% Sr	0.19
RGM	RM alloy + 0.25% Ti	0.13
RF1	RGM alloy + 0.25% Fe + 0.25% Mn	0.12
RF2	RGM alloy + 0.5% Fe + 0.5% Mn	0.14
RF3	RGM alloy + 0.25% Fe	0.15
RF4	RGM alloy + 0.5% Fe	0.17
RC1	RGM alloy + 0.5% Cu	0.14
RC2	RGM alloy + 1% Cu	0.15
RC3	RGM alloy + 0.5 Mg	0.13
RC4	RGM alloy + 0.5% Cu + 0.5 Mg	0.15
RC5	RGM alloy + 1% Cu + 0.5 Mg	0.16

A recent study by Edwards *et al.*[233] shows that the content of dispersed microporosity increases by a factor of about 4 when Cu is added to a Cu-free Al-Si-Mg alloy. They concluded that the increase in porosity which was observed can be ascribed to two main factors: (i) Cu results in a ternary reaction Liq → α-Al + Si + $CuAl_2$ at about 525°C, resulting in pools of ternary liquid which solidify when the bulk of the casting is already solid making them difficult to feed; in addition, since Cu accumulates to high levels in the eutectic liquid, the volumetric shrinkage during solidification increases; (ii) an increase in the equilibrium hydrogen gas pressure associated with a given amount of dissolved gas when Cu is present in the interdendritic liquid.[234] These authors also observed that, while the addition of 1% Cu increased the porosity to 0.7% (from 0.1% in the Cu-free alloy), increasing the Cu level beyond 1%, only resulted in a relatively small increase in porosity. They proposed, therefore, that an increase in the amount of porosity observed in their alloys does not depend on the concentration of Cu provided the Cu level is above a

certain amount. Figure 4.13 shows the percentage surface porosity, as measured using image analysis, for the different Cu and/or Mg levels. It can be observed that porosity in the RC group of alloys is hardly affected or, at most, affected only very slightly by the addition of Cu and/or Mg, as pointed out by Edwards *et al.*[233]

4.4 HARDNESS

Hardness measurements were done to assess the changes occurring in the aluminum matrix and eutectic silicon due to of the addition of modification, grain refinement, and alloying elements. These measurements were carried out on polished samples in as-cast and heat-treated conditions. The average values as well as standard deviations are presented in Table 4.7. The standard deviations, indicating the variation from one reading to another in each category, are relatively low and typical of hardness testing in general.

4.4.1 Effects of Melt Treatment

In order to study the effect of melt-treatment additions (*i.e.* grain refining and modification) and heat treatment on alloy hardness, the unmodified R alloy was compared with Sr-modified RM alloys, as shown in Table 4.7. The results indicate that, in the as-cast condition, the decrease in alloy hardness with Sr addition is less than 2%, due mainly to a change in the morphology of the eutectic Si particles. Also, Sr leads to the formation of porosity and to a depression in the eutectic temperature, causing a shift of the eutectic point to a higher Si content, in turn resulting in an increase in the amount of soft α-Al formed. All these factors lead to a noticeable decrease in the alloy hardness.[235] On the other hand,

the grain refined Sr-modified RGM alloy exhibits a slight increase in hardness compared to the R alloy. This increment may be attributed to two reasons: (a) the poisoning effect of Si on the α-Al nucleation process due to the formation of titanium silicide over $TiAl_3$ particles when the Si level is higher than 7 wt%;[107] and (b) the poisoning effect of Al-5Ti-1B grain refiner on Sr modification due to the interaction between Sr and Ti.[4]

Table 4.7 Comparison of hardness and tensile properties of as-cast and solution-treated alloys

Alloy code	Solution time, hr	HBN (MPa)	YS (MPa)	UTS (MPa)	El (%)	Q (MPa)
R	0	77.8 ± 1.38	196.8 ± 15.7	277.2 ± 24.8	1.703 ± 0.11	311.9 ± 10.5
	8	82.4 ± 1.60	220.5 ± 2.45	329.5 ± 4.6	3.31 ± 0.23	407.5 ± 11
RM	0	76.2 ± 1.24	196.5 ± 5.5	290.2 ± 16.8	1.961 ± 0.36	334.0 ± 19
	8	81.2 ± 1.44	213.5 ± 4.0	321.5 ± 14.86	3.46 ± 0.27	402.36 ± 29
RGM	0	79.5 ± 0.1	210.5 ± 2.34	295.7 ± 8.4	1.964 ± 0.25	339.67 ± 8.6
	8	84.6 ± 1.7	221.9 ± 5.16	331.6 ± 15.9	3.749 ± 0.34	417.6 ± 16.3
RF1	0	79.6 ±0.52	208.6 ± 6.6	312.5 ± 8.6	1.825 ± 0.3	351.7 ± 8.9
	8	84.8 ±1.19	225.7 ± 5.4	341.0 ± 11.3	3.184 ± 0.33	393.7 ± 11.6
RF2	0	80.0 ± 0.68	207.4 ± 15.3	296.8 ± 20	1.592 ± 0.29	327 ± 20.3
	8	85.2 ± 1.11	228.3 ± 1.8	317.6 ± 11	1.821 ± 0.32	345 ± 11.3
RF3	0	83.6 ± 1.1	209.0 ± 4.8	322.0 ± 9.9	1.779 ± 0.24	359.7 ± 10.15
	8	88.3 ± 1.27	230.7 ± 2.2	344.71 ± 14.2	3.077 ± 0.48	396 ± 14.7
RF4	0	89.0 ± 1.43	200.2 ± 12.4	280.0 ± 19	1.335 ± 0.23	298.7 ± 19.2
	8	92.0 ± 0.63	212.0 ± 6.2	316.6 ± 21	1.685 ± 0.38	340.4 ± 21.4
RC1	0	82.0 ± 1.77	215.8 ± 5.6	297.0 ± 9.12	1.418 ± 0.08	319.7 ± 9.2
	8	86.2 ± 1.99	260.2 ± 8.0	355.52 ± 7.4	3.6 ± 0.07	439 ± 7.5
RC2	0	85.6 ± 0.01	229.3 ± 6.0	299.7 ± 12.4	1.117 ± 0.15	307 ± 12.6
	8	88.3 ± 2.21	262.0 ± 8.0	365.7 ± 8.5	2.47 ± 0.19	424.6 ± 8.7
RC3	0	86.8 ± 0.76	190.8 ± 12.0	291.4 ± 7.5	1.649 ± 0.18	324 ± 7.7
	8	90.8 ± 0.63	222.7 ± 9.3	321.3 ± 16	2.306 ± 0.21	375.7 ± 16.2
RC4	0	89.4 ± 1.52	197.5 ± 19.4	291.7 ± 19.6	1.224 ± 0.04	304.8 ± 19.6
	8	95.3 ± 1.76	225.8 ± 1.2	321.7 ± 8.0	2.106 ± 0.23	370.2 ± 8.2
RC5	0	93.4 ± 0.98	198.9 ± 11.5	292.2 ± 10.4	1.113 ± 0.04	299.1 ± 10.4
	8	99.2 ± 2.69	233.2 ± 2.8	326.4 ± 19.6	1.974 ± 0.53	370.7 ± 20.1

It is clear that the hardness of the alloy is affected by each step involved in heat-treatment, namely, solution treatment and artificial aging. As expected, artificial aging

increases the hardness as a result of the formation of coherent precipitates in the matrix. The modified RM alloy exhibits slightly lower hardness values with respect to its unmodified counterparts after precipitation.

After solution treatment, the grain-refined Sr-modified RGM alloys exhibit higher hardness levels compared to the unmodified R alloy. In addition to the homogeneity in composition achieved with solution treatment, the evolution of the eutectic silicon morphology may also influence the strengthening of the alloy, where the unstable eutectic silicon modified by Sr dissolves and is fragmented due to the thermal effect.

Figure 4.14 illustrates the variation in hardness of the R, RM, and RGM alloys as a function of aging temperature. It can be observed that peak hardness is obtained at 180°C for all melt treatments/alloys. It can also be observed that the RGM alloy shows a significant improvement in hardness at all aging temperatures compared to the base R alloy. The maximum hardness value is about 125 MPa, corresponding to aging at 180°C. This implies that the combined effect of modification, grain refinement and heat treatment is excellent for obtaining superior hardness values compared to those exhibited by the untreated as-cast alloy. These changes in hardness are due mainly to the size, shape and distribution of the Al_2Cu precipitates during aging. Aging at 200°, 220°, and 240°C showed a marked decrease in the hardness values compared to those obtained at 180°C. Increasing the aging temperature increases the size of these precipitates, with a gradual change occurring in their chemical composition. As a result, the equilibrium phase (θ-Al_2Cu) in the form of incoherent particles is responsible for the drop observed in alloy hardness.

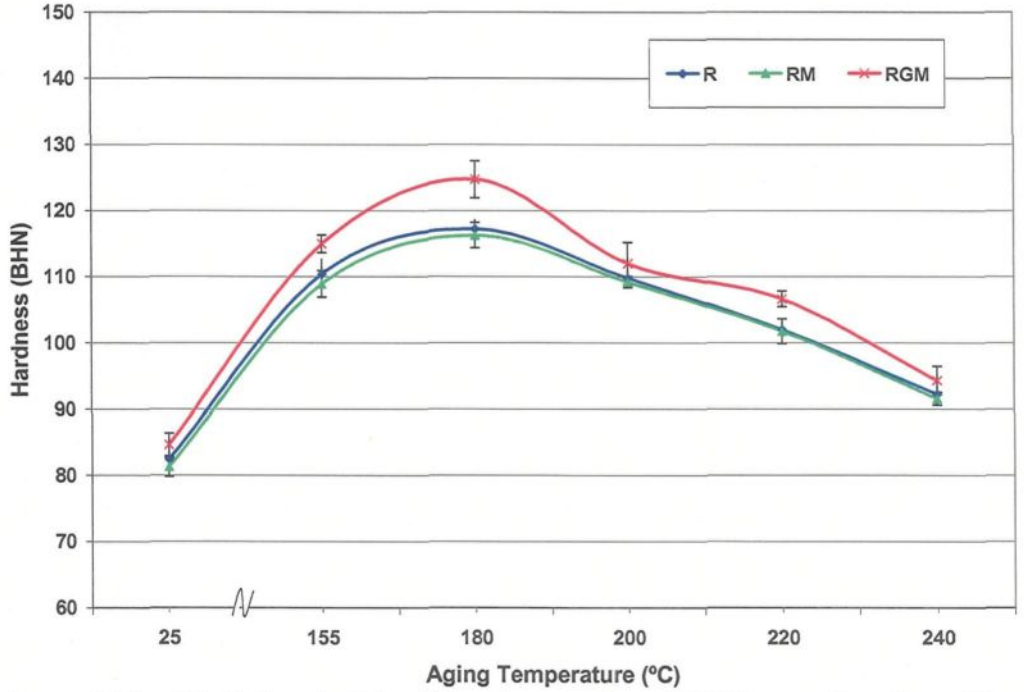

Figure 4.14 Variation in Brinell hardness values (BHN) as a function of heat-treatment conditions.

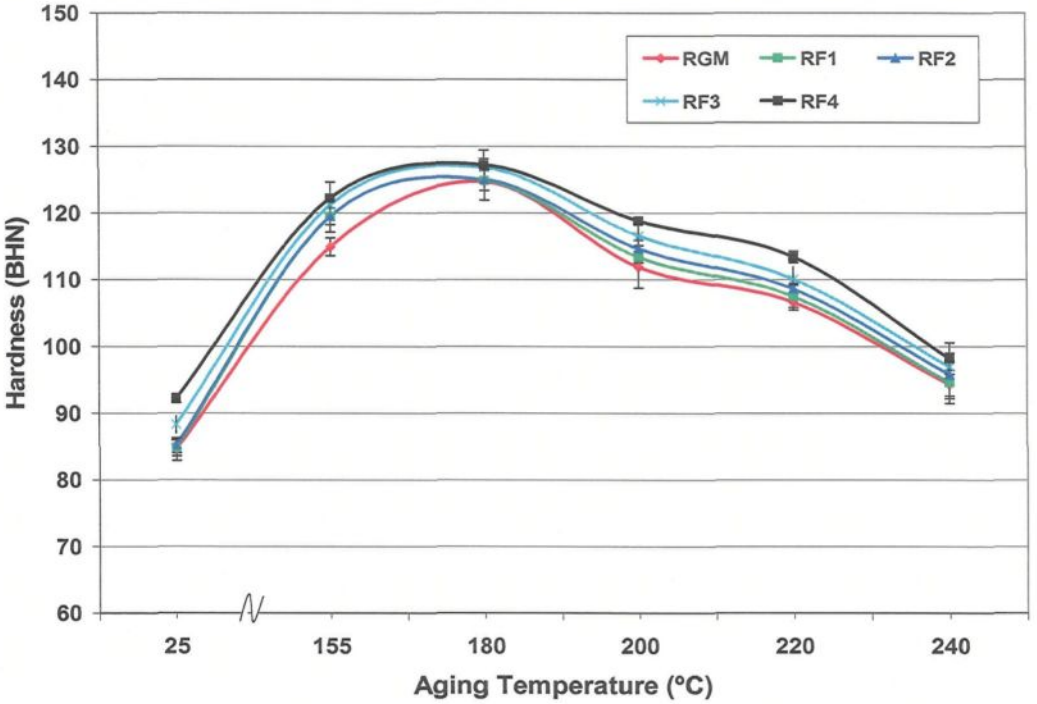

Figure 4.15 Variation in Brinell hardness values (BHN) as a function of heat-treatment conditions.

4.4.2 Effects of the Addition of Fe and Mn

From Table 4.7 it may be observed that in the as-cast condition, an increase in Fe and/or Mn content from 0.5 to 1% results in a gradual increase in hardness. In general, hardness values reflect a combination of the yield strength (YS) and work-hardening rate. Thus, a higher hardness value could result even if the YS is lower, provided that the strain-hardening rate is higher. This means that the work-hardening rate in the RF4 alloy is higher compared to the RGM alloy. The Orowan mechanism is known to lead to higher hardening rates in comparison with, for example, obstacle shearing.[236] In this mechanism, the yield stress is given by the shear stress required to bow a dislocation line between two precipitates separated by a distance λ. The same results were obtained after solution heat-treatment. The results of aging studies conducted on the RGM alloy, which is used here as a reference, with different additions of Fe and Mn, are shown in Figure 4.15. Variation in hardness with aging temperature is found to follow the same trend for all the alloys. A comparison of the peak hardness values at 180°C shows that the RF4 alloy reveals the highest hardness.

4.4.3 Effects of the Addition of Cu and Mg

The properties of alloys may be improved by adding Cu and Mg to them. Singh *et al.*[237] proposed an empirical equation to determine the effects of Cu, Mg, Si, solutionizing temperature, aging temperature and aging time on the hardness of Al-Si-Cu-Mg alloys. Their results indicate that both Cu and Mg tend to enhance the strength properties of as-cast and heat-treated alloys. Among the various interactions, those occurring between Mg and

Si, and between Mg, Cu and Si are the most significant. During solution treatment, alloying elements dissolve completely to form a supersaturated solid solution as a result of high temperature diffusion. The morphology of the eutectic silicon, however, undergoes significant changes, thereby influencing the mechanical properties greatly.

Table 4.7 summarizes the combined effects of Cu and Mg content on the hardness of the RGM alloy and the various RC alloys developed from it. It is clear that there is no marked difference in the hardness of the as-cast and solution-treated samples to be observed, thus emphasizing the influence of high solidification rates in maximizing the solubility of Cu and Mg in the Al matrix, and also improving alloy strength considerably upon subsequent aging. A recent electron-microscopy study by Reif *et al.*[238] produced a comparison of the precipitation behavior of Al-9%Si-3.5%Cu and Al-9%Si-4%Cu-0.5%Mg alloys. The strengthening observed in the ternary Al-Si-Cu alloy after aging at 160°C was attributed to the formation of θ'-Al_2Cu plates, also no Si-containing precipitates could be identified. The precipitation hardening in the quaternary Al-Si-Cu-Mg alloy was ascribed to the simultaneous formation of relatively large θ' plates and small S'-Al_2CuMg needles, again without the contribution of β''-Mg/Si or other Si-containing precipitates. Figure 4.16 shows the combined effects of Cu and Mg content with aging temperature on the RGM alloy. It is observed that the addition of Cu and Mg has the effect of improving the peak-aging hardness of the RGM alloy. For each alloy, the hardness first increases with an increase in aging temperature of up to 180°C, decreasing thereafter as the aging temperature increases further. The increase in hardness with the addition of Cu and Mg may be attributed to the formation of the hard and brittle (metastable) intermetallic phases Al_2Cu

and Al_2CuMg, and also to an increased bonding of the silicon particles with the matrix, where the thermal energy is sufficient to precipitate such intermediate phases as are coherent with the matrix. The decrease in hardness at aging temperatures above 180°C may be attributed to the coarsening of the various microconstituents and to a decrease in cohesion with the matrix. The coarsening of hard intermetallic phases may reduce the barrier to dislocation movement and, hence, to flow stress/hardness.

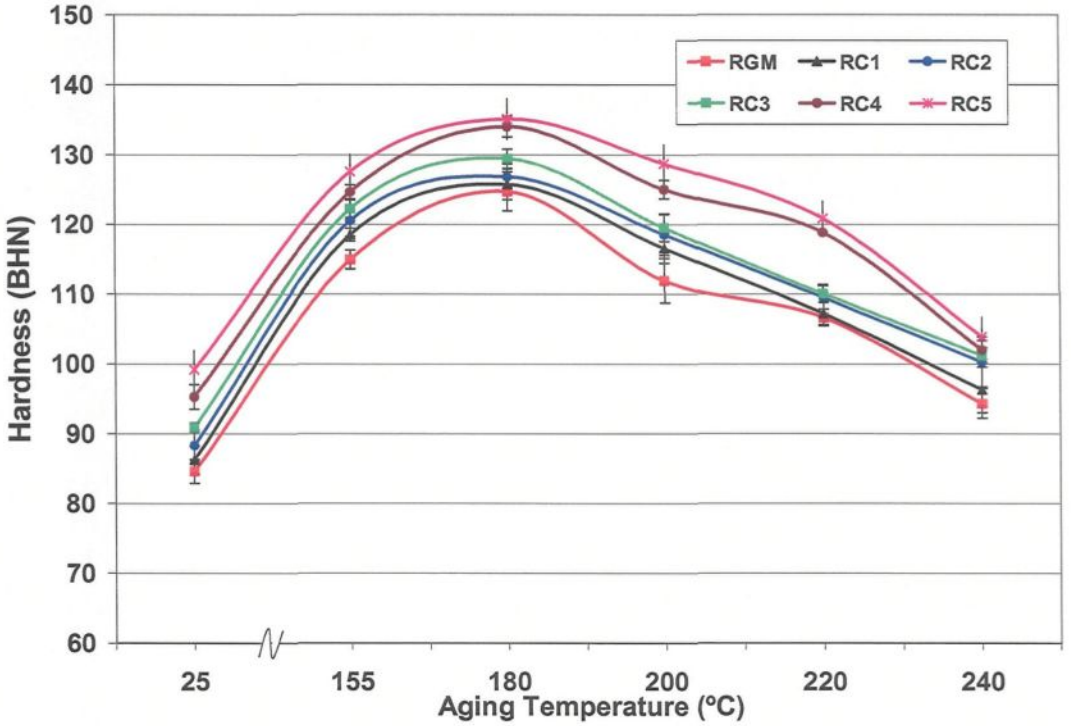

Figure 4.16 Variation in Brinell hardness values (BHN) as a function of heat-treatment conditions.

The effect of increasing the Mg content to 0.5% at different levels of Cu produces higher hardness values than those obtained for alloys containing 0.3% Mg, indicating that hardening which results from Al_2CuMg precipitation adds to that achieved due to Al_2Cu precipitation. This is also evident from a comparison of the amounts of Cu and Mg present

in the two alloys: ~2.25% Cu and ~0.5% Mg in the RC3 alloy *vs.* ~3.25% Cu and ~0.3% Mg in the RC2 alloy. In the RC5 alloy, which contains ~3.25 wt% Cu, and ~0.5 wt% Mg, the peak hardness value is seen to increase slightly by about 10% at 180°C, compared to the RGM alloy. This may be interpreted in terms of the formation of complex insoluble phases, such as $Al_5Mg_8Si_6Cu_2$, which decrease the amount of free Mg and Cu available for further hardening during the aging process, as discussed previously.[239]

4.5 TENSILE PROPERTIES

Alloys containing more than one phase in the presence of a eutectic owe their tensile properties firstly to the eutectic matrix and secondly to the primary pre-eutectic phases. The tensile properties of casting alloys are affected mainly by their microstructure, grain size, and defects. The fact that tensile properties depend on several, often interrelated, variables may explain the confusion which exists relating to the properties of cast Al alloys. The tensile properties may be determined from separately-cast test bars or from coupons cut from castings where the properties ascertained from the coupons are generally inferior to those measured on separately-cast bars.

4.5.1 Effects of Melt Treatment

The acicular morphology of the Si platelets in the eutectic, as shown in Figure 4.1(a), promotes the development of stress raisers at the edge tips in the softer phase, leading to low ductility in the unmodified alloy. This is thought to occur by a simple void formation mechanism at the Si-needle edges of the eutectic, leading rapidly to crack

formation by void coalescence. The modification of the alloy structure through the addition of Sr leads to the development of a granular eutectic structure, as shown in Figure 4.2(a). The Si phase in the eutectic develops into a globular structure and improves the mechanical properties considerably by virtue of an even distribution of the stress around these hard particles. This geometrical change also leads to the disappearance of stress raisers. The surface area per unit volume of Si in the eutectic decreases, thus favoring the isotropic distribution of the strain in the α-Al phase in the eutectic. The addition of Ti and Sr enhances the favorable effects of both elements in the microstructure, thereby leading to a general improvement in the tensile properties compared to the untreated base alloy.

Table 4.7 shows the variation in tensile properties (*i.e.* YS: 0.2% proof stress, UTS, and %El) in as-cast and solution heat-treated conditions for the untreated R alloy and the modified RM and RGM alloys. In the as-cast condition, the modified RM alloy displays somewhat higher UTS and elongation (%El) values than the unmodified R alloy, due to the improved eutectic silicon phase morphology caused by Sr modification, although the formation of porosity which accompanies Sr-addition may affect these values to some extent. The yield strength, however, seems to be independent of the Sr-addition. From the point of view of microstructure, the eutectic structure of Al-Si alloys consists of Si particles, as a second phase, embedded in the Al matrix, implying that particle size has a significant influence on the fracture strain. A theoretical analysis by Saigal *et al.*[240] showed that the stress or strain required to break a particle varied inversely with the particle size, which would signify that the void nucleation strain is higher for fine particles. Numerous studies have revealed that failure takes place when the void grows to a critical size. Since

the failure strain is inversely proportional to void growth rate, it may be suggested that this growth rate is lower in the modified RM alloy than it is in the unmodified R alloy. Thus, an increase in the void growth strain should be expected, which would, in turn, increase the fracture strain. The fine fibrous Si morphology of the modified RM alloy would thus influence the strain sustained to fracture by increasing the void nucleation and void strain simultaneously.

It may also be observed that after grain refiner and modifier have been added to the as-cast R alloy, the average values of YS, UTS, and %El are increased by 10 MPa, 24 MPa, and 0.24%, respectively, in the RGM alloy. This effect may be attributed to an increase in the number of nucleation sites for the pre-eutectic alpha aluminum phase nucleation during casting solidification. As the grain size decreases, secondary phases and porosity become more widely dispersed, and as a result, a fine grain size results not only in better castability and more uniform properties throughout the casting section, but also in the improvement of the mechanical properties of the alloy. This observation indicates that the combined effect of the grain refiner and modifier is more beneficial to the enhancement of mechanical properties than in untreated alloys. In summary, an amelioration of the tensile properties is obtained after the addition of refining and modifying elements. The total ductility of these alloys is relatively low, a finding which is consistent with the technical information available on dual-phase alloys exhibiting lamellar eutectics.[241] Higher levels of ductility result from factors which minimize the occurrence of voids, coupled with other factors that make it possible for cracks to be arrested.[242] The first is achieved by the developing microstructures capable of avoiding stress amplification factors, namely, the absence of

such stress raisers as Si eutectic lamellae and angular primary Si particles. The second factor responsible for retarding void coalescence and crack propagation through the cross-section of a tensile specimen is the volume fraction and grain size of the α-Al present. This phase is tougher and has a lower yield stress than the Si particles and provides a way of confining an advancing crack by application of the classical tip blunting mechanism.[243] According to this mechanism, when the tensile load is applied to the specimen, the crack opens and the crack tip emits dislocations and blunts. As the load is reduced is reduced, the crack tip closes down, resharpens, reweldes, and may even fold in on itself causing stretch or striation ridges or furrows. The alpha phase thus plays a role at two levels: firstly, in the eutectic, for which its volume fraction within the eutectic becomes a key issue, and secondly, as primary α-Al dendrites, for which the volume fraction and, more importantly, the grain size are critical. As expected, the Sr-treated RM alloy exhibits the best overall ductility of the alloys studied.

A theoretical analysis[240] has shown that the stress required for localized yielding varies marginally with Si-particle size or aspect ratio. Accordingly, the yield strength of the untreated R alloy does not vary significantly during solution. The stress required for crack initiation, however, depends strongly on the size and aspect ratio of Si particles. Consequently, UTS and % elongation vary significantly during solution treatment. The difference in the average values of YS and UTS between the solutionized R and RGM alloys is marginal. This can be explained in terms of the transformation mechanism of Si-particle morphology through the fragmentation, spheroidization and coarsening processes which occur during solution treatment. These results agree well with the microstructural

data presented in section (4.2). The effects of aging temperature on the tensile properties of the R alloy are shown in Figure 4.17. The average tensile properties and their standard deviations are presented in Tables 4.8 through 4.10. In general, a T6 temper allows for increased strength as well as the development of increasingly more stable mechanical properties, although with a corresponding loss of ductility. For example, at a moderate aging temperature of 155°C/5hr, hardening is due to the formation of Guinier-Preston zones, which leads to high UTS and a decreasing strain-hardening rate. Up to peak aging at 180°C, the behavior is thus similar to that of the Al-Si-Cu system. Overaging, however, results in the simultaneous formation of relatively large θ'-Al_2Cu plates[238] which are hard non-shearable obstacles to dislocations. Non-shearable obstacles lead to lower UTS and, at low strains, they result in a high strain-hardening rate because of the accumulation of Orowan loops around the strengthening particles.[244] As the strain is increased, the buildup of primary shear loops generates intense stress fields around the strengthening precipitates. These stresses are limited by the activation of cross-slip and secondary dislocation processes, which thus reduce the strain-hardening ability of the alloy.

The RM alloy, on the other hand, shows lower tensile properties at all aging temperatures used in this study; this is a result of the existence of the porosity which was observed in the modified RM alloy. A similar trend may be observed during the aging of the RGM alloy except that the rate of increase in strength is greater in the RGM alloy than it is in the R alloy. The combined addition of grain refiner (Al-5%Ti-1%B) and modifier (Sr) to the base alloy which converts large α-Al grains, eutectic plate-like silicon into fine particles and fine Al_2Cu particles in the interdendritic region resulting in improved

mechanical properties. It is apparent that overaging takes place in all alloys at temperatures above 180°C.

For aluminum foundries, a quality index, Q, can be used on as-cast and heat-treated alloys for assessing the alloy quality or for investigating the influence of a given parameter such as composition or heat treatment. Parameters such as soundness, compactness, structural fineness (*i.e.* modification, solution treatment) all affect the quality index, Q. Since Q is a function of both UTS and elongation, it is believed to be more descriptive of the true tensile properties of a casting than either the tensile strength or the elongation alone. The quality index was also calculated for all conditions; the average values and their standard deviations are provided in Tables 4.7 and 4.11. In general, for all conditions, increased Q indicates an improvement in the mechanical properties. After solution heat-treatment, the quality index of the unmodified R alloy increased from 312 MPa to 407 MPa corresponding to a 31% improvement. In the presence of Sr, Q changed from 334 MPa to 402 MPa, an increase of 20%. It should be noted however, that the standard deviation was 29 compared to 11 for the unmodified alloy. This high value indicates more scattering in the parameter, reflecting once again the increased level of porosity associated with modification. The variation of Q with aging temperature is plotted in Figure 4.18. As may be observed, the trend of the quality index decreased as the aging temperature increased for all the alloys studied. Although the peak-aged condition was observed at 180°C, the highest quality index, Q, was obtained at 155°C, which may thus be considered as the optimal aging treatment. It is also consistent with this observation that Q is more sensitive to variations in the tensile ductility than to tensile strength. Thus it would appear that, among

all the castings, the combined addition of grain refiner and modifier produces the best overall quality index. With regard to the quality index, Figure 4.19 shows a correlation between UTS and elongation for the aged R, RM, and RGM alloys. The circular contour shown by the correlation is thus the result of the transition from a high correlation value in the underaged and peak-aged conditions to the lower correlation value associated with the overaged condition. Again, the combined addition of grain refiner and modifier displays the best correlation overall, among all the castings.

Table 4.8 Yield strength as a function of aging temperature for Al-10.8%Si alloy

Alloy code	155 °C	180 °C	200 °C	220 °C	240 °C
R	288.31 ± 3.6	329.39 ± 3.2	326.11 ± 10.2	303 ± 8.28	265.25 ± 3.36
RM	275 ± 3.4	325.86 ± 4.8	322.33 ±12	296.45 ±7.5	256.58 ± 4.6
RGM	293.84 ± 5.2	336.63 ± 6.9	332.1 ± 8.7	306.1 ± 9.2	271.34 ± 7.6
RF1	317.7 ± 4.5	344.6 ± 8.4	335.6 ± 12.2	309.1 ± 9	263.24 ± 4
RF2	314.2 ± 3.3	340.85 ± 7.7	339.15 ± 8.6	316.3 ± 5.5	265.96 ± 3.8
RF3	319.4 ± 5.6	353.1 ± 10.6	345.2 ± 8.5	307.6 ± 11.5	265.79 ± 4.3
RF4	298.48 ± 3.2	337.13 ± 7.7	320.4 ± 12.7	294.2 ± 10.7	247.57 ± 4
RC1	318.7 ± 18.9	377.3 ± 11.7	368.9 ± 7	342.1 ± 10	292.35 ± 5.3
RC2	334.8 ± 9	382.51 ± 4.5	377.54 ± 2.7	354.3 ± 8.2	295.8 ± 11.5
RC3	288.3 ± 7	343.9 ± 6	323.8 ± 16.1	301.1 ± 2.2	247.8 ± 3.5
RC4	299.5 ± 9	348.8 ± 4.2	338.9 ± 4.7	308.9 ± 2.2	282.5 ± 6.2
RC5	302.2 ± 6.6	368.8 ± 6.6	355.7 ± 6.8	325.48 ± 8.5	267.3 ± 3.2

Table 4.9 UTS as a function of aging temperature for Al-10.8%Si alloy

Alloy code	155 °C	180 °C	200 °C	220 °C	240 °C
R	350.9 ± 6.8	365.1 ± 5.8	358.8 ± 14.6	343.8 ± 13.2	314.2 ± 5.5
RM	346.7 ± 9.2	358.6 ± 13.3	353.3 ± 6.3	334.5 ± 11.6	309.4 ± 8.8
RGM	362 ± 19.5	374.5 ± 15.2	366.9 ± 12.3	346.9 ± 8.7	328.3 ± 15.6
RF1	367.16 ± 3.4	377.7 ± 8.6	368.3 ± 6.7	351.4 ± 13.6	317.1 ± 9.3
RF2	338.5 ± 5.6	351.5 ± 11.2	345.5 ± 15.5	324.5 ± 10.8	303.9 ± 13
RF3	370.6 ± 9.6	380.8 ± 21.8	370.2 ± 8.2	355.2 ± 19.2	324.9 ± 5.0
RF4	331.7 ± 9.6	347.6 ± 8	339.5 ± 16	321.1 ± 10.3	286.3 ± 15
RC1	374.3 ± 18.7	398.2 ± 10.6	386.3 ± 12.3	371.15 ± 8.7	348.0 ± 15.6
RC2	394.2 ± 19.7	401.9 ± 14.6	388.89 ± 8.6	377.52 ± 13	352.1 ± 20
RC3	357.9 ± 17.3	368.6 ± 19.5	354.14 ± 4.35	334.8 ± 18.4	314.1 ± 28.5
RC4	364.6 ± 10	372.4 ± 19.6	365.1 ± 11.6	340.1 ± 12.3	325.82 ± 5.7
RC5	367.1 ± 10.4	389.3 ± 10.2	372.24 ± 6.8	351.56 ± 12	329.24 ± 11.4

Table 4.10 Pct elongation as a function of aging temperature for Al-10.8%Si alloy

Alloy code	155 °C	180 °C	200 °C	220 °C	240 °C
R	1.74 ± 0.25	0.92 ± 0.01	0.95 ± 0.04	1 ± 0.07	1.41 ± 0.13
RM	1.81 ± 0.33	0.93 ± 0.1	0.98 ± 0.06	1.03 ± 0.003	1.45 ± 0.13
RGM	2.0 ± 0.29	1.127 ± 0.25	1.128 ± 0.14	1.36 ± 0.32	1.45 ± 0.24
RF1	1.24 ± 0.06	0.972 ± 0.15	1.031 ± 0.19	1.17 ± 0.15	1.396 ± 0.22
RF2	0.915 ± 0.16	0.709 ± 0.09	0.718 ± 0.16	0.72 ± 0.09	1.02 ± 0.24
RF3	1.25 ± 0.17	0.889 ± 0.20	0.955 ± 0.21	1.15 ± 0.21	1.34 ± 0.33
RF4	0.887 ± 0.14	0.599 ± 0.03	0.631 ± 0.05	0.642 ± 0.05	0.985 ± 0.16
RC1	1.93 ± 0.2	0.88 ± 0.07	0.94 ± 0.24	0.97 ± 0.12	1.41 ± 0.35
RC2	1.7 ± 0.18	0.74 ± 0.06	0.76 ± 0.14	0.89 ± 0.12	1.42 ± 0.18
RC3	1.65 ± 0.03	0.93 ± 0.34	0.96 ± 0.11	0.98 ± 0.29	1.37 ± 0.29
RC4	1.5 ± 0.2	0.86 ± 0.21	0.92 ± 0.18	0.96 ± 0.16	1.33 ± 0.03
RC5	1.41 ± 0.13	0.78 ± 0.06	0.82 ± 0.02	0.93 ± 0.17	1.29 ± 0.23

Table 4.11 Quality index, Q, as a function of aging temperature for Al-10.8%Si alloy

Alloy code	155 °C	180 °C	200 °C	220 °C	240 °C
R	386.9 ± 7.1	359.67 ± 5.8	355.54 ± 14.6	343.87 ± 13	336.63 ± 5.6
RM	385.31 ± 9.6	354 ± 13.4	351.76 ± 6.3	336.3 ± 11.7	330.55 ± 8.9
RGM	407.2 ± 19.8	382.3 ± 15.4	374.77 ± 12.5	366.87 ± 9	352.49 ± 15.8
RF1	381.1 ± 3.5	375.8 ± 8.8	370.2 ± 6.9	361.7 ± 13.8	338.8 ± 9.5
RF2	332.7 ± 5.8	329.2 ± 11.3	323.9 ± 15.7	303.2 ± 10.8	305.3 ± 13.2
RF3	385.2 ± 9.8	373.2 ± 22	367.2 ± 8.4	364.4 ± 19.4	343.9 ± 5.3
RF4	323.9 ± 9.7	314.2 ± 8	309.4 ± 16.1	292.2 ± 10.4	285.3 ± 15.2
RC1	417.2 ± 18.9	389.6 ± 10.7	382.4 ± 8.6	369.6 ± 15.5	370.5 ± 17.7
RC2	427.9 ± 19.8	381.8 ± 2.2	371.8 ± 6.9	370.5 ± 13	374.7 ± 20
RC3	390.5 ± 17.3	363.5 ± 19.8	351.3 ± 4.5	334 ± 18.7	334.7 ± 28.7
RC4	391.1 ± 10.2	362.2 ± 20	359.6 ± 11.8	337.6 ± 12.5	344.4 ± 5.7
RC5	389.7 ± 10.5	372.8 ± 10.3	359.4 ± 6.8	346.8 ± 12.2	345.7 ± 11.6

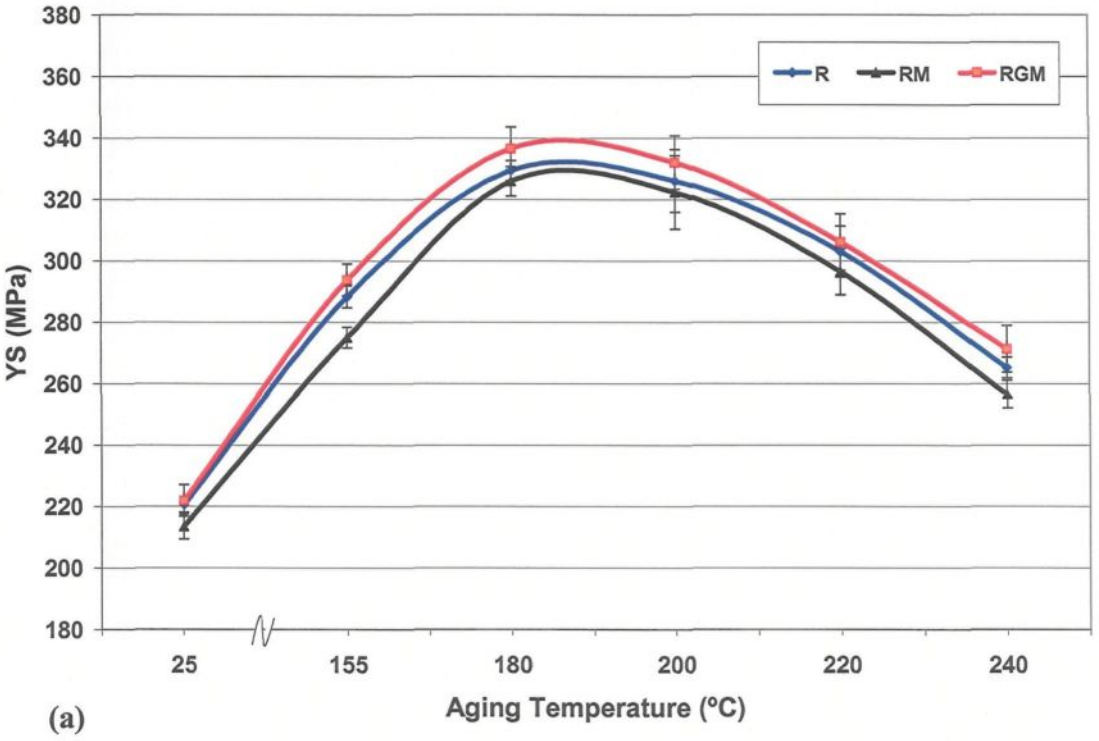

(a)

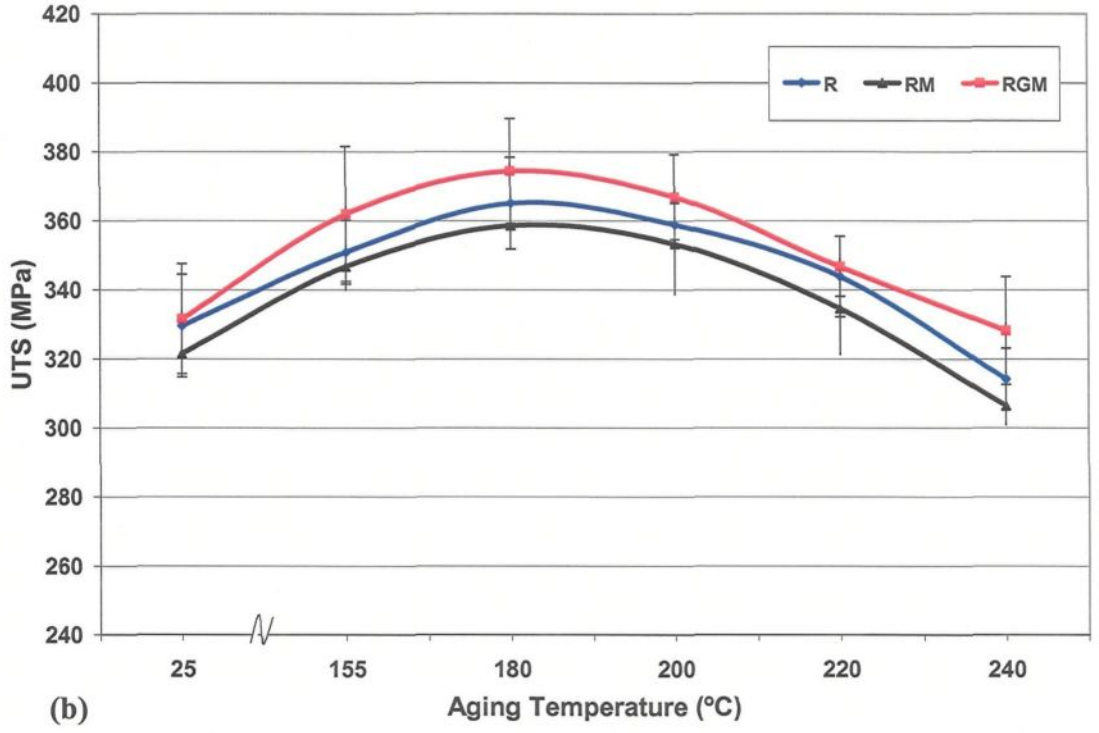

(b)

Figure 4.17 ⟶ Continued

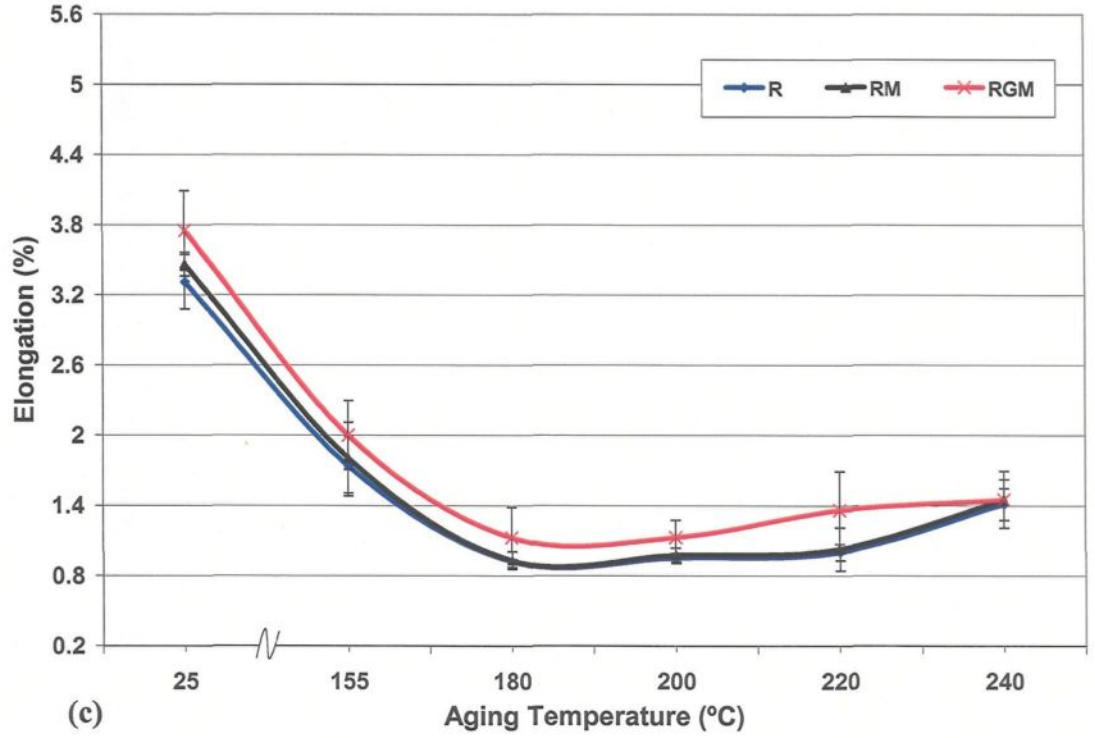

Figure 4.17 Variation in (a) YS, (b) UTS, and (c) %El as a function of aging temperature in R, RM and RGM alloys.

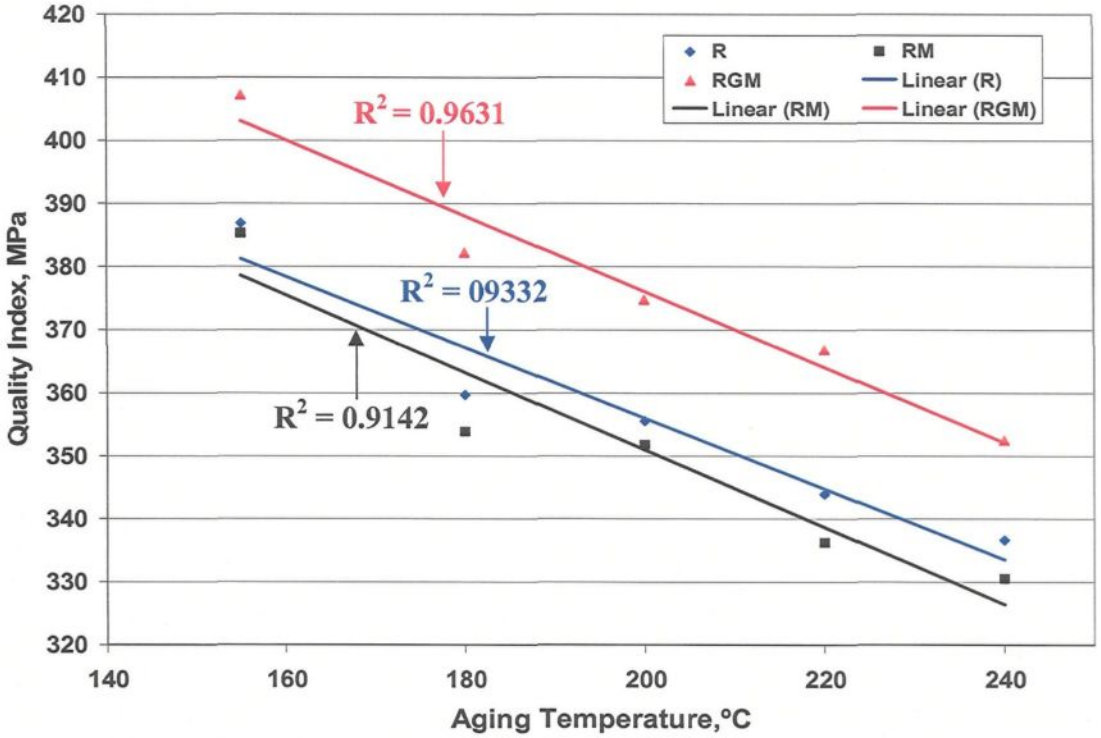

Figure 4.18 Effect of aging temperature on the quality index of R, RM and RGM alloys.

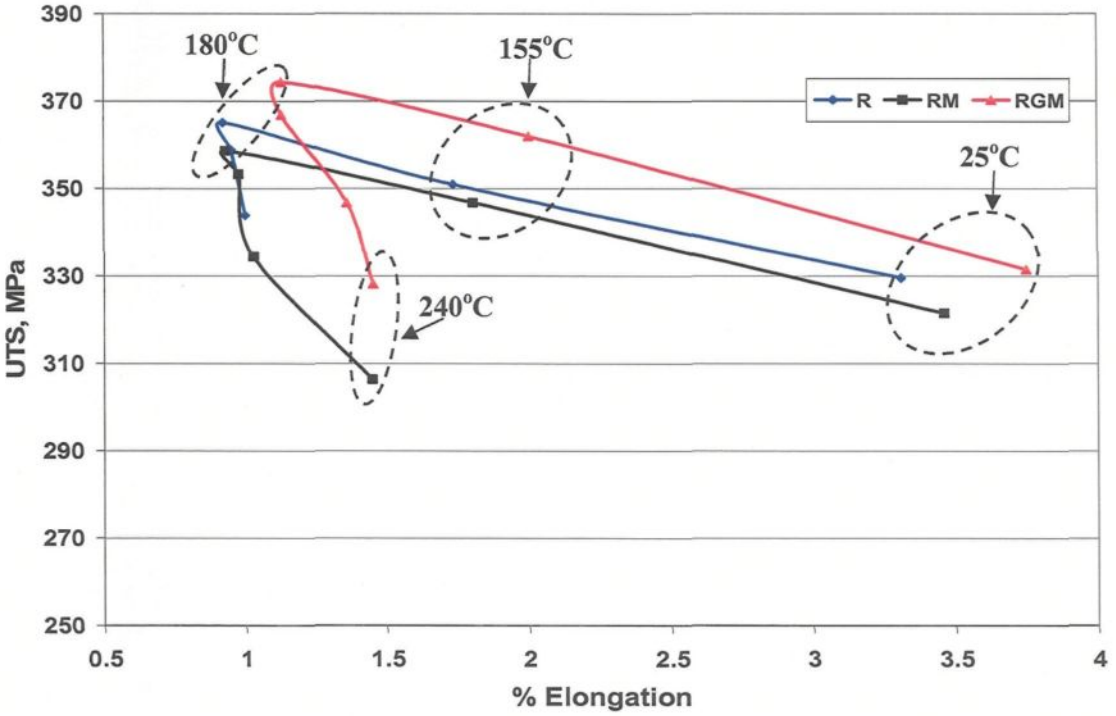

Figure 4.19 Plot of UTS *vs.* %El for R, RM, and RGM alloys.

4.5.2 Effects of the Addition of Fe and Mn

In general, it has been found that iron and manganese, which form complex compounds and intermetallic phases, have a deleterious effect on alloy properties. The presence of these compounds can lower the energy required for fracture. The effects of Fe and Mn on the tensile properties were studied by pulling test bars of alloy samples containing ~0.5% Fe + 0.5% Mn (the RGM or reference alloy); ~0.75% Fe + 0.75% Mn (RF1 alloy); ~1% Fe + 1% Mn (RF2 alloy); ~0.75% Fe + 0.5% Mn (RF3 alloy); and ~1% Fe + 0.5% Mn (RF4 alloy), in the as-cast and solution-treated conditions. A summary of the tensile properties obtained is given in Table 4.7 where, in the as-cast condition, the UTS increased slightly as the Fe level increased from ~0.5% in the RGM alloy to ~0.75% in the

RF1 alloy at ~0.75% Mn, and increased to a maximum at ~0.5% Mn in the RF3 alloy; concurrently, elongation in both alloys decreased from 1.945% in RGM alloy to 1.825% and 1.779%, respectively.

It may be also seen, however, that as the percentage of Fe and/or Mn increases beyond 0.75%, strength and ductility decrease dramatically, a fact which may be attributed to the presence of Fe- and Mn-bearing phases (*i.e.* sludge and β-Fe) in the structure of the RF2 and RF4 alloys, respectively; which has little beneficial effect on the properties of the as-cast alloy. From the point of view of the mechanical behavior of the alloy, yield strength is an important parameter and should be taken into account. If the Fe-intermetallic compounds are considered as inclusions in the alloy, the yield strength will then depend strongly on the type and critical size of these Fe-intermetallic compounds (mainly β-Fe). This would explain the reduction in yield stress upon attaining an Fe content of 1% in RF4 alloy.

The average YS, UTS, and %El curves for these alloys, as a function of aging temperature are shown in Figure 4.20. It may be observed that the UTS and YS increase while the elongation decreases with an increase in aging temperature of up to 180°C for all alloys. This observation may be attributed to the dispersion of massive Fe-rich phases throughout the matrix, in addition to the formation of age-hardening compounds. Thereafter, a continuous decrease in the YS and UTS may be observed with a further increase in aging temperature. The decrease in strength properties is accompanied by an enhancement of the ductility in all the alloys.

The quality index evaluated for the aging condition under consideration is displayed in Figure 4.21. It may be observed that the quality index, Q, depends strongly on the morphology of Fe-intermetallics for all the aging temperatures investigated. With regard to their quality indices in Table 4.11, the RF3 and RF1 alloys are characterized by the highest quality values compared to the RF2 and RF4 alloys. From a general point of view, it will be observed that the quality is dominated by the tensile ductility values and is much more sensitive to variations in tensile ductility than to changes in tensile strength. A comparison of the dependencies of the quality index in Figure 4.21 and the elongation-to-fracture in Figure 4.20(c) with the aging temperatures confirms the strong sensitivity of Q to variations in the tensile ductility. It may be concluded that the analytical quality index is a sensitive tool capable of detecting variations in the ductility.

Figure 4.22 displays the correlation between UTS and elongation at different aging temperatures. It is also interesting to note that the curves produced by the UTS – elongation relationship are substantially circular. The circular pattern is a result of the transition from high Q values of the underaged condition to the low Q values of the overaged condition. In general terms, however, the pattern of behaviour of the alloys studied is remarkably similar. As noted with regard to Figure 4.22, the presence of ~1% Fe and ~1% Mn in the RF2 alloy lowers the circular pattern due to the formation of sludge. The same result may be observed in the RF4 alloy due to the formation of the β-Fe phase.

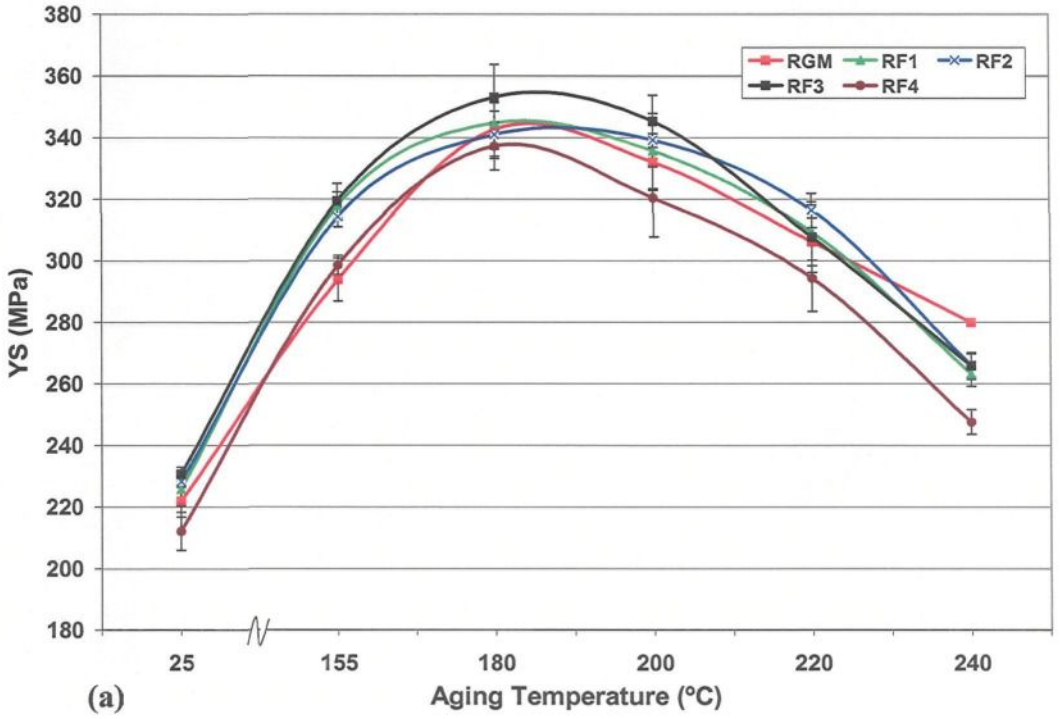

(a)

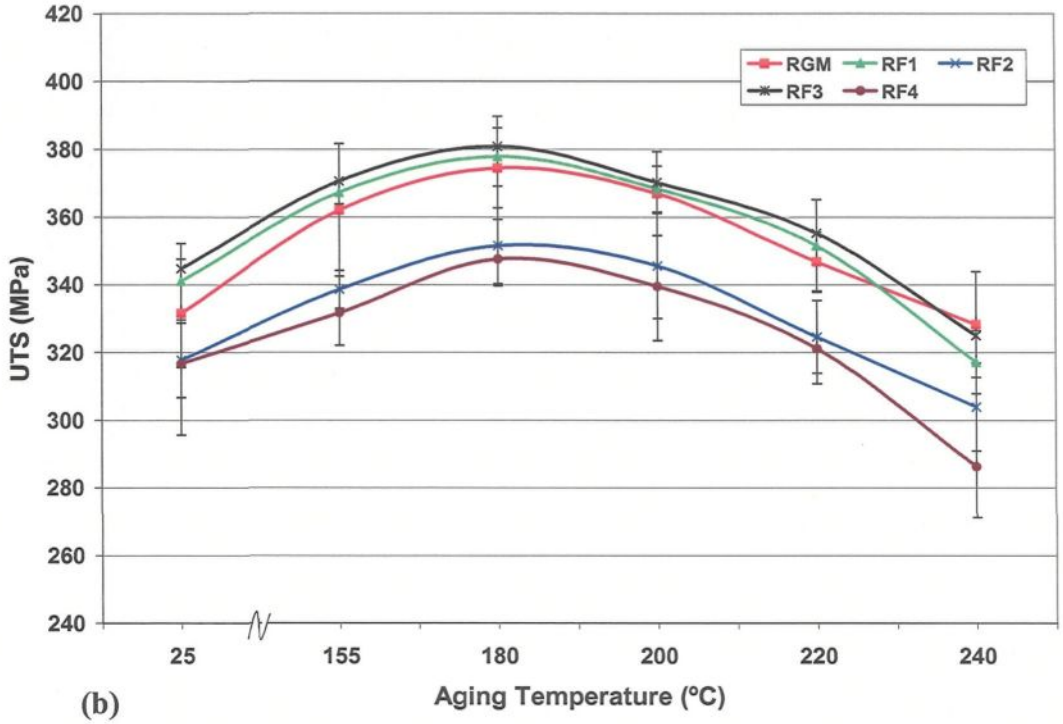

(b)

Figure 4.20 ⟶ **Continued**

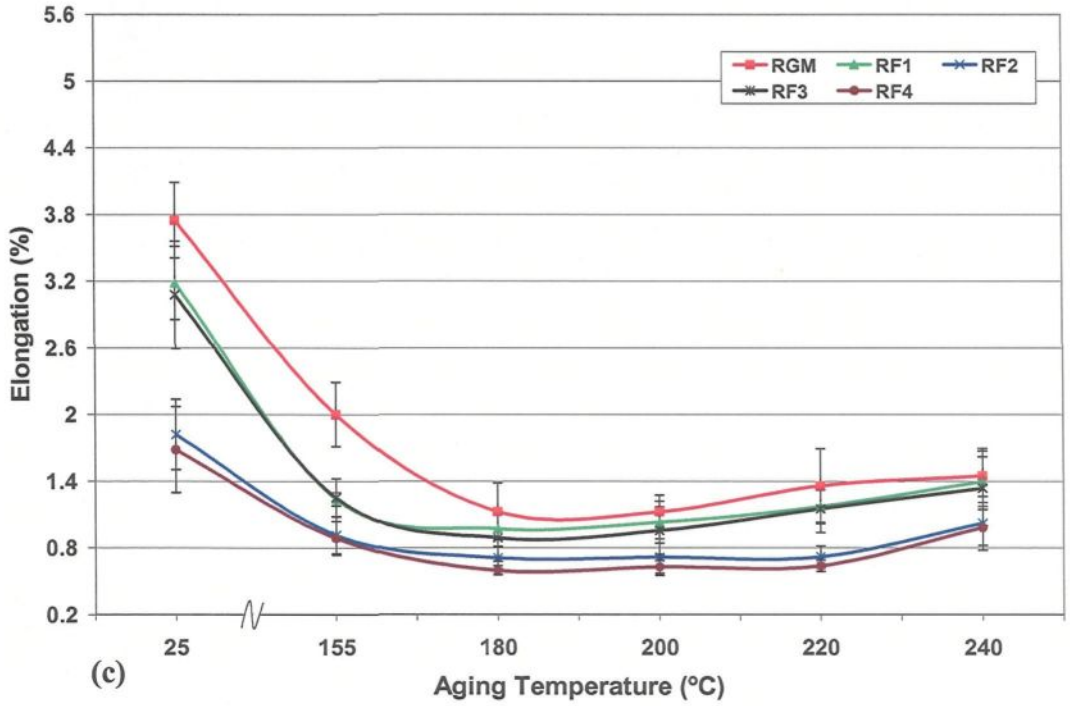

Figure 4.20 Variation in (a) YS, (b) UTS, and (c) %El as a function of aging temperatures.

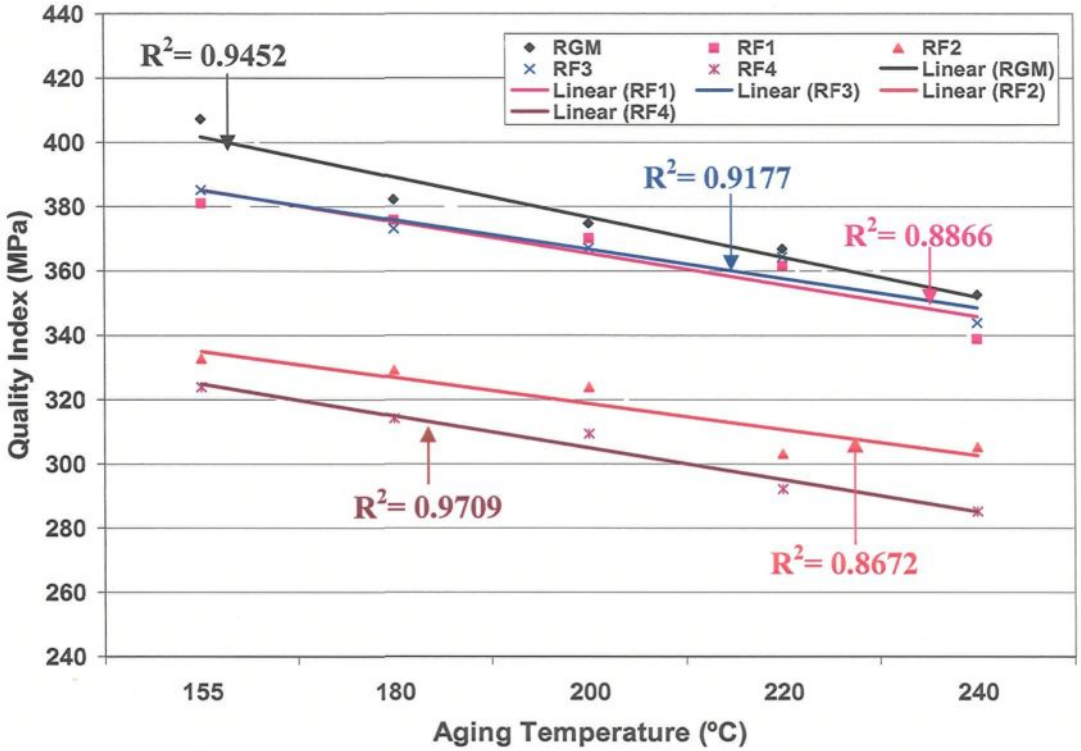

Figure 4.21 Effect of aging temperature on the quality index of the alloys investigated.

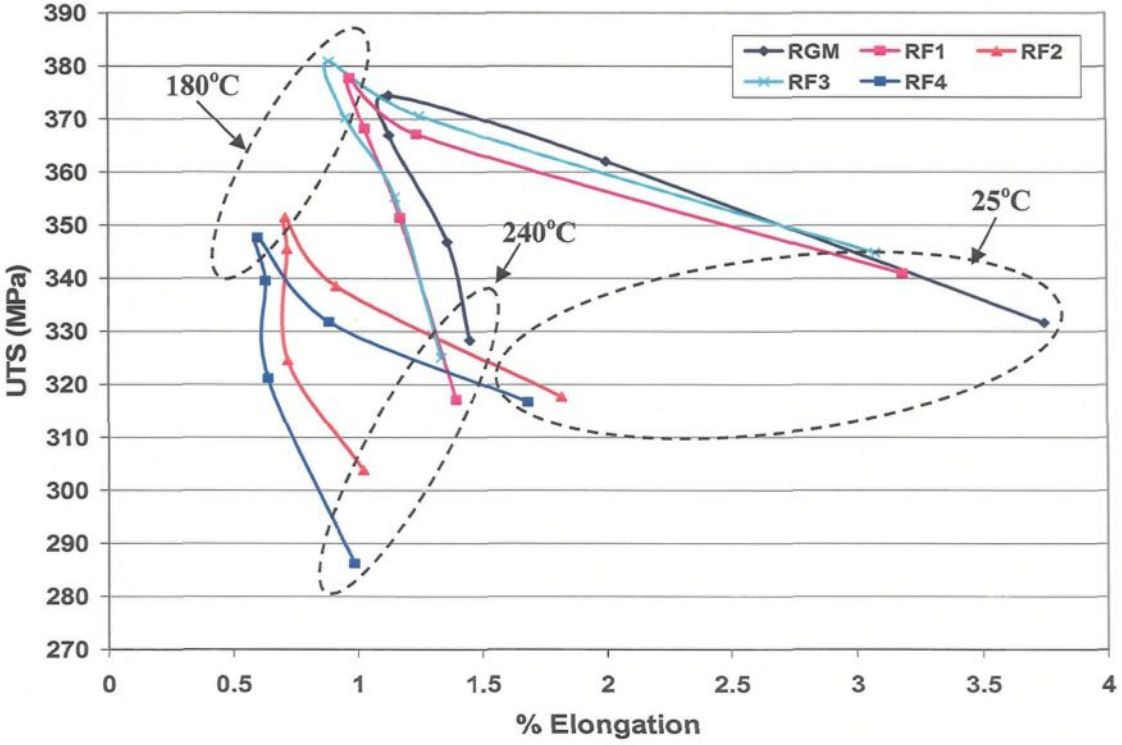

Figure 4.22 Plot of UTS *vs.* %El for the alloys investigated.

4.5.3 Effects of the Addition of Cu and Mg

In general, an improvement in the mechanical properties of Cu- and Mg-containing aluminum alloys is attributed to the formation of the age-hardening compounds Al_2Cu and Mg_2Si, respectively, which precipitate from the solid solution during aging.[245] The degree of strengthening depends on the copper and magnesium content, and an increase in strength due to higher copper and magnesium levels is always accompanied by a corresponding decrease in ductility. An overview of the tensile properties obtained for the artificial aging conditions investigated may be found in Tables 4.8-4.10. All values in these tables represent average values for the five tensile tests. The dependence of YS, UTS, and %El on the aging temperatures is displayed in Figures 4.23(a), (b), and (c) respectively. The tensile

strength (UTS) increases with the Cu and Mg content in the alloys. A significant improvement in the tensile strength was obtained for the RC2 alloy containing 3.25% Cu and 0.3% Mg. Also, this alloy shows much higher yield strength (YS) than does the RGM alloy containing 2.25% Cu and 0.3% Mg. An increase in the Cu-level at a given Mg-content causes a rapid loss in the relative ductility and the samples fall short of the necking strain, which is in principle an expected result. Figure 4.23(c), however, shows that a proportionally larger loss of the relative ductility occurs at higher Cu and Mg contents. The noticeable difference in strength between the RC2 and RGM alloys is due mainly to the precipitation of a large amount of the θ'-Al_2Cu phase.

The precipitation of θ'-Al_2Cu is not only attributable to the Cu-content but is also dependent upon the concentration of Si and the Cu/Mg ratio. A high Si-content and a high ratio of Cu:Mg have the effect of enhancing the precipitation of the θ'-Al_2Cu phase.[246] It was found that only when the Si-content was higher than 0.3 wt% could the θ'-Al_2Cu phase precipitate in Al-1.5%Cu-0.75%Mg alloy during artificial aging at 175°C,[246] whereas there was no precipitation of θ'-Al_2Cu to be found in the Al-2.0%Cu-0.9%Mg-0.25%Si alloy after artificial aging.[247] Since the Si-content in the alloy under study is much higher than the solubility of Si in Al, there must be a threshold value for the Cu-content lying between 1.0 and 1.5 wt%, above which the θ'-Al_2Cu phase precipitates during artificial aging. In addition, load-shedding onto the dispersed particles is increased and particle cracking occurs at lower strains. Lowering the ductility when the alloy matrix is strengthened by precipitation can lead to delays in the onset of plastic relaxation.[248] The ductility also diminishes when the reinforcing particles are either large or elongated.[249] For example, at

180°C, increasing the amount of Cu from ~2.25 wt% (RGM alloy) up to ~3.25 wt% (RC2 alloy) in the presence of a low Mg-content (0.3 wt%) is found to improve the alloy YS and UTS values by 26% and 13%, respectively, with a corresponding decrease of ~35% in elongation. At 0.5 wt% Mg, an increase in the Cu level from ~2.25 wt% (RC3 alloy) up to ~3.25 wt% (RC5 alloy) produces an increase of ~9.7% and 5.5% in the YS and UTS, respectively, with a corresponding decrease in elongation of ~16% at peak aging.

All of the preceding would thus indicate that a high level of Mg addition is of no great effectiveness, possibly due to the formation of $Al_5Mg_8Si_6Cu_2$ which decreases the amount of free Mg available for forming the Al_2CuMg phase. This observation is in agreement with the results reported by Dunn and Dickert.[35] Thereafter, a continuous decrease in the YS and UTS takes place with increasing aging temperature; the decrease in strength properties is accompanied by an improvement in the ductility.

It was observed that the alloy with 3.25 wt% Cu and 0.3 wt% Mg is significantly stronger but less ductile. In general terms, as the alloys undergo progressive treatments toward peak aging, the YS and UTS increase while the ductility decreases. Overaging, on the other hand, lowers the YS and UTS but does not increase the ductility except for the overaged samples at 240°C. Alloys containing high levels of Mg were also found to be significantly less ductile than the alloys with a low Mg content at the same content of Cu for all heat/aging treatment studied.

Again, the tensile properties can be evaluated using the quality index. With regard to the respective mechanical properties listed in Tables 4.9 and 4.10, the use of Q for quality evaluation leads to very reasonable results. Figure 4.24 shows a comparison of the

results obtained with the additions of varying quantities of Cu and Mg and by applying different aging temperatures. As can be expected, the RC2 alloy (3.25% Cu and 0.3% Mg) displays the best quality index compared to the other alloys investigated at all aging temperatures. It is also consistent that the Q value is more sensitive to tensile ductility than it is to tensile strength variations. The highest quality index was obtained at 155°C for all the alloys investigated. Thus, this temperature may be considered the optimal aging treatment according to this particular quality index.

It may be concluded from the above investigation that the use of Q will lead to satisfactory results in engineering applications where variations in tensile ductility may be considered as an essential parameter for alloy quality evaluation. Various events occurring during the aging treatment can be analyzed by plotting the UTS as a function of %El, as shown in Figure 4.25. The curves begin at point A, which represents the value in the solution heat-treated condition. As precipitation begins to occur, the alloys containing the additions of Cu and/or Mg begin to harden, and the strength increases, while there is an overall reduction in ductility. At 180°C, the alloys attain a peak strength value. This point corresponds to a minimum in elongation. A purely overaging phenomenon would suggest that increases in elongation should be accompanied by a reduction in the strength levels.

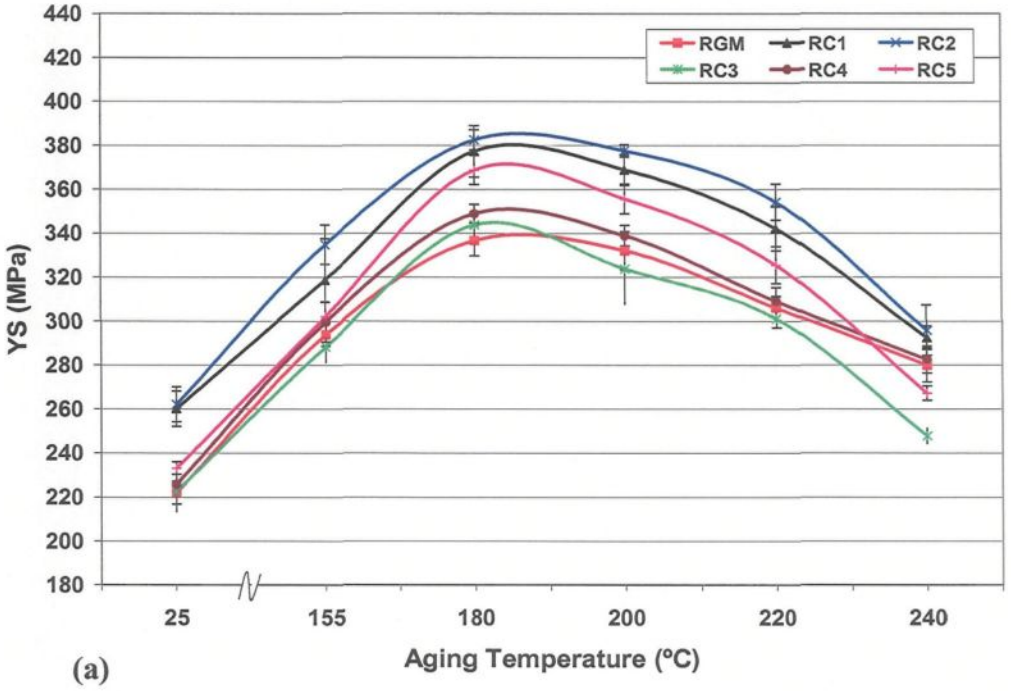

(a)

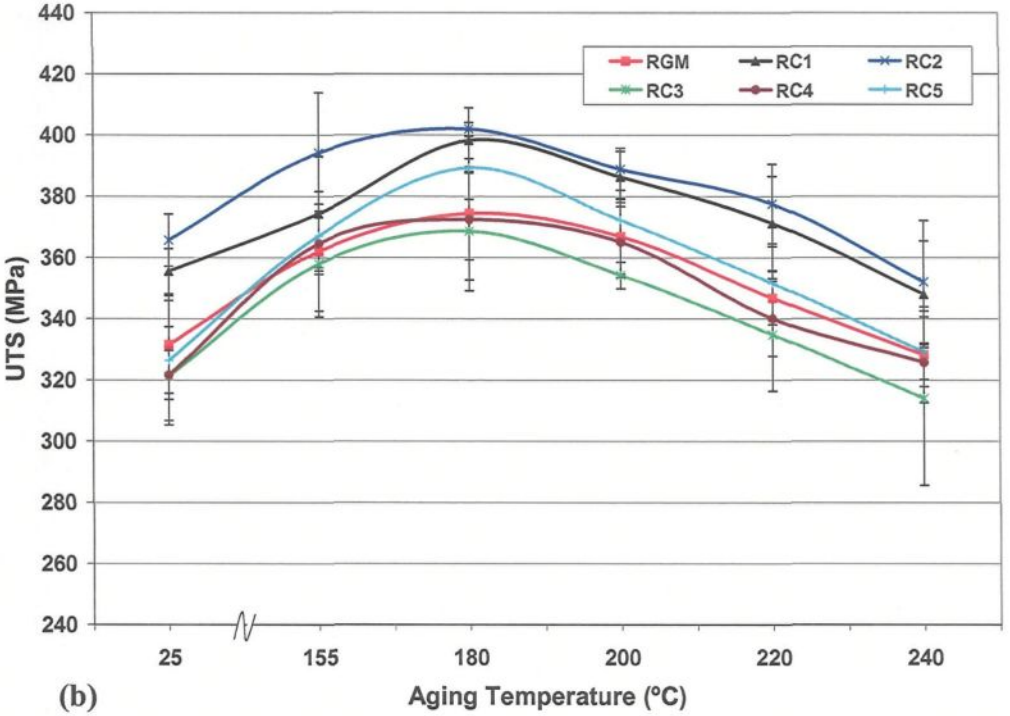

(b)

Figure 4.23 ⟶ **Continued**

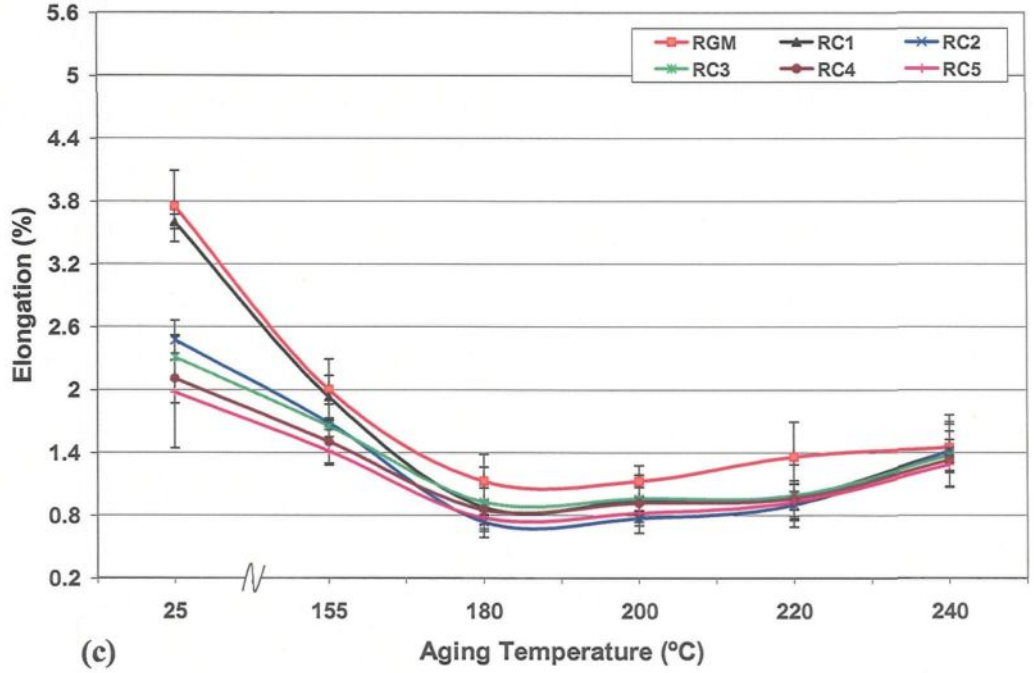

Figure 4.23 Variation in (a) YS, (b) UTS, and (c) %El as a function of aging temperature.

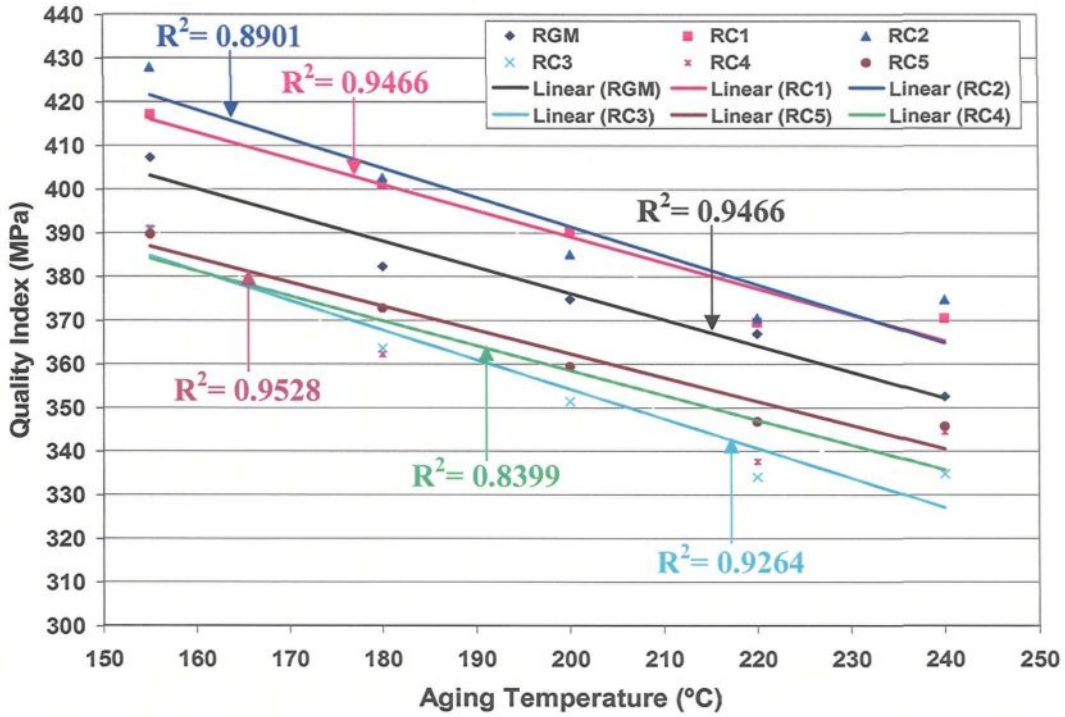

Figure 4.24 Effect of aging temperature on the quality index of the investigated alloys.

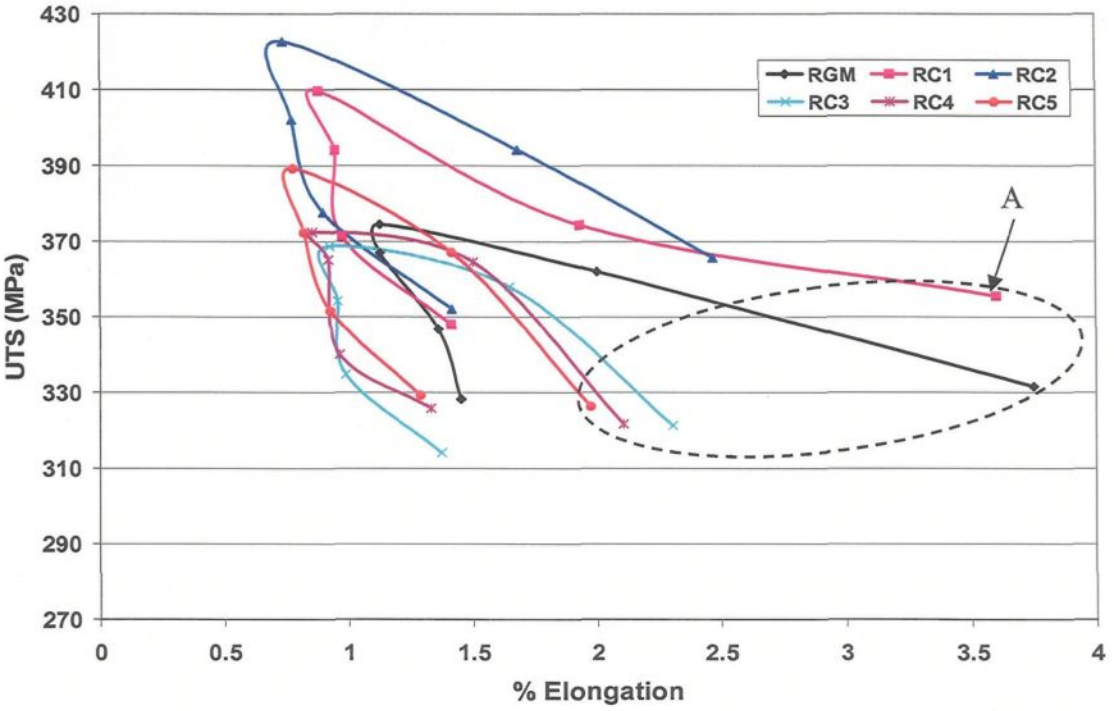

Figure 4.25 Plot of UTS *vs.* %El for the investigated alloys.

CHAPTER 5

IMPACT PROPERTIES OF Al-10%Si ALLOYS AND EXPERIMENTAL DESIGN

CHAPTER 5

IMPACT PROPERTIES OF Al-10%Si ALLOYS AND EXPERIMENTAL DESIGN

5.1 IMPACT PROPERTIES

5.1.1 Introduction

Tensile testing is the most commonly used method for quantifying the mechanical properties of aluminum alloys. Impact strength, however, is also of importance in certain applications and can provide an informative estimation of the ductility of an aluminum alloy. The Charpy test is the most frequently used means for laboratory measurement of impact energy. This energy, as recorded by the Charpy test, correlates with the area under the total stress-strain curve shown in Figure 2.7 from an earlier chapter.

From the few data available in the literature for the impact strength of Al-Si alloys, it would appear that this property is influenced by the fineness of the microstructure and the morphology of the constituents. In this subsection, the impact behaviour of different alloys will be investigated with reference to the way they relate to the as-cast and heat-treated conditions. In each case, the traditional impact strength or the total absorbed energy during impact will be determined together with more specific parameters such as crack initiation and propagation energies and the load required to break the sample. In view of the fact that the total absorbed energy, E_t, is normally taken to represent impact energy, this parameter will be used mainly to discuss impact properties from the point of view of the type of melt treatment and alloying elements added, as was done earlier for tensile properties. Also

presented will be the relationship between impact energy and tensile and ductility with reference to the alloys studied.

5.1.2 Effects of Melt Treatment

As pointed out by Kobayashi and Niinomi,[250] the impact toughness of the as-cast Al-Si alloy is related mainly to: (i) aluminum dendrite cell size and dendrite arm spacing; (ii) the shape of eutectic silicon crystals; (iii) other second-phase particles such as intermetallic compounds; (iv) casting defects such as voids; and (v) primary silicon particles. Unnotched, untreated and melt-treated impact bars were tested to investigate the effects of modification and grain refining. It was decided not to notch the impact bars in order to increase the accuracy of the measurements and to emphasize the effects of the microstructure. The instrumented impact testing equipment allows the fracture response of the impact specimen to be studied in terms of absorbed fracture energy. This may be determined directly from the dial of the pendulum machine as in the traditional test, or else calculated from the curves obtained on the oscilloscope. When the system is well calibrated, the calculated E_t value will match the dial energy. This correspondence was verified for each sample, and only the results obtained from the curves themselves will be considered here. The results of the instrumented impact test were provided in the form of a visual record of the applied load and energy absorbed during fracture. The relative shape of the load-time curve is indicative of the deformation and fracture history of the impacted test sample. The interpretation of the load record may be done using concepts which are similar to those already employed for the conventional tensile test, while the curve itself can be subdivided into deformation stages.

Figures 5.1 and 5.2 provide examples of the recorded results for untreated and melt-treated impact bars in the as-cast condition. The variation of the load with time is shown by the upper curve. The total energy absorbed during impact can be estimated from the area under the load-time curve; however, as the Dynatup System also provides the energy-time signal (the lower curve), the absorbed energy can be calculated directly, as mentioned earlier in Chapter 2. The effect of modification can be observed easily upon comparing Figures 5.1 and 5.2(a). The first part of the curve, where the load varies linearly with time, corresponds to the elastic deformation up to the yield load; it should be noted that this zone remains unaffected by the presence of Sr or the addition of Sr and Ti. This observation is in agreement with the results from the tensile tests. After yielding, plastic or permanent deformation occurs, where the damage is generally distributed over a relatively large volume of alloy so that a decrease of the load is not observed. This zone, where the load may increase up to a maximum, is wider for the RM and RGM alloys than it is for the R alloy. In other words, it takes a longer time for a crack to be initiated and to begin to propagate. Finally, there is a sharp decrease in load after the ultimate point (corresponding to the maximum load) is reached, which is associated with the catastrophic cracking leading to failure. As can be seen in Figure 5.2(b), a more gradual decrease in load after the maximum load can occur for the Sr-modified and grain-refined RGM alloy; it too can be associated with localized cracking which propagates more slowly leading to gradual failure. In such a case the percentage of the total energy attributed to the crack propagation will be larger and lead to a higher ductility index, as will be shown later on in the text.

Table 5.1 shows the results for the different parameters as determined from the instrumented impact tests for untreated and melt-treated alloys. The total absorbed energy, E_t, the crack initiation energy, E_i, the maximum load, total time, and time to maximum load were all determined from the curves, whereas the crack propagation, E_p, ductility index (DI), and average crack speed were obtained by means of calculation. The results represent the average values and their standard deviation. The impact strength, or the total absorbed energy, increased from 5.42 J for the unmodified R alloy to 7.13 J for the modified RM alloy, corresponding to an improvement of about 31%. These results reflect the structural changes associated with modification from acicular to fibrous eutectic Si.

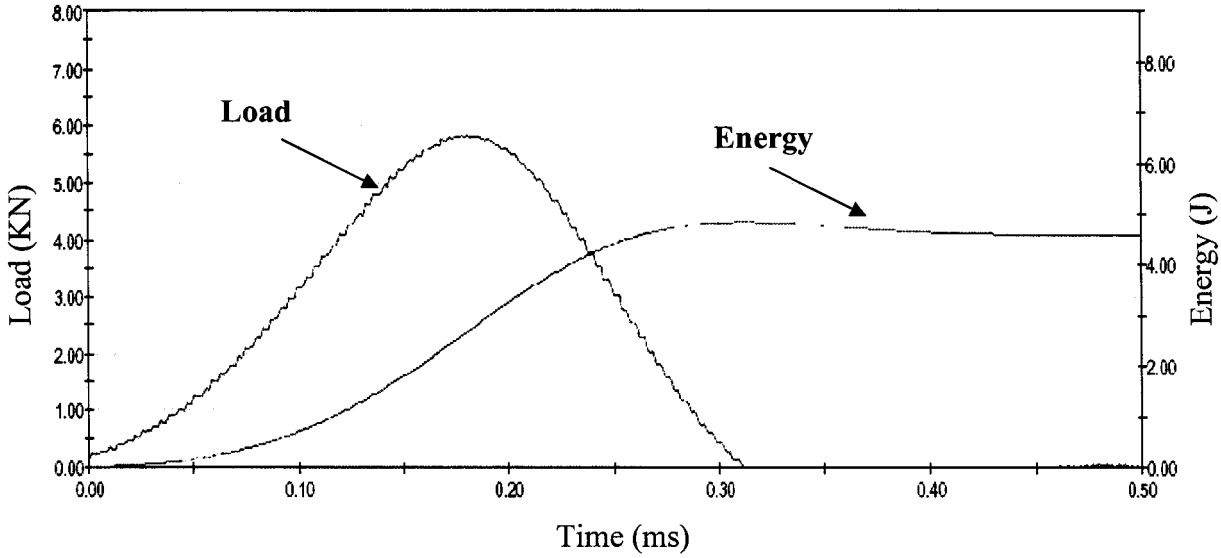

Figure 5.1 Load-time and energy-time curves for untreated R alloy in the as-cast condition.

Impact strength is imparted to the alloy by the ductile aluminum matrix which separates the brittle silicon phase. The acicular or needle-like morphology of the silicon phase in the unmodified alloy, as observed by metallography, gives rise to stress

concentration at the sharp silicon corners. This stress concentration rapidly creates a crack which propagates easily, resulting in fracture under load. Modification with strontium changes the Si particles from the acicular to the fibrous form, but also refines the size of this brittle phase which results in significant improvement of the impact strength of the alloy. It is interesting to note that the combined addition of modifier and grain refiner leads to an increase in the impact strength by 33% compared to the untreated alloy.

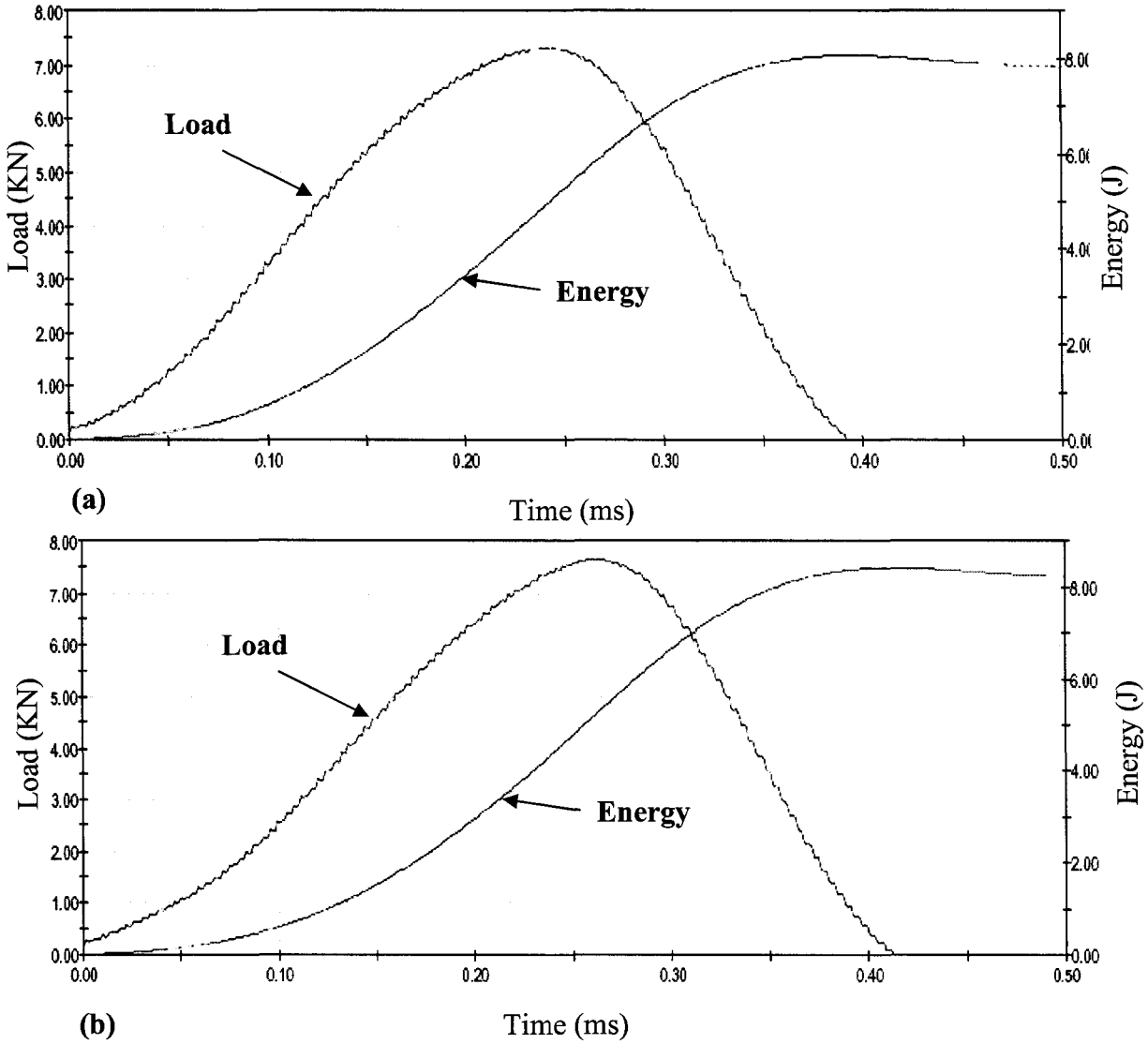

Figure 5.2 Load-time and energy-time curves for (a) Sr-modified RM, and (b) Sr-modified and grain refined RGM alloys in the as-cast condition.

Table 5.1 Effect of modification, grain refining, and aging temperature on the impact properties of Al-10% Si alloys

Alloy Code	Condition	Total absorbed energy E_T (J)	Crack initiation energy E_i (J)	Crack propagation energy E_p (J)	Ductility index DI	Maximum load (KN)	Total Time (ms)	Time to maximum load (ms)	Average crack speed (mm/ms)
R	As-cast	5.42 ± 0.98	4.3 ± 0.87	1.12 ± 0.12	0.26 ± 0.027	5.971 ± 0.54	0.34 ± 0.039	0.203 ± 0.032	29.5 ± 3.3
	SHT	17.0 ± 2.5	12.7 ± 1.22	4.3 ± 0.43	0.34 ± 0.03	10.410 ± 0.26	0.62 ± 0.002	0.44 ± 0.01	16 ± 0.6
	A @ 155	12.37 ± 2	9.35 ± 0.97	3.02 ± 0.88	0.32 ± 0.07	9.480 ± 0.12	0.43 ± 0.02	0.27 ± 0.013	23 ± 2.2
	A @ 180	8.38 ± 2.8	6.54 ± 2.2	1.94 ± 0.67	0.28 ± 0.03	9.48 ± 0.87	0.316 ± 0.01	0.21 ± 0.05	31.6 ± 1.1
	A @ 200	11.31 ± 1.0	8.78 ± 0.74	2.53 ± 0.31	0.29 ± 0.027	10.513 ± 0.29	0.41 ± 0.02	0.26 ± 0.02	24 ± 1.97
	A @ 220	12.69 ± 1.7	9.68 ± 0.92	3.01 ± 0.82	0.31 ± 0.05	10.414 ± 0.82	0.45 ± 0.034	0.29 ± 0.033	22 ± 5.2
	A @ 240	12.9 ± 2.0	9.72 ± 1.78	3.18 ± 0.54	0.33 ± 0.01	10.794 ± 0.97	0.49 ± 0.01	0.31 ± 0.013	20.4 ± 1.6
RM	As-cast	7.13 ± 2.1	5.47 ± 0.69	1.66 ± 0.62	0.30 ± 0.01	6.845 ± 0.55	0.37 ± 0.05	0.22 ± 0.06	27 ± 1.2
	SHT	23.22 ± 3.5	17.1 ± 2.7	6.12 ± 0.35	0.36 ± 0.07	10.895 ± 0.52	0.65 ± 0.05	0.45 ± 0.013	15.4 ± 1.2
	A @ 155	14.15 ± 1.3	10.65 ± 0.81	3.5 ± 0.59	0.33 ± 0.05	10.675 ± 0.14	0.45 ± 0.03	0.28 ± 0.02	22 ± 1.6
	A @ 180	9.1 ± 2.3	7.03 ± 1.7	2.02 ± 0.54	0.28 ± 0.01	10.400 ± 0.15	0.34 ± 0.03	0.2 ± 0.01	29.3 ± 3.6
	A @ 200	12.17 ± 3.4	9.66 ± 2.82	3.15 ± 1.01	0.33 ± 0.04	11.035 ± 1	0.41 ± 0.059	0.26 ± 0.04	24.4 ± 3.7
	A @ 220	13.1 ± 1.35	9.76 ± 0.99	3.31 ± 0.69	0.34 ± 0.07	11.555 ± 0.11	0.35 ± 0.02	0.20 ± 0.02	28.6 ± 1.9
	A @ 240	13.3 ± 0.04	9.90 ± 0.98	3.43 ± 0.95	0.35 ± 0.013	11.716 ± 0.62	0.48 ± 0.003	0.28 ± 0.02	20.8 ± 1.5
RGM	As-cast	7.21 ± 1.36	5.48 ± 1	1.73 ± 0.39	0.32 ± 0.05	7.100 ± 0.52	0.38 ± 0.036	0.20 ± 0.03	26.6 ± 2.5
	SHT	23.5 ± 3.85	17.2 ± 1.88	6.3 ± 0.99	0.37 ± 0.04	10.469 ± 0.28	0.66 ± 0.048	0.48 ± 0.035	15.2 ± 1.1
	A @ 155	14.37 ± 2.6	10.8 ± 2.6	3.57 ± 0.52	0.33 ± 0.09	10.369 ± 0.50	0.45 ± 0.049	0.32 ± 0.039	22.3 ± 2.2
	A @ 180	9.34 ± 1.31	7.19 ± 0.91	2.14 ± 0.42	0.297 ± 0.02	10.1 ± 1.1	0.34 ± 0.04	0.2 ± 0.03	29.4 ± 3.4
	A @ 200	13.73 ± 1.5	10.3 ± 1.36	3.43 ± 0.11	0.334 ± 0.03	11.138 ± 0.64	0.37 ± 0.02	0.22 ± 0.03	27 ± 1.1
	A @ 220	14 ± 1.93	10.4 ± 1.36	3.6 ± 0.59	0.346 ± 0.02	11.346 ± 0.73	0.45 ± 0.034	0.29 ± 0.026	22.1 ± 2.2
	A @ 240	14.33 ± 3.4	10.57 ± 2.49	3.76 ± 0.25	0.36 ± 0.05	10.402 ± 0.48	0.52 ± 0.07	0.32 ± 0.06	19.2 ± 2.6

Although the tensile and impact properties were not determined from exactly the same samples with identical microstructures, it is of interest to compare the improvement obtained with modification. In both cases, the samples (impact bars and tensile bars) were cast in permanent molds. Impact strength increased by about 31% when the alloy was modified, while tensile elongation improved by about 15%. This relatively poor improvement in tensile properties was explained by the presence of porosity associated with modification. It appears, therefore, that impact properties are more sensitive to the modification itself and are less affected by porosity than simple tensile properties. The standard deviation in the total impact energy for the modified alloy (± 2.1), however, remains higher than for the unmodified alloy (± 0.98). Similar observations were reported by Tsukuda[251] who indicated that impact results are more sensitive to the as-cast microstructure of Al-Si alloys than are the tensile test results, and the influence of porosity on impact test results is not as significant as it is on tensile test results.

The total absorbed energy does not provide much information on the details of the fracture behaviour of a material, hence the interest of dividing the energy into two parts: crack initiation energy (E_i) and crack propagation energy (E_p). In real terms, any brittle, high strength material will manifest high crack initiation energy, E_i, and low crack propagation energy, E_p. Conversely, a low strength ductile material will have low E_i and high E_p. Therefore, even though the Charpy energy for each of the two materials may be the same, their fracture behavior is quite different. These observations indicate that the use of a "ductility index" (DI), which is the ratio of the propagation to initiation energies is to be recommended highly.

Modification and grain refinement affect not only the total absorbed energy but also the fracture behavior of the impact samples. This is illustrated by the two energy values involved in the fracture of the impact specimens shown in Figure 5.3. For a particular stacked column, the lower bar represents the energy required to initiate fracture, E_i, and the top bar represents the energy required to propagate fracture, E_p. The sum of these two bars is the total absorbed energy, or the impact strength of the alloy. As expected, the crack initiation energy is improved by modification, increasing by 28% from 4.3 J to 5.5 J. This may be explained by the change in silicon morphology from an acicular to a fibrous form resulting in a diminution of stress concentration at the silicon-aluminum interface. Strontium also reduces the size of the Si particles resulting in higher crack propagation energy, since a crack has more chance of propagating in the ductile matrix without encountering a brittle silicon particle.

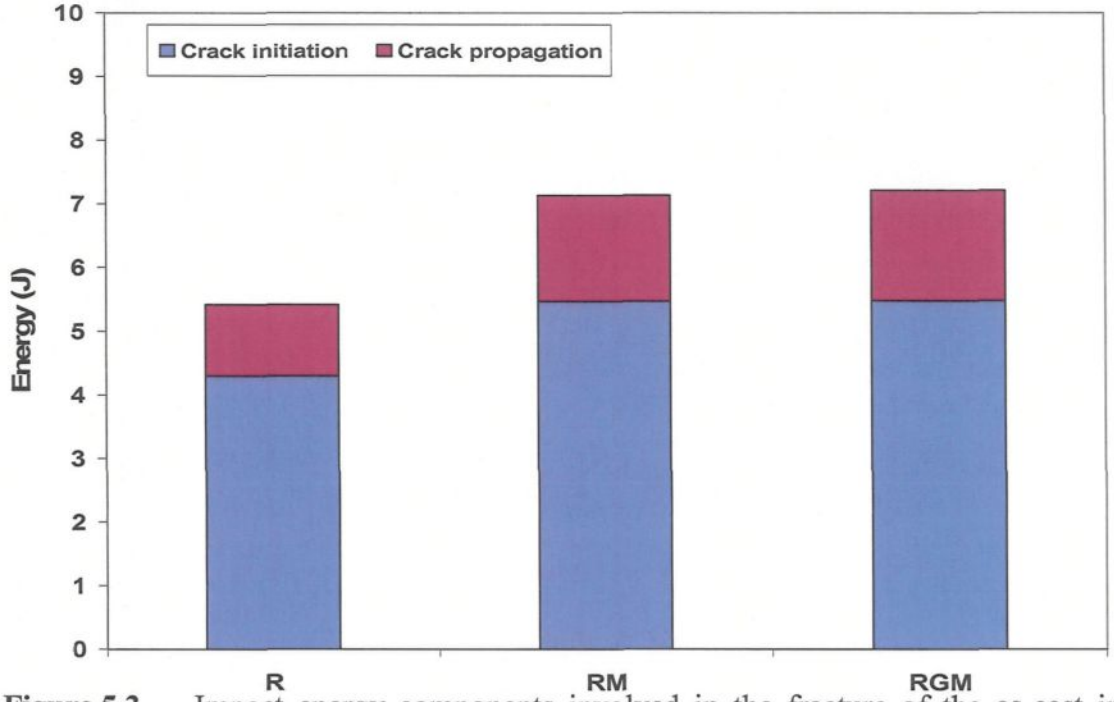

Figure 5.3 Impact energy components involved in the fracture of the as-cast impact samples.

The crack propagation energy changed from 1.1 J to 1.7 J with an addition of strontium, corresponding to a 55% increase. Consequently, the ductility index, which is defined as the ratio of propagation to initiation energies, increased from 0.26 to 0.30 with modification (see Table 5.1). As expected, the combined addition of modifier and grain refiner displays the best ductility index of all the alloys studied. The maximum load was of the order of 6845 N and 7100 N for both the RM and the RGM alloys corresponding to an increase of 15% and 19%, respectively, compared to the R alloy. Average crack speed is a useful parameter with which to characterize the crack propagation phenomenon; it may be defined as the sample width divided by the total time elapsed from the moment the load was exerted to the moment it was removed. From Table 5.1, it is clear that the untreated R alloy displays the highest crack speeds compared to the modified RM and modified grain-refined RGM alloys. This untreated alloy also reveals the lowest impact energy components. Figures 5.4 and 5.5 show examples of curves recorded for solutionized untreated and melt-treated alloys, respectively. Significant changes were observed in the impact behavior of the alloys after solution heat-treatment, although the difference between untreated and treated samples persisted. The average values as well as the standard deviations of the impact parameters are presented in Table 5.1 for solution heat-treated alloys. All the impact properties of solutionized heat-treated samples were largely superior to the corresponding values of the as-cast samples. As may be observed from the curves already recorded, the scattering in the impact properties was greater for the solutionized alloys than it was for as-cast alloys. This fact is reflected in the higher standard deviations

observed for the solution-treated samples of R and RM alloys (±2.5 and ±3.5, respectively) compared to those obtained for the as-cast condition (±1 and ±2, respectively).

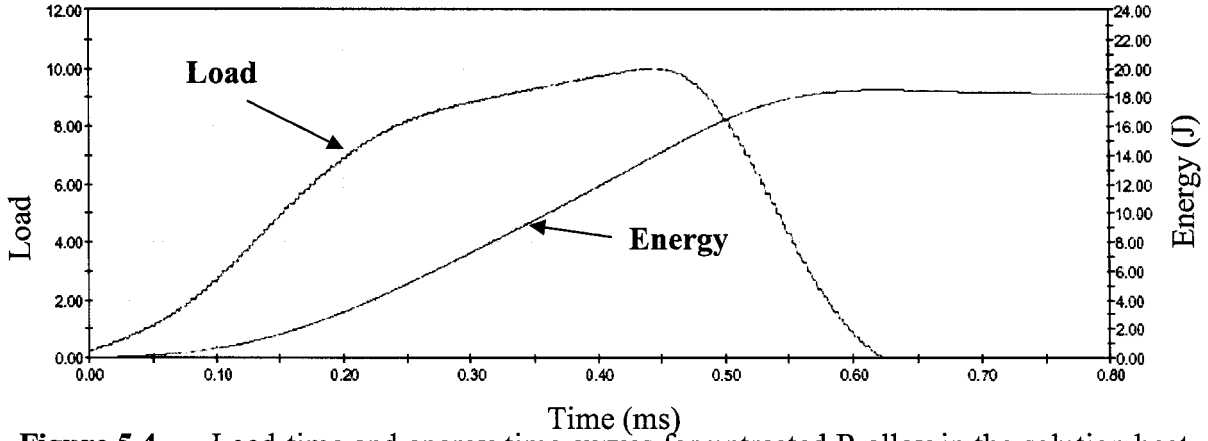

Figure 5.4 Load-time and energy-time curves for untreated R alloy in the solution heat-treated condition.

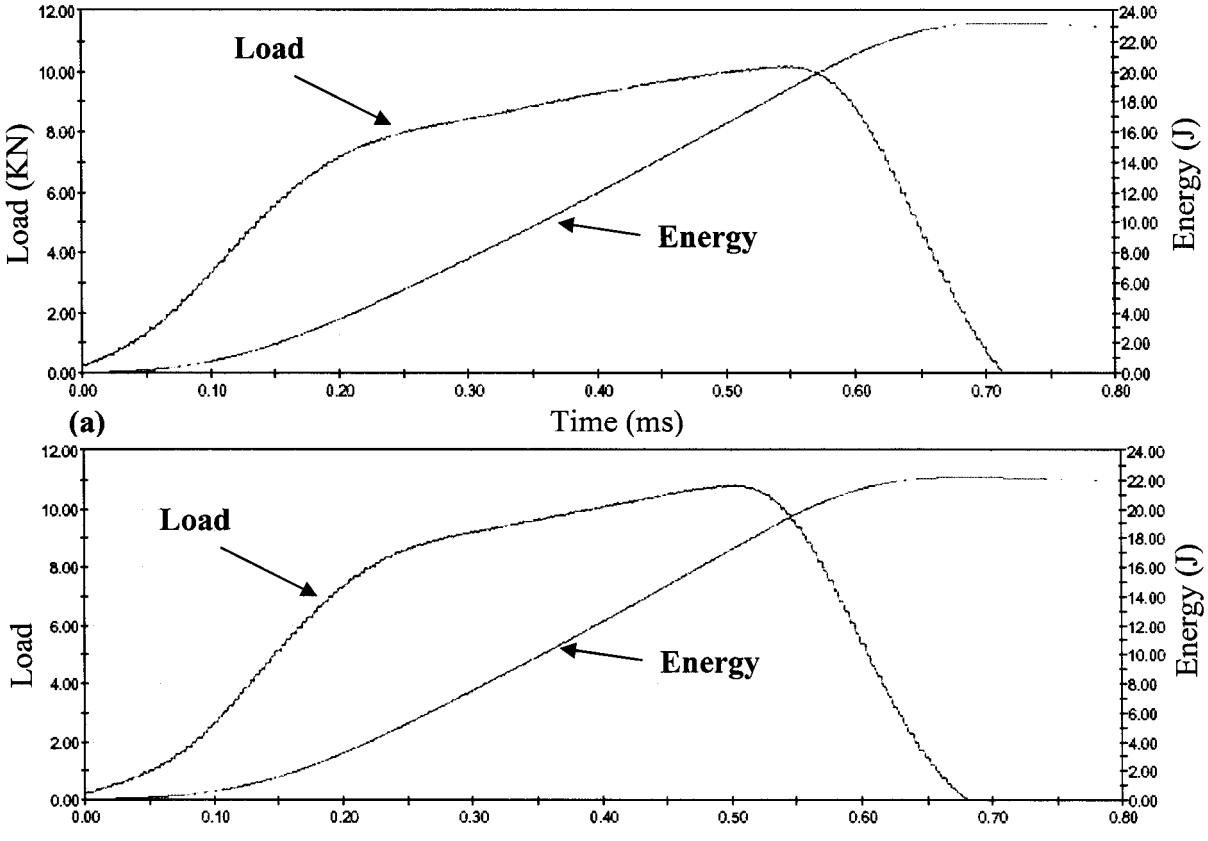

Figure 5.5 Load-time and energy-time curves for (a) Sr-modified RM, and (b) Sr-modified and grain refined RGM alloys in the solution heat-treated condition.

After solution heat-treatment, the total absorbed energy of the unmodified R alloy was 14.3 J, corresponding to a 213% improvement due to the decrease of stress concentration as the eutectic silicon changed from acicular to spherical form during the holding period at elevated temperature. It also should be noted that the impact strength of the *solution-treated* unmodified R alloy was greater than that of the *as-cast* modified RM alloy. The microstructural change of the eutectic silicon from acicular to fibrous form yielded only a 31% increase. From this point of view, heat treatment is deemed to be better than modification in improving the impact properties.

When modification was combined with solution heat treatment, however, still higher values of total absorbed energy were obtained: the solution-treated RM modified alloy showed an improvement of about 226%, with a total absorbed energy of 23.22 J. This increase resulted from the fragmentation of the branched and fibrous eutectic silicon into small segments which rapidly spheroidized and coarsened, as indicated by the quantitative study of the microstructures. It should be noted that the maximum load of solutionized unmodified R alloy was of the order of 10410 N, corresponding to an increase of 74%, which implies that the solution heat treatment caused larger changes in this parameter than did modification.

The influence of aging temperatures on untreated and melt-treated alloys is shown in Figure 5.6, where the total absorbed energy was plotted as a function of aging temperature. The impact strength of the alloys decreased with an increase in aging temperature of up to 180°C and then rebounded 25-30% up to 240°C. These results are

consistent with those obtained for tensile ductility, as observed for the range of alloys examined.

Crack initiation and propagation energies of the alloys were both affected by aging treatment with variations in temperature similar to those obtained for the total absorbed energy. Figure 5.7 indicates how the total absorbed energy is distributed between the two energy values involved in the fracture of the impact specimens, *i.e* E_i and E_p. Consequently, the ductility index varied with aging temperature as shown in Figure 5.8.

In view of the fact that different alloys exhibit different microstructures, it is natural to expect that their impact energies will also differ, depending on the type and amount of microconstituents and defects present. The effects of the combined additions of Fe and Mn, and of Cu and Mg, on the impact strength of the Sr-modified grain-refined RGM alloy in as-cast and heat-treated conditions, used as a reference, will be discussed below.

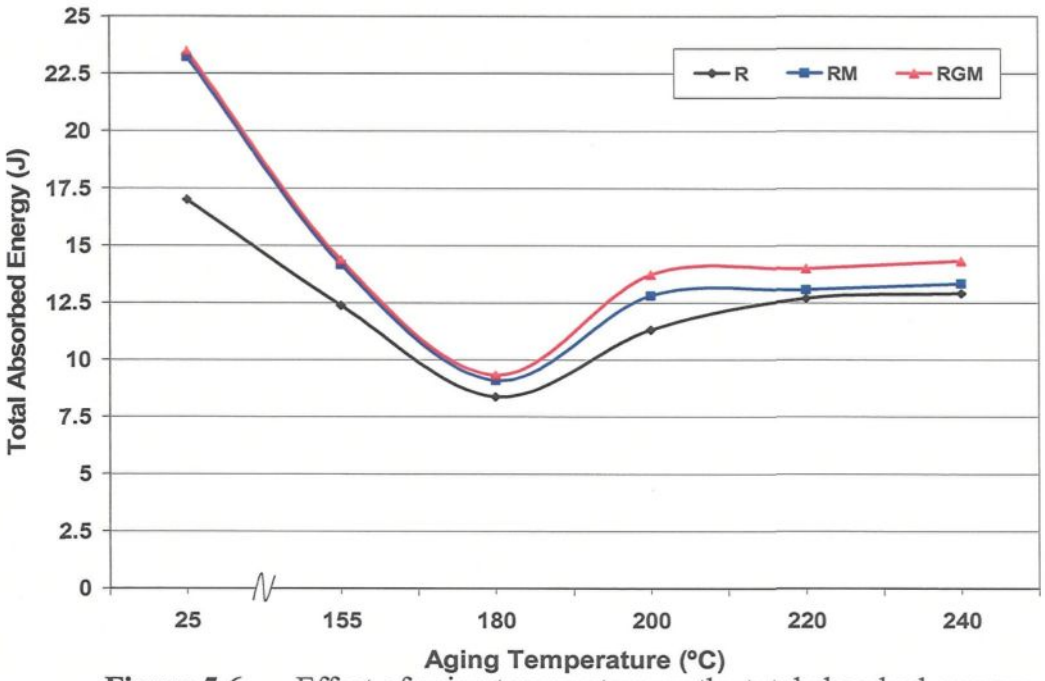

Figure 5.6 Effect of aging temperature on the total absorbed energy.

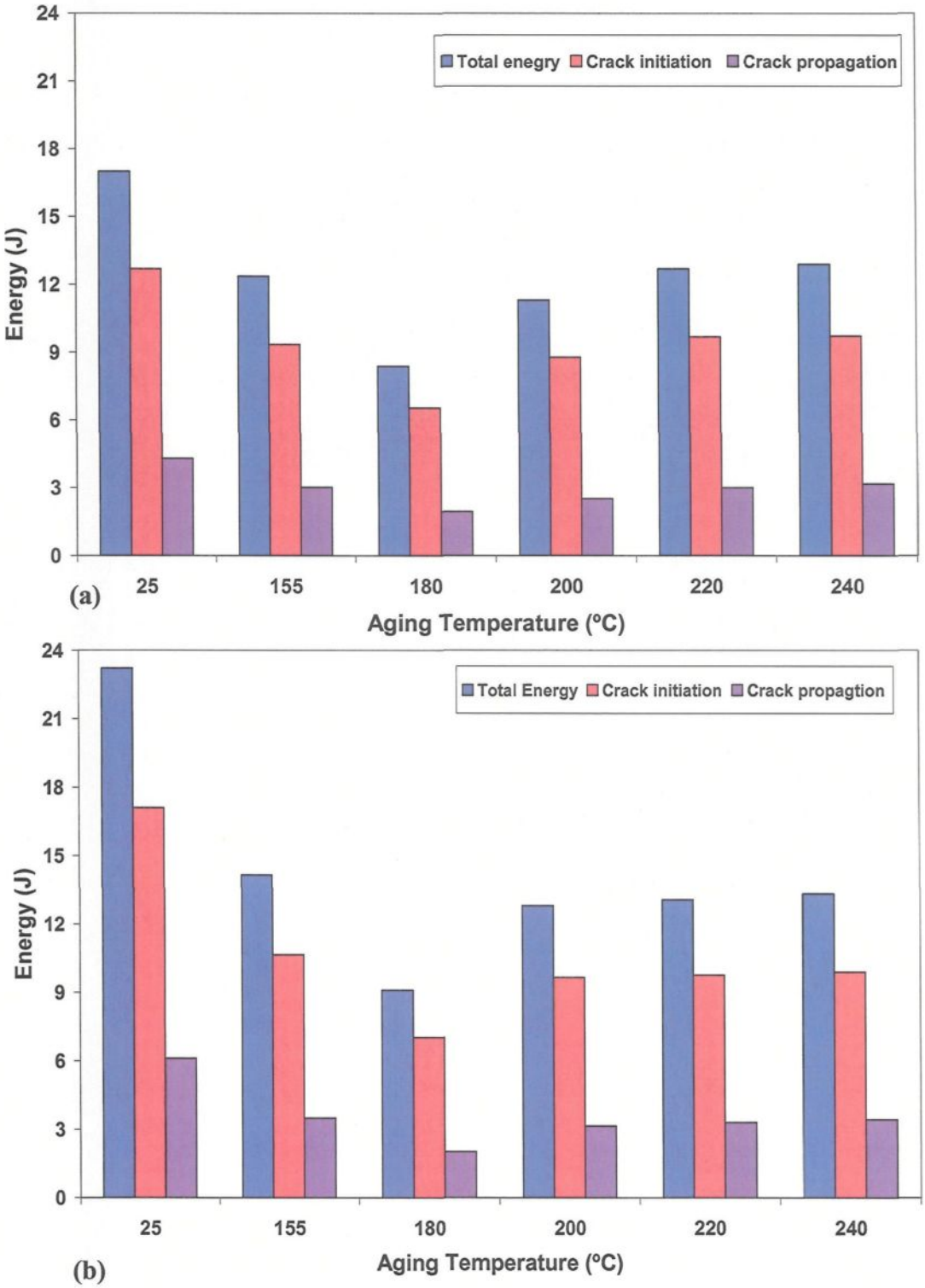

Figure 5.7 Effect of aging temperature on the energies involved in the fracture of impact bars for (a) unmodified R, and (b) modified RM alloys.

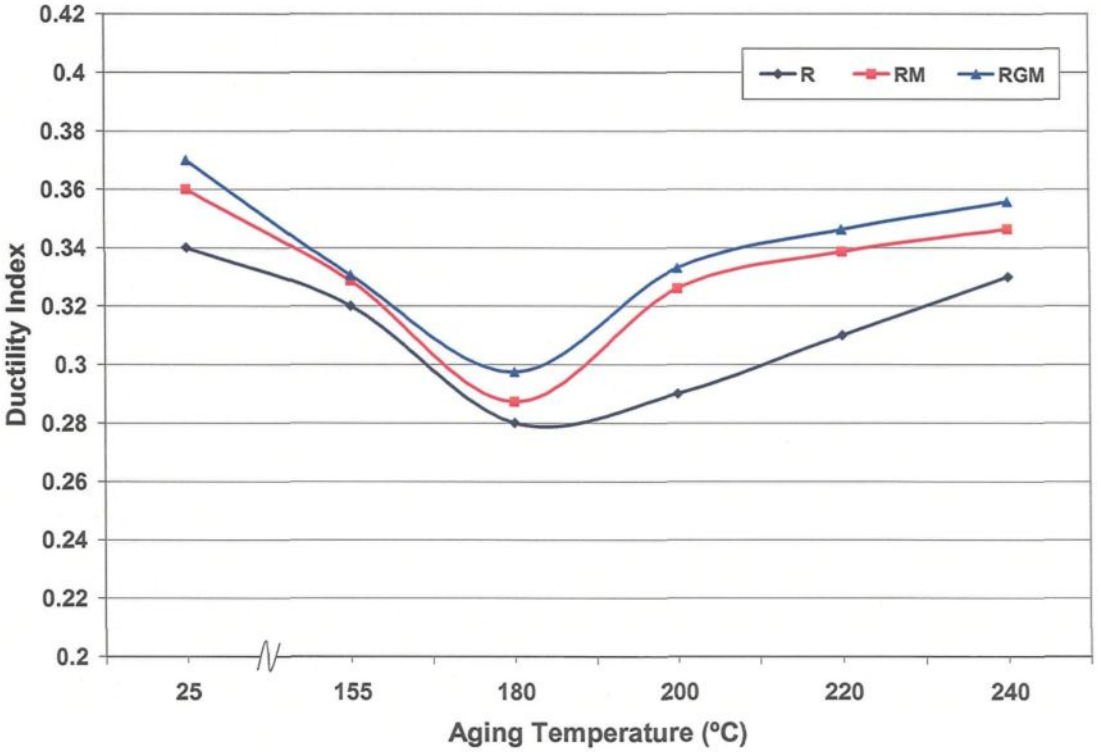

Figure 5.8 Effect of aging temperature on the ductility index.

5.1.3 Effects of the Addition of Fe and Mn

The effect of iron on the mechanical properties of Al-Si alloys was investigated by Komastu *et al.*[252] Their results show that iron has a detrimental effect on the impact strength of these alloys because of the formation of Al-Si-Fe compounds. Table 5.2 shows the results for the different parameters as determined from the instrumented impact tests for the Sr-modified grain-refined RGM alloy, thus making it possible to investigate the effects of various additions of Fe, whether individually or in combination with Mn, in as-cast and heat-treated conditions. In the as-cast condition, the total absorbed energy, E_t, of the RGM alloy is found to decrease with an increase in Fe whether added individually, or in

combination with Mn. For example, the E_t value of the RF1 alloy (containing ~0.75% Fe and ~0.75% Mn) is decreased by 12% compared to its value in the RGM alloy. The decreasing of E_t for the RF1 alloy may be attributed to an increase in the volume fraction of iron intermetallics, as discussed previously in Chapter 4, section 4.2.

At high Fe levels of ~1%, the impact energy is considerably lower due to the formation of sludge and β-Fe, respectively, as was to be observed in the case of the RF2 and RF4 alloys. Such intermetallics serve as stress concentration sites and tend to promote crack propagation, ultimately resulting in low impact energy values. The total absorbed energy of the RF4 alloy (containing ~1% Fe and ~0.5% Mn) is low compared to the other alloys studied. It is also interesting to note that the impact strength is more sensitive to minimal variations in the microstructure than elongation. Similar observations were made by Richard,[253] who indicated that impact energy values are more sensitive to the as-cast microstructure of Al-Si alloys than the tensile properties.

Figure 5.9 indicates how the crack initiation and propagation energies of the alloys were affected by the addition of Fe, either individually or in combination with Mn. As expected, the crack initiation energy decreased with an increase in the iron content. For example, the crack initiation energy decreased by ~11%, from 5.48 J for RGM alloy to 4.9 J for RF1 alloy, with the addition of Fe. Since a crack has little chance to propagate in the brittle matrix, the crack propagation energy changed from 1.73 J in the RGM alloy to 1.47 in the RF1 alloy. Consequently, the ductility index decreased from 0.32 in the RGM alloy to 0.30 in the RF1 alloy. The average crack speed for the alloys studied with respect to Fe and Mn contents is shown in Figure 5.10. It may be observed that the highest crack speeds

were obtained for the alloys containing the highest iron levels, thus indicating that these alloys possessed the lowest energies. Even after solution heat treatment, these alloys displayed no significant increase in the impact energy due to the brittle and hard nature of the iron microconstituents. The formation of these undesirable phases is not changed or only slightly changed by solution heat treatment at 495°C, resulting in low impact energy values. Figure 5.11 shows the impact strength of the RGM alloy as a function of aging temperature with the various additions of Fe and Mn. It is seen that the addition of Fe individually or in combination with Mn reduces the total absorbed energy of the RGM alloy at all aging temperatures. The impact energy of all the alloys displays the same behavior undergoing artificial aging procedures; it decreases with increasing aging temperatures of up to 180°C, and then increases slightly with further increase in aging temperature. As a result, the ductility index also decreases as the aging temperature increases up to 180°C, increasing thereafter with further increase in aging temperature, as shown in Figure 5.12. It may be observed that the RF1 alloy (~0.75% Fe, ~0.75% Mn) displays the highest ductility index followed by RF3 alloy (~0.75% Fe, ~0.5% Mn) at all aging temperatures. It may thus be deduced that optimum impact properties for the RGM alloy can be achieved by keeping the Fe and Mn levels at a minimum (< 0.75%).

Table 5.2 Effects of Fe and Mn addition and aging temperature on the impact properties

Alloy Code	Condition	Total absorbed energy, E_T (J)	Crack initiation energy, E_i (J)	Crack propagation energy, E_p (J)	Ductility index DI	Total Time (ms)	Time to maximum load, (ms)	Average crack speed (mm/ms)
RF1	As-cast	6.37 ± 1.29	4.9 ± 0.89	1.47 ± 0.56	0.3 ± 0.08	0.348 ± 0.036	0.21 ± 0.02	29 ± 3.2
	SHT	12.9 ± 2.5	9.83 ± 2.03	3.073 ± 0.58	0.32 ± 0.06	0.469 ± 0.052	0.304 ± 0.05	21.6 ± 2.6
	A @ 155	10.02 ± 1.6	7.71 ± 1.15	2.3 ± 0.49	0.297 ± 0.02	0.367 ± 0.03	0.206 ± 0.03	27.3 ± 2.1
	A @ 180	6.1 ± 0.66	4.83 ± 0.81	1.25 ± 0.55	0.27 ± 0.02	0.298 ± 0.01	0.168 ± 0.01	33.6 ± 0.14
	A @ 200	7.33 ± 0.31	5.66 ± 0.15	1.66 ± 0.14	0.29 ± 0.02	0.31 ± 0.01	0.167 ± 0.02	32 ± 5.3
	A @ 220	7.58 ± 0.49	5.62 ± 0.53	1.97 ± 0.97	0.3 ± 0.02	0.334 ± 0.01	0.181 ± 0.01	29.9 ± 0.1
	A @ 240	9.36 ± 0.88	7.1 ± 0.91	2.26 ± 0.39	0.32 ± 0.07	0.386 ± 0.03	0.23 ± 0.02	26 ± 0.2
RF2	As-cast	6.13 ± 0.95	4.8 ± 0.01	1.25 ± 0.23	0.255 ± 0.05	0.30 ± 0.003	0.19 ± 0.004	33 ± 0.8
	SHT	9.04 ± 2.1	7.13 ± 1.7	1.9 ± 0.35	0.269 ± 0.01	0.44 ± 0.04	0.41 ± 0.06	23 ± 6.7
	A @ 155	6.42 ± 0.88	5.1 ± 0.61	1.32 ± 0.27	0.26 ± 0.02	0.366 ± 0.1	0.16 ± 0.07	29.9 ± 5.7
	A @ 180	5.81 ± 0.45	4.65 ± 0.49	1.16 ± 0.13	0.25 ± 0.04	0.286 ± 0.01	0.23 ± 0.01	34.9 ± 1.1
	A @ 200	6.74 ± 1.28	5.29 ± 0.84	1.45 ± 0.44	0.27 ± 0.04	0.359 ± 0.001	0.26 ± 0.01	27.8 ± 1.0
	A @ 220	6.87 ± 0.35	5.29 ± 0.1	1.58 ± 0.37	0.295 ± 0.04	0.367 ± 0.02	0.24 ± 0.02	27.2 ± 1.4
	A @ 240	8.59 ± 0.86	6.61 ± 0.88	1.98 ± 0.37	0.31 ± 0.08	0.367 ± 0.02	0.21 ± 0.09	27.2 ± 1.2
RF3	As-cast	6.35 ± 1.1	4.97 ± 0.86	1.38 ± 0.27	0.28 ± 0.04	0.34± 0.03	0.20 ± 0.02	29.4 ± 2.4
	SHT	12.24 ± 0.94	9.38 ± 1.03	2.86 ± 0.12	0.31 ± 0.04	0.46 ± 0.04	0.36 ± 0.01	22 ± 1.8
	A @ 155	9.14 ± 2.1	7.11 ± 1.7	2.02 ± 0.42	0.28 ± 0.01	0.35 ± 0.04	0.21 ± 0.03	28.7 ± 3.7
	A @ 180	6.16 ± 1.1	4.89 ± 0.81	1.27 ± 0.24	0.26 ± 0.01	0.325 ± 0.02	0.19 ± 0.02	30.8 ± 2.1
	A @ 200	6.89 ± 1.2	5.4 ± 0.96	1.49 ± 0.28	0.28 ± 0.02	0.33 ± 0.02	0.19 ± 0.03	30.2 ± 1.9
	A @ 220	7.31 ± 0.88	5.64 ± 0.71	1.67 ± 0.18	0.30 ± 0.01	0.35 ± 0.02	0.2 ± 0.02	29 ± 1.4
	A @ 240	9 ± 0.96	6.89 ± 0.9	2.11 ± 0.07	0.31 ± 0.03	0.4 ± 0.03	0.25 ± 0.02	24.9 ± 1.6
RF4	As-cast	5.69 ± 1.5	4.66 ± 1.17	1.04 ± 0.34	0.22 ± 0.03	0.33 ± 0.03	0.19 ± 0.03	30.6 ± 2.4
	SHT	7.5 ± 0.87	5.99 ± 0.78	1.52 ± 0.13	0.26 ± 0.03	0.34 ± 0.03	0.20 ± 0.02	29.3 ± 2.2
	A @ 155	6.82 ± 0.65	5.37 ± 0.52	1.46 ± 0.13	0.24 ± 0.04	0.32 ± 0.01	0.18 ± 0.01	30.9 ± 1.1
	A @ 180	4.25 ± 0.64	3.43 ± 0.51	0.82 ± 0.16	0.238 ± 0.03	0.266 ± 0.01	0.14 ± 0.01	37.6 ± 1.4
	A @ 200	4.73 ± 0.36	3.75 ± 0.22	0.98 ± 0.17	0.26 ± 0.03	0.286 ± 0.01	0.16 ± 0.02	34.9 ± 2.1
	A @ 220	4.95 ± 0.43	3.88 ± 0.43	1.09 ± 0.01	0.28 ± 0.03	0.305 ± 0.02	0.18 ± 0.01	32.8 ± 2.1
	A @ 240	5.93 ± 0.97	4.55 ± 0.54	1.38 ± 0.25	0.30 ± 0.02	0.315 ± 0.02	0.18 ± 0.02	31.8 ± 2.5

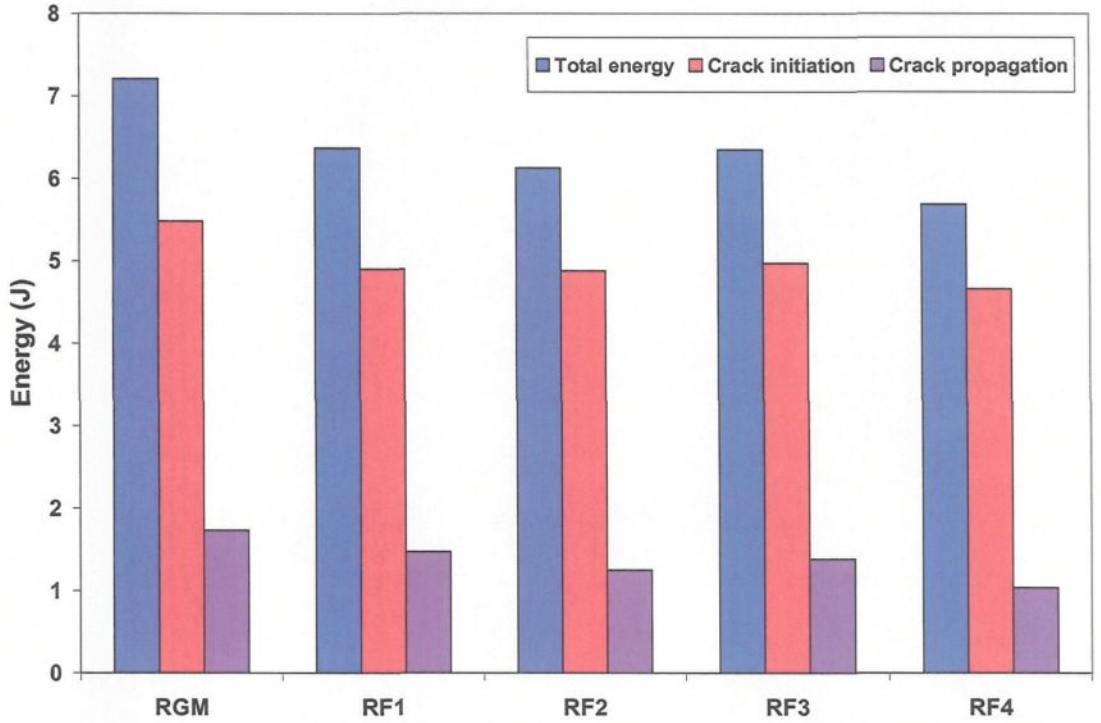

Figure 5.9 Effects of the addition of Fe and Mn on the energies involved in the fracture of impact bars in as-cast condition.

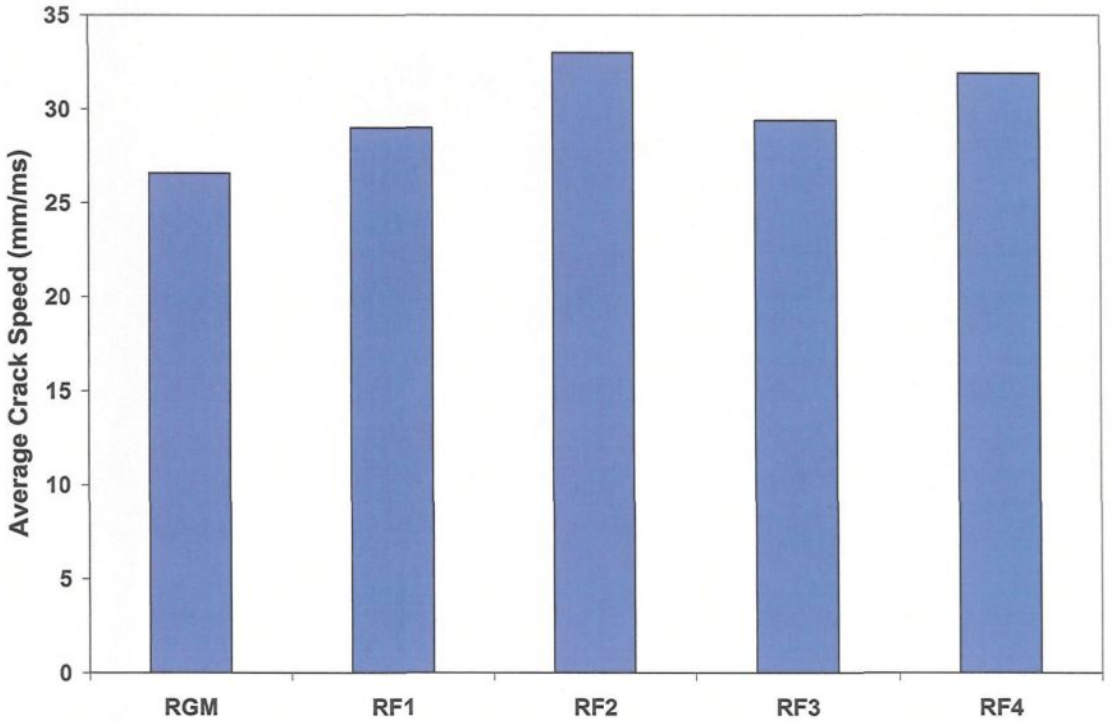

Figure 5.10 Average crack speeds as a function of Fe and Mn additions to RGM alloy (as-cast condition).

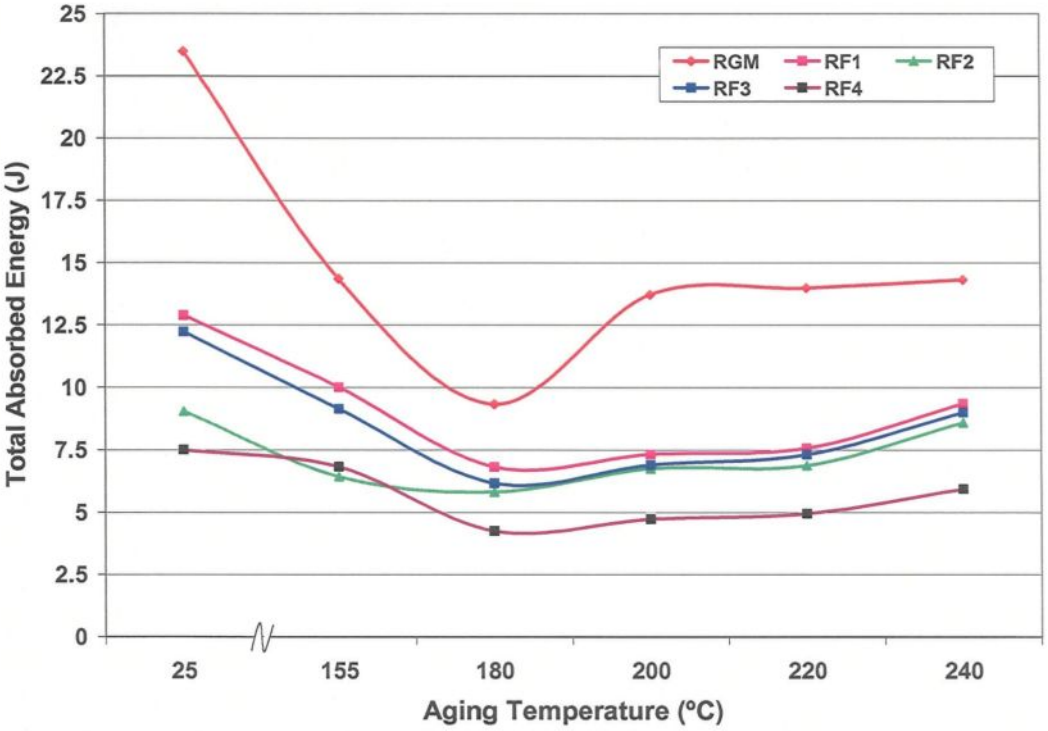

Figure 5.11 Total absorbed energy of the alloys studied as a function of aging temperature.

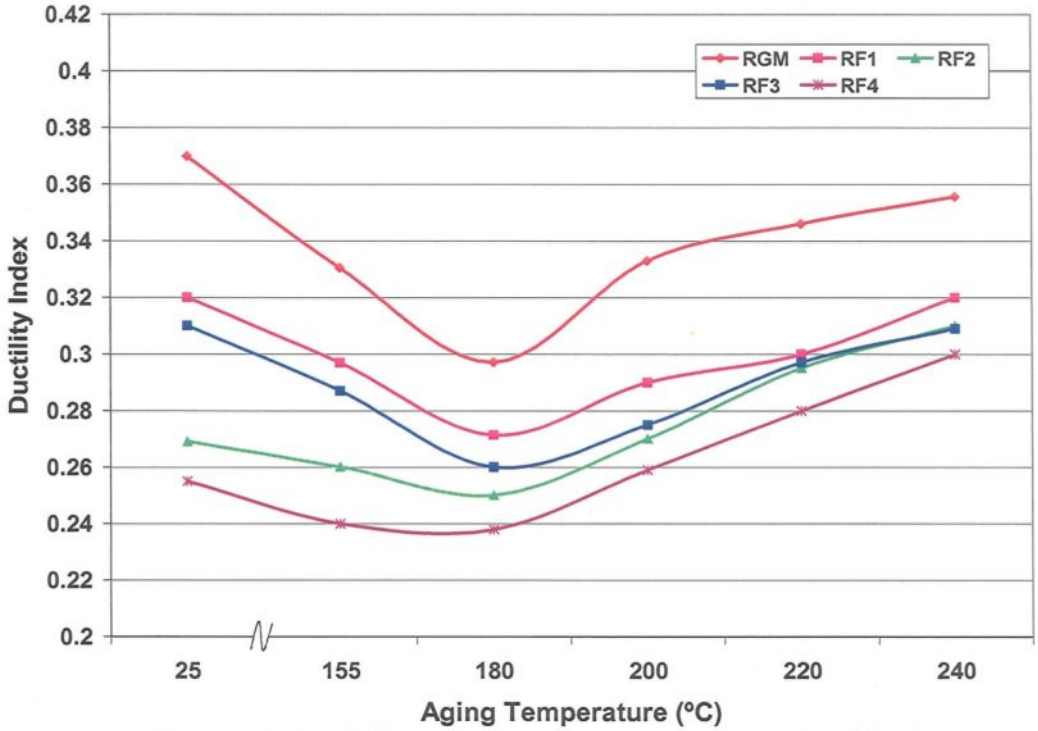

Figure 5.12 Effect of aging temperature on the ductility index.

5.1.4 Effects of the Addition of Cu and Mg

With regard to the addition of Cu and Mg to the RGM alloy, Table 5.3 provides the average values and standard deviations for the different parameters as determined from the instrumented impact tests. In general, the impact energies are relatively low with increases in the Cu and/or Mg content. As mentioned previously in Chapter 4 and shown in Figure 4.8, the volume fraction of the blocky Al_2Cu phase increases with an increase in Cu content. In addition to the modification of the silicon phase, there is a tendency to form an increased amount of blocky Al_2Cu in the presence of Sr, although dispersed Al_2Cu also forms. These particles provide further crack-initiations sites in addition to those of the brittle Si particles. Paray *et al.*[254] have suggested that in Cu-containing alloys such as 319 and 332, the fracture behavior is controlled by the Al_2Cu particles rather than by the Si particles.

It may be observed that at a high Mg level of ~0.5%, the impact energy is considerably lower, as observed in the case of the RC3, RC4, and RC5 alloys, in both as-cast and solution heat-treated conditions. This result may be attributed to the brittle and hard nature of the $Al_5Cu_2Mg_8Si_6$ particles which are habitually unaffected by solution heat-treatment. Magnesium has also been reported to negate the effects of Sr-modification, as shown previously in Table 4.1. In addition, the influence of both Sr and Mg on the segregation of Al_2Cu phase is expected to increase the severity of the segregation, resulting in the formation of large amounts of the coarse block-like form of the phase, thus providing a further cause of the reduction in the impact energy. The decrease in the total absorbed

energy from one alloy to another is more significant at the highest Cu and Mg contents, compared to that observed for low Cu and Mg contents.

The dependence of the total absorbed energy, E_t, on aging temperature is shown in Figure 5.13. All the impact properties of the solutionized alloys were largely superior to the corresponding values in the as-cast condition. The improvement in the impact energy values may be explained by the even distribution of microconstituents and their dissolution in the aluminum matrix achieved through the solution heat treatment/quenching step. It may be observed that as the aging temperature increases from 155° to 180°C, a continuous decrease in E_t is noted for all the alloys studied. Further increase in aging temperature, between 200° and 240°C, reduces the impact energy of the alloys. It may also be observed, from Figure 5.14, that alloys with a low Mg-content have higher impact energy values compared to alloys with a high Mg-content at the same Cu-content and aging temperature. Consequently, the ductility indices for high Mg-containing alloys are lower than those for low Mg-containing alloys under the same conditions.

Table 5.3 Effects of Cu and Mg addition and aging temperature on the impact properties

Alloy Code	Condition	Total absorbed energy, E_T (J)	Crack initiation energy, E_i (J)	Crack propagation energy, E_p (J)	Ductility index, DI	Total Time, (ms)	Time to maximum load, (ms)	Average crack speed (mm/ms)
RC1	As-cast	6.79 ± 1.5	5.44 ± 1.28	1.35 ± 0.25	0.28 ± 0.04	0.369 ± 0.04	0.253 ± 0.03	27.2 ± 1.9
	SHT	18.59 ± 3.65	13.79 ± 3.14	4.79 ± 0.51	0.36 ± 0.04	0.61 ± 0.11	0.44 ± 0.11	17 ± 3.1
	A @ 155	13.6 ± 4.46	10.39 ± 3.4	3.21 ± 1.0	0.31 ± 0.02	0.36 ± 0.05	0.24 ± 0.02	27.8 ± 2.5
	A @ 180	9.17 ± 0.19	7.05 ± 0.17	2.05 ± 0.01	0.29 ± 0.02	0.338 ± 0.01	0.24 ± 0.02	29.6 ± 0.02
	A @ 200	10.92 ± 1.3	8.25 ± 1	2.67 ± 0.42	0.32 ± 0.05	0.34 ± 0.01	0.21 ± 0.01	29.4 ± 1
	A @ 220	11.33 ± 2.6	8.5 ± 2	2.8 ± 0.58	0.34 ± 0.03	0.42 ± 0.04	0.27 ± 0.03	24.12 ± 2.2
	A @ 240	11.92 ± 0.3	8.89 ± 0.77	3.03 ± 0.46	0.35 ± 0.08	0.45 ± 0.01	0.28 ± 0.01	22.3 ± 0.5
RC2	As-cast	6.87 ± 1.13	5.42 ± 0.97	1.45 ± 0.39	0.27 ± 0.01	0.354 ± 0.01	0.238 ± 0.03	28.2 ± 0.9
	SHT	13.48 ± 1.49	10.21 ± 0.9	3.27 ± 0.35	0.32 ± 0.04	0.435 ± 0.01	0.307 ± 0.02	23 ± 1.1
	A @ 155	10.16 ± 0.57	7.85 ± 0.73	2.3 ± 0.27	0.295 ± 0.07	0.33 ± 0.1	0.216 ± 0.01	30 ± 1.4
	A @ 180	7.39 ± 1.13	5.83 ± 0.85	1.56 ± 0.13	0.27 ± 0.03	0.32 ± 0.02	0.203 ± 0.01	31.2 ± 1.7
	A @ 200	7.5 ± 0.68	5.82 ± 0.61	1.67 ± 0.13	0.285 ± 0.03	0.33 ± 0.01	0.208 ± 0.01	30.4 ± 1
	A @ 220	8.73 ± 2.53	6.73 ± 2	2 ± 0.52	0.3 ± 0.02	0.36 ± 0.03	0.219 ± 0.02	28 ± 2.7
	A @ 240	10.64 ± 1.6	8.05 ± 1.15	2.58 ± 0.44	0.32 ± 0.03	0.43 ± 0.04	0.27 ± 0.03	23.5 ± 1.9
RC3	As-cast	6.64 ± 0.75	5.2 ± 0.55	1.44 ± 0.27	0.278 ± 0.04	0.355 ± 0.03	0.22 ± 0.02	28.5 ± 2.4
	SHT	13.42 ± 0.88	10.24 ± 0.81	3.19 ± 0.39	0.31 ± 0.02	0.48 ± 0.04	0.35 ± 0.01	20.9 ± 1.8
	A @ 155	9.38 ± 0.56	7.21 ± 0.51	2.17 ± 0.42	0.30 ± 0.01	0.35 ± 0.04	0.22 ± 0.03	28.7 ± 3.7
	A @ 180	7.73 ± 2.3	5.99 ± 1.79	1.74 ± 0.24	0.29 ± 0.01	0.346 ± 0.02	0.21 ± 0.02	30 ± 2.1
	A @ 200	8.11 ± 1.59	6.24 ± 1.21	1.86 ± 0.28	0.30 ± 0.02	0.35 ± 0.02	0.21 ± 0.03	28.3 ± 1.9
	A @ 220	9.1 ± 2.2	6.95 ± 1.75	2.15 ± 0.18	0.31 ± 0.01	0.41 ± 0.02	0.27 ± 0.02	24.3 ± 1.4
	A @ 240	10.94 ± 1.58	8.25 ± 1.1	2.69 ± 0.07	0.32 ± 0.03	0.46 ± 0.03	0.3 ± 0.02	22 ± 1.6
RC4	As-cast	6.42 ± 0.94	5.02 ± 0.74	1.40 ± 0.19	0.278 ± 0.01	0.35 ± 0.01	0.233 ± 0.01	28.3 ± 0.3
	SHT	13.38 ± 1.67	10.32 ± 1.42	3.06 ± 0.43	0.31 ± 0.04	0.5 ± 0.01	0.33 ± 0.01	20 ± 0.5
	A @ 155	8.98 ± 0.13	6.89 ± 0.25	2.09 ± 0.02	0.29 ± 0.04	0.34 ± 0.02	0.246 ± 0.02	29.2 ± 1.6
	A @ 180	7.41 ± 0.83	5.82 ± 0.65	1.58 ± 0.02	0.272 ± 0.02	0.33 ± 0.03	0.21 ± 0.03	31.2 ± 2.2
	A @ 200	7.82 ± 1.24	6.1 ± 1.1	1.74 ± 0.17	0.288 ± 0.02	0.33 ± 0.01	0.201 ± 0.01	30 ± 2.6

	A @ 220	8.29 ± 1.56	6.33 ± 0.4	1.96 ± 0.04	0.305 ± 0.01	0.357 ± 0.04	0.226 ± 0.03	28.2 ± 2.9
	A @ 240	9.74 ± 1.6	7.43 ± 0.19	2.31 ± 0.02	0.319 ± 0.06	0.4 ± 0.02	0.29 ± 0.02	24.8 ± 1.4
RC5	As-cast	4.86 ± 0.78	3.85 ± 0.59	1.01 ± 0.19	0.26 ± 0.02	0.31 ± 0.02	0.187 ± 0.01	32.7 ± 2.1
	SHT	11.16 ± 2.71	8.39 ± 2.1	2.77 ± 0.62	0.33 ± 0.01	0.43 ± 0.07	0.274 ± 0.06	24 ± 4.5
	A @ 155	8.26 ± 2.7	6.34 ± 2.4	1.92 ± 0.18	0.28 ± 0.05	0.33 ± 0.06	0.192 ± 0.05	27.6 ± 0.5
	A @ 180	7.13 ± 1.67	5.65 ± 1.56	1.48 ± 0.42	0.26 ± 0.01	0.306 ± 0.03	0.176 ± 0.02	32.7 ± 3.7
	A @ 200	7.25 ± 0.72	5.66 ± 0.53	1.59 ± 0.2	0.279 ± 0.01	0.314 ± 0.01	0.162 ± 0.01	31.8 ± 1.7
	A @ 220	7.39 ± 1.9	5.72 ± 1.55	1.67 ± 0.45	0.29 ± 0.01	0.33 ± 0.03	0.21 ± 0.04	29.9 ± 3.1
	A @ 240	8.45 ± 1.89	6.52 ± 1.54	1.93 ± 0.35	0.30 ± 0.02	0.36 ± 0.03	0.215 ± 0.03	27.8 ± 2.7

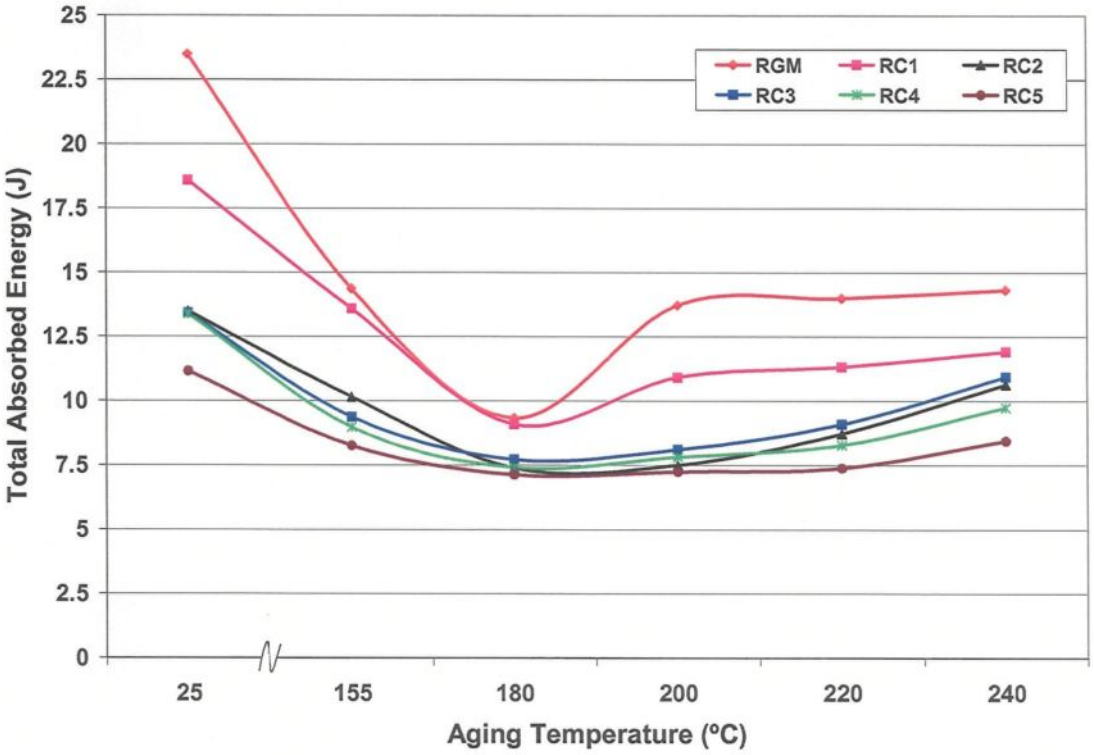

Figure 5.13 Effect of aging temperature on the total absorbed energy.

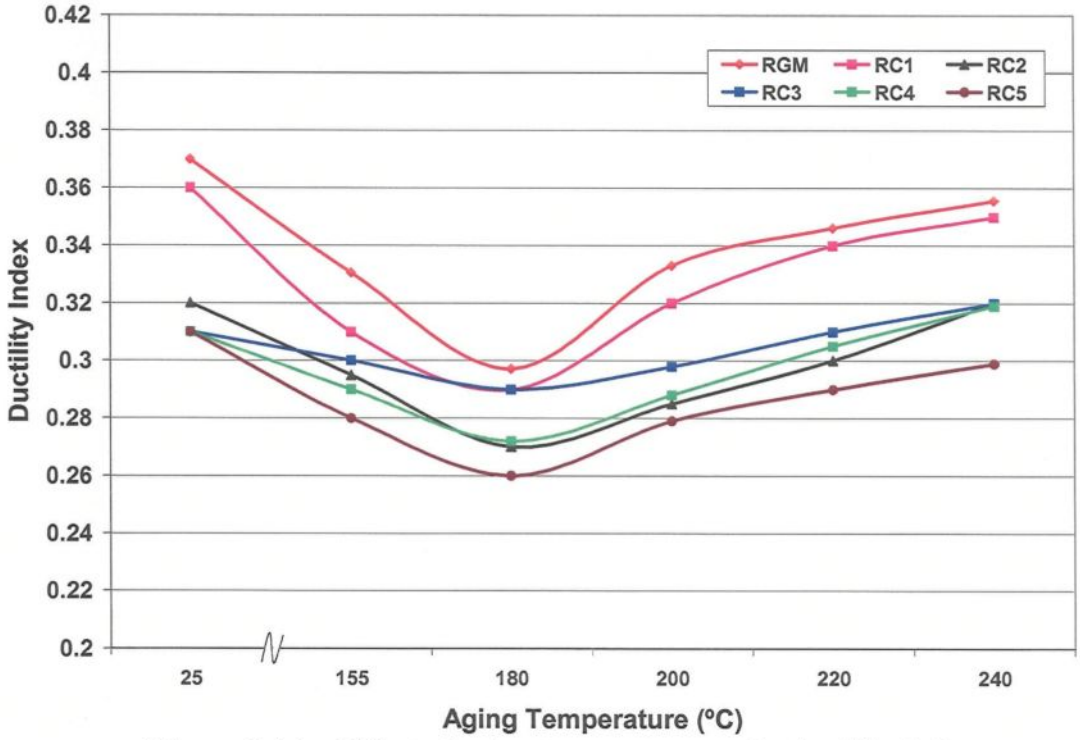

Figure 5.14 Effect of aging temperature on the ductility index.

5.1.5 Relationship between Impact Energy and Ductility

The relationship between impact energy and elongation is shown in Figures 5.15 through 5.17 for the alloys studied. In all cases, the graphs plotted for impact energy *vs.* elongation follow linear relationships, while the R^2 values are listed in Table 5.4. It may be observed that with an increase in percent elongation, the total absorbed energy of impact testing (E_t) increases for all alloys.

The impact energy *vs.* percent elongation relationships for the R, RM, and RGM alloys as a function of aging temperature are shown in Figure 5.15. With respect to ductility, linear correlations may be observed for both unmodified and modified alloys. The plots clearly depict that the increase in E_t and %El in the modified RM alloy and the grain-refined modified RGM alloy are much higher than those observed for the untreated R alloy, due mainly to the acicular eutectic Si phase in the later.

Figure 5.16 illustrates the dependence of the impact energy on the percent elongation of the alloys studied as a function of aging temperature and additions of Fe and Mn. It may be observed that the RF1 alloy (containing ~0.75% Fe, ~0.75% Mn) and the RF3 alloy (containing ~0.75% Fe and ~0.5% Mn) both possess relatively high E_t and %El values. However, alloys with a high Fe content, such as RF4 (containing ~1% Fe, ~0.5% Mn), or a high Fe and Mn content, such as RF2 (containing ~1% Fe and ~1% Mn), are characterized by low E_t and low %El values. Thus, it is clear that the presence of a high Fe-level is detrimental to both impact energy and ductility. In these high Fe-containing alloys, the persistence of the platelet-like β-Al_5FeSi, and sludge phases in RF4 and RF2, respectively, lowers the impact energy and ductility. This observation is consistent with

that of Grand,[255] who reported that increasing the iron content from 0.5 to 1.2% in an Al-13%Si casting alloy dramatically reduced its mechanical properties, particularly ductility, due to the formation of the β-Fe phase platelets.

Figure 5.17 shows the plots of impact energy, E_t, versus percent elongation of the alloys studied as a function of aging temperature and additions of Cu and Mg. In general, alloys with a Mg-content of 0.5% at different levels of Cu are characterized by low E_t and low %El, while alloys with a Mg content of 0.3% possess relatively high E_t and %El values. In all the cases, the correlations are quite good, as seen from the R^2 values listed in Table 5.4.

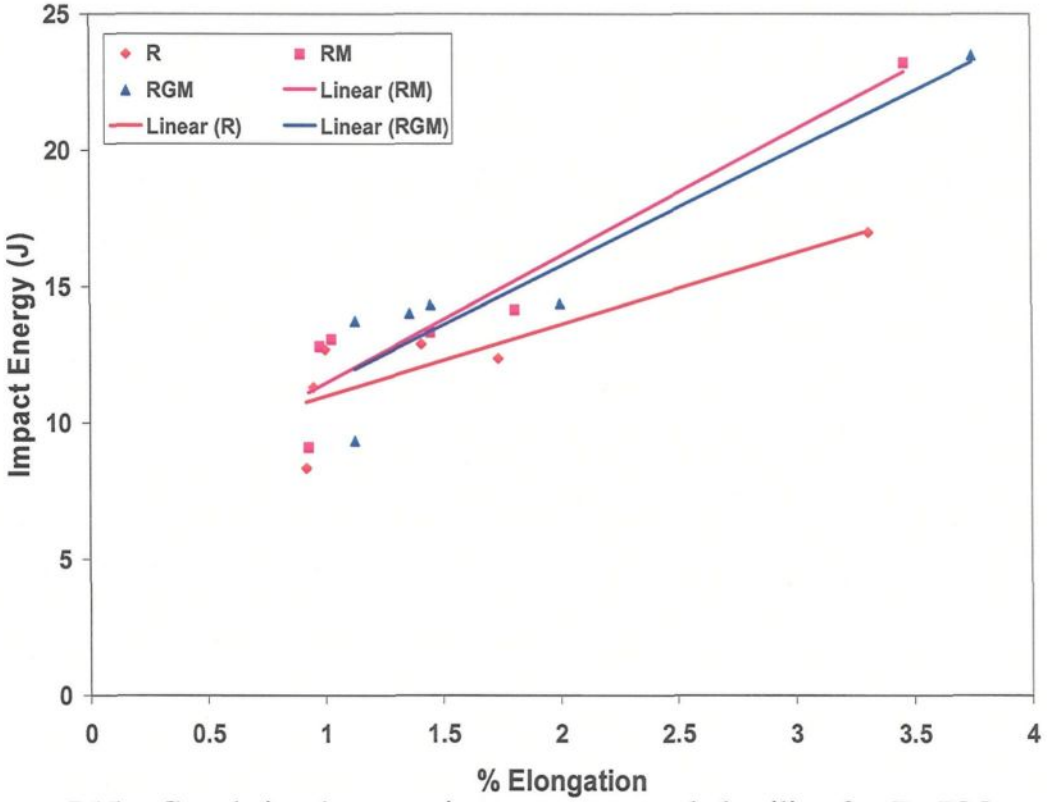

Figure 5.15 Correlation between impact energy and ductility for R, RM, and RGM alloys (heat-treated condition).

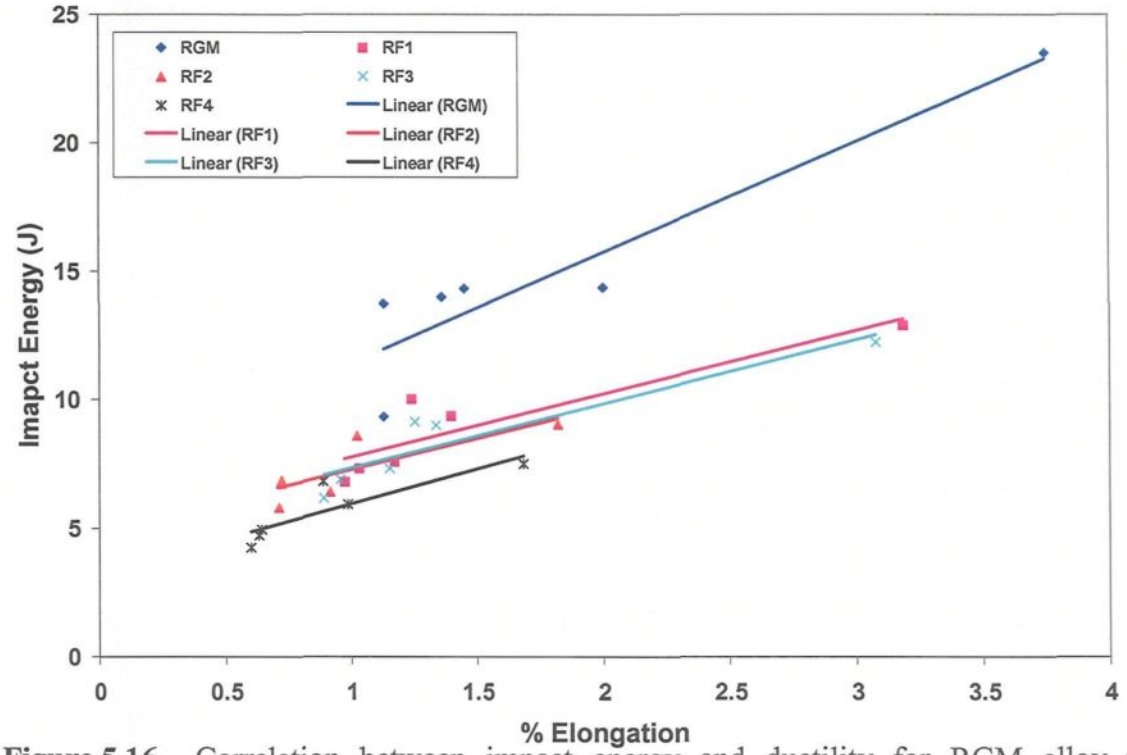

Figure 5.16 Correlation between impact energy and ductility for RGM alloy with different additions of Fe and Mn (heat-treated condition).

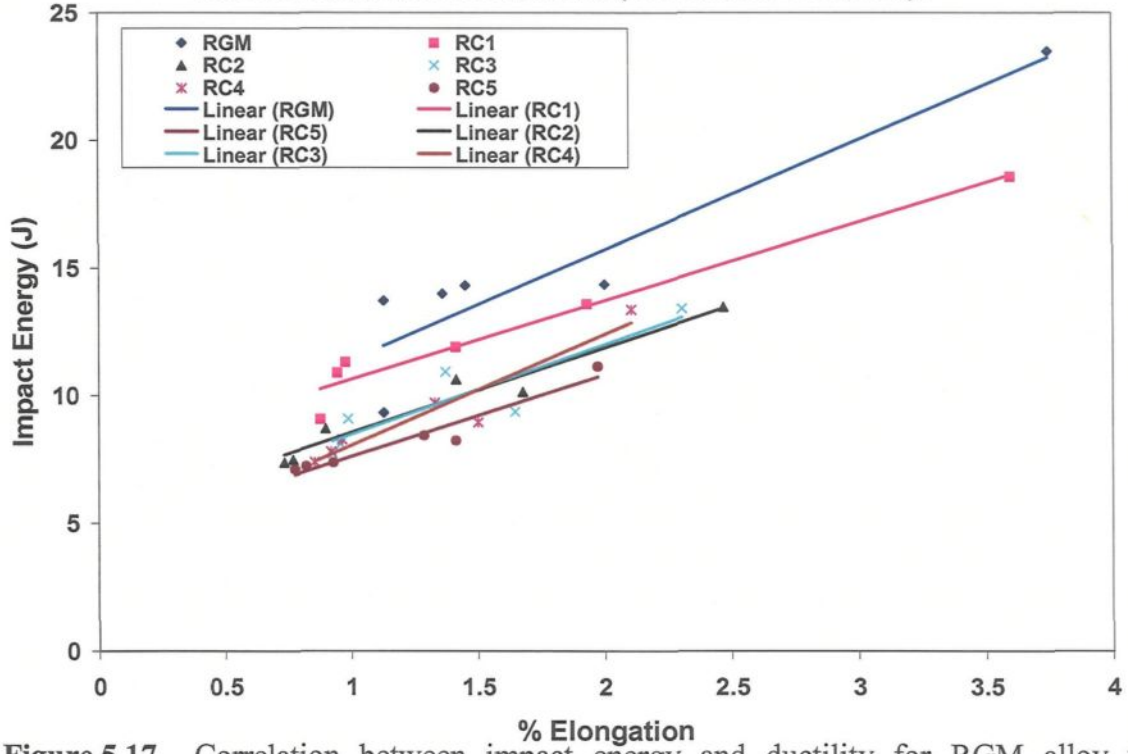

Figure 5.17 Correlation between impact energy and ductility for RGM alloy with different additions of Cu and Mg (heat treatment condition).

Table 5.4 R^2 values of trend lines in the impact energy – elongation plots shown in Figures 5.15, 5.16, and 5.17

Alloy	R^2 value
R	0.75
RM	0.91
RGM	0.87
RF1	0.80
RF2	0.70
RF3	0.87
RF4	0.77
RC1	0.96
RC2	0.95
RC3	0.82
RC4	0.91
RC5	0.94

5.2 STATISTICAL ANALYSIS

5.2.1 Introduction

Several experimental studies have been carried out over the past years to determine the effects of content variation of alloying elements on the microstructure and mechanical properties of Al-Si alloys. Selection of an alloy with certain specific properties is extremely laborious and time-consuming, particularly since classical methods have not always led to the development of a quantitative relationship between the mechanical properties of alloys on the one hand, and their composition or heat-treatment parameters on the other. Therefore, if two or more variables are alternated or interchanged amongst themselves, it could become difficult to quantify the effect that any interaction between different variables would have on mechanical properties.

Under these circumstances, physical metallurgists have used empirical methods based on physicomechanical models in order to solve problems of this calibre. Experiments were made to determine the effect of the independent variable (factor) on the dependent variable (response), while the relationship between them was illustrated using a regression model involving experimental data. Statistical design of experiments (DOE) is widely used as an efficient experimentation technique which has been applied to produce high quality products, to facilitate the economical operation of a number of procedures, and to ensure the stable and reliable progress of these same procedures.[15,16]

Studies involving the application of DOE methods have been made for more than four decades, and the advance of DOE applications has been assisted by developments in the field of computer science. Carr *et al.*[256] applied statistical program-planning to process improvement by applying fractional factorial design for the purpose of reducing development time. Major *et al.*[257] applied fractional factorial design to evaluate the microstructure of the Al-Mg_2Si casting alloy system in order to optimize alloy composition. Carranza-Barraza *et al.*[258] applied a Taguchi L8 orthogonal experimental design to evaluate the effect of chemical composition on the mechanical properties of a 319-type alloy. Ganguly *et al.*[259] used the statistical design of experiments to study and control the properties and behavior of Al-Mg-Si alloys.

Two-level factorial experimental designs are highly efficient, although the number of experimental runs increases exponentially with the number of factors. Some of these factors may be turn out to be inactive and, in such cases, would be dropped in further experiments; researchers may wish to use different factor settings in follow-up

experiments; a two-level design will identify interactions, but not quadratic effects, thus the design may need to be augmented and then subjected to further testing; some of the experiments may even need to be repeated; and/or the entire design may need to be replicated with a view to improving the accuracy of the estimates. The reason for which *fractional factorial designs* appeal to researchers is that they provide an efficient strategy for reducing work when relatively few effects are realistically to be expected, or that they are sufficiently noteworthy to require screening for more significant experimental settings.[16]

A fractional factorial design is an experimental layout where a full factorial design is augmented by one or more factors (independent variables) to be analyzed without increasing the number of experimental runs. These designs are labelled 2^{k-p}, where k is the number of factors which may be evaluated in a full factorial design of size 2^k, and p is the number of additional factors to be included. When a fourth factor requires to be incorporated in a 2^3 design of eight runs, the resulting design is a 2^{4-1} fractional factorial which also has $2^3 = 8$ runs. The full 2^4 factorial would thus have 16 runs. The 2^{4-1} factorial has only eight runs in that it is a half-fractional of the full four-factor design.

Statistical design of experiments, as a method, will be used in this chapter to develop regression models for the influence of the addition of alloying elements on the mechanical properties of the experimental Al-10.8%Si alloy. These models may be analyzed quantitatively in order to acquire an understanding of the effects of the variables and their interactions on the mechanical properties of the alloys under investigation. Furthermore, within the variation range of the variables studied, these equations may be

used to predict the composition of an alloy which, after the requisite heat treatment, would have the desired properties. The presence of strong interaction coefficients, as evidenced by non-linearity in the equations, justifies the adoption of an appropriate higher order design. A current and well-established system will be selected to examine the relevance of this mathematical technique by correlating the results generated in this section with those obtained experimentally by the conventional methods described in Chapter 3.

5.2.2 Factorial Design of Experiment

A number of factors which affect the mechanical properties of Al-Si alloys include (i) the alloy content; (ii) solutionizing time and temperature; (iii) aging time and temperature; and (iv) mode of casting. Four parameters were selected as independent variables while at the same time maintaining other factors such as solution heat-treatment temperature and time, quenching conditions, and aging time and temperature, constant. The four independent variables were tested at two levels in order to carry out the factorial design method. Table 5.5 lists these main variables and the code values used for each of them in these trials.

Table 5.5 Independent variables and their codes

Independent Variable	**Code**
Copper Content (wt%)	X_1
Magnesium Content (wt%)	X_2
Iron Content (wt%)	X_3
Manganese Content (wt%)	X_4

Five new alloys were prepared in the same way as was explained in Chapter 3, in order to design the matrix required for studying the effects of all the alloying elements on

the mechanical properties of the experimental Al-10.8%Si alloy, as presented in Chapters 4 and 5. The chemical compositions of these alloys and their respective codes are shown in Table 5.6. The hardness, tensile, and impact test bars obtained from these alloys were solution heat-treated at 495°C/8 h, then quenched in warm water at 65°C (quench delay was maintained at under 3 seconds), followed by artificial aging at 180°C for 5 hours (*i.e.* the bars were T6-tempered). The entire heat-treatment process was carried out in a Blue M forced-air furnace in which temperature uniformity was controlled to within ± 2°C.

Table 5.6 Chemical composition of the various alloys prepared for factorial analysis

Alloy code	Chemical Composition (wt %)							
	Si	Cu	Mg	Fe	Mn	Sr	Ti	Al
A	10.89	2.243	0.49	0.464	0.745	0.03	0.27	bal.
B	10.93	2.221	0.47	0.749	0.494	0.03	0.26	bal.
C	10.91	3.21	0.28	0.48	0.746	0.03	0.26	bal.
D	10.92	3.18	0.273	0.729	0.471	0.03	0.28	bal.
E	10.93	3.23	0.48	0.744	0.746	0.03	0.27	bal.

Four factors were varied on two levels, *i.e.* at an upper level and a lower level. The upper and lower levels of these four factors are as follows: Cu was varied between 2.25 and 3.25 wt%, Mg between 0.3 and 0.5 wt%, Fe between 0.5 and 0.75 wt%, and Mn between 0.5 and 0.75 wt%. Level values of these factors are listed in Table 5.7. The response of these data is characterized by the mean values of the mechanical properties; Table 5.8 lists the properties studied and the codes used to specify each property in the final regression equations obtained. According to the two-level experimental design, a nonlinear object may be approximated by a nonlinear regression function of Equations 5.1 and 5.2. Regression

models were obtained for the response variables with the level of confidence, $\alpha = 0.05$. The aim of the analysis was to find out the effect of independent variables on the response:

$$Y = f(X_1, X_2, X_3, X_4) \qquad \text{Eq. (5.1)}$$

using the polynomial equation:

$$Y = b_o + b_1X_1 + b_2X_2 + b_3X_3 + b_4X_4 + b_1b_2\,X_1X_2 + b_1b_3\,X_1 \ldots\ldots\ldots\ldots \qquad \text{Eq. (5.2)}$$

where Y is the response variable (hardness, YS, UTS, %El. or E_T); b_o, b_1, b_2, *etc.* are constants representing the effects of the respective factors; and b_1b_2, b_1b_3, etc. represent the respective interactions. Also, X_1, X_2, X_3 and X_4 are the coded values of the factors for copper, magnesium, iron and manganese content, respectively.

It should be pointed out that, according to the statistical design procedure, the regression coefficients were calculated using standardized values of inlet variables, X_{jz}:

$$X_{jz} = (X_i - X_{j0})/I_j \qquad \text{Eq. (5.3)}$$

where X_{jz} is the standardized value of the inlet variable; X_j the real value of the inlet variable; X_{j0} the value at 0; and I_j the variation interval. This means that Eq. 5.3 may be applied for evaluating the response variable (*e.g.* hardness) using the standardized inlet variables, X_{jz}, since the real values of X_j cannot be used for this purpose. For the evolution of four-variables at two levels, a Box-Hunter design with only eight experiments is described instead of $2^4 = 16$ which is required for a full factorial design. The Box-Hunter matrix in Table 5.9 shows that the low (-1) and high (+1) levels indicated are the same as those specified in Table 5.7. The experiment was conducted according to the design matrix shown in Table 5.10, where the factors (independent variables) X_1, X_2, X_3, and X_4 are identified as 1, 2, 3, and 4, respectively.

Table 5.7 Experimental setting for the independent variables

Setting	%Cu content (X_1)	% Mg content (X_2)	%Fe content (X_3)	%Mn content (X_4)
High level (+1)	3.25	0.5	0.75	0.75
Low level (-1)	2.25	0.3	0.5	0.5

Table 5.8 Response variables, units, and codes

Response variables	Unit	Code
Hardness	BHN	Y_1
YS	MPa	Y_2
UTS	MPa	Y_3
Elongation	%	Y_4
Impact energy	Joule	Y_5

Table 5.9 Experimental parameters and average response variables from the trial experiments (runs) used for factorial design

Run	Independent Variable				Dependent Variables				
	1	2	3	4	Y_1	Y_2	Y_3	Y_4	Y_5
RGM	-1	-1	-1	-1	124.7±2.8	342.63±6.9	374.45±15.2	1.127±0.25	9.34±1.31
C	1	-1	-1	1	137±3.7	372±1.2	394.8±1.2	0.62±0.05	5.98±0.64
A	-1	1	-1	1	130±0.1	355.5±3.5	380.89±4.8	0.85±0.09	7.76±0.83
RC5	1	1	-1	-1	135±2.9	368.8±6.6	389.23±10.2	0.776±0.06	7.13±1.67
RF1	-1	-1	1	1	125±1.5	344.61±8.4	377.73±8.6	0.972±0.15	6.8±0.31
D	1	-1	1	-1	128±1.6	367.29±17.2	379.62±17.2	0.67±0.08	6.41±0.42
B	-1	1	1	-1	122.6±2.8	352.64±4.5	371.1±13.6	0.8±0.05	7.37±0.39
E	1	1	1	1	136±2.1	370±12.6	392.7±9.3	0.64±0.07	6.16±0.14

Table 5.10 Model matrix for the 2^{4-1} fractional factorial design

Run	Average 1234	1 = 234	2 = 134	3 = 124	4 = 123	12 = 34	13 = 24	23 = 14
RGM	+	-1	-1	-1	-1	1	1	1
C	+	1	-1	-1	1	-1	-1	1
A	+	-1	1	-1	1	-1	1	-1
RC5	+	1	1	-1	-1	1	-1	-1
RF1	+	-1	-1	1	1	1	-1	-1
D	+	1	-1	1	-1	-1	1	-1
B	+	-1	1	1	-1	-1	-1	1
E	+	1	1	1	1	1	1	1

5.2.3 Results and Discussion

A Statistica Version 7 software program was used for computing the main effects as well as the interactions of the independent variables (alloying elements) on the response variables (mechanical properties) of the experimental Al-10.8%Si alloy. The main effect of these alloying elements or independent variables is the difference in average response observed as a result of a change in the level of the variable, in this case, a change from level -1 to level +1. The use of main effect graph plots is to determine which set of independent variables influences the response as well as to compare the relative strength of these effects. Coded values, instead of actual compositional percentages, should be inserted into Equations 5.1 and 5.2 in order to calculate the value of a response variable for an alloy within a given variation range. The equations are non-linear in nature and there are several binary and ternary coefficients. The experimental factors and the response variables (hardness, YS, UTS, %El, and E_t) for eight sets of experiments are shown in Table 5.9. The standard deviation associated with the average value of the response variables is also reported.

In general, positive values of the coefficient signify an increase in the property (*e.g.* hardness) due to a concomitant increase in the individual parameters and their interactions, whereas the magnitude of the coefficients signifies the extent of the influence of individual parameters, or their interactions, on the response variable. For example, positive and higher values of b_1 in Equation 5.2 signify an increase in the response variable, and to a greater extent. Similarly, lower values of the coefficients suggest that the action of associated individual parameters, or their interactions, is insignificant in a given response variable. By

processing the data provided in Table 5.9, regression Equations 5.4-5.8 were developed for hardness, BHN; yield strength, YS; ultimate tensile strength, UTS; percent elongation, %El; impact energy, E_t; and the variation of a number of different factors, as follows:

$$Y_H = 129.745 + 4.255\ X_1 + 1.070\ X_2 - 1.930\ X_3 + 2.25\ X_4 + 0.43\ X_1X_2 - 0.070\ X_1X_3 + 0.245\ X_1X_4 \qquad \text{Eq. (5.4)}$$

$$Y_{YS} = 359.184 + 10.339\ X_1 + 2.551\ X_2 - 0.549\ X_3 + 1.344\ X_4 - 2.674\ X_1X_2 - 0.329\ X_1X_3 - 0.138\ X_1X_4 \qquad \text{Eq. (5.5)}$$

$$Y_{UTS} = 383.052 + 6.036\ X_1 + 1.403\ X_2 - 1.791\ X_3 + 3.477\ X_4 + 0.477\ X_1X_2 - 1.137\ X_1X_3 + 1.186\ X_1X_4 \qquad \text{Eq. (5.6)}$$

$$Y_{\%El} = 0.807 - 0.130\ X_1 - 0.040\ X_2 - 0.037\ X_3 - 0.037\ X_4 + 0.072\ X_1X_2 + 0.015\ X_1X_3 - 0.010\ X_1X_4 \qquad \text{Eq. (5.7)}$$

$$Y_{ET} = 7.30 - 0.880\ X_1 - 0.195\ X_2 - 0.253\ X_3 - 0.263\ X_4 + 0.420\ X_1X_2 + 0.118\ X_1X_3 - 0.088\ X_1X_4 \qquad \text{Eq. (5.8)}$$

where X_1, X_2, X_3, and X_4 are in reduced form and can be decoded for their natural values using the following relationships:

$$X_1 = (\%Cu - 2.75)/0.5, \quad X_2 = (\%Mg - 0.4)/0.1, \quad X_3 = (\%Fe - 0.625)/0.125, \quad X_4 = (\%Mn - 0.625)/0.125 \qquad \text{Eq. (5.9)}$$

By substituting the essential regression coefficients in the polynomial Equation 5.2, Equations 5.4-5.8 were produced and provide valuable information about the conjugated and non-conjugated effects of the four independent variables on the response variables:

- The influence of the addition of Cu on the response variables Y_H, Y_{YS}, Y_{UTS}, $Y_{\%El}$, and Y_{ET}, is represented by the coefficients b_1, b_{12}, b_{13}, and b_{14}; a comparison of the values of these coefficients indicates that the non-conjugated coefficient, b_1, is of crucial importance.
- When considering the effect of the addition of Mg on response variables, the coefficients b_2 and b_{12} should be taken into account; in this particular case, the conjugated coefficient, b_2, is of major significance.
- The addition of Mn has an effect on the response variables due to the coefficients b_4 and b_{14}, where the former is a decisive factor.
- The dependence of response variables on Fe addition is represented by coefficients b_3 and b_{13}; coefficient b_3 appears to have a greater influence on the value of response variables than b_{13}.

The models which were developed for this study display varying degrees of accuracy. Correlation coefficients are provided in Table 5.11. Multiple correlation coefficients are estimates of how well the model accounts for variations in the data set. For example, an R^2 value of 0.96 means that 96% of the variation is accounted for by the model and 4% is accounted for either by variables which are assumed to be constant or by the inability of the data to be modelled by a quadratic equation. The R^2 value for prediction is an estimate of how well the model will predict the response of new data which falls within the bounds of the set variable ranges. For the purposes of this study, it is recommended that the value of R^2 should be maximized. The models for hardness, ultimate tensile strength, and yield strength have high multiple correlation coefficients, while those for elongation

and toughness are less significant, suggesting that these two variables are sensitive to some factor, or group of factors, which do not lie within the scope of this study.

Table 5.11 Multiple regression coefficients

Dependent variable	R^2	R^2 for prediction
Hardness	0.99	0.98
Yield stress	0.94	0.86
UTS	0.95	0.88
Elongation	0.79	0.52
Toughness	0.83	0.65

Figure 5.18 represents a Pareto chart which is a horizontal bar-chart plotting hardness values in descending order. The length of each bar is proportional to the value of the estimated effect. The most significant effects correspond to independent variable X_1 (%Cu content), independent variable X_4 (%Mn content), and independent variable X_3 (%Fe content), respectively.

After processing the data provided in Table 5.9, Equation 5.4 shows the effect produced by the simultaneous variation of alloying elements on the hardness of heat-treated alloys. This equation further conveys the fact that the coefficients associated with copper (X_1) are significantly higher than those associated with Mg (X_2), Fe (X_3), and Mn (X_4). The coefficients associated with X_1, X_2, X_3, and X_4 are 4.26, 1.1, -1.93, and 2.25, respectively, indicating that out of these four alloying elements, Cu appears to have the greatest effect on hardness, while Mg has the least. The addition of Cu has been shown to have approximately four times as much effect on hardness as the addition of Mg does. This fact may be ascribed to the formation of complex insoluble phases, such as $Al_5Mg_8Si_6Cu_2$,

which decrease the amount of free Mg as well as Cu available for further hardening during the aging process, as shown previously in Chapter 4.

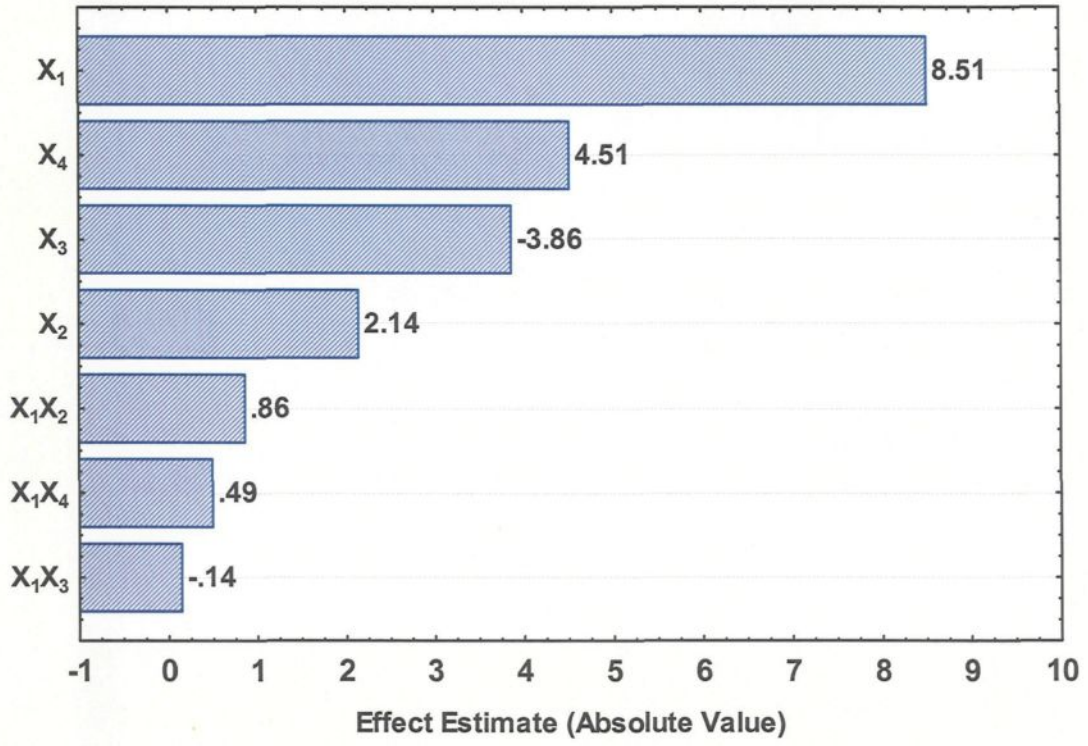

Figure 5.18 Pareto chart of estimated effects for hardness.

Figure 5.19 shows the 3-D representation of the response surface for hardness as a function of the coded values of Cu content (X_1) and Mg content (X_2) for alloys containing (a) low and (b) high Fe and Mn contents. Hardness is most sensitive to the copper content and relatively insensitive to the magnesium level, as shown in Figure 5.18. These figures once again point to the fact that the optimum combination for hardness prevails at Cu and Mn contents of over 2.75 and 0.625 wt%, respectively; and at Mg and Fe contents of under 0.4 and 0.625 wt%, respectively.

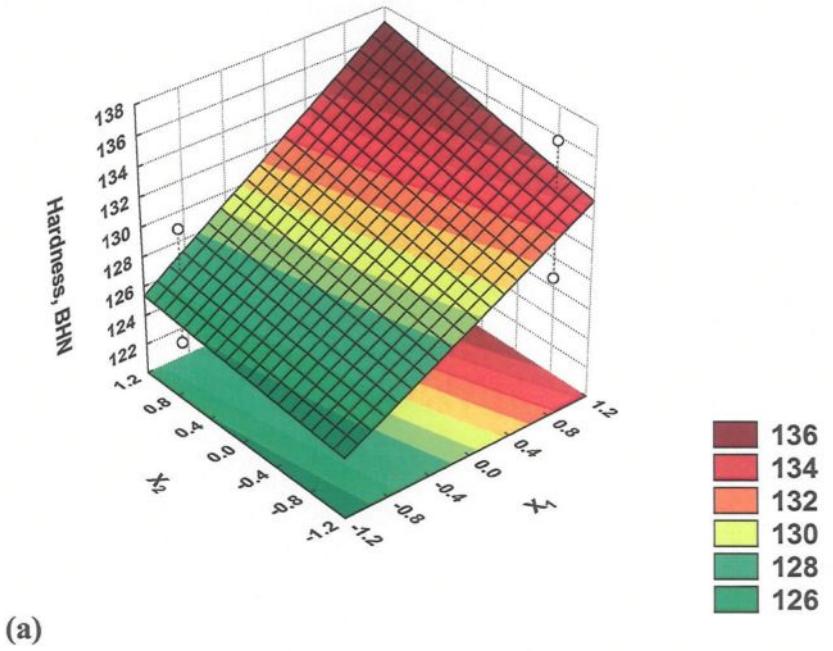

(a)

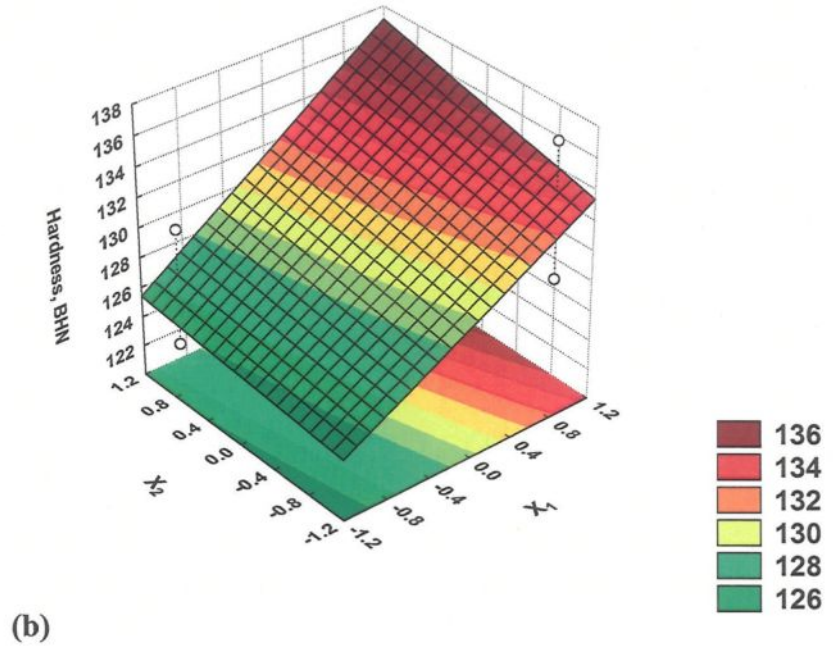

(b)

Figure 5.19 Regression model for hardness as a function of Cu and Mg content for aged Al-10.8%Si alloys: (a) alloys containing 0.5% Fe and 0.5% Mn, and (b) alloys containing 0.75% Fe and 0.75% Mn.

The interaction coefficients obtained in Equation 5.4 show that alloying elements interact with each other to a significant degree. The coefficients associated with X_1X_2, X_1X_3, and X_1X_4 are 0.43, -0.1, and 0.245, respectively. The coefficient of X_1X_2 is the most significant in comparison with the other interaction coefficients present in Equation 5.4; this would tend to suggest that there are indeed efficacious interactions between Cu, Mg, Si, and Al.

Equations 5.5 and 5.6 show the effect of alloying elements on the yield stress and tensile strength of heat-treated alloys. It will be observed that, of the four alloying elements, Cu has the greatest effect by increasing the YS and UTS values. Cu is, thus, a superior strengthener and its addition as an alloying element is desirable; Mg and Mn also increase the strength although this effect is mild. In another respect the presence of a number of binary interactions indicates the formation of various intermetallic compounds, and in spite of the fact that several interaction coefficients are present, they may not be of any significance. Equations 5.5 and 5.6 are similar in nature except for the fact that the tensile strength is affected slightly more by the variables when compared to yield strength. It would be possible to construct the response surfaces shown in Figures 5.20 and 5.21 using the same variables. Copper has the greatest effect, with maximum YS and UTS occurring at high levels (+1) of Cu. The addition of Mg improves tensile properties only slightly at low levels of Cu.

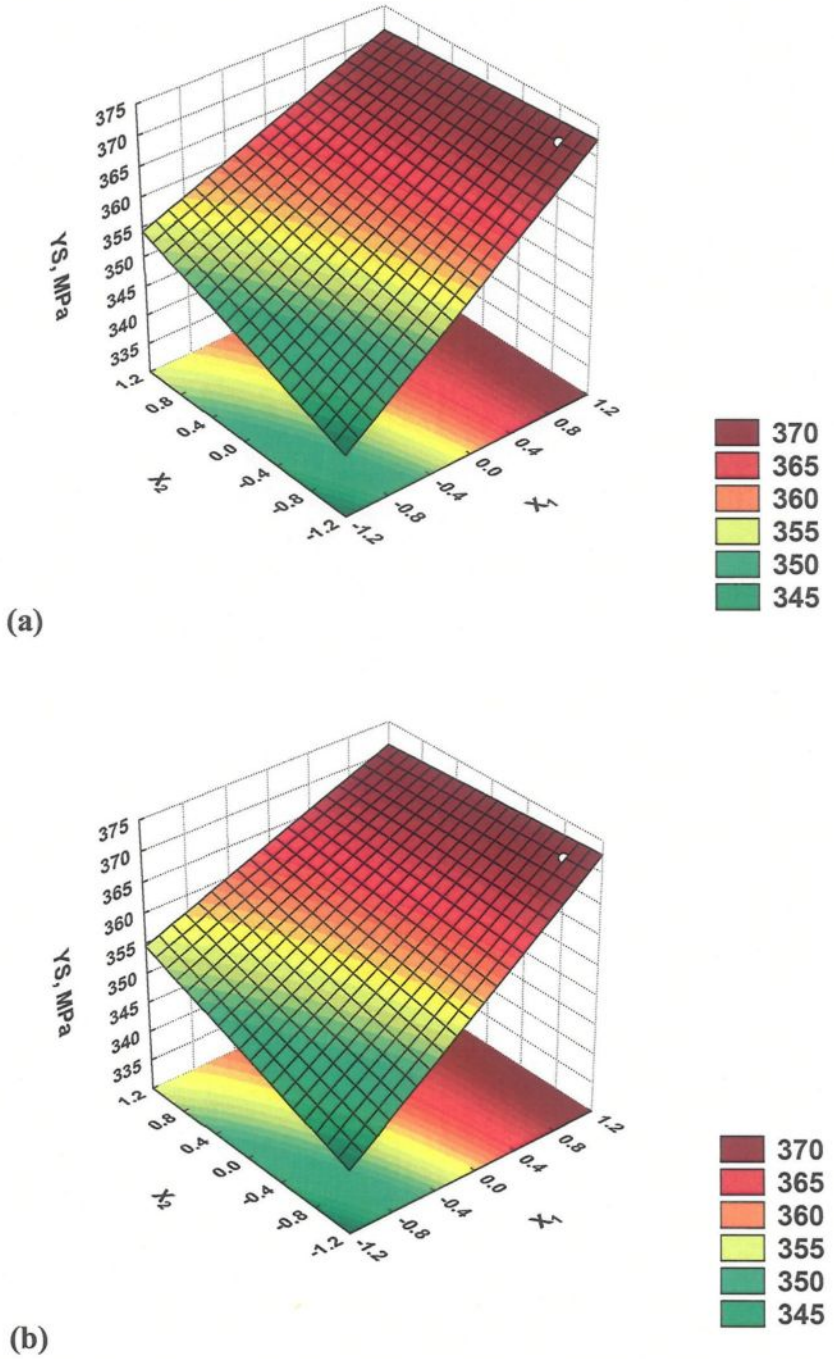

Figure 5.20 Regression model for the YS as a function of Cu and Mg contents for aged Al-10.8%Si alloys: (a) alloys containing 0.5% Fe and 0.5% Mn, and (b) alloys containing 0.75% Fe and 0.75% Mn.

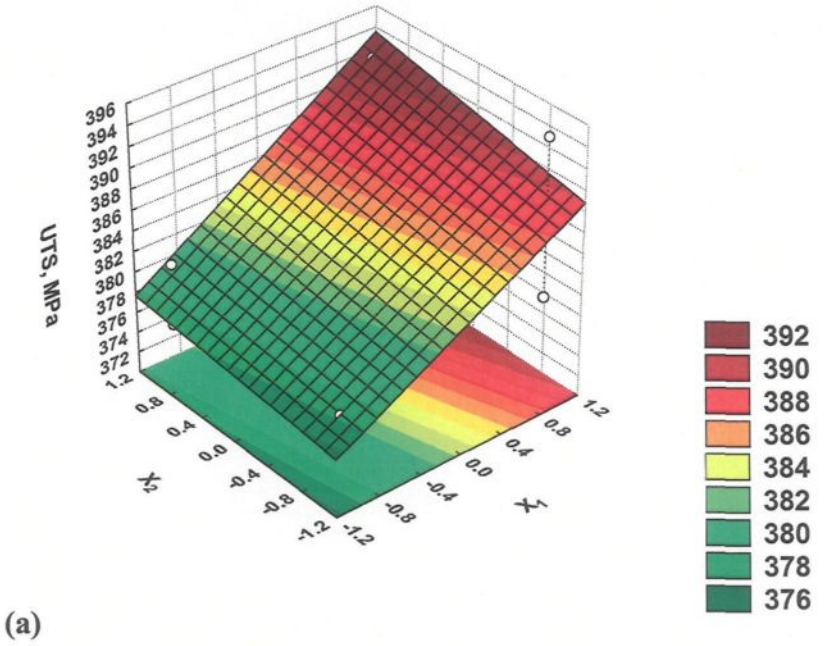

(a)

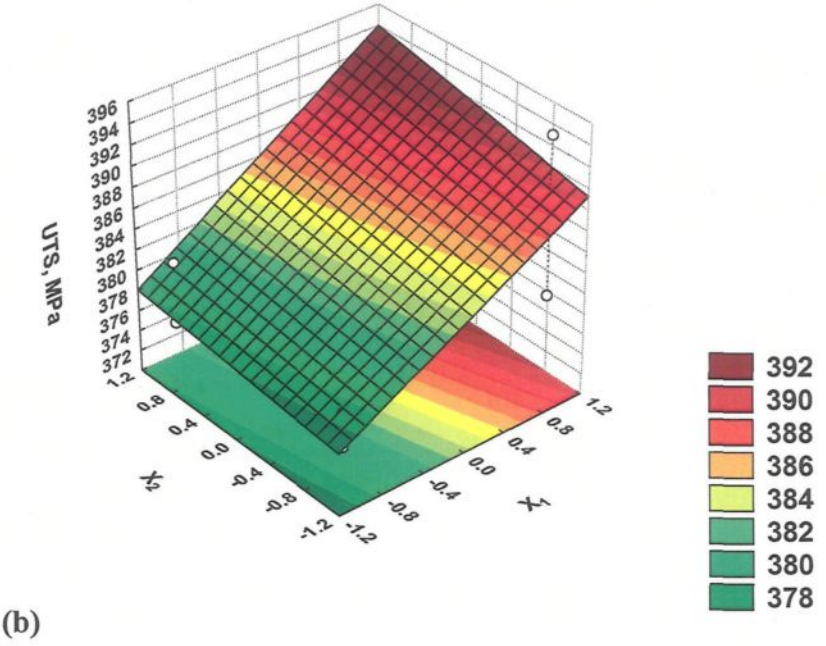

(b)

Figure 5.21 Regression model for the UTS as a function of Cu and Mg contents for aged Al-10.8%Si alloys: (a) alloys containing 0.5% Fe and 0.5% Mn, and (b) alloys containing 0.75% Fe and 0.75% Mn.

Equation 5.7 shows the dependence of percent elongation on the variables. From this equation, it will be seen that all the variables contribute negatively to the percent elongation. Both Cu and Mg appear to affect the elongation adversely; and Fe and Mn also have a mild effect in that they lower the elongation. Here, the binary interactions between X_1 and X_2, and X_1 and X_3 show a positive effect on the percent elongation while other interactions are not in any way significant.

Equation 5.8 reveals a trend noticeably similar to that observed in Equation 5.7 regarding percent elongation, thereby providing a good indication of the magnitude of the impact that alloying elements have on these alloys. The effects of the interaction of these independent variables, however, were found to be insignificant.

The models for elongation and toughness are shown in Figures 5.22 and 5.23. These models show that ductility and toughness are highly sensitive to alloy composition. Once the values of the effects have been obtained at each level, the overall effect and response surfaces may be constructed. Similarly, the response surfaces for other variables may also be obtained. The tendency of ductility and toughness to increase may be observed when the lower level of Cu content is combined with the lower level of Mg.

The validity of the equations was verified by performing random experiments in the range of the variation of Cu, Mg, Fe, and Mn content. Table 5.12 provides a comparison between the calculated values of the mechanical properties obtained from Equations 5.4-5.8 and the values obtained experimentally from the random experiments. The experimental values in Table 5.12 are the average results of three randomly performed experiments using the same treatment combinations. As suggested by the multiple correlation coefficients, the

models are suitable for predicting the hardness, yield strength, and ultimate tensile strength, but do not provide good estimates for the elongation and impact energy.

An examination of the results indicates that there is a close match between the properties obtained by performing random experiments and those calculated from the respective regression equations. The preceding operation was carried out by inserting the reduced values of the parameters corresponding to the random experiments in the associated equations. The closeness of the match indicates that the equations are sufficiently accurate within an acceptable range of variations in the variables.

From the proposed two-level factorial design experiments on the mechanical properties of an experimental Al-10.8%Si alloy, it is obvious that by using this type of polynomial regression equation, the effect of each of the individual variables and that of their interactions on the mechanical properties may be grasped. In other words, the model makes it possible to predict the performance behavior of the samples as a function of variations in the additions made of the given alloying element within the range specified by this study. Modification of the equation-model may suitably be applied in order to clarify the mechanical property response of the samples beyond the specified range. Finally, for a better understanding of the effects of individual variables and their interaction on the mechanical properties, a higher level of factorial experimental design is recommended, wherein the influence of other parameters such as solution treatment temperature and time, quenching conditions, aging time and temperature, and so forth, could also be examined.

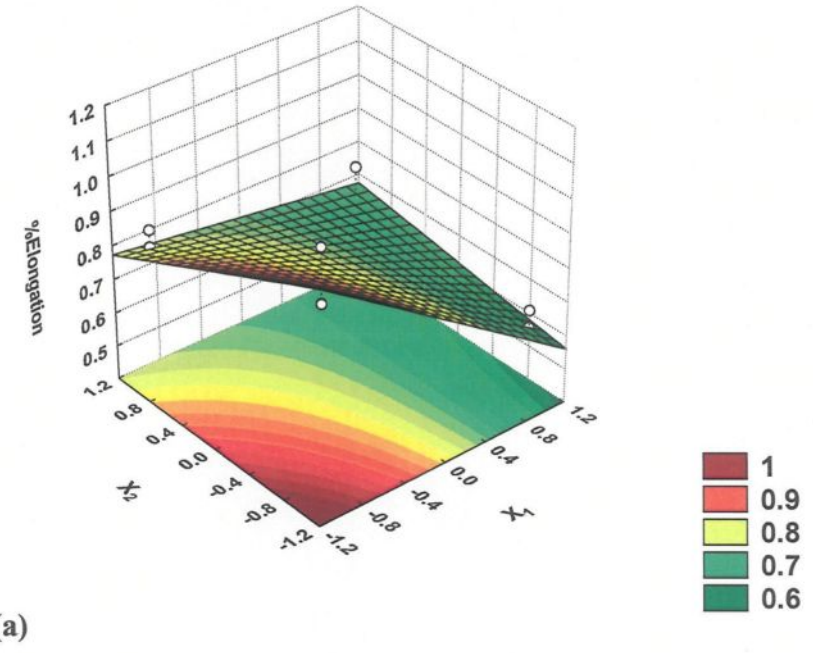

(a)

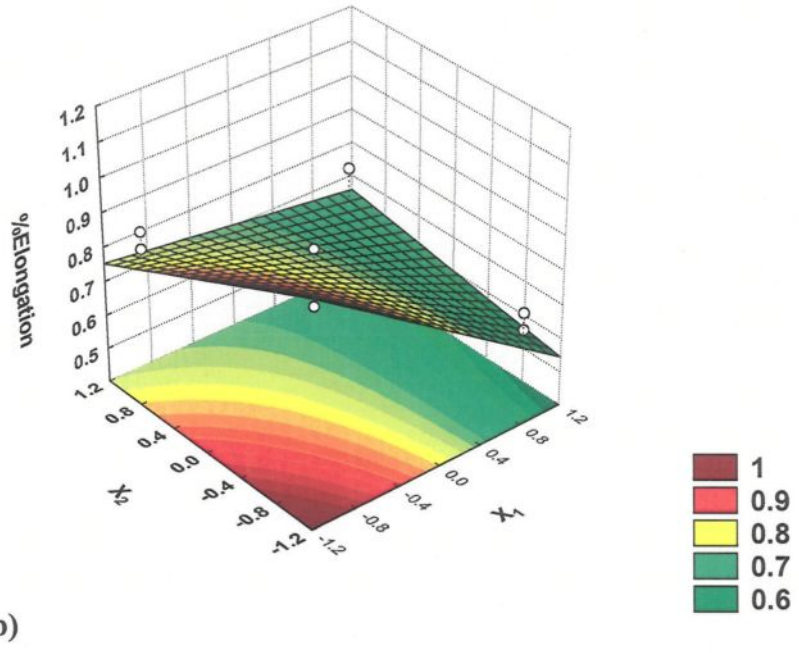

(b)

Figure 5.22 Regression model for percent elongation as a function of Cu and Mg content for aged Al-10.8%Si alloys: (a) alloys containing 0.5% Fe and 0.5% Mn, and (b) alloys containing 0.75% Fe and 0.75% Mn.

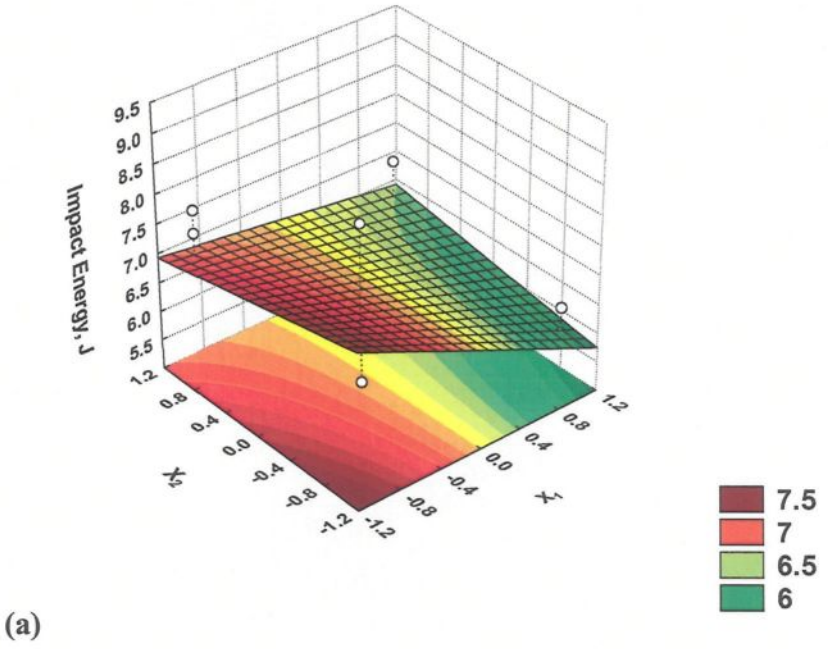

(a)

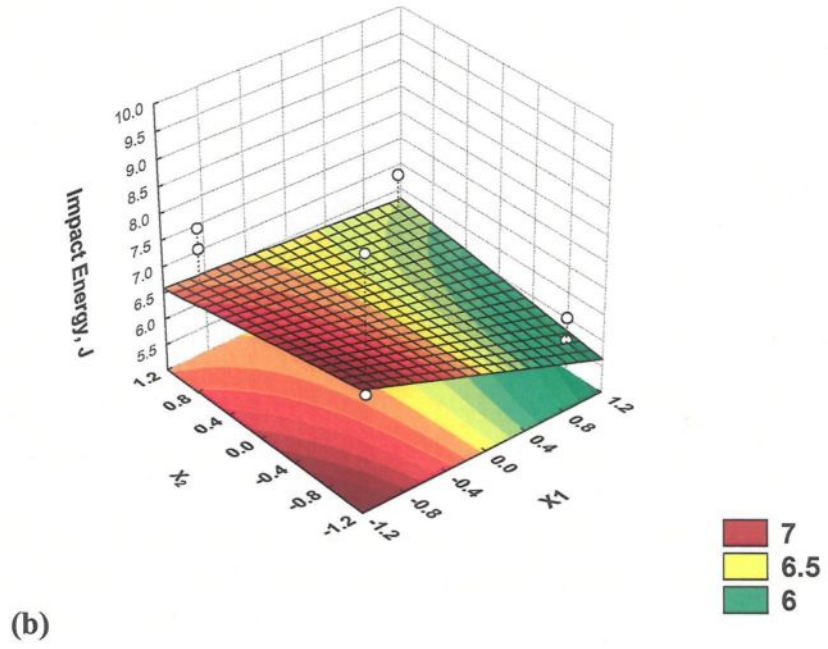

(b)

Figure 5.23 Regression model for total impact energy as a function of Cu and Mg content for aged Al-10%Si alloys: (a) alloys containing 0.5% Fe and 0.5% Mn, and (b) alloys containing 0.75% Fe and 0.75% Mn.

Table 5.12 Comparison of the mechanical properties calculated from Equations 5.4-5.8 and values from random experiments

Alloy Code	Predicted Values					Experimental Values				
	BHN	**YS, MPa**	**UTS, MPa**	**%El**	**E_T, J**	**BHN**	**YS, MPa**	**UTS, MPa**	**%El**	**E_T, J**
RF3	122.1	341.92	373.15	1.02	7.878	126.8 ± 1.1	346.5 ± 8.2	380.8 ± 21	0.889 ± 0.2	6.16 ± 1.1
RC1	128.4	355.84	379.96	0.92	8.01	125.7 ± 2.2	377.3 ± 11.7	382.5 ± 4	0.88 ± 0.1	9.1 ± 0.2
RC2	132	369.32	385.47	0.694	6.68	126.8 ± 1.8	382.5 ± 4.5	401.9 ± 3	0.74 ± 0.1	7.39 ± 1.1
RC3	126.1	353.74	378.56	0.894	8.05	129.4 ± 1.4	343.9 ± 6	368.6 ± 19	0.93 ± 0.3	7.73 ± 2.3
RC4	130.5	360.94	382.77	0.841	7.98	134 ± 1.5	348.8 ± 4.2	372.4 ± 19	0.86 ± 0.2	7.41± 0.83

CHAPTER 6

ADDITION OF TRACE ELEMENTS

CHAPTER 6

ADDITION OF TRACE ELEMENTS

6.1 INTRODUCTION

Through metallographical analyses, Chapter 4 explored the specific microstructural changes resulting from the addition of melt treatment and alloying elements with and without heat treatment to an experimental Al-10.8%Si near-eutectic alloy. The study involved collating a large number of micrographs in order to provide a summary of all the factors relating to the microstructural investigation. The mechanical properties were discussed in Chapters 4 and 5 where evaluation was made by means of tensile and impact tests; also hardness measurements were taken for all samples.

In spite of the published literature available, there is very little data describing the effects that adding lead, bismuth, tin, and indium would have on the microstructure and mechanical properties of Al-Si alloys. The first part of this chapter will thus examine the effects of the Al-insoluble elements Pb, Bi, Sn, and In on the microstructure and mechanical properties of a grain-refined and modified Al-10.8%Si near-eutectic alloy. The RGM alloy was selected as an investigation reference for the purposes of this study. In the second part of this chapter, an intensive investigation will be carried out to study the precipitation of Sn and its effects on the mechanical properties of B319.2 and A356.2 alloys. It should be kept in mind here that these elements all have extremely low distribution coefficients in both Al and Si. Of most significant interest in the pursuit of this study is determining the effect that these elements have on the morphology and size of Si

particles, and whether the refinements observed do indeed translate into an increase in tensile and ductility.

6.2 EFFECTS OF LEAD, BISMUTH, AND TIN ON MICROSTRUCTURE AND MECHANICAL PROPERTIES OF AN EXPERIMENTAL Al-10.8%Si ALLOY

6.2.1 Characterization of Microstructures

The microstructure of Al-Si alloys depends on the chemical composition, casting process, and the heat treatment regime applied. The microstructures of experimental Al-10.8%Si alloy with minor additions of Pb, Bi, and Sn, in as-cast and solution heat-treated conditions were thus investigated for this research work. The samples were prepared using the standard metallographic techniques as described in Chapter 3. Optical microscopy and electron probe microanalysis were used to record the microstructures. The Si-particle characteristics of the various alloy samples were examined and quantified using image analysis; these specific characteristics include particle area, length, roundness, aspect ratio and density.

6.2.1.1 Effects on Microstructure of Adding Pb, Bi, and Sn Individually

Figures 6.1 through 6.3 show the effects of the trace elements Pb, Bi, and Sn on the microstructure of the grain-refined and modified RGM alloy in the as-cast condition. In general, these figures indicate that eutectic Si is somewhat coarse because of the presence of the incompletely modified structures; in particular, Figure 6.2 shows that there is the appearance of acicular needle-like Si formation in RB alloy. Table 6.1 summarizes the

eutectic Si particle characteristics obtained for the alloys investigated. It may be observed that the addition of 0.5% Pb to the RGM alloy (*i.e.* the RP alloy) leads to a slight coarsening of the eutectic Si particles, as seen in Figure 6.1. For example, the average Si particle area, length, and aspect ratio increase by 17%, 14%, and 4%, respectively, compared to the RGM alloy, whereas the average roundness and density decrease by 4% and 11%, respectively.

The addition of 0.5% Bi to the RGM alloy counteracts the modifying effect of Sr, as shown in Figure 6.2, leading to a noticeable coarsening of the Si crystals; thus agreeing with the results obtained by Cho *et al.*[260] The eutectic Si particle parameters are approximately comparable to those of the base alloy R. The corresponding data on the average particle area showed a jump in this parameter from 2.67 μm^2 in the RGM alloy to 8.23 μm^2 in the RB alloy. Also, particle length increased from 2.69 μm in the RGM alloy to 5.41 μm after the addition of Bi. Although no specific bismuth intermetallic compounds were identified in the microstructure of the RB alloy, it is possible that a ternary compound, Bi_2Mg_2Sr, and/or the binary compounds, Bi_3Sr, BiSr, Bi_2Sr_3, and $BiSr_2$, might form, leading to a reduction in the amount of Sr available for modification.

The addition of 1.1% Sn to the Sr-modified RGM alloy is shown in Figure 6.3. This particular element was selected for a numbers of reasons: (i) it decreases the surface tension of Al considerably, as shown by Eustathopoulos *et al.*,[261] (ii) it has a rapid diffusion coefficient in Al; also, (iii) Sn segregates to the grain boundaries, as observed by Song *et al.*,[262] and by Erb and Aust.[263] A coarser and partially modified eutectic structure is thus to be observed with the addition of 1.1% Sn, and the modification level corresponds to that of

a class 3 type, namely, partial modification. It may also be observed that there is no significant difference in microstructure between Sn-free and Sn-containing alloys in the as-cast condition except for the precipitation of finely distributed Sn in the form of black reticulate particles of β-Sn (free machining inclusions). These β-Sn particles always solidify within the Al_2Cu network and at the interfaces of Al-α/Si or Al-α/Fe rich intermetallics, as shown in Figure 6.3. The distribution of the β-Sn particles is not uniform; rather, they are distributed in small clusters. Apparently, no Mg_2Sn formation has been observed in Al-Mg-Si-Sn alloys by other authors.[264]

To date the equilibrium diagram of Al-Si-Sn ternary system has never been reported. The phase transformation of the crystallization processes for the alloys may be analyzed, however, by means of the three known binary systems. The Al-Sn and Sn-Si alloys both belong to a special binary eutectic system, where there is hardly any solid solubility between Al and Sn or between Sn and Si. With this regard, the Sn content for the eutectic composition of Al-Sn and Sn-Si systems is about 99.8 and 100%, respectively, while the corresponding equilibrium temperatures are ~229°C and ~232°C, respectively; these temperatures approach or are equal to the melting point of Sn. According to the experimental results, there are no Al-Sn compounds to be found in the RN alloy. It may thus be inferred that, according to the rules of equilibrium diagrams, the Al-Si-Sn system should belong to a ternary eutectic system. The projection drawing of the liquid phase surface unfolded diagrams for the ternary system are shown in Figure 6.4. Based on three binary system diagrams and the experimental results, it may be determined that the projection of the ternary eutectic point is near corner Sn. Since the Sn content of the

eutectic composition almost approaches 100%, the equilibrium temperature should be below 229°C; it may therefore be concluded that Sn precipitates mainly in the form of the β-phase.

Table 6.1 Silicon particle characteristics of the alloys

Alloy code	Solution time	Particle area (μm^2)		Particle length (μm)		Roundness ratio (%)		Aspect ratio		Density (particles/ mm^2)
		Av	SD	Av	SD	Av	SD	Av	SD	
R	0[a]	8.59	14.11	5.86	6.37	57.34	29.46	2.41	1.23	10096
	8	7.25	13.1	5.58	6.02	62.0	20	2.21	1.27	14457
RGM	0[a]	2.67	4.71	2.69	2.65	71.29	24.97	2.11	0.94	40807
	8	5.22	7.04	3.66	3.25	75.42	21.47	1.93	0.84	20903
RP	0[a]	3.13	7.65	3.07	4.33	68.14	26.72	2.20	1.04	33293
	8	5.65	7.19	3.49	2.91	72.95	19.7	1.96	0.71	20377
RB	0[a]	8.225	13.60	5.41	6.55	57.26	32.16	2.37	1.58	17855
	8	6.85	12.3	5.26	6.0	65	19.1	2.16	0.97	18965
RN	0[a]	4.57	6.56	3.45	4.72	66.78	27.12	2.28	1.19	25979
	8	6.69	5.91	4.17	3.56	70.15	19.71	2.04	0.83	19699
RBP	0[a]	6.10	10.75	3.4	4.67	61.49	22.91	2.28	1.45	23850
	8	8.25	10.25	3.55	3.47	65.29	21.09	2.15	1.41	18280
RBN	0[a]	6.28	11.72	4.68	4.36	59.41	32.49	2.34	1.28	20734
	8	11.04	13.89	5.74	4.92	63.59	29.56	2.12	1.41	15292
R2BN	0[a]	5.34	4.56	4.52	6.69	61.95	32.83	2.25	1.42	22116
	8	7.27	4.27	5.20	4.12	66.18	29.25	2.12	1.42	17672
RZ	0[a]	5.13	2.64	3.17	2.69	65.28	22.73	2.25	1.24	24472
	8	7.23	4.03	3.98	2.55	68.26	29.47	2.03	1.41	19540
RNN	0[a]	3.92	2.19	2.80	2.14	70.77	22.83	2.17	0.83	32433
	8	5.86	3.75	2.87	2.49	73.37	19.76	1.97	0.81	20226

a: as-cast; Av: average; SD: standard deviation.

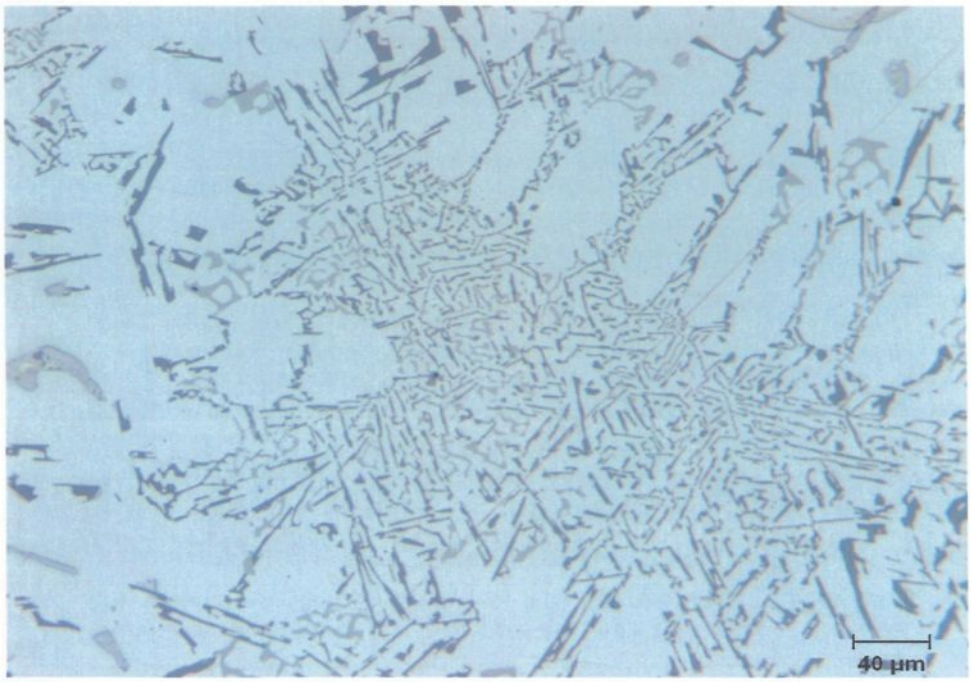

Figure 6.1 Optical micrograph showing microstructure of RP alloy (RGM + 0.5% Pb) in the as-cast condition.

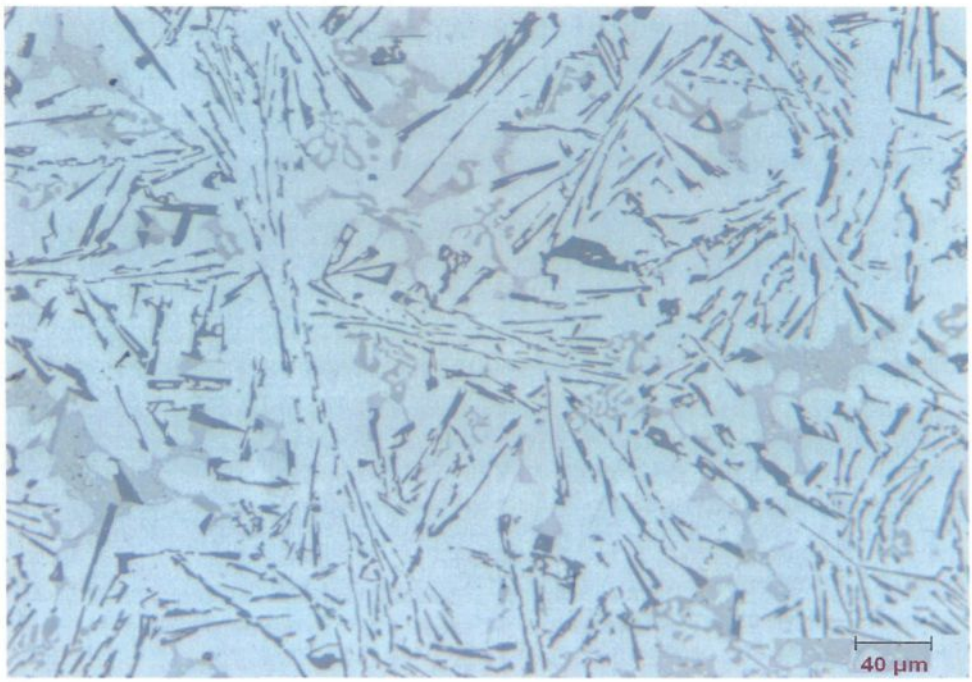

Figure 6.2 Optical micrograph showing microstructure of RB alloy (RGM + 0.5% Bi) in the as-cast condition.

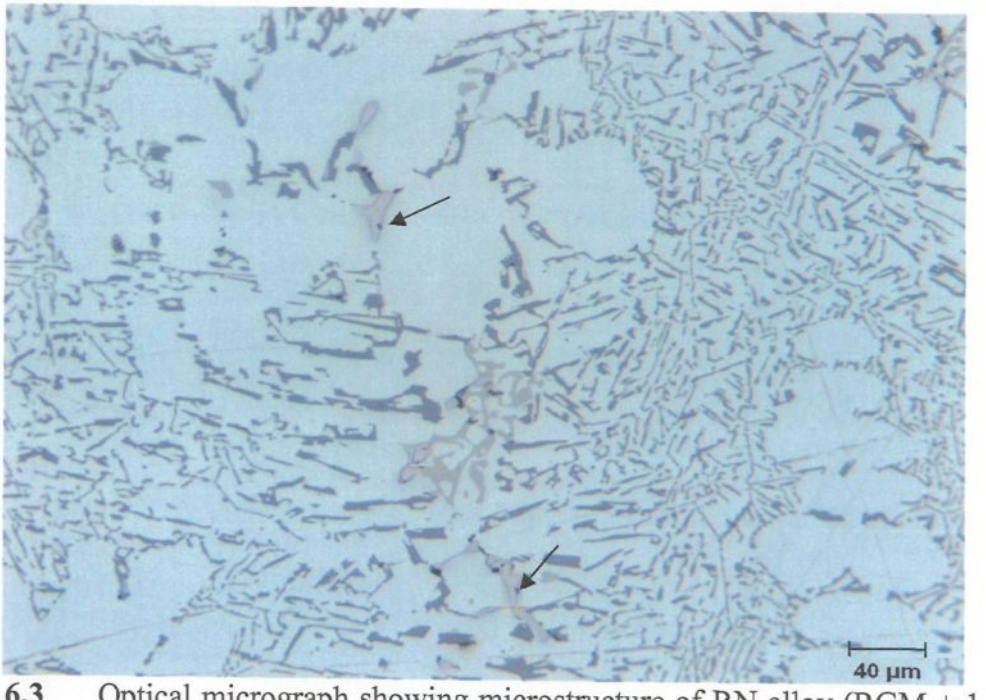

Figure 6.3 Optical micrograph showing microstructure of RN alloy (RGM + 1.1% Sn) in the as-cast condition. Arrows point to β-Sn particles.

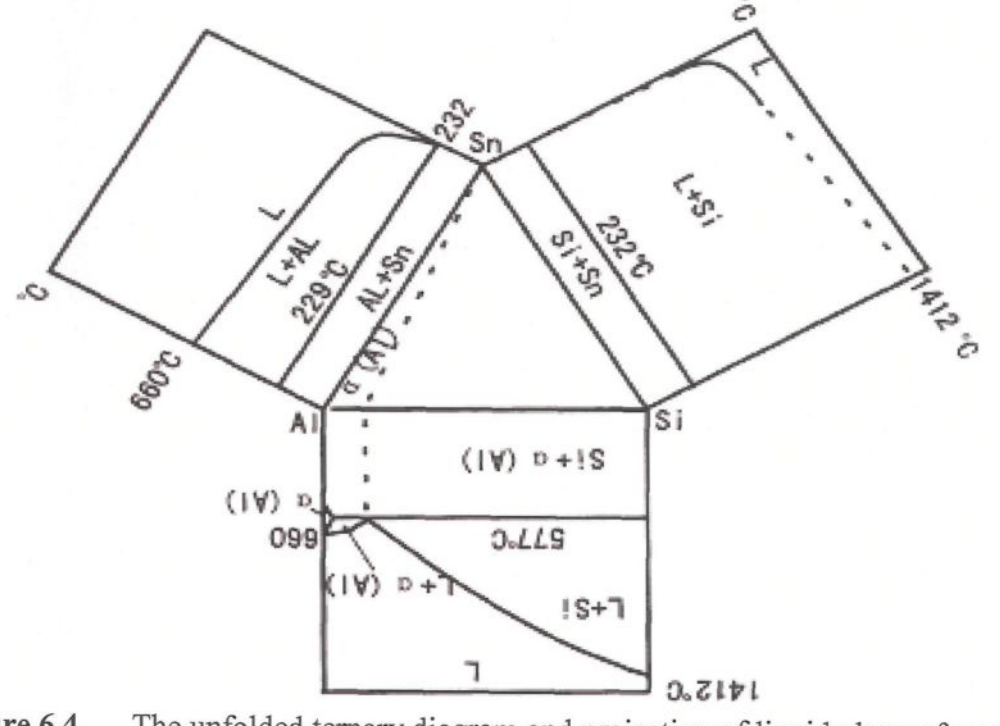

Figure 6.4 The unfolded ternary diagram and projection of liquid phases face for Al-Si-Sn system.

Figure 6.5 shows a backscattered image taken of the RN alloy, according to atomic number sequence; the white phases in the matrix are β-Sn which precipitated within the light grey Al_2Cu network (light grey). For further investigation, X-ray mapping of the β-Sn phase was carried out to determine the distribution of Sn, Cu, and Si, as shown in Figure 6.6. The WDS analysis shown in Table 6.2 suggests that the chemical composition of this phase is β-Sn. A minimum of ten measurements were taken in different regions of the microstructure, and the standard deviations in composition were calculated. The corresponding EDX spectrum, shown in Figure 6.7, displays strong reflections due to the presence of Sn, which is consistent with the WDS analysis. Figure 6.8 shows the backscattered images obtained at high magnification of the RN alloy (RGM alloy + 1.1% Sn) illustrating the morphology of Sn-containing particles precipitated in the alloy.

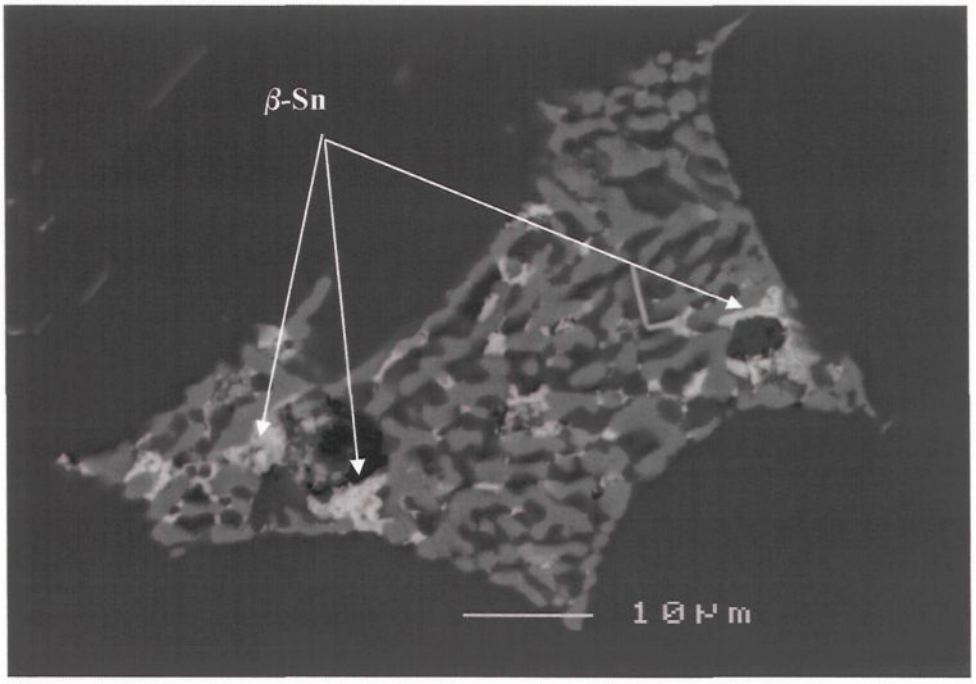

Figure 6.5 Backscattered image obtained from RN alloy showing the precipitation of β-Sn.

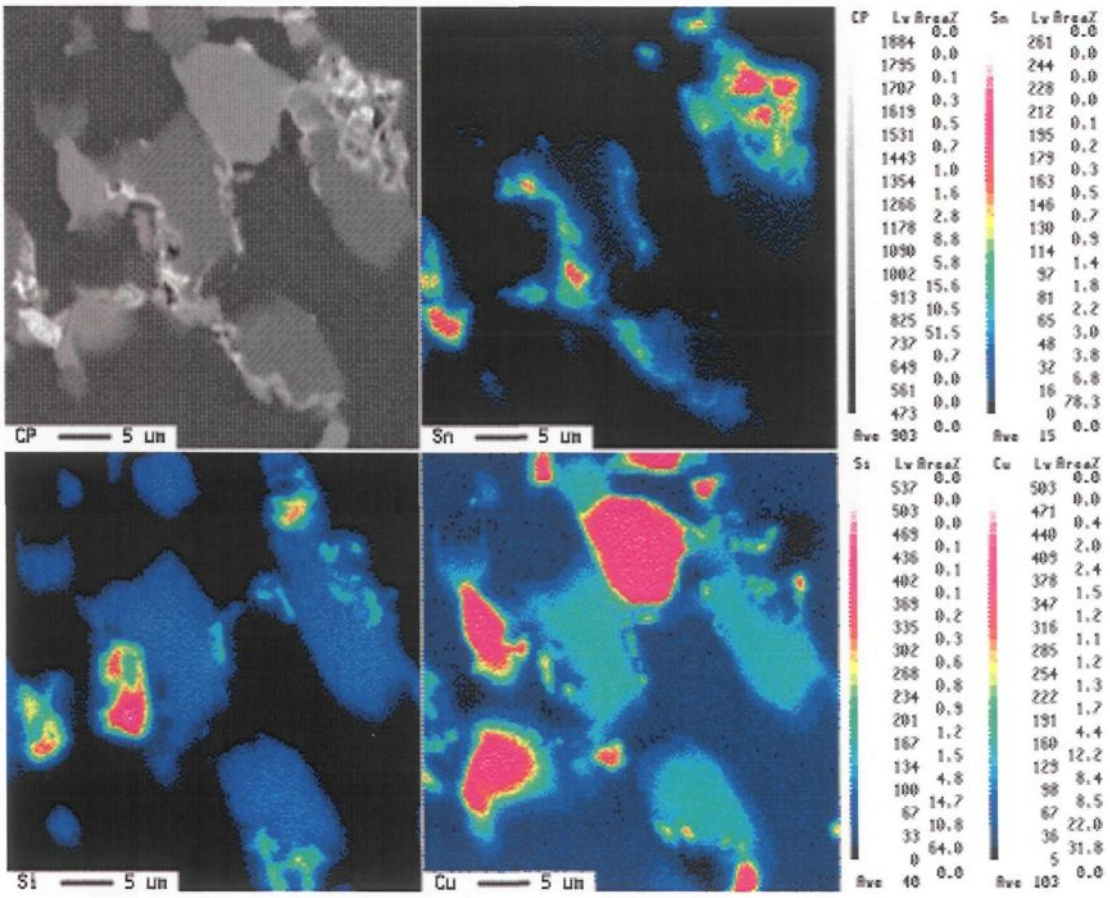

Figure 6.6 Backscattered image taken of the RN alloy showing the precipitation of β-Sn and the corresponding X-ray image of Sn, Cu and Si.

Table 6.2 Chemical composition of the examined Sn-containing phase particles in as-cast RN alloy obtained from WDS analysis

Alloy Code	Element	wt %	at. %	Color & Shape	Phase
RN	Sn	99.1 ± 1.39	96.16 ± 1.58	white & reticulate	β-Sn phase
	Cu	0.95 ± 0.43	1.53 ± 0.72		
	Total	**100.05**	**97.69**		

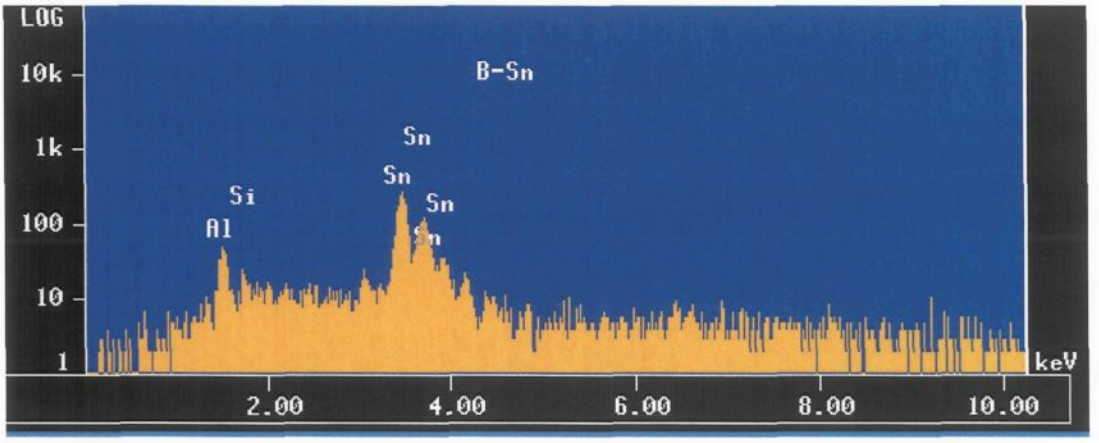

Figure 6.7 EDX spectrum corresponding to a β-Sn particle observed in RN alloy (containing 1.1% Sn).

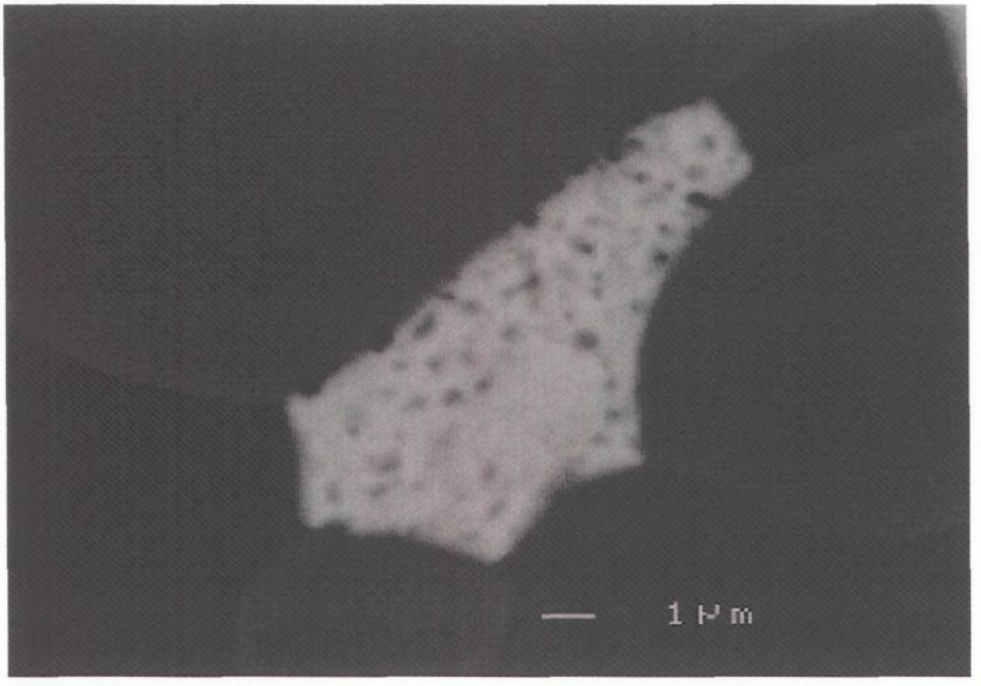

Figure 6.8 Backscattered images at high magnification of the RN alloy showing the precipitation of β-Sn.

As mentioned previously in Chapter 4, solution heat treatment is performed to dissolve Al_2Cu, homogenize the solid solution, and fragment and spherodize the eutectic silicon. It may be seen clearly from Figures 6.9 through 6.11 that the 8-hour solution heat treatment caused the dissolution of Al_2Cu particles. Upon considering the various stages of the solution treatment as a whole, it can be observed that the three stages of fragmentation, spheroidization and coarsening may also occur together in the same microstructure, depending upon the variety of Si particle sizes present in the as-cast structure. Thus, while some longer particles may undergo fragmentation, other smaller Si particles may become spheroidized, and those already spheroidized could start coarsening, at any particular time during the solution treatment process. As Table 6.1 shows, after solution treatment of the RP, and RN alloys, the average Si particle area and roundness increase, while the aspect ratio and density decrease, compared to the as-cast condition, as may also be observed in Figures 6.9 and 6.10. The decrease in Si particle density by 39%, and 24% for the RP, and RN alloys, respectively, may indicate the commencement of the coarsening process. The aspect ratio, defined as the ratio of the length to the width of the particle, decreased with solution heat-treatment, thereby leading to shorter, more rounded particles.

As may be seen in Figure 6.11, the microstructure of the RN alloy after solution treatment for 8 hours at 495°C reveals: (a) a heightened tendency towards Si-particle spheroidization; (b) the absence of any sign of incipient melting of Cu-base intermetallics; and (c) β-Sn, present in black reticulate form, melts due to solution treatment at 495°C, leading to the formation of spherical voids.

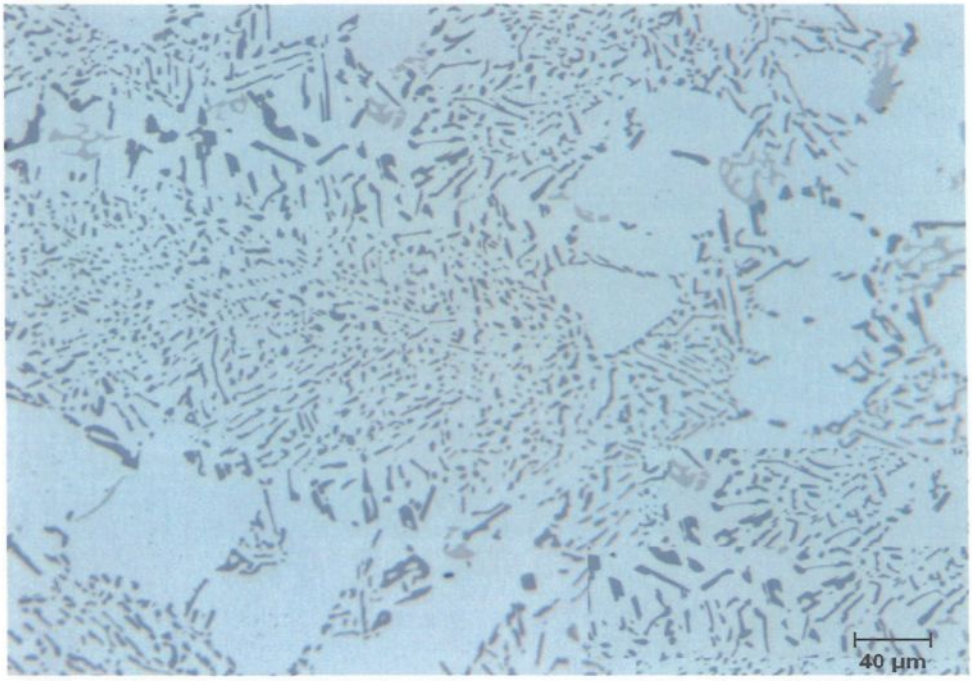

Figure 6.9 Optical micrograph showing structure of RP alloy (RGM + 0.5% Pb) in the solution treatment condition.

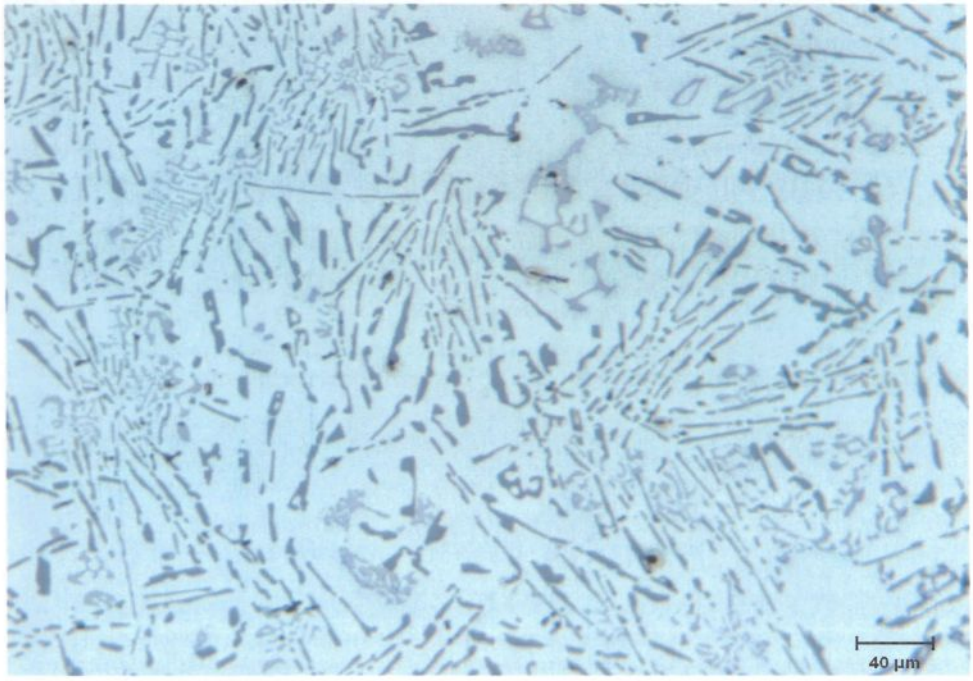

Figure 6.10 Optical micrograph showing structure of RB alloy (RGM + 0.5% Bi) in the solution treatment condition.

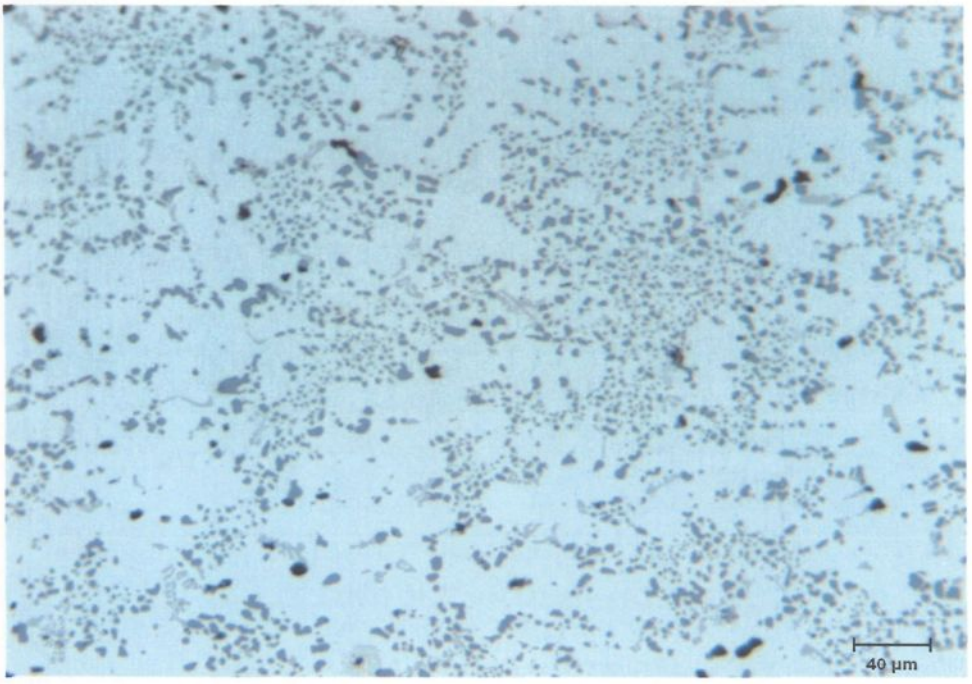

Figure 6.11 Optical micrograph showing structure of RN alloy (RGM + 1.1% Sn) in the heat-treated condition.

6.2.1.2 Effects on Microstructure of Adding Pb, Bi, and Sn in Combination

Table 6.1 also summarizes the eutectic Si-particle characteristics obtained from the image analysis measurements for the RGM alloy with respect to the combined Pb+Bi, Sn+Bi, and Sn+In additions. It may be observed that the combined additions of these elements for the RGM alloy in the as-cast condition have a moderate-to-significant influence on the eutectic Si particle size, in that the particle size increases in the presence of a combined addition of Pb and Bi (in the RPB alloy) or Sn and Bi (for the RBN alloy) as shown in Figures 6.12 and 6.13, respectively. The moderate effect may be observed with the combined addition of Sn and In (for the RNN alloy) as shown in Figure 6.14. With respect to the roundness parameter, the best results are obtained with the RNN alloy which displays the highest roundness values compared to the RBN and RPB alloys.

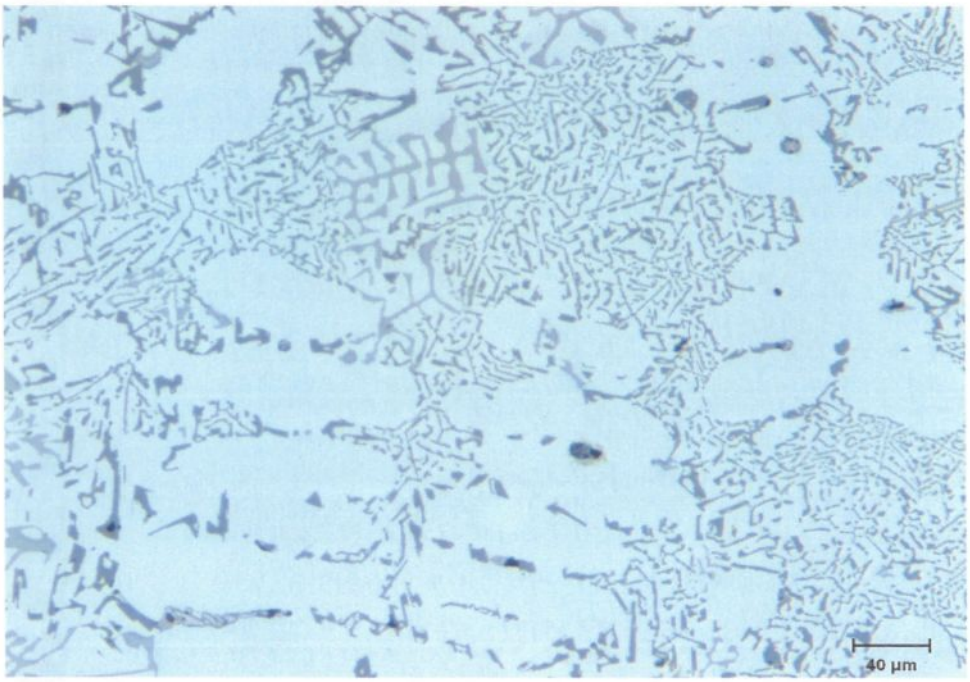

Figure 6.12 Optical micrograph showing microstructure of RPB alloy (RGM + 0.5% Pb + 0.5% Bi) in the as-cast condition.

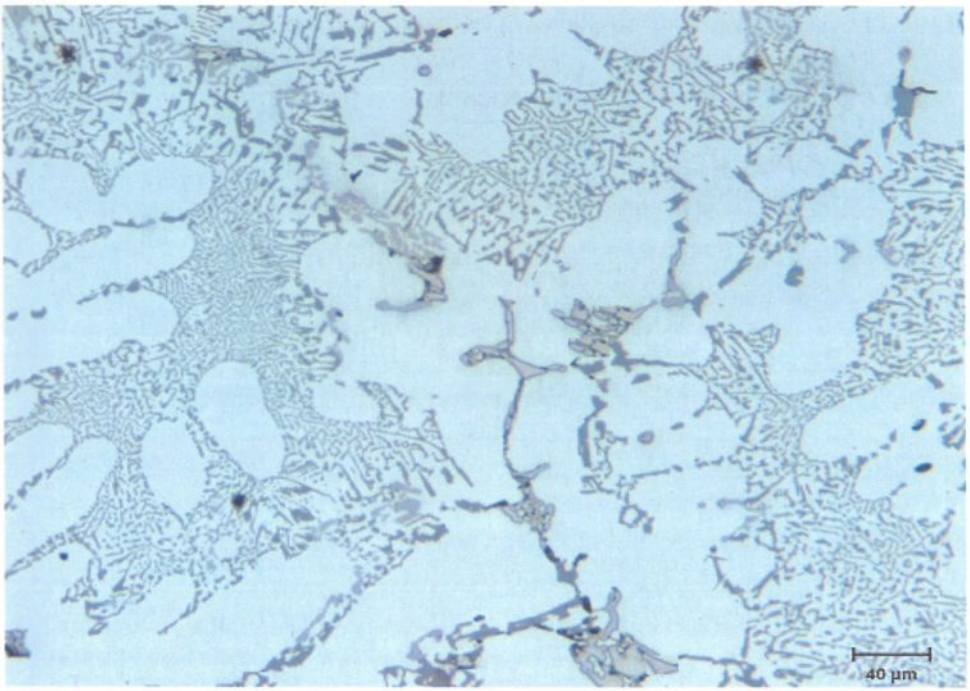

Figure 6.13 Optical micrograph showing microstructure of RBN alloy (RGM + 0.5% Bi + 1.1% Sn) in the as-cast condition.

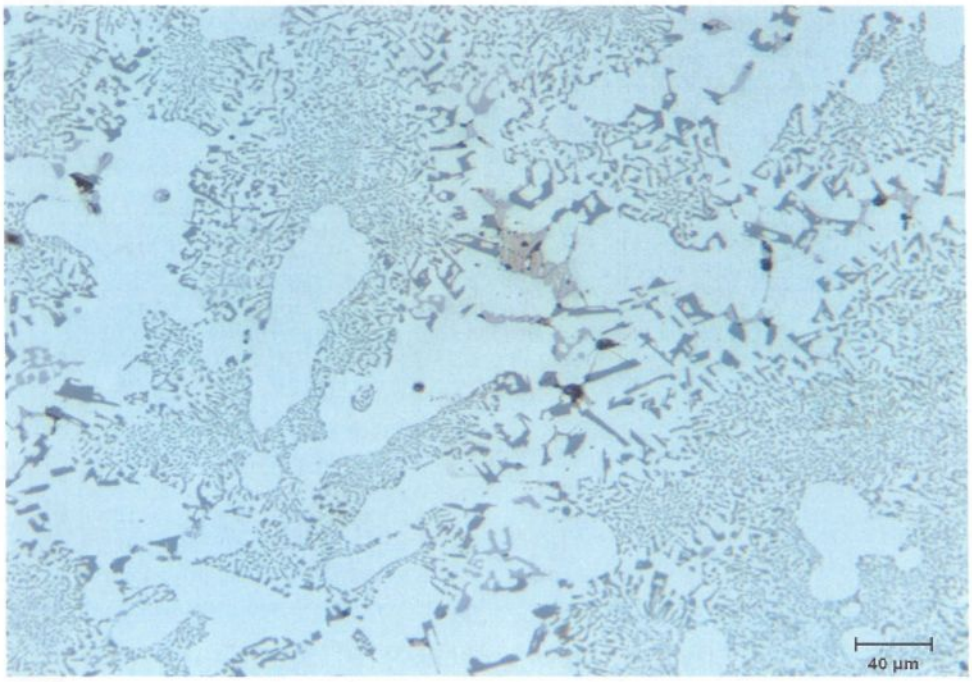

Figure 6.14 Optical micrograph showing microstructure of RNN alloy (RGM + 0.5% Sn + 0.5% In) in the as-cast condition.

Figure 6.15 shows a backscattered image of the RBP alloy (RGM alloy + 0.5% Pb + 0.5% Bi) in the as-cast condition. Due to a large difference in the atomic numbers (Z), the Pb-Bi particles (free machining inclusions) are easily deciphered as being the brightest, with an irregular morphology; they consist of primary Bi crystals enveloped with the Pb_3Bi phase. The high magnification backscattered image displayed in Figure 6.16 shows these features clearly. Besides lead and bismuth, these inclusions also contained Al, Cu, and impurity elements. The contents in impurity elements varied from a few tenths to about 1 at%. The high Bi and Pb concentrations observed in Figure 6.17 for the Pb_3Bi particle shown in Figure 6.16 is in keeping with the WDS analysis provided in Table 6.3.

Similar observations may be noted for the In-Sn inclusions observed in RNN alloy, as shown in Figure 6.18. The backscattered image of RNN alloy shows a more even distribution of the In-Sn particles, compared to the irregular distribution of the Pb-Bi particles seen in Figures 6.15. The In-Sn inclusions were smaller and more densely distributed compared to the Pb-Bi inclusions in the RBP alloy. Figure 6.19 shows a high magnification backscattered image of the RNN alloy (RGM alloy + 0.5% Sn + 0.5% In) showing the morphology of the In_3Sn particles which precipitated in an irregular form. The high In and Sn concentrations observed in Figure 6.20 for the In_3Sn particles shown in Figure 6.19 is in keeping with the WDS analysis provided in Table 6.4.

Figure 6.21 shows the backscattered image corresponding to the optical micrograph seen in Figure 6.13, as taken from the RBN alloy (RGM + 0.5% Bi +1.1% Sn). Both figures show the morphology of Bi- and Sn- particles precipitated in the alloy. The distribution of Bi-and-Sn containing particles is shown in Figure 6.22(a) and (b), respectively. It is clear from these that there is no evidence for the formation of any intermetallic compound between Bi and Sn in the RBN alloy. The Bi-phase is not formed as an intermetallic compound with Al, because it is independently distributed. The Bi-phase is thus not uniformly distributed in the alloy structure and has a tendency to segregate and form a coarse phase. Figure 6.23 is a backscattered image of the R2BN alloy (RGM alloy + 0.5% Sn + 0.5% Bi), also showing the precipitation of Sn and Bi particles whose distribution is shown in Figure 6.24. Bismuth precipitation in the R2BN alloy was well-distributed as small particles compared to its precipitation in the RBN alloy.

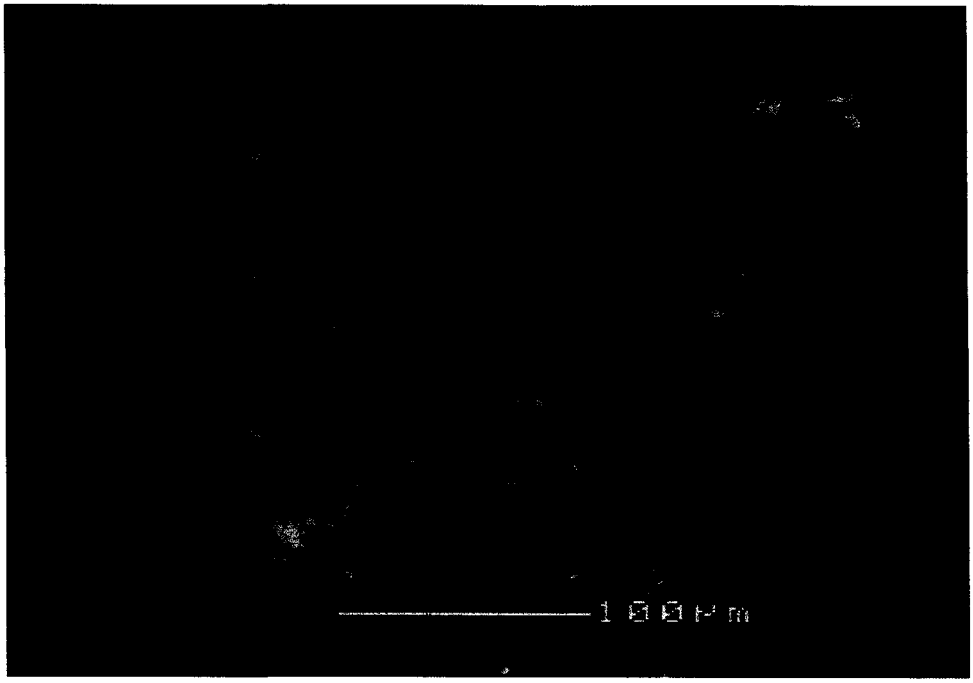

Figure 6.15 Backscattered image obtained from RBP alloy showing the precipitation of Pb-Bi particles.

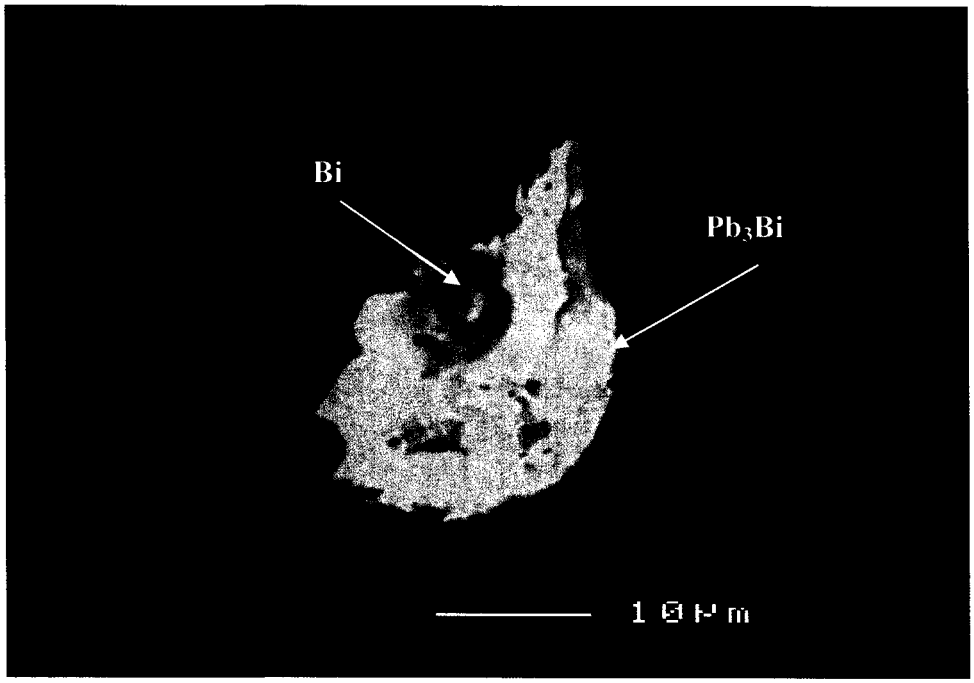

Figure 6.16 High magnification backscattered image taken from RBP alloy (RGM + 0.5% Bi, and 0.5% Pb), showing the presence of a Pb_3Bi particle.

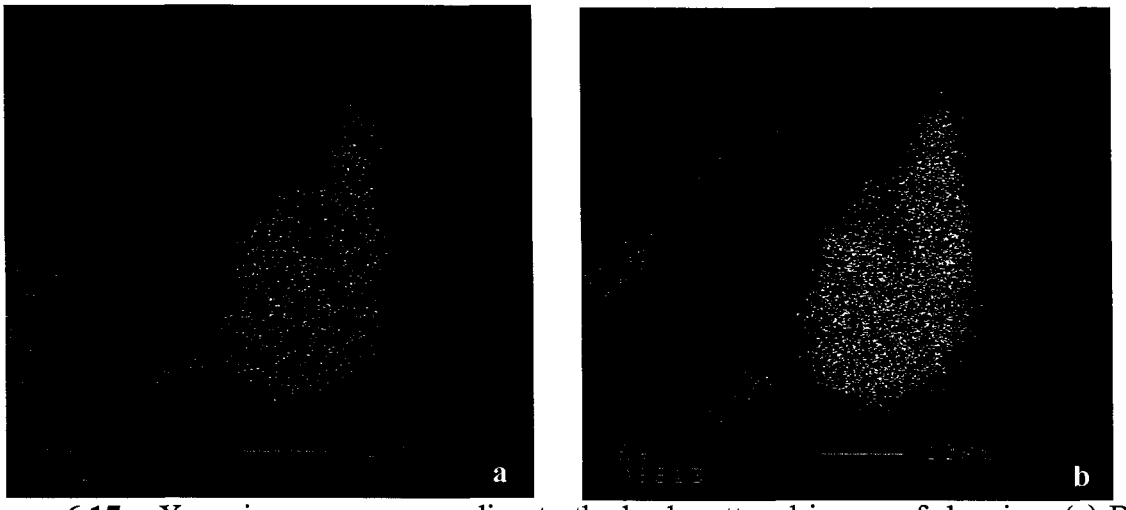

Figure 6.17 X-ray images corresponding to the backscattered image of showing: (a) Bi, and (b) Pb distribution for the Pb_3Bi particle illustrated in Figure 6.16.

Table 6.3 Chemical composition of Pb_3Bi phase particles in as-cast RBP alloy obtained from WDS analysis

Alloy Code	Element	wt %	at. %	Phase
RBP	Pb	70.86 ± 2.37	72.56 ± 4.17	Pb_3Bi phase
	Bi	24.71 ± 3	23.79 ± 3.9	
	Total	**95.57**	**96.35**	

Figure 6.18 Backscattered image obtained from RNN alloy (RGM + 0.5%Sn and 0.5% In), showing the precipitation of In-Sn particles (bright white spots).

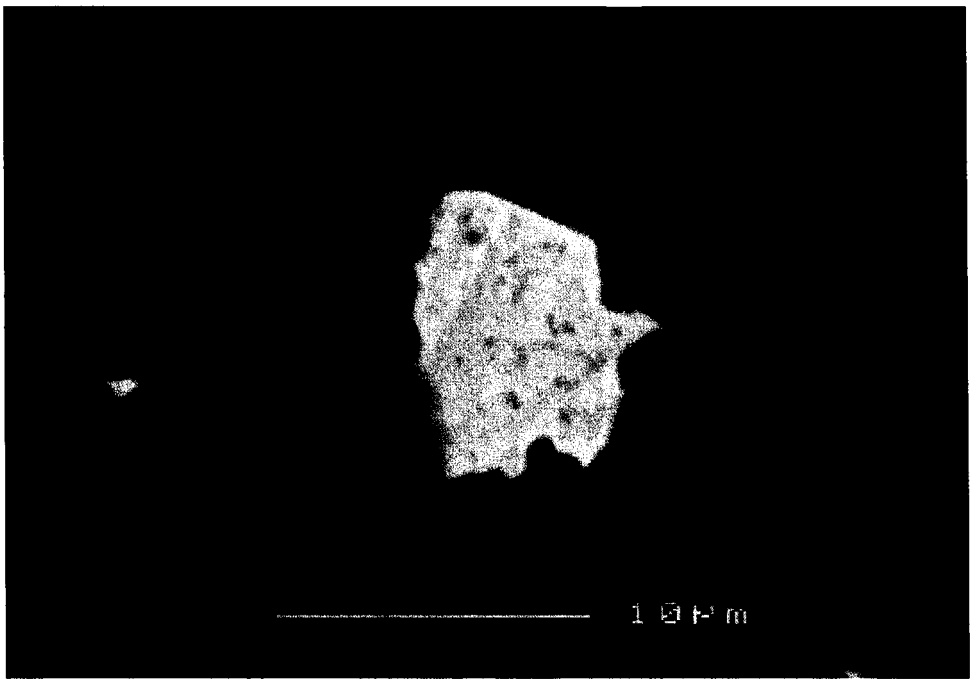

Figure 6.19 High magnification backscattered image taken from RNN alloy (RGM + 0.5% Sn, and 0.5% In), showing the presence of an In_3Sn particle.

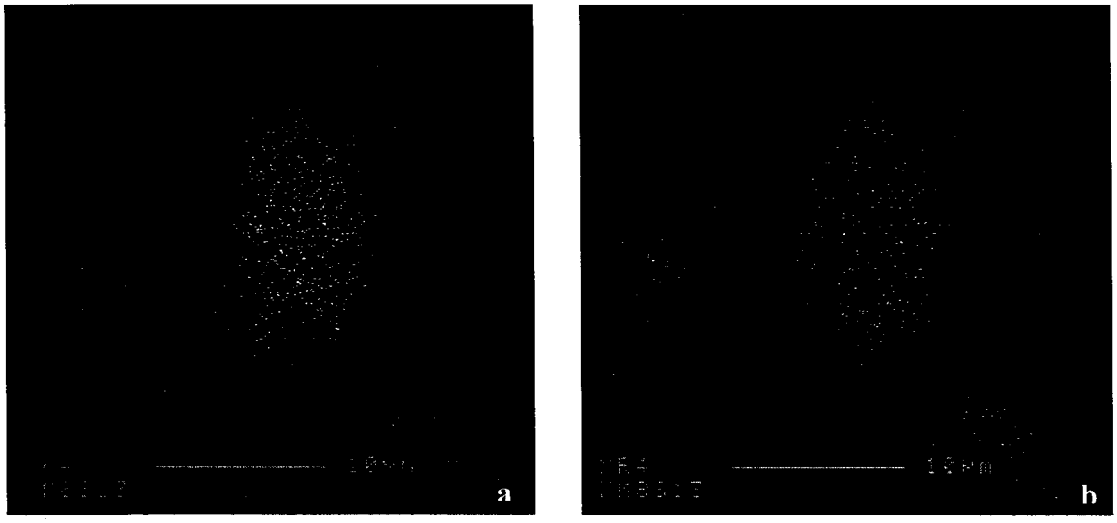

Figure 6.20 X-ray images of (a) In, and (b) Sn distribution in the In_3Sn particle shown in the backscattered image of Figure 6.19.

Table 6.4 Chemical composition of In_3Sn phase particles in as-cast RNN alloy obtained from WDS analysis

Alloy Code	Element	wt %	at. %	Color & Shape	Phase
RNN	In	72.37 ± 1.35	72.17 ± 1.49	white &	In_3Sn
	Sn	26.81 ± 0.42	22.87 ± 1.9	spherical	phase
	Total	**99.18**	**95.04**		

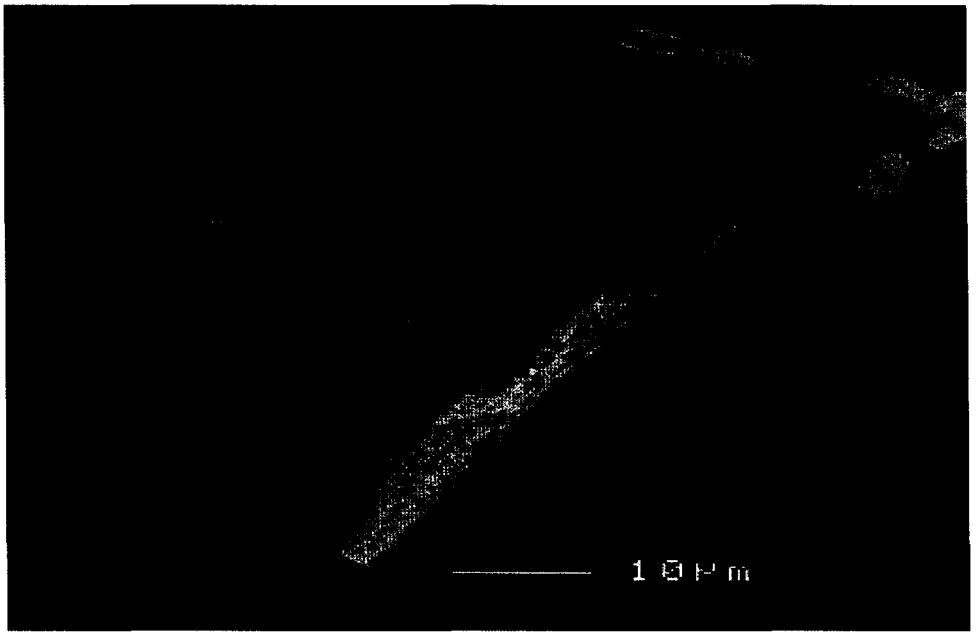

Figure 6.21 Backscattered image taken from RBN alloy (RGM + 0.5% Bi, and 1.1% Sn), showing the presence of Bi and Sn particles.

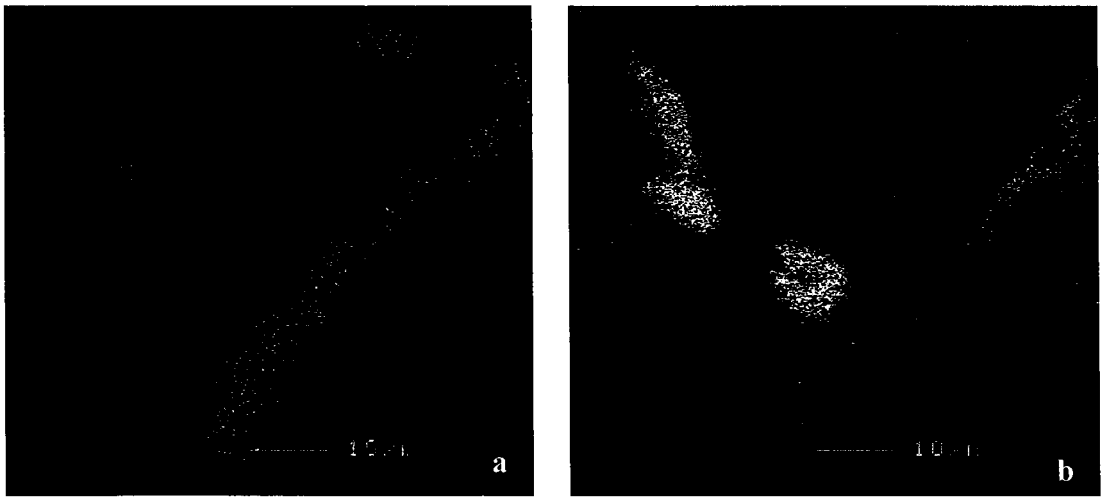

Figure 6.22 X-ray images of: (a) Bi, and (b) Sn, corresponding to the Bi and Sn particles shown in Figure 6.21.

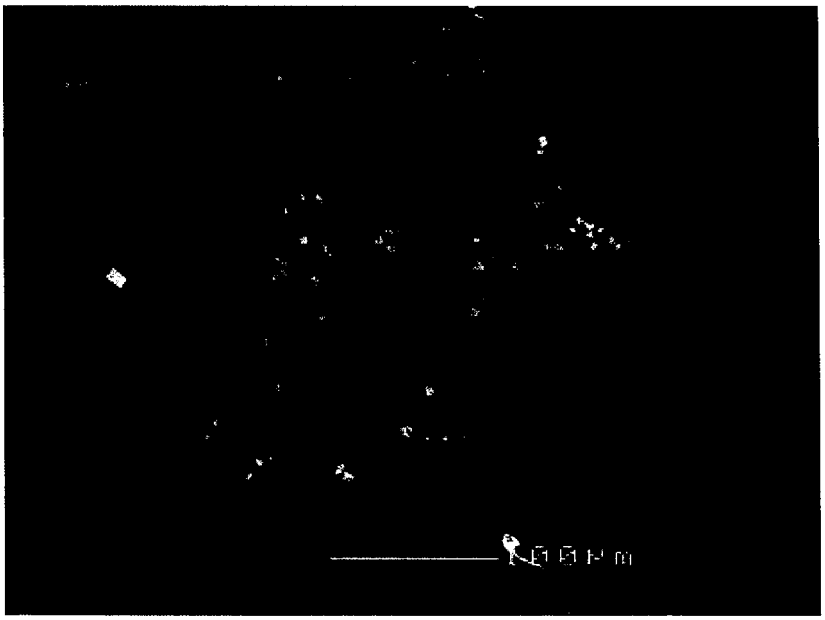

Figure 6.23 Backscattered image taken from R2BN alloy (RGM + 0.5% Bi, and 0.5% Sn), showing the presence of Bi and Sn particles.

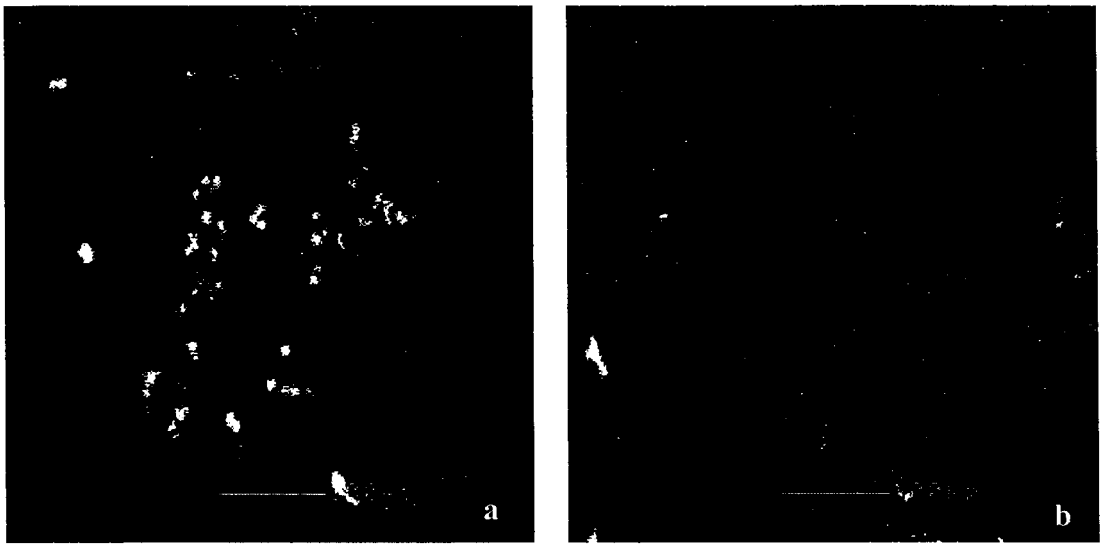

Figure 6.24 X-ray images of: (a) Bi, and (b) Sn corresponding to the Bi and Sn particles shown in Figure 6.23.

Zinc (Zn) is often credited with improvements in the machinability of aluminum casting alloys.[265] Some proponents claim that Zn benefits an alloy by hardening the matrix; others claim that it has a lubricating effect, while still others claim that it does both. Figure 6.25 shows the backscattered image of the as-cast RZ alloy (R2BN alloy + 0.5% Zn). According to atomic number sequence, the white phases in the matrix are well-distributed Bi particles, whereas the lighter white particles are β-Sn which precipitated within the grey Al_2Cu network, see inset to the left.

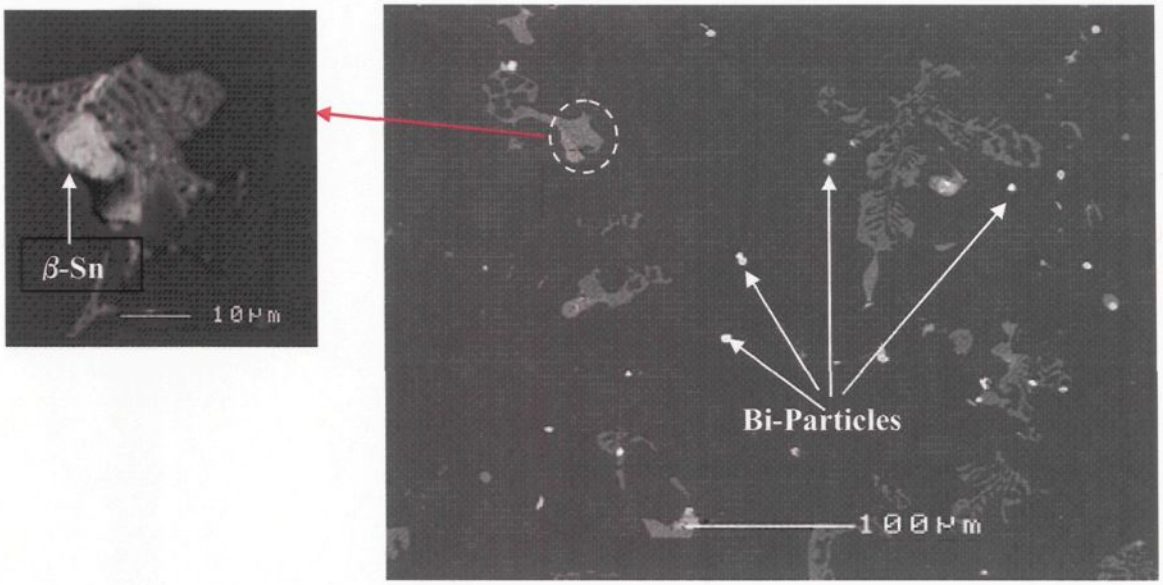

Figure 6.25 Backscattered image taken from RZ alloy (RGM alloy + 0.5% Bi + 0.5% Sn + 0.5% Zn), showing the presence of Bi and Sn particles.

6.2.2 Mechanical Properties

As a general rule, the mechanical properties of Al-Si alloys display a strong dependence on heat treatment, porosity levels, and the nature, size and morphology of second phase constituents.

6.2.2.1 As-Cast Condition

Figure 6.26 and the tabulation in Table 6.5 show the pertinent data relating to as-cast mechanical properties; these include the hardness, yield strength, ultimate tensile strength, and percent elongation of the Sr-modified Al-10.8%Si (RGM) alloy after the addition of Pb, Bi, and Sn, either individually or in combination. The overall results reveal that the mechanical properties ascertained for all nine experimental compositions are somewhat similar to those of the RGM alloy, in that they show better ductility at the

expense of low YS and UTS. It may be observed that there is no marked difference to be seen in the yield strength of the as-cast samples due to the individual or combined addition of these trace elements.

The addition of 0.5% Pb causes no significant deterioration in either the hardness or the tensile properties of the RGM alloy. The same results were observed in the case of the addition of 0.5% Bi, except for elongation which diminishes by 35% compared to the RGM alloy, even though this same element has a marked influence on microstructure, as mentioned earlier. On the other hand, the addition of 1.1% Sn reduces the hardness and UTS by 10% and 7%, respectively, compared to the RGM alloy. The lower strength and hardness values may be interpreted in terms of the presence of Sn, which results in the formation of a certain amount of soft β-Sn particles precipitated mainly at the grain boundaries. Likewise, for the same reason, the elongation increases slightly by 2%.

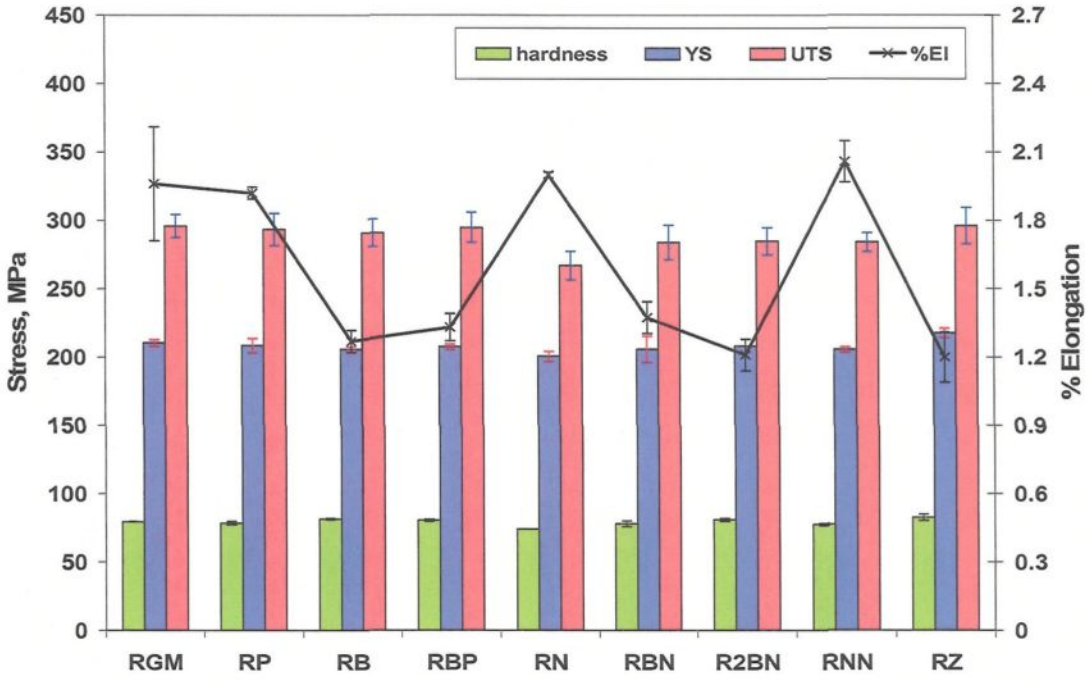

Figure 6.26 Mechanical properties of experimental alloys in the as-cast condition.

It may also be observed that the mechanical properties of alloys containing Sn are marginally lower compared to those of alloys containing Pb. The combined addition of Pb (0.5%) and Bi (0.5%) to the RGM alloy produces better mechanical properties than does the combined addition of Bi (0.5%) and Sn (1.1%). It may also be observed that the combined addition of Sn (0.5%) and In (0.5%) to the RGM alloy leads to an improvement of 3, 6, and 5% in YS, UTS, and %El, respectively, compared to the addition of Sn alone.

Table 6.5 Mechanical properties of RGM alloy after addition of trace elements

Alloy Code	Yield stress (MPa)	UTS (MPa)	Elongation (%)	Hardness BHN
RGM	210.54 ± 2.34	295.31 ± 8.4	1.96 ± 0.25	79.5 ± 0.1
RP	208.7 ± 5.17	293.31 ± 11.7	1.92 ± 0.03	78.5 ± 1.29
RB	206.00 ± 1.92	290.85 ± 10	1.27 ± 0.05	81.5 ± 0.54
RBP	207.72 ± 1.94	294.75 ± 11	1.33 ± 0.06	80.5 ± 0.88
RN	200.68 ± 3.76	267 ± 10.4	1.99 ± 0.013	74 ± 0.0
RBN	205.94 ± 9.7	283.92 ± 12.7	1.37 ± 0.07	78 ± 2.1
R2BN	208.37 ± 4.75	284.66 ± 9.85	1.21 ± 0.08	80.93 ± 1.1
RNN	205.67 ± 1.94	284 ± 6.8	2.06 ± 0.09	77.5 ± 0.81
RZ	217.90 ± 3.33	296 ± 13.23	1.285 ± 0.11	82.65 ± 2.41

6.2.2.2 T6 and T7 Heat-Treated Conditions

Figure 6.27 shows the effects of the addition of Pb, Bi, and Sn, both individually and in combination, on the hardness of T6 and T7 heat-treated Sr-modified Al-10.8%Si alloys. In general, it can be observed that peak hardness is obtained at 180°C for all the alloys studied. A comparison of peak hardness values at 180°C shows that the RB alloy (RGM alloy + 0.5% Bi) has the highest hardness compared to the other alloys. Variations occurring in hardness values with changes in aging temperature are found to follow a

similar trend for all the alloys. The changes which are to be observed in hardness values are due mainly to the size, shape and distribution of Al_2Cu precipitates during aging. Aging at 200°, 220°, and 240°C causes a noticeable decrease in the hardness values compared to those obtained at 180°C. These precipitates show an increase in size accompanied by a gradual change in chemical composition upon increasing the aging temperature. The resulting equilibrium phase, *i.e.* θ-Al_2Cu, in the form of incoherent particles, is responsible for the drop to be observed in the alloy hardness. The results provided in Figure 6.27 also show that the level of hardness in the T6-treated condition is generally lower for the RN alloy (RGM alloy + 1.1% Sn) than it is for other alloys. Alloy RB (RGM alloy + 0.5% Bi), however, displays the maximum hardness at all the aging temperatures applied.

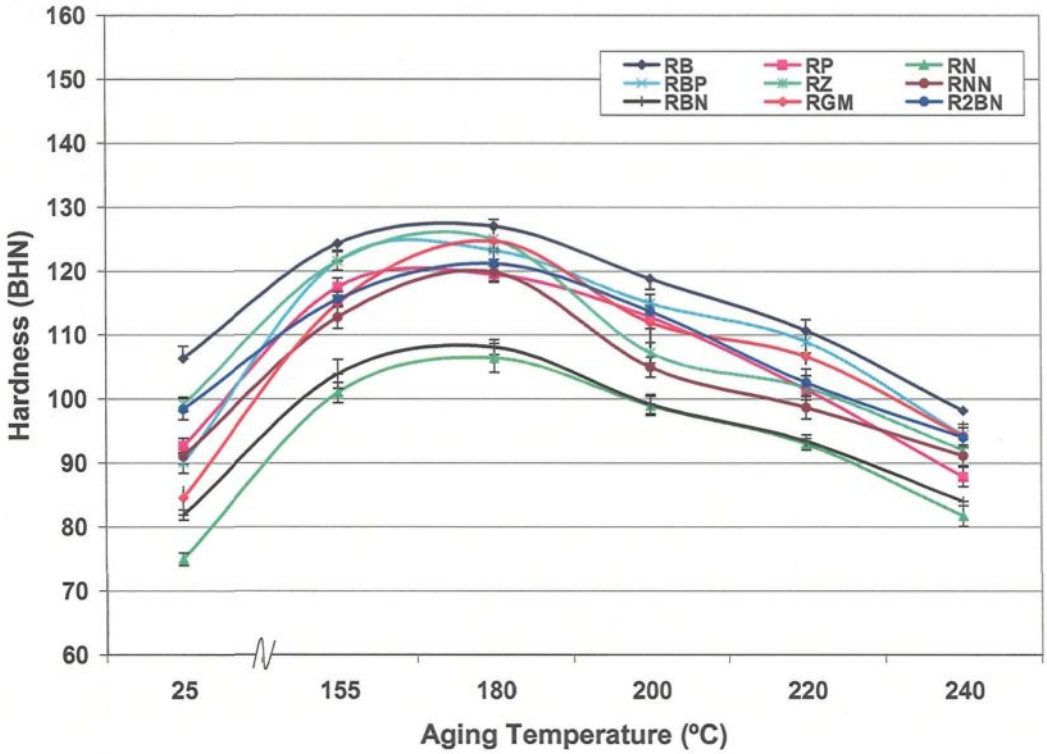

Figure 6.27 Hardness of RGM alloy as a function of Pb, Bi, and Sn additions and heat treatment conditions.

Figures 6.28(a) to (c) show the YS, UTS and % El of these alloys plotted as a function of aging temperature. The average tensile properties and their standard deviations are presented in Tables 6.6 through 6.8. Since the value of the UTS and %El would be influenced by any localized defect concentration, only the best results were taken into account in determining the average values plotted in Figures 6.28(b) and (c), in view of the fact that the scatter was too large.

In general, T6-temper produces increased strength with a corresponding loss in ductility, as well as the development of more stable mechanical properties. For example, with an aging time of 5 hours, the tensile strength increases and elongation decreases with an increase in aging temperature of up to 180°C for all the alloys studied. The YS, shown in Figure 6.28(a), increases with aging temperature and attains a maximum at 180°C for all the alloys. Softening commences when the alloy is aged at 200°C, reaching a maximum at 240°C. The UTS exhibits a trend similar to that shown by YS, as shown in Figure 6.28(b).

It can be observed that the RB alloy containing 0.5% Bi behaves in much the same way as the RP alloy with 0.5% Pb at the different aging temperatures applied. On the other hand, the RN alloy shows lower tensile properties at all aging temperatures. For example, at 180°C, the alloy YS, UTS, and %El diminish by 12%, 21%, and 56%, respectively, compared to the RGM alloy. The reduced strength and ductility of the Sn-containing alloys may be attributed to the increase in percentage porosity observed in these alloys compared to the RGM alloys. The combined addition of Sn and In to the RGM alloy produces an increase of 1%, 2% and 5% in the YS, UTS, and %El, respectively, compared to the RN

alloy at 180°C. Similarly, a combined addition of Sn and Bi improves the tensile properties significantly compared to the RN alloy.

The combined addition of Bi (0.5%) and Pb (0.5%) to the RGM alloy (or RPB alloy) produces properties which are more or less similar to those of the RB and RP alloys, while the RNN alloy (RGM alloy + 0.5% Sn + 0.5% In) possesses tensile properties which are higher than those obtained for the RN alloy (RGM + 1.1% Sn) at any of the five aging temperatures applied. For example, aging the RNN alloy for 5 h at 180°C is associated with increases of 1%, 2%, and 5% in YS, UTS, and %El, respectively, compared to the values exhibited by the RN alloy. It is evident, from the results, that the Sn-In interaction enhances the alloy strength parameters above those obtained from the RN alloy which contained only the addition of Sn.

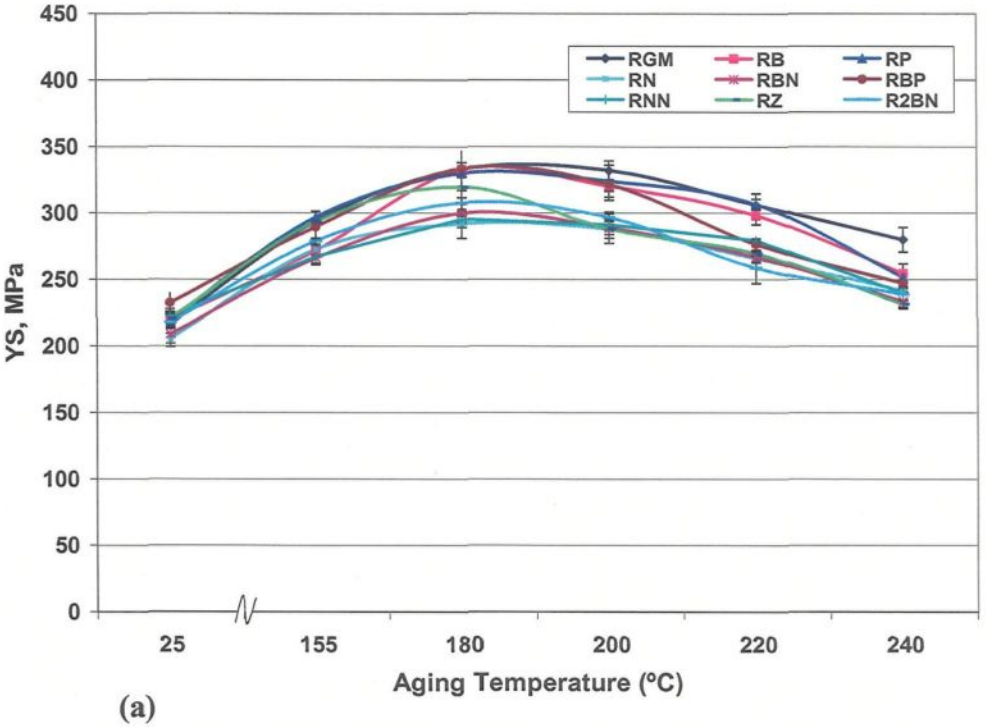

(a)

Figure 6.28 ⟶ **Continued**

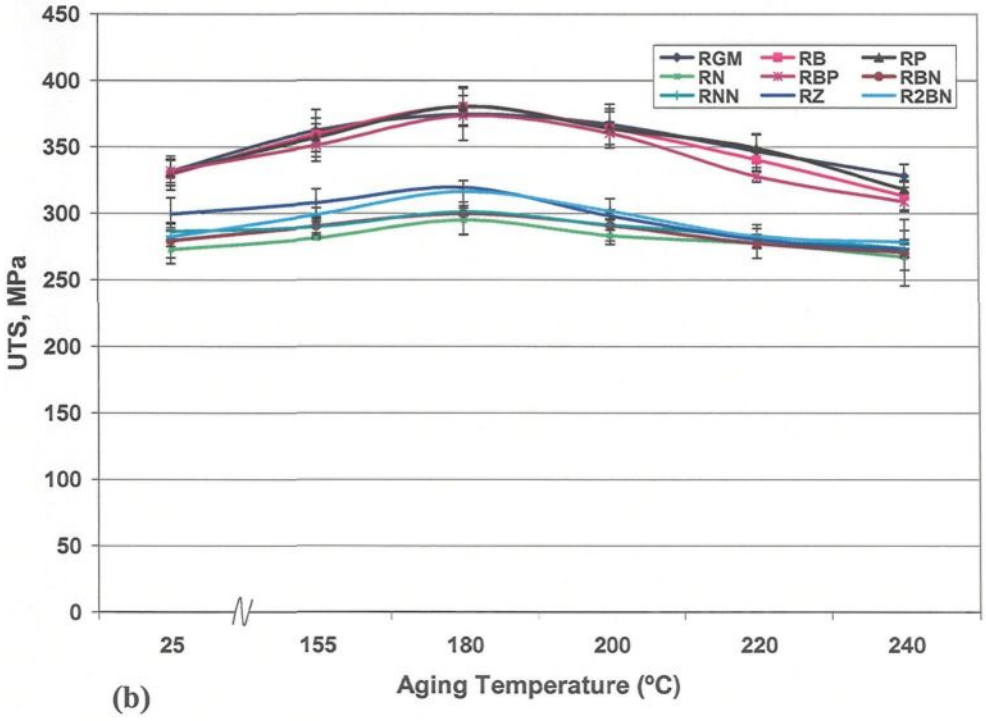

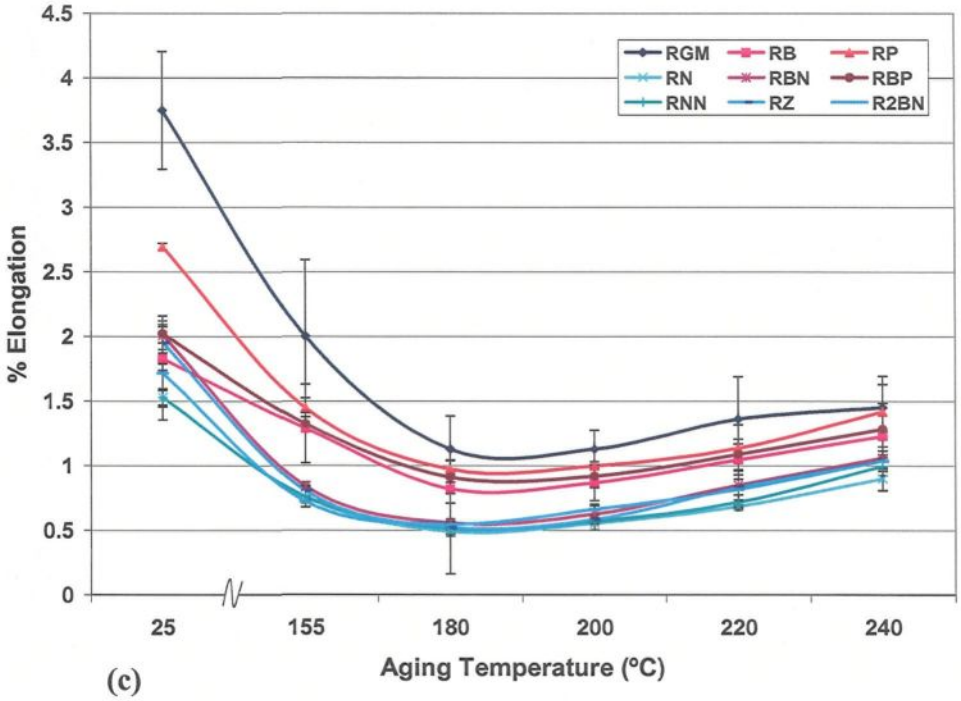

Figure 6.28 Variation in (a) YS, (b) UTS, and (c) %El as function of Pb, Bi, and Sn additions and heat-treatment conditions.

Table 6.6 Yield strength as a function of aging temperature for Al-10.8%Si alloy

Alloy code	155 °C	180 °C	200 °C	220 °C	240 °C
RGM	293.84 ± 5.2	336.63 ± 6.9	332.1 ± 8.7	306.1 ± 9.2	271.34 ± 7.6
RP	296.8 ± 2.2	329.8 ± 12	324 ± 4	306.6 ± 2.5	251.8 ± 2.6
RB	271.8 ± 5.2	332.75 ± 4	320.49 ± 7.2	298.4 ± 7	254.67 ± 7.5
RN	272.6 ± 11	291.89 ± 4	287.79 ± 3.2	265.9 ± 1.4	241.69 ± 3.6
RBP	289.66 ± 13	333.47 ± 12	321.59 ± 4.6	276.6 ± 6.6	247.26 ± 7.3
RBN	366.1 ± 6.8	299.9 ± 11.7	289 ± 2.7	266.9 ± 5.5	233.6 ± 6.6
R2BN	278.8 ± 9.6	307.49 ± 2.8	296.6 ± 11.7	258.8 ± 10.2	238.9 ± 9.3
RNN	267.1 ± 6.2	295.38 ± 3.8	291.27 ± 1.3	279.5 ± 4.9	239.75 ± 5.4
RZ	293.49 ± 0.5	319.45 ± 7.8	288.2 ± 7.2	269.6 ± 2	231.66 ± 2.4

Table 6.7 UTS as a function of aging temperature for Al-10.8%Si alloy

Alloy code	155 °C	180 °C	200 °C	220 °C	240 °C
RGM	362 ± 19.5	374.5 ± 15.2	366.9 ± 12.3	346.9 ± 8.7	328.3 ± 15.6
RP	356.96 ± 8	380.5 ± 14.7	364 ± 11	349 ± 6.7	318.1 ± 11.2
RB	359.4 ± 15	380.38 ± 12	364.18 ± 9	340.5 ± 10.5	313.16 ± 4.1
RN	281.3 ± 10.7	294.94 ± 6.5	283.19 ± 2.8	277.45 ± 9.8	267.22 ± 9.1
RBP	351.21 ± 7	373.39 ± 8.4	360.33 ± 4.3	327.82 ± 7.4	308.78 ± 5.8
RBN	290.23 ± 16	299.94 ± 11	290.99 ± 11	277.38 ± 25	270.7 ± 4.34
R2BN	298.86 ± 5.2	316.39 ± 8	301.55 ± 9.6	282.66 ± 8.9	278.38 ± 8.9
RNN	289.88 ± 2.8	301.1 ± 3.8	291.27 ± 1.3	282.86 ± 6.8	273.51 ± 5.3
RZ	307.89 ± 10	319.45 ± 2.3	298.21 ± 2.4	380.31 ± 2.3	273.12 ± 5.6

Table 6.8 Pct elongation as a function of aging temperature for Al-10.8%Si alloy

Alloy code	155 °C	180 °C	200 °C	220 °C	240 °C
RGM	2.0 ± 0.29	1.127 ± 0.25	1.128 ± 0.14	1.36 ± 0.32	1.45 ± 0.24
RP	1.449 ± 0.07	0.973 ± 0.03	1.0 ± 0.18	1.138 ± 0.2	1.42 ± 0.03
RB	1.29 ± 0.02	0.82 ± 0.11	0.87 ± 0.14	1.048 ± 0.12	1.23 ± 0.003
RN	0.749 ± 0.01	0.487 ± 0.03	0.552 ± 0.05	0.682 ± 0.01	0.896 ± 0.08
RBP	1.325 ± 0.3	0.911 ± 0.12	0.919 ± 0.08	1.087 ± 0.11	1.285 ± 0.2
RBN	0.84 ± 0.01	0.557 ± 0.39	0.626 ± 0.06	0.85 ± 0.17	1.06 ± 0.08
R2BN	0.719 ± 0.04	0.547 ± 0.04	0.660 ± 0.04	0.814 ± 0.08	1.036 ± 0.23
RNN	0.758 ± 0.05	0.511 ± 0.05	0.568 ± 0.02	0.714 ± 0.06	0.993 ± 0.07
RZ	0.803 ± 0.07	0.52 ± 0.05	0.58 ± 0.01	0.83 ± 0.01	1.035 ± 0.08

6.3 INFLUENCE OF TIN ADDITION ON THE MICROSTRUCTURE AND MECHANICAL PROPERTIES OF B319.2 AND A356.2 ALLOYS

6.3.1 Microstructure

The microstructure of Al-Si alloys depends on the chemical composition, casting process, and heat treatment applied. The B319.2 and A356.2 alloys are popular hypoeutectic Al-Si alloys used extensively by automotive and aircraft industries mainly for their high strength and ductility. In the context of this research study, where the main focus has been the development of the Al-10.8%Si alloys with a view to optimizing their machining characteristics and, hence, productivity, it was also thought worthwhile to investigate the microstructure and mechanical properties of the B319.2 and A356.2 alloys from this point of view. For this purpose, an examination of the microstructures of these alloys was thus undertaken after minor amounts of Sn had been added. The study was carried out for the as-cast and heat-treated conditions, using optical microscopy and electron probe microanalysis (EPMA).

6.3.1.1 Alloy B319.2

In the 319-type aluminum alloys, the microstructure is typically composed of an aluminum matrix containing eutectic silicon which may be present in the form of acicular needles, blocky plates, or a refined fibrous structure, depending upon the level of chemical modification and the cooling rate of the cast section. In general, the eutectic silicon is not uniformly distributed, but tends to be concentrated at the interdendritic boundaries. The as-cast microstructure of the Sn-free alloy (coded N alloy) is shown in Figure 6.29(a). Eutectic

silicon particles, precipitated in the fibrous form typical of a modified structure, constitute the main microstructural feature observed. Both of the Fe-containing phases, *i.e* α-$Al_{15}(Fe,Mn)_3Si_2$ Chinese script and needle-like β-Al_5FeSi, as well as the Cu-containing phases, mainly Al_2Cu, are seen to nucleate within the matrix or at the interface of such pre-existing constituents as Si or intermetallic particles. The presence of Sr and Mg leads to an increase in the tendency of Al_2Cu to segregate to areas free of eutectic silicon. Samuel *et al.*[232] proposed a schematic model explaining the mechanism of this phenomenon which was also commented upon by Mulazimoglu *et al.*[266] The copper phase occurs in block form as Al_2Cu, or as fine pockets of eutectic Al-Al_2Cu.

The typical optical microstructure of the Sn-containing B319.2 alloy, coded as NSS, is shown in Figure 6.29(b). It can be observed that, there is no significant difference in microstructure for Sn-free and Sn-containing alloys in the as-cast condition except for the precipitation of Sn as black reticulate particles of β-Sn. These β-Sn particles always solidify within the Al_2Cu network, attached to the Si particles. The distribution of the β-Sn particles is not uniform; rather, they are distributed as small clusters.

Figure 6.30 is a backscattered image taken from the NSS alloy sample. According to atomic number sequence, the white phases in the matrix are β-Sn which precipitated within the Al_2Cu network (lighter grey particles). Tiny Mg_2Sn particles (300-500 nm) which had also precipitated on the eutectic Si particles could not be observed using optical microscopy, but were discernable with the EPMA technique. Unfortunately, it was impossible to quantify the Mg_2Sn phase by EDX using point analysis because of the fine size of this phase. This inability indicates that the magnesium level in B319.2 alloy needs to

be high enough to tie up the tin in the form of the higher melting Mg_2Sn while still leaving enough for magnesium intermetallics/precipitates to impart typical properties, suggesting a critical Mg level in the presence of Sn.

It is also clear that the spherical precipitates are not Cu-Sn intermetallic particles, since no Cu enrichment was found in the Sn precipitates. It is also unlikely that these particles are an Al-Sn compound, since no compounds are reported in the equilibrium phase diagram.[220] Moreover, from the WDS analysis shown in Table 6.9, the chemical composition of this phase appears to be β-Sn. A minimum of ten measurements were performed in different regions of the microstructures, and the standard deviations in composition were calculated. The corresponding EDX spectrum, as shown in Figure 6.31, displays strong reflections due to Sn, a fact which is consistent with the WDS analysis. Figures 6.32(a) and (b) are the backscattered micrographs taken of the NSS alloy (N alloy + 0.15% Sn) at high magnification, showing the morphology of Sn-containing particles precipitated in the alloy.

As in the case of the RN alloy (RGM alloy + 1.1%Sn), the microstructure of the NSS alloy solutionized for 8 h at 495°C followed by quenching in hot water (~65°C) and aging at 180°C/5h, as shown in Figure 6.33, reveals (a) a high tendency towards eutectic Si particles spheroidization, (b) the absence of any sign of incipient melting of Cu-base intermetallics, and (c) β-Sn, present in black reticulate form, which melts due to solution treatment at 495°C, leading to the formation of spherical voids. Figure 6.34 shows a backscattered image obtained from the NSS alloy, where the molten state of the tin particles (which occurred during solution heat treatment) can be observed clearly.

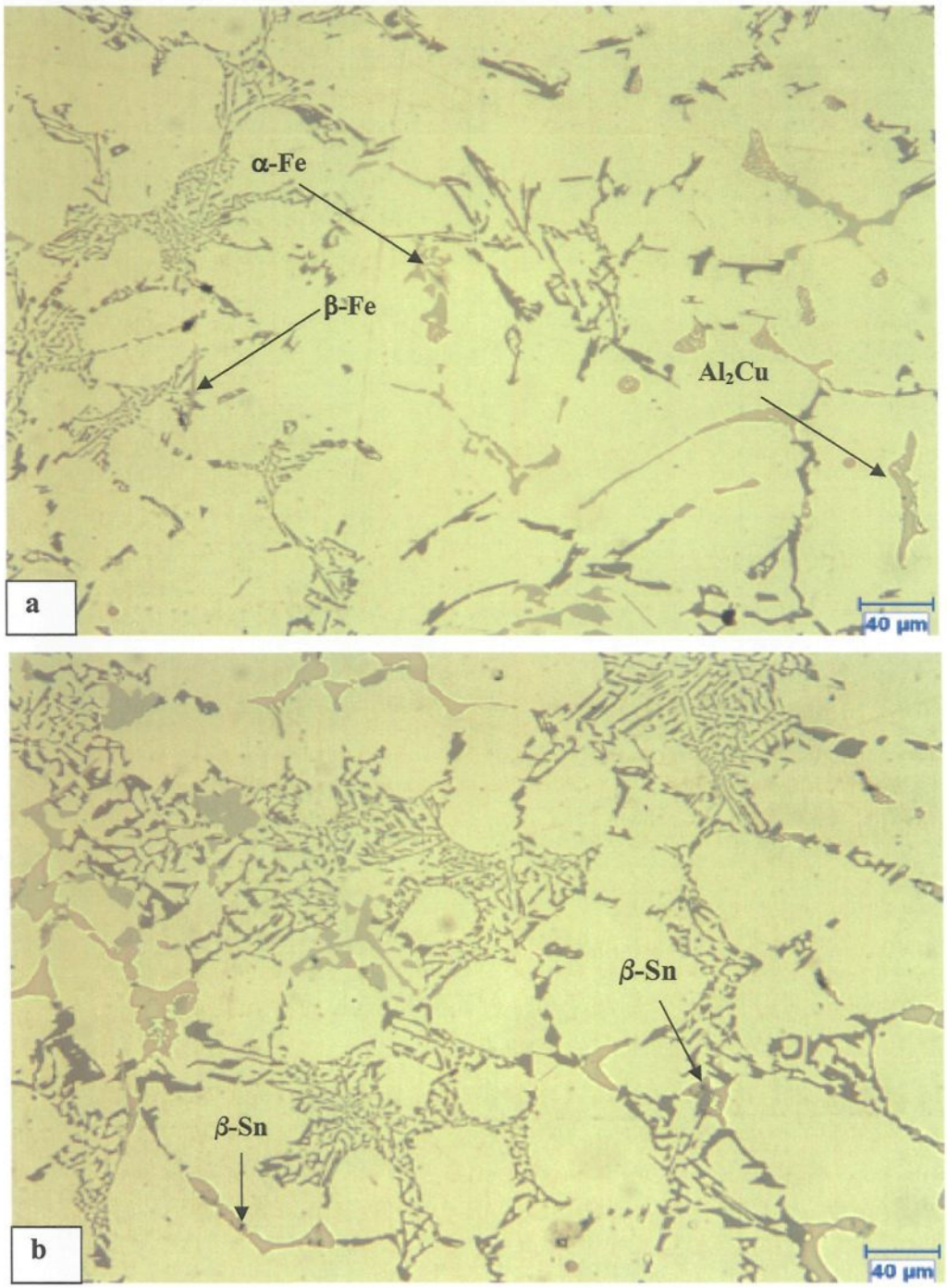

Figure 6.29 Optical micrographs of: (a) N, and (b) NSS alloys in the as-cast condition.

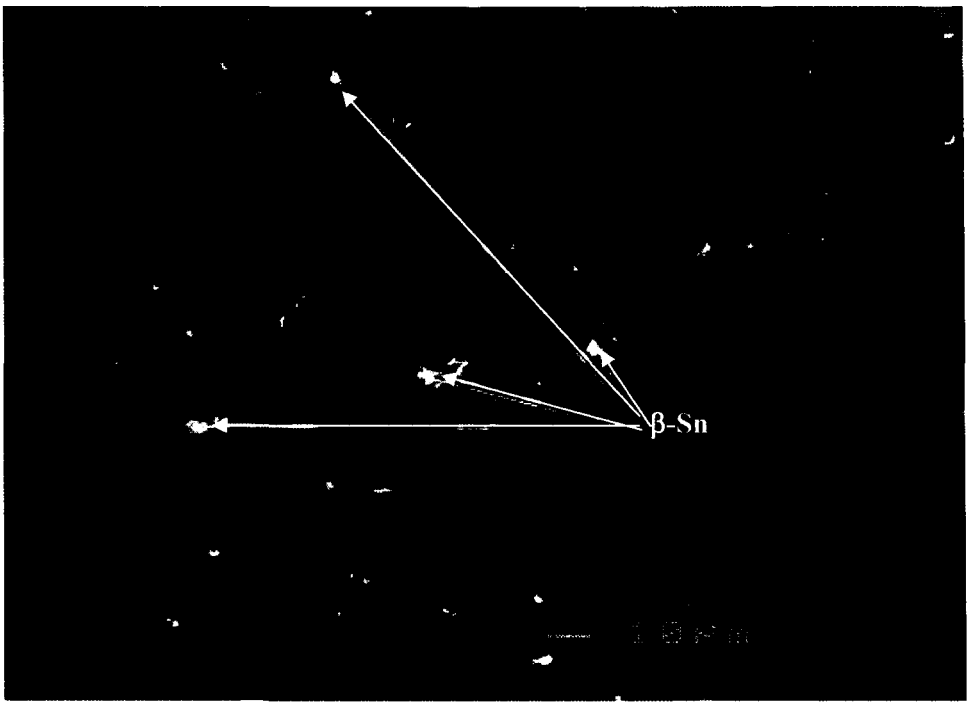

Figure 6.30 Backscattered image obtained from NSS alloy showing β-Sn precipitation.

Table 6.9 Chemical composition of the Sn-containing phase particles in as-cast NSS and KSS alloys containing 0.15% Sn obtained from WDS analysis

Alloy Code	Element	wt %	at. %	Brightness & Shape	Phase
NSS	Sn	98.11 ± 0.22	97.93 ± 0.16	white &	β- Sn
	Cu	1.15 ± 0.29	2.10 ± 0.29	polyhedral	
	Total	**99.26**	**100.03**		
KSS	Mg	30.03 ± 1.0	64.5 ± 1.2	grey & Chinese	Mg_2Sn
	Sn	64.78 ± 1.5	28.5 ± 0.29	script	
	Si	2.88 ± 0.49	5.35 ± 0.61		
	Total	**98.55**	**99.99**		

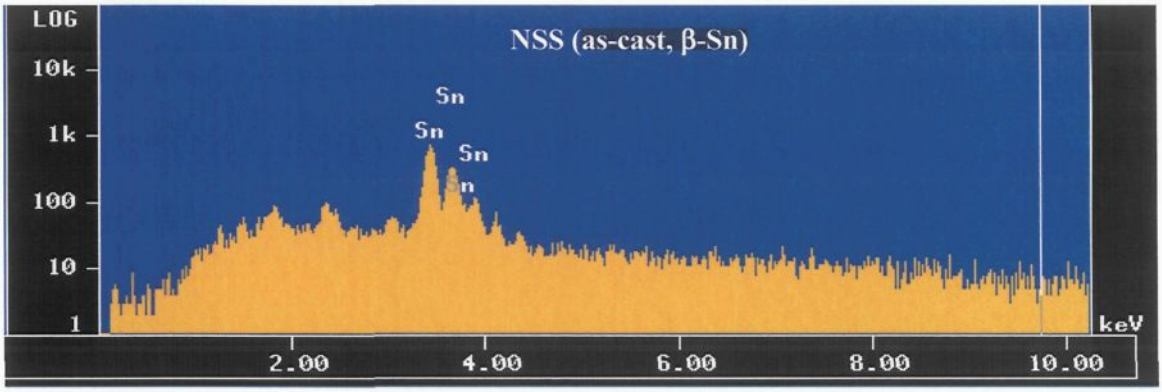

Figure 6.31 EDX spectrum corresponding to β-Sn particles observed in NSS alloy containing 0.15% Sn.

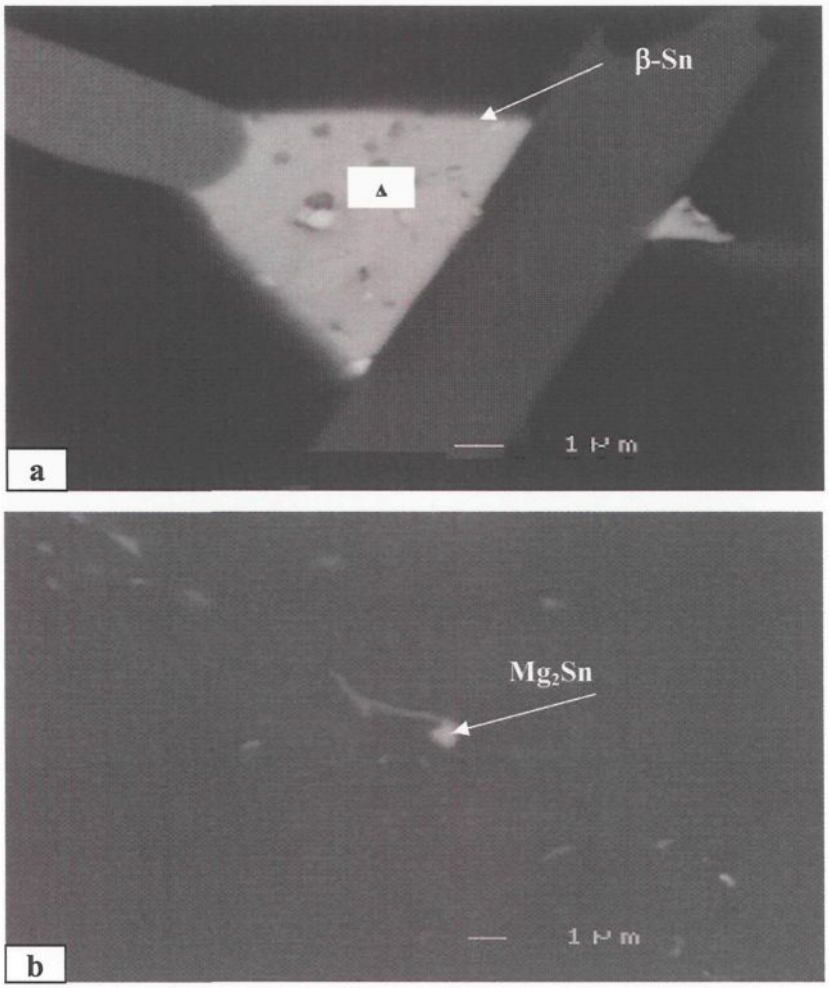

Figure 6.32 Backscattered images taken at high magnification of the NSS alloy showing the precipitation of (a) β-Sn, and (b) Mg_2Sn. Spot analysis of point A is given in Table 6.9.

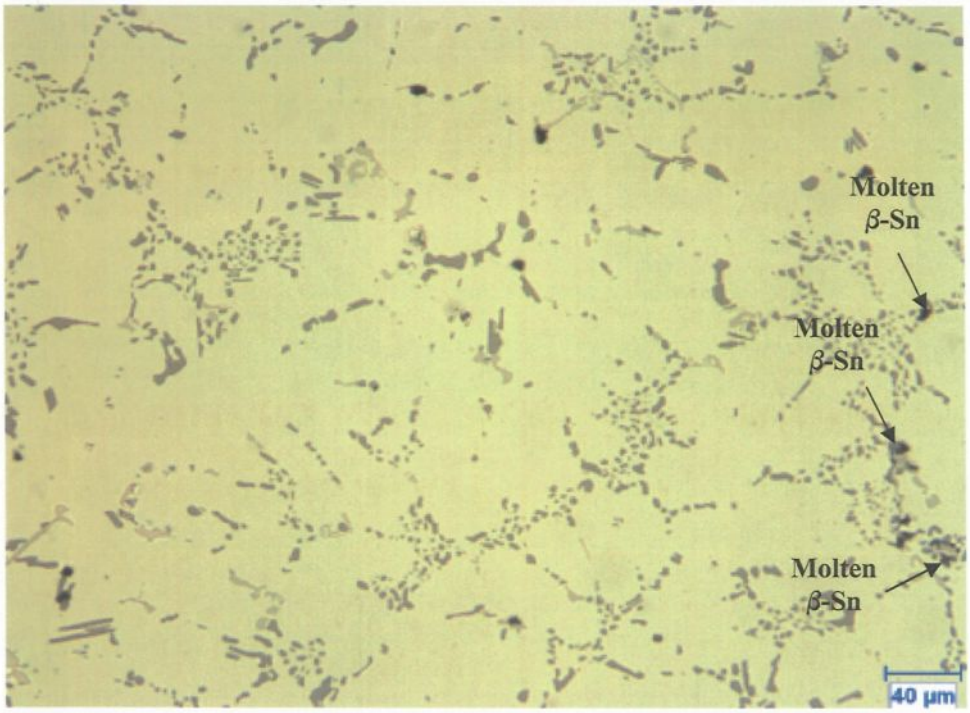

Figure 6.33 Optical micrograph of NSS (N + 0.15% Sn) alloy in the T6 condition.

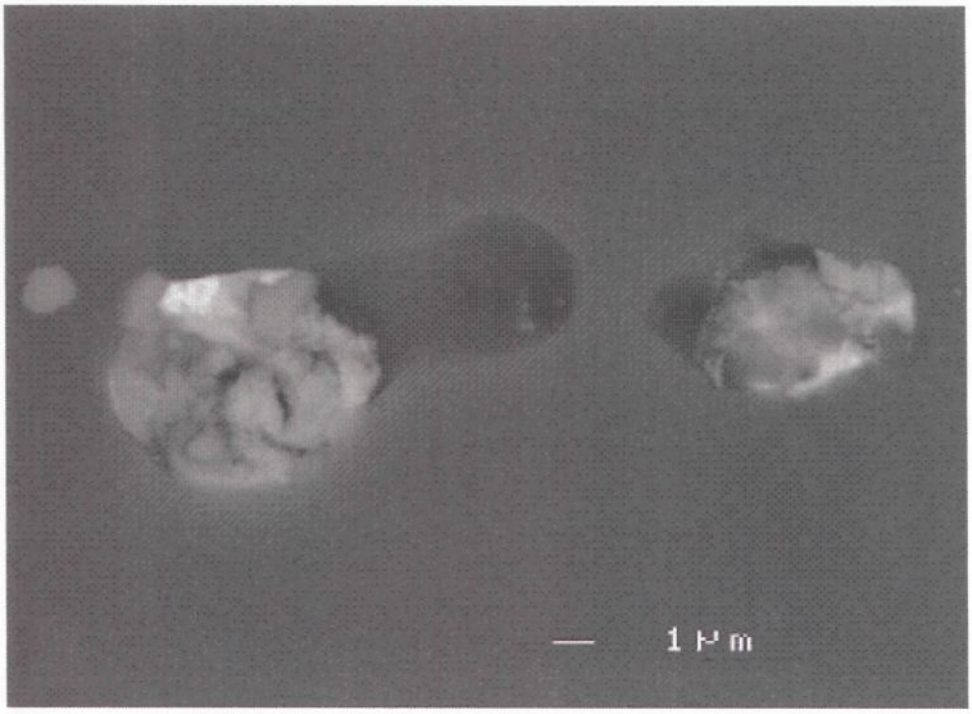

Figure 6.34 Backscattered image taken from NSS alloy in T6 condition showing molten β-Sn particles.

6.3.1.2 Alloy A356.2

The alloy A356.2 has high Mg, but is very low in Cu content. Its microstructural characteristics and tensile properties will therefore be controlled by compositional factors. Figure 6.35 shows the typical microstructures for the as-cast conditions of the K and KSS alloys containing 0.0 and 0.15% Sn, respectively. The microconstituents of the KSS alloy were similar to those of the K alloy except that the Mg_2Sn particles were observed in the form of Chinese script as shown in Figure 5.35(b).

Figure 6.36 is a backscattered image of the KSS alloy, from which it is clear that Sn was precipitated as a single crystal of Mg_2Sn with embedded nano-sized particles of Mg_2Sn-Sn eutectic, leading to the conclusion that there is usually more Sn than required for Mg_2Sn. The Mg_2Sn phase occurs in grey Chinese script form.

The high Mg and Sn concentrations observed in Figure 6.36 for the Mg_2Sn particles are shown in Figure 6.37. Figure 6.38 is a backscattered image of the KSS alloy (K alloy + 0.15% Sn) taken at high magnification, showing the morphology of the Mg_2Sn particle in Chinese script form. Mg has a higher affinity for such elements as Si, Sn, Pb, and so forth, than it does for Al; it can form binary intermetallic compounds with Al only after these elements are completely combined. On the other hand, the distribution of phases in the solid state in the aluminum corner of the Al-Si-Mg and Al-Sn-Mg phase diagrams[23] indicates their similarity. In all cases, the path of Al + Mg_2B divides the corner into two regions: Al + Mg_2B + Mg_5Al_8 (or Mg_2Al_3), where B is Si or Sn. An examination of the regions of the Al-Si-Mg and Al-Sn-Mg phase diagrams which concern this study leads to the conclusion that, in the Al-Si-Mg system, compounds of Sn with magnesium (Mg_2Sn)

form as the result of an excess of Mg from the unstable compound Mg_5Al_8 and the Mg in the stable compound Mg_2Si through the following reactions:[217]

$$Al + Mg_2Si + Mg_5Al_8 + Sn \rightarrow Al + Mg_2Si + Mg_2Sn \quad \text{Eq. (1)}$$

$$Al + Mg_2Si + Si + Sn \rightarrow Al + Mg_2(Si, Sn) + Si \quad \text{Eq. (2)}$$

In the most interesting region of Al + Mg_2Si + Si, which is the region of cast Al-Si alloys, the formation of Mg_2Sn without excess magnesium is possible only with partial or complete anions, with isovalent replacement of silicon in Mg_2Si with tin through the reaction expressed in Eq.(2). This type of replacement would be possible with comparable thermodynamic characteristics of the compounds Mg_2Si and Mg_2Sn, characterizing the binding force, and also with the crystallochemical correspondence between them. Mg_2Si and Mg_2Sn have the same cubic crystal structure of the CaF_2 type with similar lattice constants: 6.33 and 6.765°A, respectively.[267] For further investigation, X-ray mapping of the Mg_2Sn phase was carried out to determine the distribution of Sn and Mg, as shown in Figure 6.39. The corresponding EDX spectrum of the compound is shown in Figure 6.40. The quantitative WDS analysis provided in Table 6.9 indicates that this phase contains approximately 64.5 at% Mg, 28.5 at% Sn and 5.3 at% Si, with an approximate composition of $Mg_2Si_{0.2}Sn_{0.8}$. Thus, it may be concluded that Sn tends to interact with Mg more than with Si.

Figure 6.41, showing a backscattered image obtained from the T6 heat-treated KSS alloy (K alloy + 0.15% Sn - solutionized for 8 h at 540°C, followed by quenching in hot water at~65°C and aging at 180°C/5h), reveals the formation of spherical voids. While the melting point of Mg_2Sn is about 783°C, the temperature of the Mg_2Sn-Sn eutectic is

~209°C and its composition is very close to 91 at% (98 wt%) Sn.[267] From this, it can be concluded that the formation of voids is related to the melting of the Mg_2Sn-Sn eutectic phase during solution treatment. Also, since the as-cast structure contained Mg_2Sn, as well as mixtures of Sn and Mg_2Sn, following heat treatment, the tin was predominantly present as the Mg_2Sn-Sn eutectic.

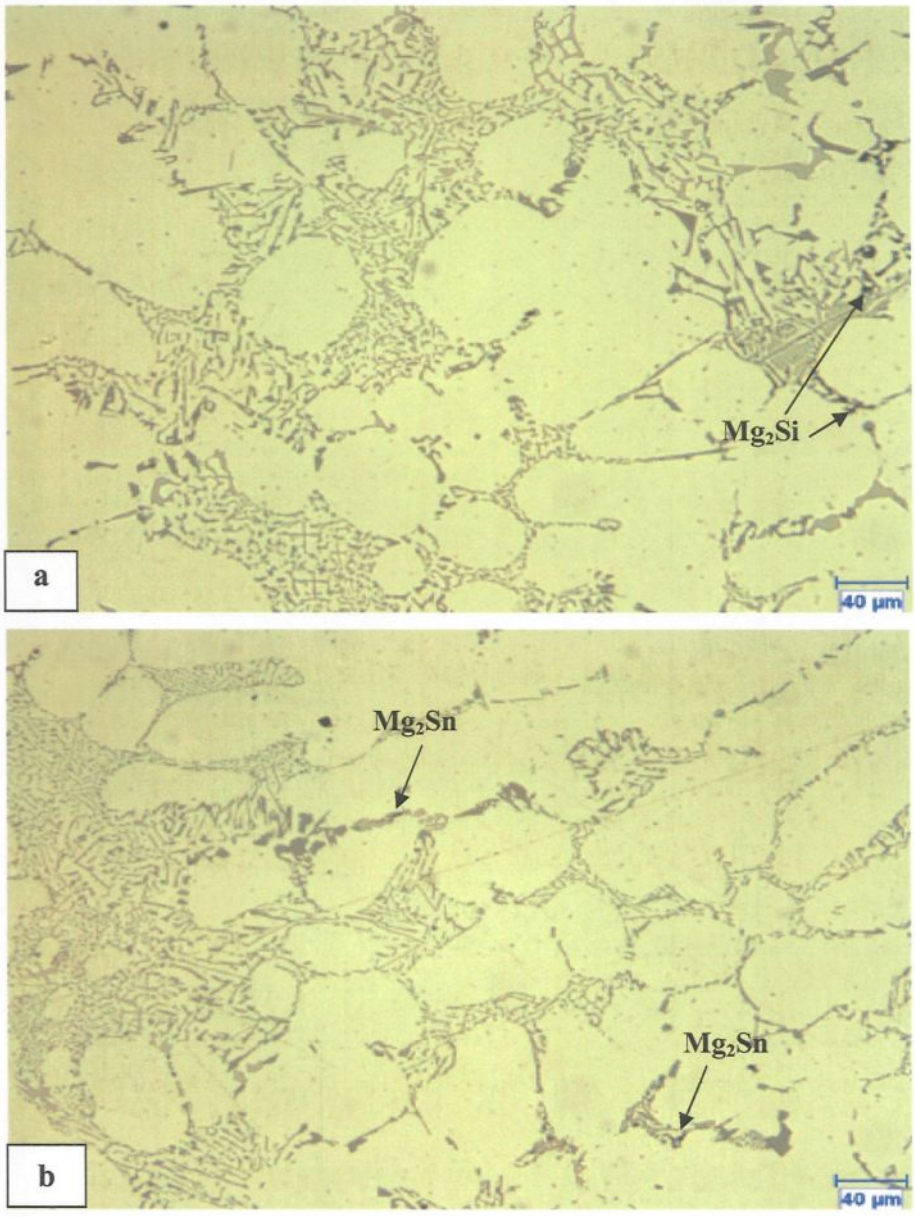

Figure 6.35 Optical micrographs of: (a) K, and (b) KSS alloys in the as-cast condition.

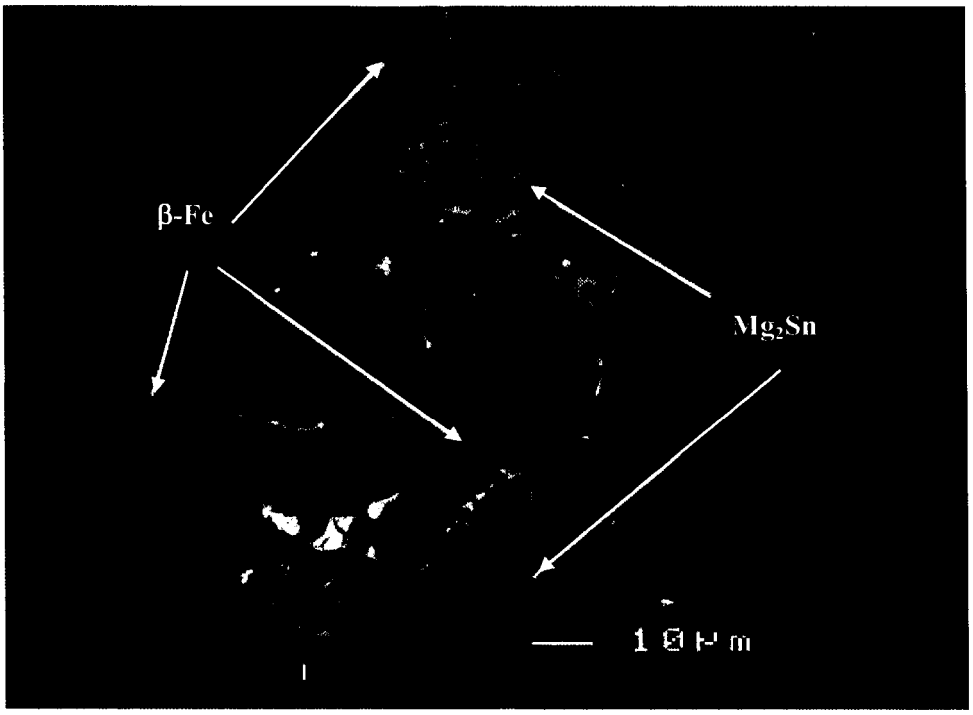

Figure 6.36 Backscattered image of KSS alloy showing the precipitation of Mg_2Sn phase.

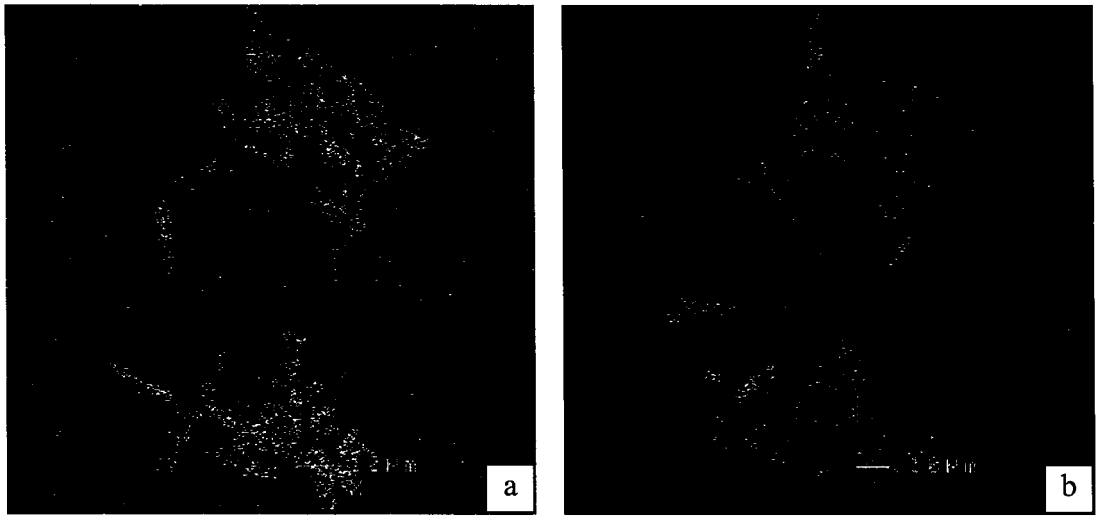

Figure 6.37 X-ray images corresponding to Figure 6.36 showing (a) Mg, and (b) Sn distribution.

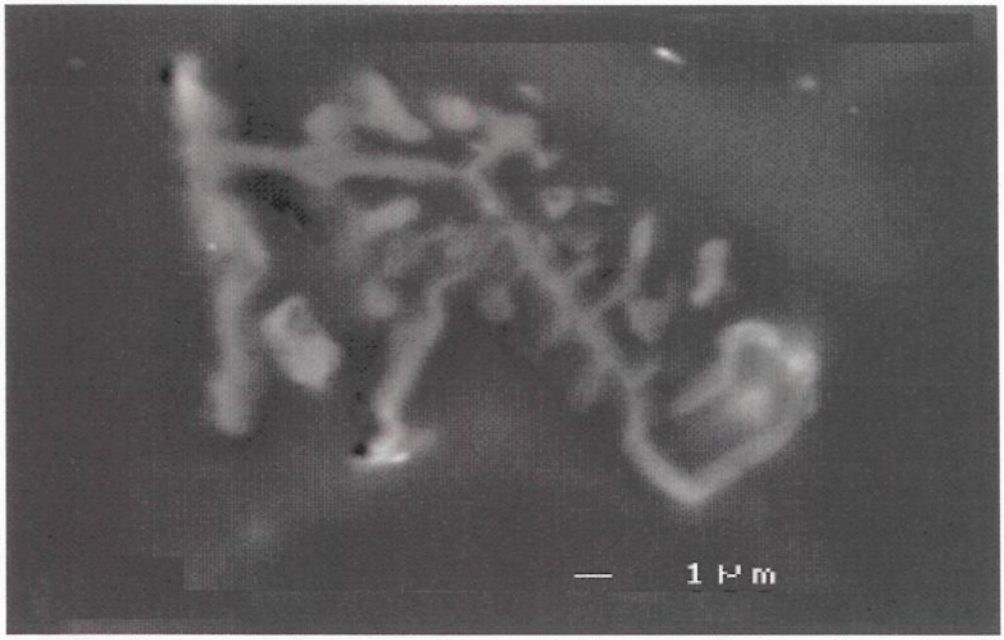

Figure 6.38 Backscattered image taken at high magnification from the KSS alloy showing the precipitation of Mg_2Sn in Chinese script form.

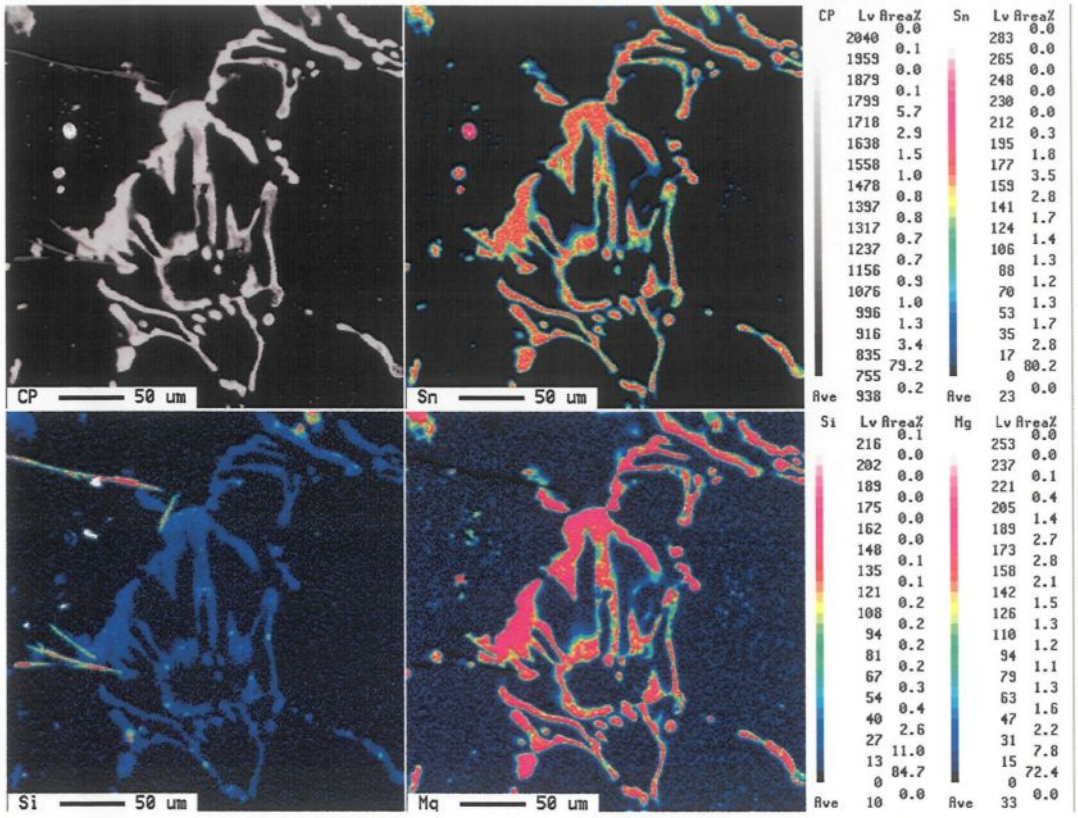

Figure 6.39 Backscattered image of the KSS alloy showing the precipitation of Mg_2Sn and the corresponding X-ray images of Sn, Mg and Si.

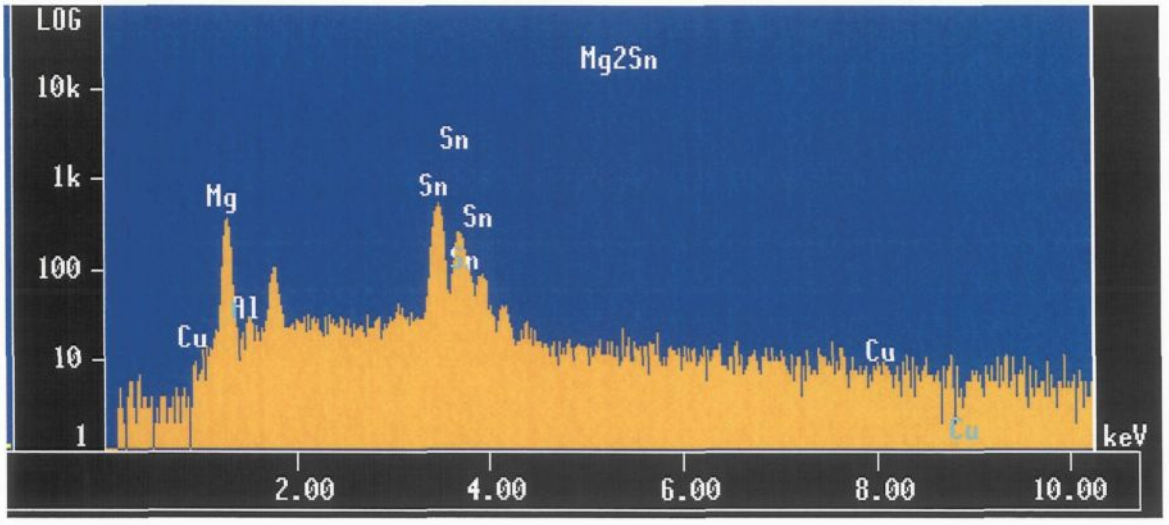

Figure 6.40 EDX spectrum corresponding to an Mg_2Sn particle observed in KSS alloy containing 0.15% Sn.

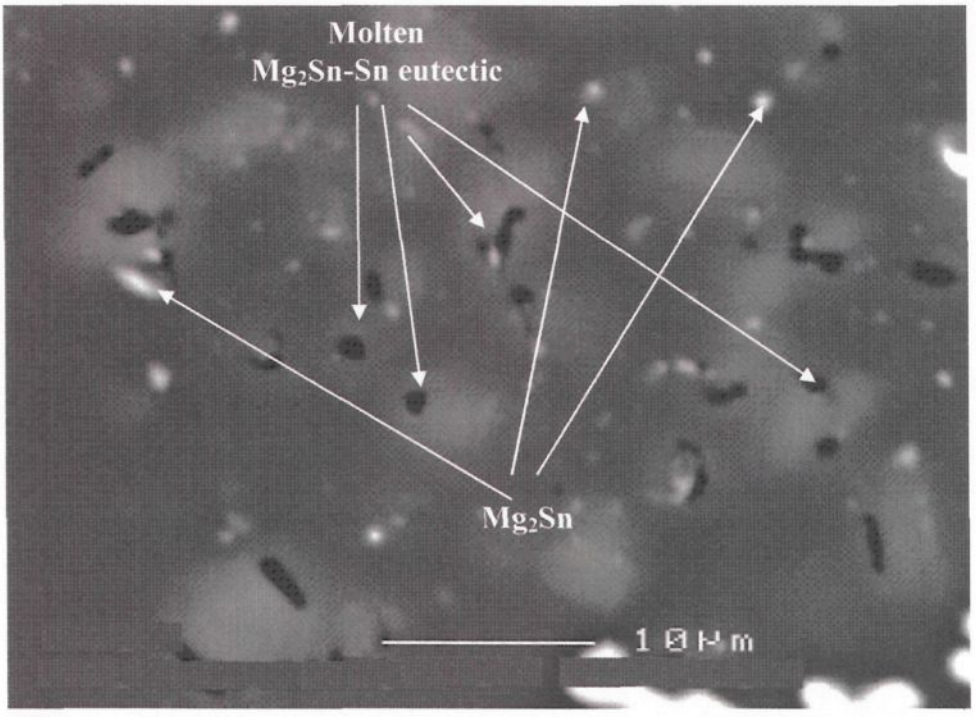

Figure 6.41 Backscattered image taken from KSS alloy in the T6-condition showing the melting of the Mg_2Sn-Sn eutectic phase.

6.3.3 Porosity

Figure 6.42 shows the surface percentage porosity values obtained from image analysis measurements of samples of as-cast and heat-treated B319.2 and A356.2 alloys containing different Sn levels.

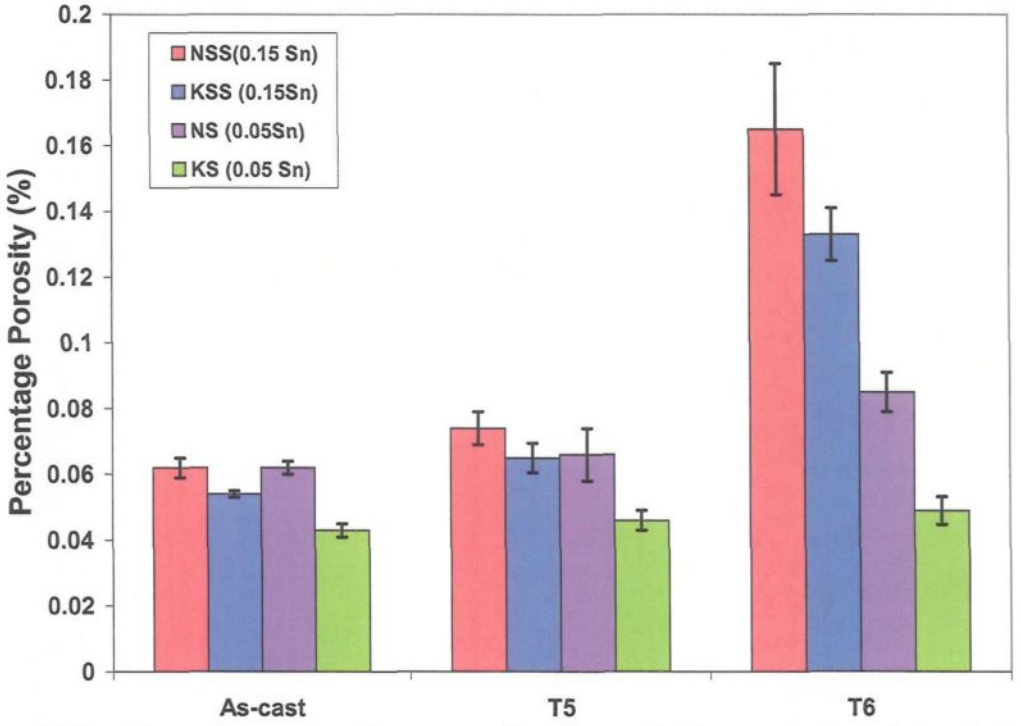

Figure 6.42 Percentage porosity as a function of Sn content and heat treatment conditions for B319.2 and A356.2 alloys.

It can be seen that, in the T6 condition, the surface percentage porosity increases when the Sn level increases beyond 0.05% for both B319.2 and A356.2 alloys. This indicates that Sn additions exceeding ~0.05% Sn are enough to trigger the development of a large amount of voids. The development of porosity in B319.2 and A356.2 alloys seems to be connected to the melting of the β-Sn and Mg_2Sn-Sn eutectic phases, respectively, during solution heat treatment. These observations are consistent with the idea that the formation

of transitional liquid phases at temperatures below the Al-Si eutectic is responsible for the increased levels of porosity observed in the Sn-containing alloys. Such porosity levels would explain the low values of tensile properties in the T6 condition. It may thus be concluded that β-Sn and the Mg_2Sn-Sn eutectic phases are undesirable in such heat-treatable alloys, in view of the fact that solution treatment would melt the Sn phases and lead to voids in the structure.

6.3.4 Mechanical Properties

All mechanical property measurements were made at ambient temperature. Macro-hardness (Brinell) was measured using a 500-kg load and a 10-mm diameter steel ball. Tensile properties (UTS, YS, %El) were determined on specimens with dimensions of 12.7 mm diameter and 50.8 mm gauge length. Tests were conducted according to ASTM Standards.[57] Charpy impact tests were conducted using ASTM Standard procedures on unnotched bar specimens measuring 10 mm x 10 mm x 55 mm according to ASTM standard specifications.[58]

6.3.4.1 Hardness

Alloy B319.2

Variations of macrohardness with Sn content for the as-cast and heat-treated conditions are shown in Figure 6.43. The trend of variation in hardness with Sn content was found to be the same for all conditions. Typical average hardness values of the N alloy in as-cast, and T5 and T6-heat-treated conditions were 84, 94, and 128 BHN, respectively. At

0.05% Sn content (NS alloy), the hardness values registered a slight decrease for all conditions, compared with the corresponding hardness values of the N alloy. The hardness values decreased further when the Sn content was increased to 0.15% (NSS alloy). The lower hardness of NS and NSS alloys can be ascribed to the formation of the soft β-Sn phase. Table 6.10 lists the average hardness and tensile property values with their standard deviations.

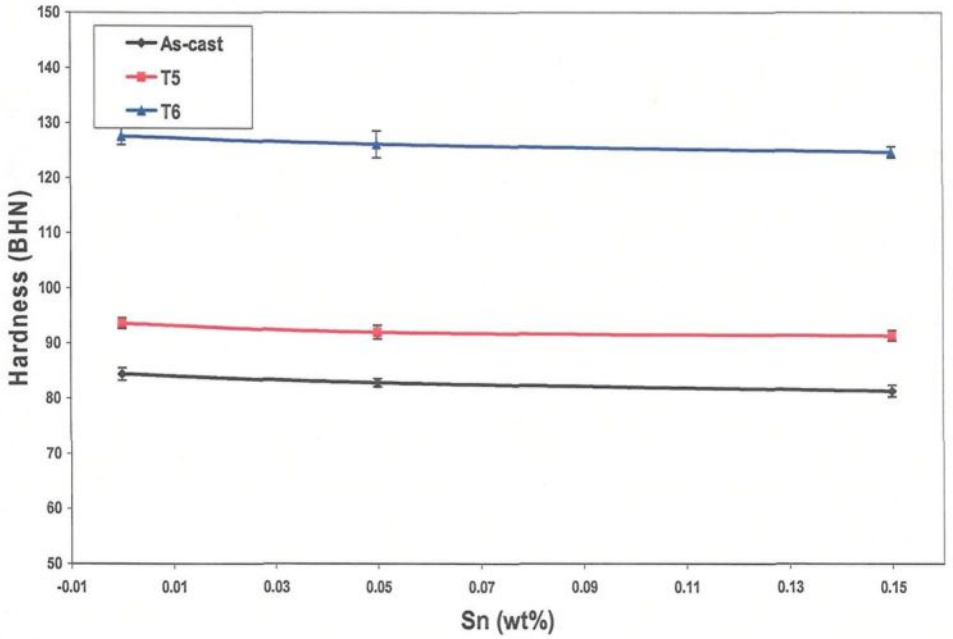

Figure 6.43 Hardness as a function of Sn content and heat treatment conditions for B319.2 alloy.

Alloy A356.2

In the as-cast condition, the hardness of the K alloy was 63 BHN; the addition of 0.15% Sn (KSS alloy) reduced the hardness to 61 BHN. In the T5 and T6 heat-treated conditions, the hardness values of KSS alloy reduced by 2 and 7 BHN, respectively, compared with the K alloy under the same conditions, see Table 6.11. The results shown in

Figure 6.44 show that the level of hardness in T5 and T6 heat treated conditions is generally lower for A356.2 alloy in comparison to B319.2 alloy, especially at high Sn levels. This observation may be attributed to the formation of the Mg_2Sn phase. The presence of this phase is undesirable because the magnesium, which is bound to the tin, is not available for age-hardening, thereby reducing the effect of precipitation hardening. Table 6.11 lists the average hardness and tensile property values obtained and their standard deviations.

Table 6.10 Effects of Sn addition and heat treatment conditions on the hardness and tensile properties of B319.2 alloy

Alloy Code	Condition	YS (MPa)	UTS (MPa)	Elongation (%)	Hardness (BHN)
N (0% Sn)	As-cast	223.03 ± 7.1	307.46 ± 13.9	1.40 ± 0.14	84.39 ± 1.1
	T5	257.51 ± 14.3	312.0 ± 10.2	1.17 ± 0.16	93.61 ± 0.9
	T6	396.20 ± 1.2	426.57 ± 6	1.10 ± 0.11	127.55 ± 1.5
NS (0.05% Sn)	As-cast	219.42 ± 1.2	282.20 ± 3.7	1.48 ± 0.12	82.82 ± 0.7
	T5	246.57 ± 2.3	287.60 ± 4.3	0.85 ± 0.04	92.34 ± 1.2
	T6	395.02 ± 8.6	400.42 ± 7.7	0.80 ± 0.01	126.1 ± 2.4
NSS (0.15% Sn)	As-cast	218.21 ± 5.5	280.63 ± 5.5	1.50 ± 0.05	81.3 ± 1.1
	T5	245.16 ± 2.0	284.49 ± 14.2	0.80 ± 0.06	91.34 ± 0.9
	T6	386.0 ± 0.02	386.0 ± 0.02	0.67 ± 0.01	124.65 ± 1.0

Table 6.11 Effect of Sn additions and heat treatment conditions on the tensile properties of A356.2 alloy

Alloy Code	Condition	YS (MPa)	UTS (MPa)	Elongation (%)	Hardness (BHN)
K (0% Sn)	As-cast	184.10 ± 2.1	288.5 ± 3.4	5.44 ± 0.67	63.45 ± 0.01
	T5	249.39 ± 7.1	300.25 ± 7.4	1.85 ± 0.43	76.62 ± 0.65
	T6	318.37 ± 6.4	357.48 ± 5.1	1.48 ± 0.32	107.41 ± 0.01
KS (0.05% Sn)	As-cast	182.1 ± 2.6	287.0 ± 3.9	5.89 ± 0.15	62.43 ± 0.01
	T5	238.51 ± 7.2	296.53 ± 9.4	2.59 ± 0.21	75.28 ± 1.43
	T6	313.5 ± 3.53	351.46 ± 3.26	2.46 ± 0.14	103.87 ± 0.99
KSS (0.15% Sn)	As-cast	181.84 ± 5.6	285.71 ± 9.25	6.37 ± 0.53	60.94 ± 0.91
	T5	235.26 ± 4.4	290.17 ± 2.46	2.49 ± 0.32	74.76 ± 0.68
	T6	302.1 ± 5.7	344.1 ± 6.9	1.78 ± 0.01	100.18 ± 0.01

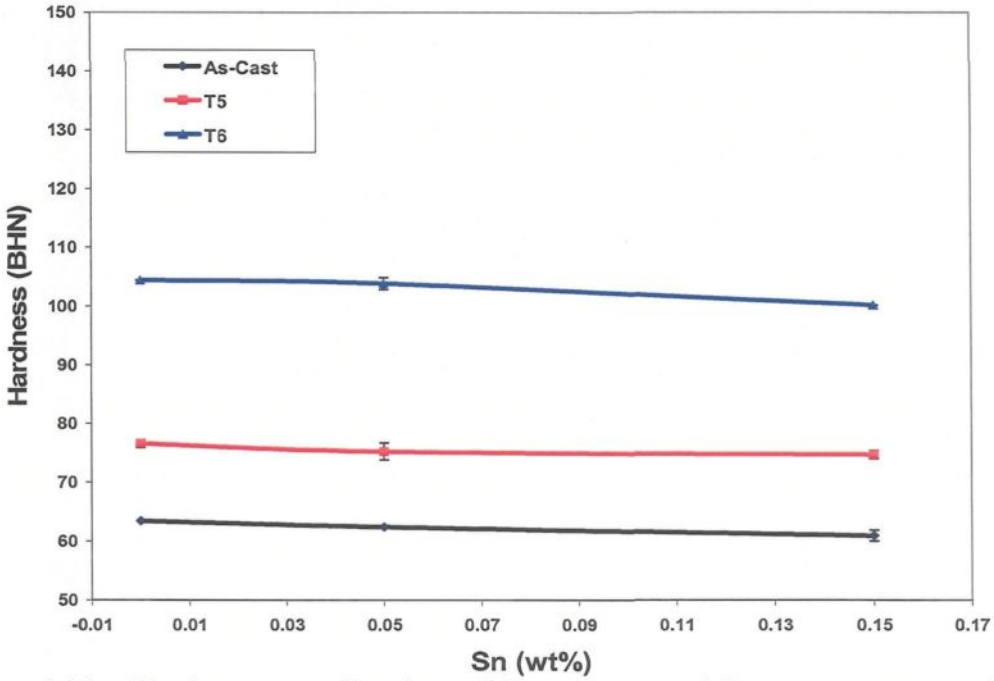

Figure 6.44 Hardness as a function of Sn content and heat treatment conditions for A356.2 alloy.

6.3.4.2 Tensile Properties

Alloy B319.2

The ultimate tensile strength (UTS), yield strength (YS, at 0.2% offset strain), and percentage elongation (%El) were determined for as-cast and T5- and T6-tempered tensile bars. The effect of Sn on the tensile properties of B319.2 alloy is shown in Figure 6.45, while Table 6.10 lists the average tensile properties and standard deviations for each level of Sn addition. It is clear that the strength properties decrease with increasing Sn content and are lower in all the conditions examined compared to the Sn-free alloy. This decreasing trend was similar for each of the levels of Sn investigated. In the case of as-cast alloys, the UTS and YS were reduced by 9%, and 2%, respectively, with an increase in Sn content from 0 to 0.15 wt%. Lower strength properties of the alloys containing Sn resulted firstly

from the distribution of fine, soft β-Sn mainly at the grain boundaries, and secondly from fine particles of other intermetallic compounds such as Mg_2Sn; likewise, due to the same reason, the elongation increased by 7%. In the T5-aged condition, a small decrease in YS was observed with the addition of 0.05% Sn (NS alloy), with no further decrease at a 0.15% Sn addition. The UTS, however, decreased much more noticeably, from 312 MPa for the N alloy to 288 MPa in the NS alloy (0.05% Sn), and to 285 MPa in the NSS alloy (0.15% Sn). The results also show that elongation decreased with increasing tin content. Similar results were obtained for the T6 condition. The reduced strength and ductility of the Sn-containing alloys may be attributed to the increase in percentage porosity compared to the Sn-free alloy.

Alloy A356.2

The effects of tin content on the tensile properties of A356.2 alloy are plotted in Figure 6.46, while Table 6.11 lists the average tensile properties and standard deviations obtained at each level of Sn content. In the as-cast condition, the UTS and YS values appear to remain more or less stable with an increase in Sn content, decreasing slightly from 288 MPa and 184 MPa in the K alloy to 286 MPa and 182 MPa in the KSS alloy, respectively. This decrease may be attributed to the formation of the Mg_2Sn phase embedded with nano-sized particles of Mg_2Sn-Sn eutectic. For the same reason, the elongation increases dramatically, i.e. by 17%.

After aging, the UTS and YS decrease slightly with increasing Sn content. Table 6.11 lists the variations in these properties in the T5 and T6 conditions for the low and high

Sn-containing alloys. The results also show that the elongation to failure increased by 34% and 20% in the T5 and T6 heat-treated conditions, respectively, with an increase in Sn-content from 0% to 0.15% Sn. Elongation increases because of the precipitation of Mg_2Sn which decreases the amount of free Mg available for hardening during the aging process. Although it is expected that the elongation will increase further with a higher Sn-content, this may not necessarily be the case, since the formation of porosity would increase due to melting of the Mg_2Sn-Sn eutectic.

The presence of these pores, which act as stress concentration sites, causes a decrease in ductility of the 0.15% Sn-containing alloy, whereby the negative effect of porosity *overrides* the positive effect of the Sn-bearing precipitates.

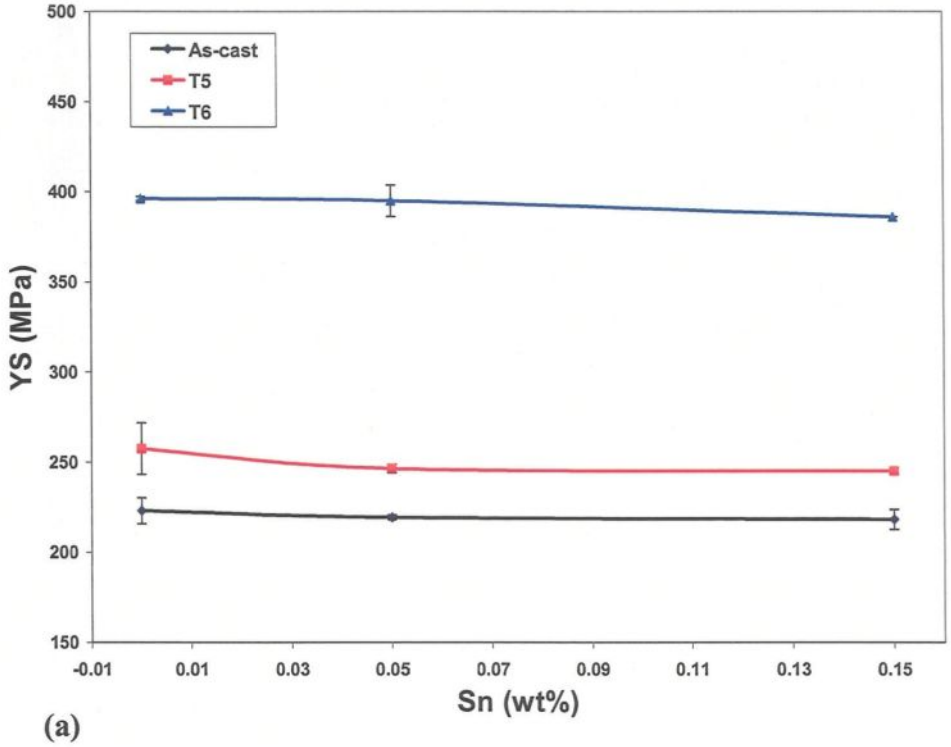

(a)

Figure 6.45 ⟶ **Continued**

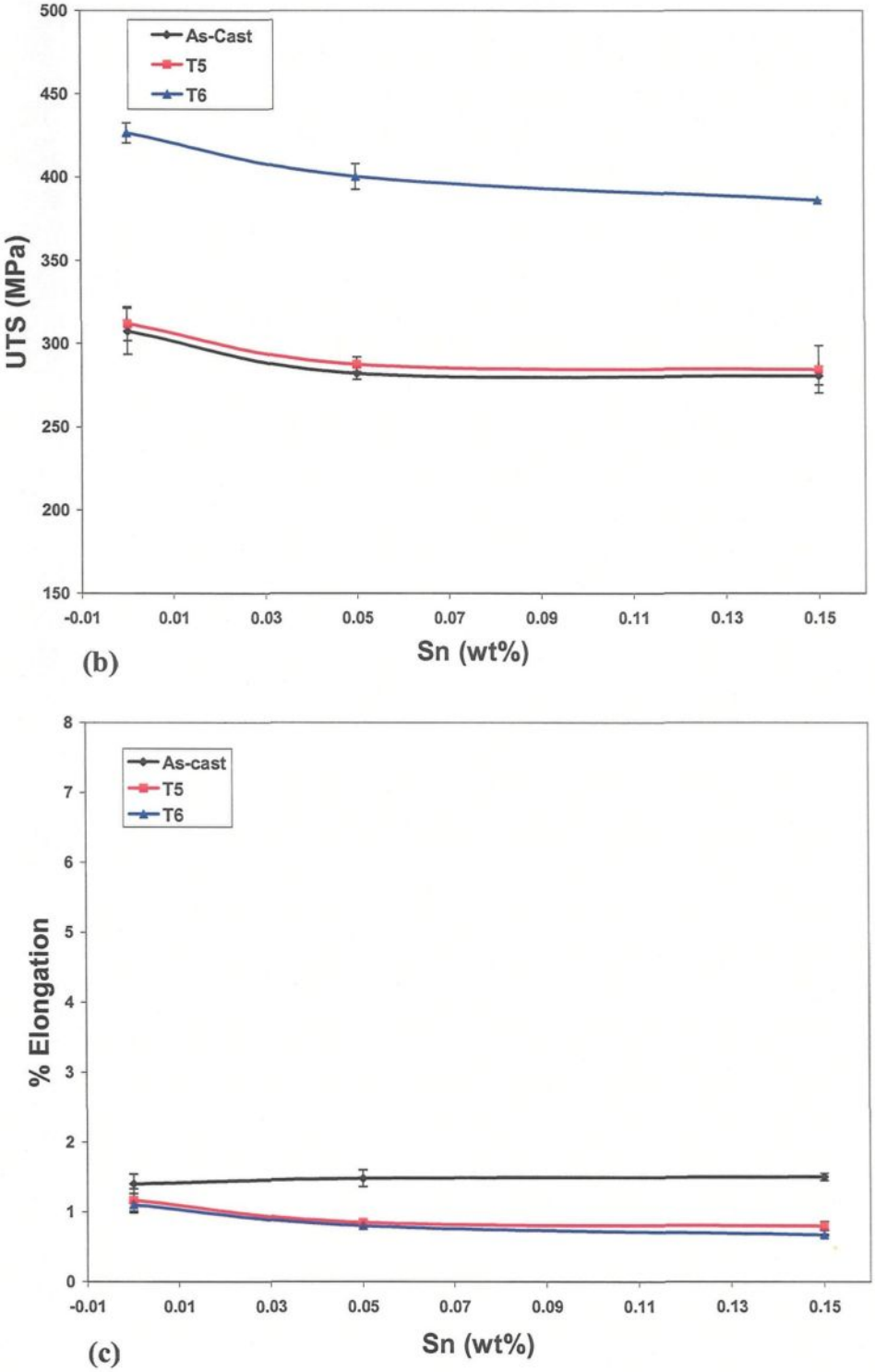

Figure 6.45 Variation in (a) YS, (b) UTS, and (c) %El as a function of Sn-content and heat treatment conditions for B319.2 alloy.

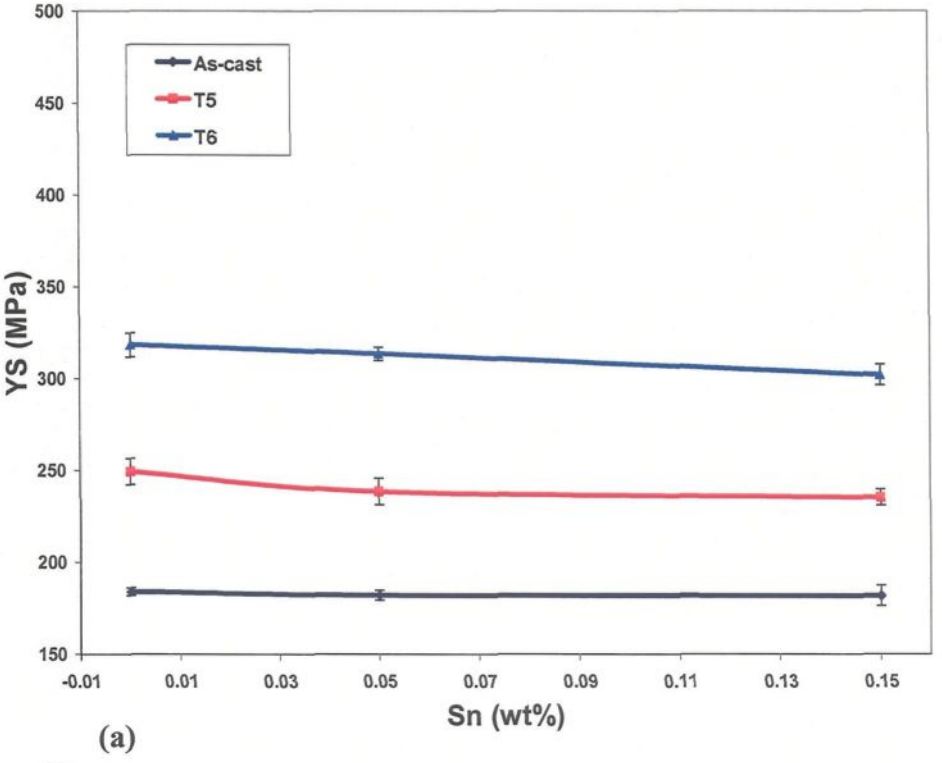

(a)

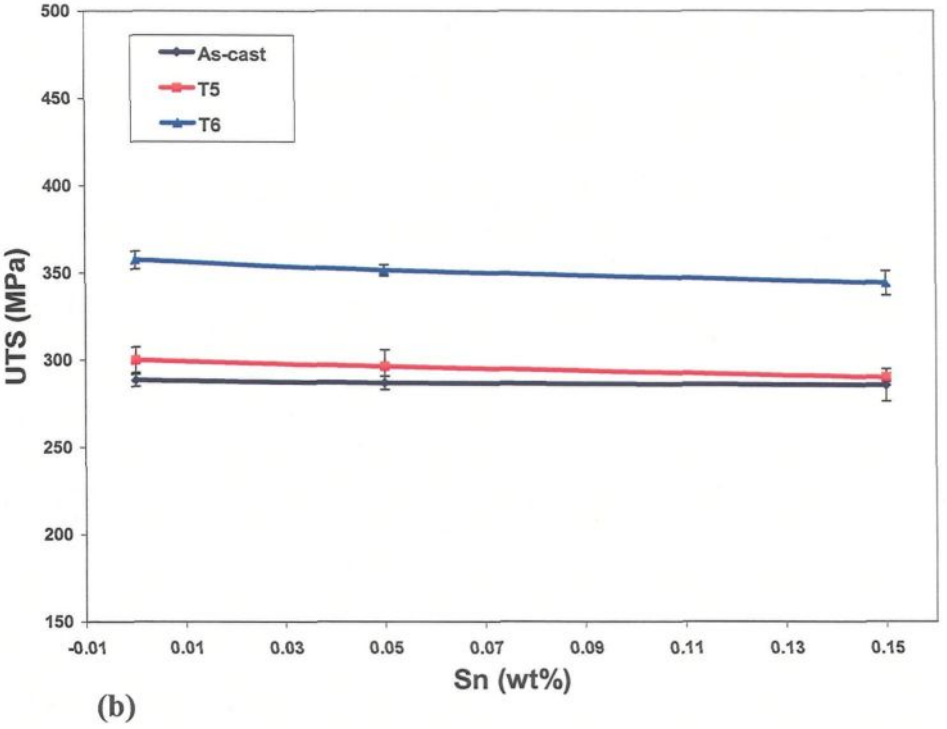

(b)

Figure 6.46 ⟶ **Continued**

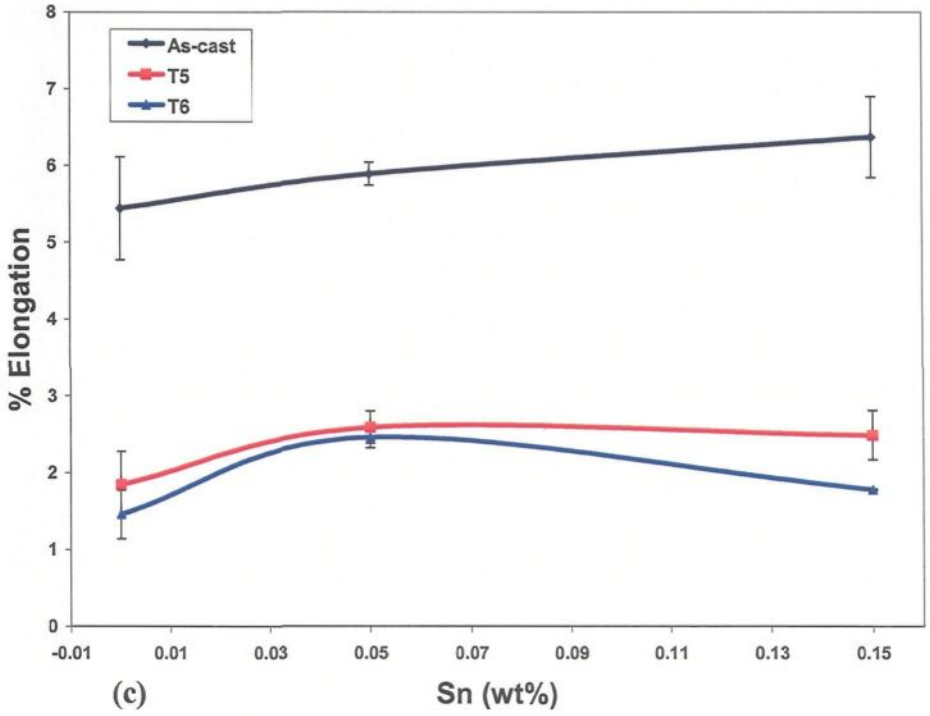

Figure 6.46 Variation in (a) YS, (b) UTS, and (c) %El as a function of Sn-content and heat treatment conditions for A356.2 alloy.

6.3.4.3 Impact Properties

Although tensile testing is the most commonly used method to quantify the mechanical properties of aluminum alloys, the impact strength is of importance when evaluating certain applications and may provide a useful estimation of the ductility of an alloy under conditions of rapid loading. A survey of the available literature clearly indicates that information available on the effect of Sn addition on the fracture toughness of Al-Si-Cu (Mg) and Al-Si-Mg alloys is not only meagre but also inconclusive. Also, the impact values depend strongly on the testing technique used, and particularly on the size and shape of the specimens.[42] A crack is generally considered to be initiated at maximum load, L_{max}, and therefore the area under the load-time curve before the maximum load will be the

energy for crack initiation, E_i, and the remaining area of the curve will be the energy for crack propagation, E_p. As the total absorbed energy, E_t, is normally taken to represent the impact energy, this parameter will be used mainly to discuss the impact properties in relation to the addition of tin, as was done for the tensile properties. Since, the impact toughness is composed of these two values (*i.e.* $E_t = E_i + E_p$), thus E_i and E_p can also be considered as toughness parameters. When the curve changes from triangular to sinusoidal form, both E_i and E_p increase. This has also been observed with alloys containing high amounts of Sn.

Alloy B319.2

Some typical load-time curves for B319.2 alloy with different levels of tin in the as-cast condition are shown in Figure 6.47. At minimal Sn levels of ~0%, the shape of the load-time curve is sinusoidal; as the Sn content increases to 0.15%, the area under the load-time curve increases while the shape of the curve remains sinusoidal. These observations indicate that the alloy exhibits ductile behavior as the Sn content increases. The area under the load-time curve represents the total energy absorbed E_t (J) during fracture or the impact toughness.

The variation of the impact toughness, E_t in the B319.2 alloy as a function of Sn content is shown in Figure 6.48, while the various average energies are tabulated in Table 6.12. In the as-cast condition, the impact toughness of the N alloy improved from 4.67 J to 5.3 J corresponding to an Sn addition of 0.15%. This represents an increase of about 13%.

It is obvious that the improvement in the toughness is a consequence of the gradual improvement in its parameters (*i.e.* E_i and E_p) with increasing amounts of Sn.

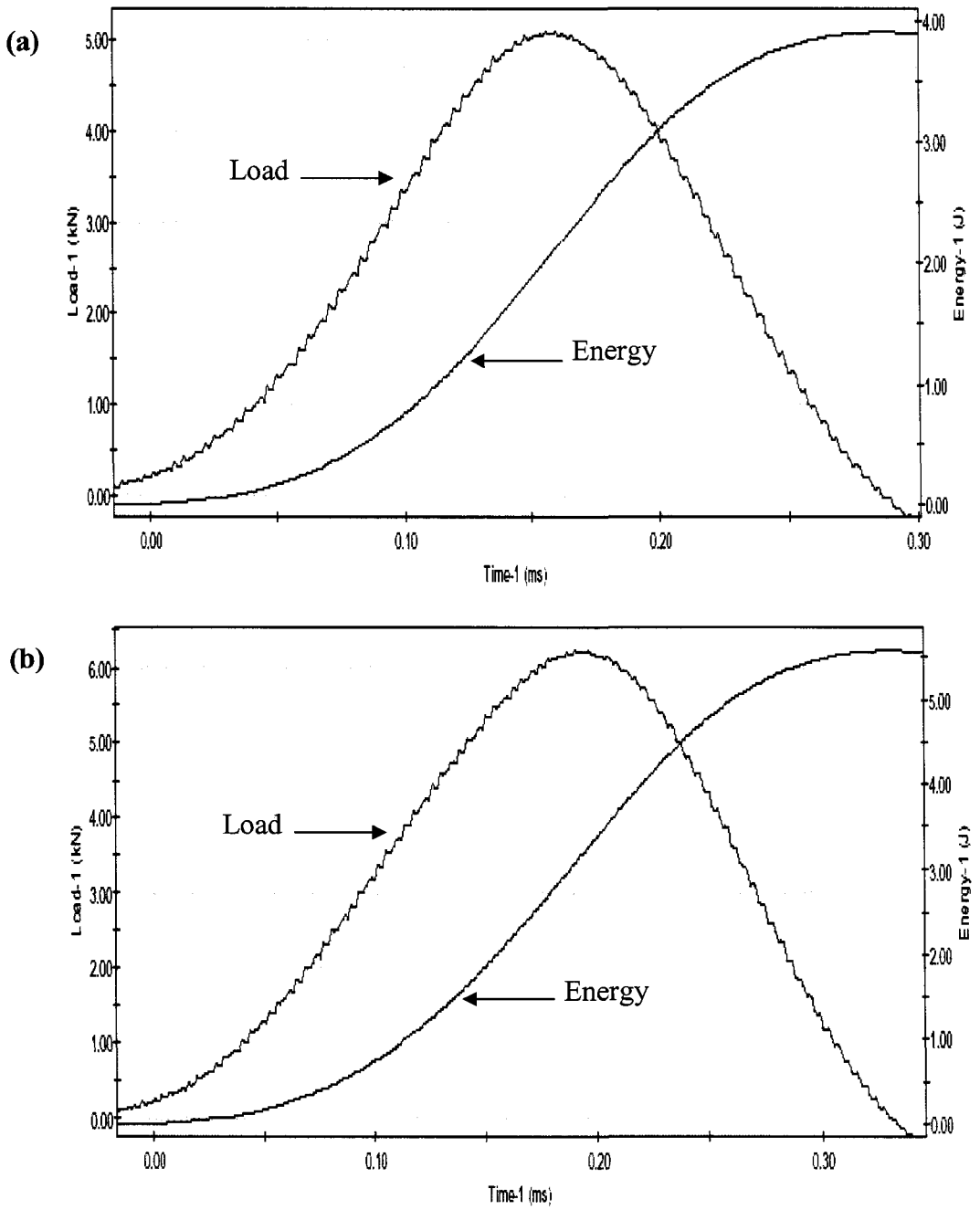

Figure 6.47 Typical results from the instrumented impact test for B319.2 alloy with (a) 0% Sn, and (b) 0.15% Sn. Note the difference in scales in the two cases.

In T5-aged conditions, a decrease in impact energy as a function of an increase in tin content was observed in alloy B319.2, as may be seen in Figure 6.48. The decrease in the total absorbed energy is more significant at the highest Sn level of ~0.15%, compared to that observed at ~0% Sn. This observation may be explained by the presence of β-Sn which reduced the cohesion of crystal grains during aging and led to the accelerated rupture of material during dynamic loading. The same result was observed in the T6 heat-treated condition as a result of the formation of voids due to the melting of β-Sn during solution heat treatment. An analysis of the plotted graphs shows that the impact energy displays a linear relationship with the Sn-content at all conditions.

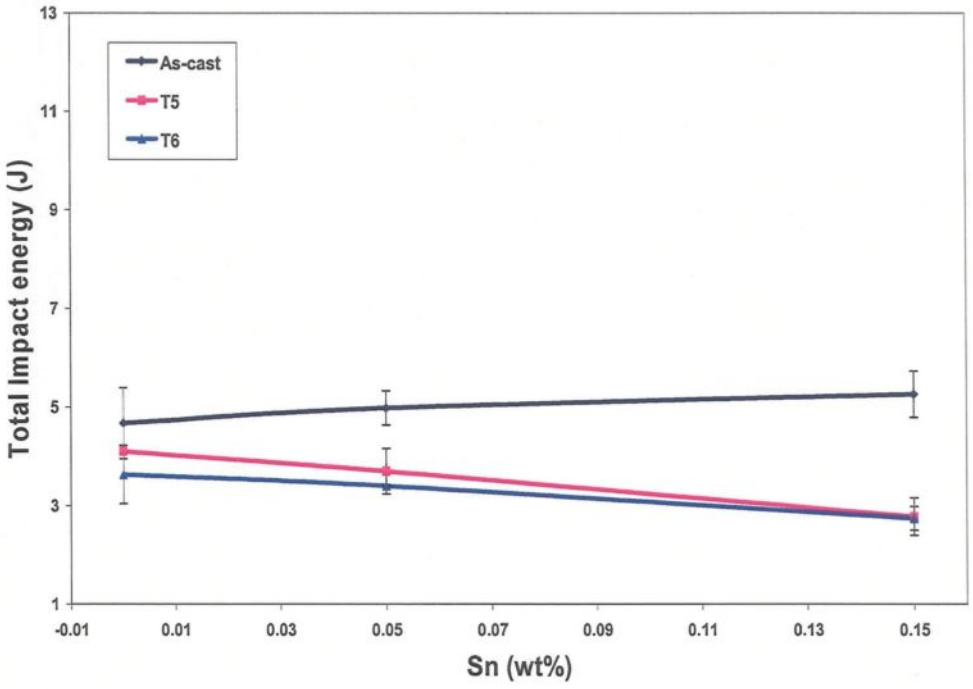

Figure 6.48 Total impact energy as a function of Sn-content and heat treatment conditions for B319.2 alloy.

Table 6.12 Average impact properties of B319.2 alloy with different Sn levels

Alloy code	Condition	E_T (J)	E_I (J)	E_P (J)	Max. Load (N)
N (0.0% Sn)	As-Cast	4.67 ± 0.72	2.50 ± 0.54	2.17 ± 0.31	5115 ± 544
	T5	4.1 ± 0.02	3.03 ± 0.23	1.07 ± 0.20	4198 ± 732
	T6	3.63 ± 0.59	2.82 ± 0.30	0.81 ± 0.29	3788 ± 612
NS (0.05% Sn)	As-Cast	4.98 ± 0.35	2.74 ± 0.20	2.24 ± 0.32	5773 ± 861
	T5	3.7 ± 0.46	2.77 ± 0.10	0.92 ± 0.39	3838 ± 747
	T6	3.4 ± 0.02	2.67 ± 0.19	0.73 ± 0.19	3595 ± 713
NSS (0.15% Sn)	As-Cast	5.26 ± 0.47	2.9 ± 0.46	2.36 ± 0.25	6432 ± 707
	T5	2.78 ± 0.38	2.1 ± 0.35	0.68 ± 0.27	3312 ± 414
	T6	2.74 ± 0.24	2.18 ± 0.11	0.56 ± 0.12	3210 ± 312

Alloy A356.2

Figure 6.49 provides examples of results recorded for impact bars of the as-cast A356.2 alloy containing different levels of Sn. The variation of the load with time and the variation of energy absorbed are represented by the upper and lower curves, respectively. The effects of Sn content can be easily observed upon comparing Figures 6.49(a) and 6.49(b). The first part of the curve, in which the load varies linearly with time, corresponds to the elastic deformation, up to the yield load, and this zone is not affected by any increase in tin content. After yielding, plastic or permanent deformation occurs; the damage is generally distributed over a relatively large volume of material so that a decrease in the load is not observed. This zone is wider for the alloy containing 0.15% Sn, implying that more time is required before a crack is initiated and begins to propagate. Finally, there is a sharp decrease in load after the maximum value has been recorded. This decrease is associated with the type of catastrophic cracking which leads to failure. As can be seen in Figure 6.49(b), there is a gradual decrease in load after the maximum load occurs in the Sn-

containing 0.15% alloy. Localized cracking propagates at a slower rate, leading to a gradual occurrence of failure.

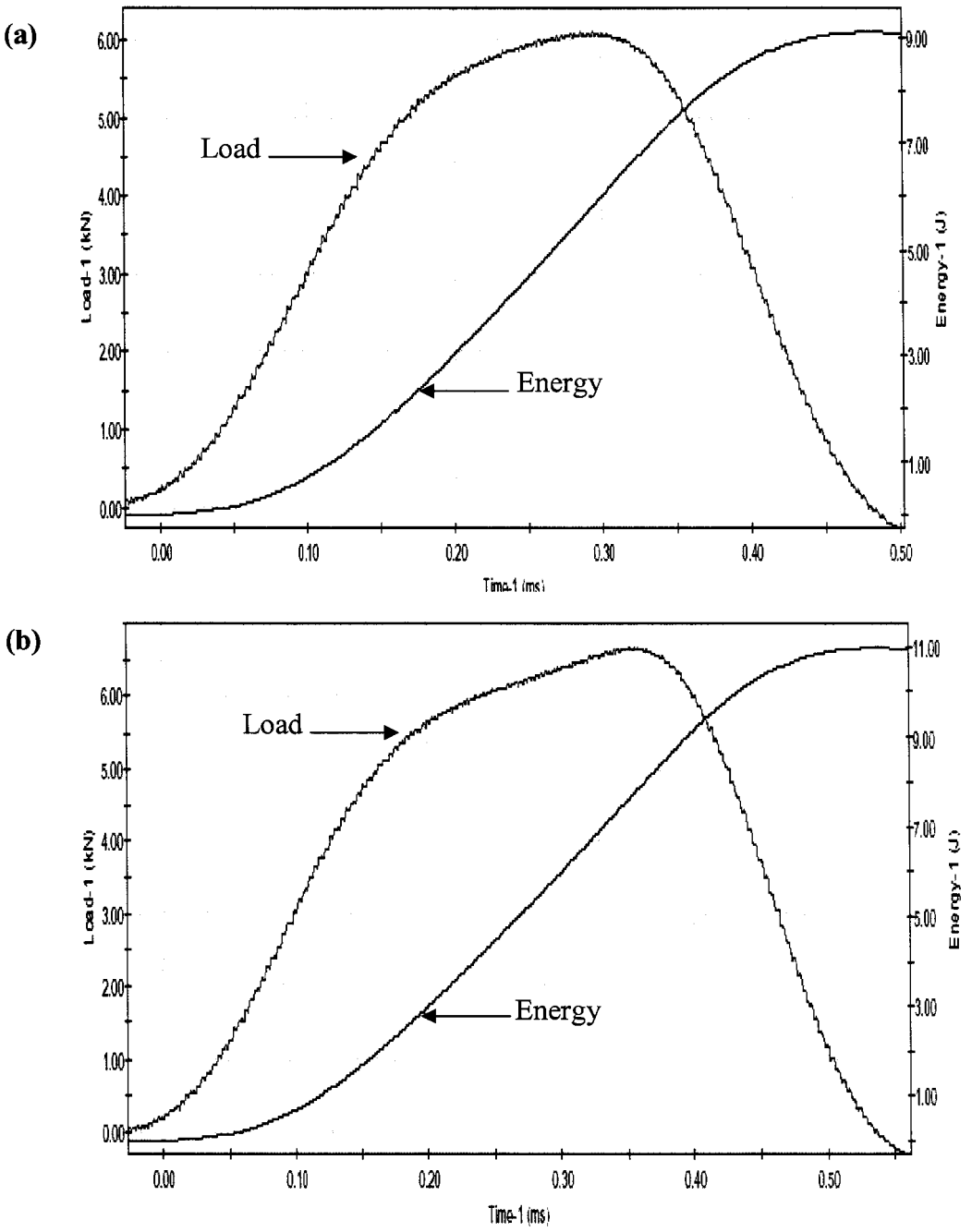

Figure 6.49 Typical results from the instrumented impact test for A356.2 alloy with (a) 0% Sn, and (b) 0.15% Sn.

Table 6.13 provides the average values and their standard deviations for the different parameters which have been determined from the instrumented impact tests for A356.2 alloys as a function of Sn-content. In the as-cast condition, the Sn addition has a greater effect on impact energy, increasing from 9.3 J for the K alloy containing 0% Sn to 10.8 J for the KSS alloy containing 0.15% Sn, as shown in Figure 6.50. This represents an increase of about 16% in the toughness of the alloy. The improvement in the toughness parameters and, consequently, in the toughness due to the addition of tin reflects the sensitivity of the behavior of the alloy to the microstructural variations on the one hand, and also emphasizes the importance of the fine and soft Sn-bearing phases in upgrading the toughness values, on the other. The reduction in toughness observed in the heat-treated alloys containing tin was the consequence of the prevailing influence of the melting of the Mg_2Sn-Sn eutectic phase on the rupture of the material over the softening effect of the Sn-bearing phases, in addition to the formation of voids as a result of said melting.

Table 6.13 Average impact properties of A356.2 alloy with different Sn levels

Alloy code	Condition	E_T (J)	E_I (J)	E_P (J)	Max. Load (N)
K (0.0% Sn)	As-Cast	9.30 ± 0.49	6.10 ± 0.13	3.00 ± 0.86	8028 ± 565
	T5	5.72 ± 0.4	4.16 ± 0.24	1.56 ± 0.16	6011 ± 541
	T6	5.1 ± 0.49	3.79 ± 0.28	1.29 ± 0.21	5843 ± 420
KS (0.05% Sn)	As-Cast	9.82 ± 0.13	6.63 ± 0.91	3.19 ± 0.48	8360 ± 927
	T5	6.49 ± 0.34	4.59 ± 0.29	1.89 ± 0.05	5959 ± 981
	T6	6.25 ± 0.11	4.48 ± 0.19	1.76 ± 0.16	5186 ± 507
KSS (0.15% Sn)	As-Cast	10.8 ± 0.22	7.37 ± 0.79	3.44 ± 0.24	8899 ± 491
	T5	6.33 ± 0.11	4.51 ± 0.1	1.82 ± 0.12	5574 ± 365
	T6	5.62 ± 0.14	4.11 ± 0.74	1.56 ± 0.4	5252 ± 256

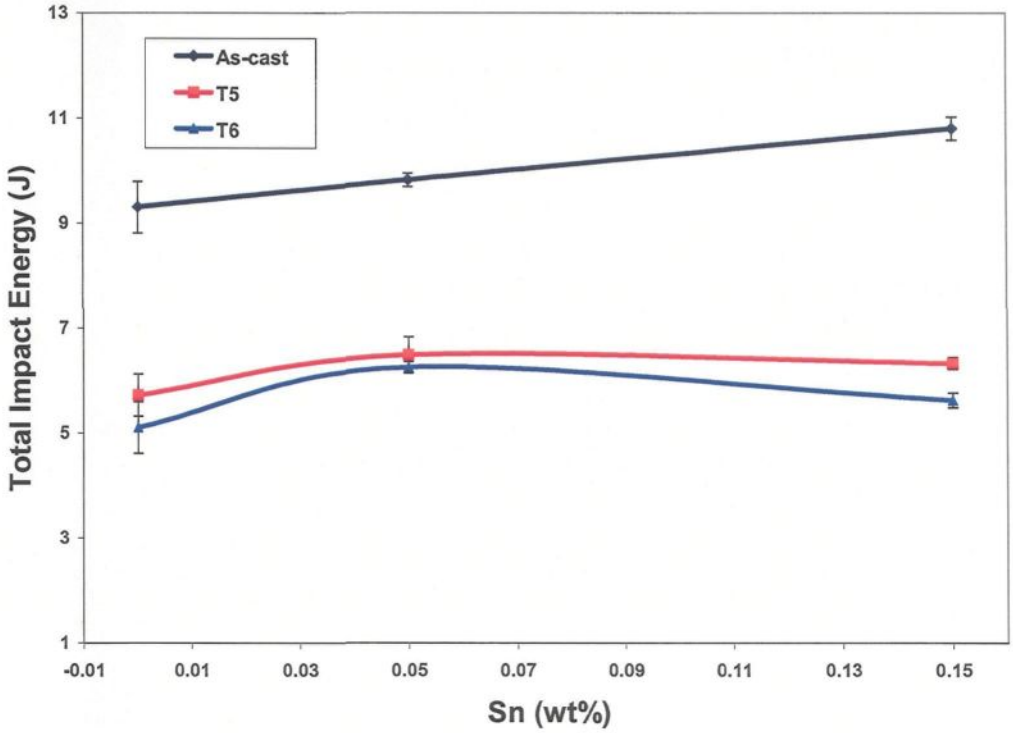

Figure 6.50 Total energy as a function of Sn-content and heat treatment conditions for A356.2 alloy.

CHAPTER 7

CONCLUSIONS AND RECOMMENDATIONS

CHAPTER 7

CONCLUSIONS AND RECOMMENDATIONS

The main objective of this thesis has been to investigate the effects of adding alloying and trace elements together with heat treatment parameters on the microstructural characteristics and mechanical properties of an experimental Al-10.8%Si near-eutectic alloy. Microstructural assessment was carried out by quantitative metallography using optical microscopy and EPMA techniques, while mechanical testing included tensile testing and hardness measurement as well as impact tests. Section 7.1 of this chapter will present a summary of the research findings obtained from this study, following which, a number of suggestions and recommendations for further research have been provided.

7.1 CONCLUSIONS

From the analysis and discussion of the results presented in Chapters 4, 5, and 6 of this thesis, the following conclusions may be drawn:

Addition of Alloying Elements

1- Image analysis, optical microscopy, and EPMA make it possible to quantify any microstructural changes occurring in the experimental Al-10.8%Si alloy. Modification increases the eutectic Si particle count per unit area in the as-cast condition, indicating a refinement of the microstructure. Both the size and the shape parameters of eutectic silicon are also affected.

2- The addition of Sr leads to the segregation of the copper phase in areas away from the modified eutectic Si; it also alters the precipitation of the α-$Al_{12}(Fe,Mn)_3Si_2$ phase from a post-dendritic reaction in the unmodified alloy to a pre-dendritic one in the modified alloy. This observation is consistent with the published data.

3- An increase in the level of Mg and Cu supplied to the Sr-containing alloys results in an increase in the Si-particle size (area, length, and aspect ratio) and reduces the roundness ratio and particle density, thereby, in effect, diminishing the modifying influence of Sr. The addition of Fe and/or Mn, however, has no significant effect on the Si-particle characteristics.

4- As the Fe content increases, more intermetallic compounds form at each level of Mn, and the volume percent of Fe-intermetallics increases. The stoichiometry of polyhedral (sludge) and Chinese-script (α-Fe) intermetallics corresponds to $Al_{12}(Fe,Mn)_3Si_2$, while needle-like or platelet compounds (β-Fe) have the stoichiometry $Al_5(Fe,Mn)Si$.

5- The percentage surface porosity increases significantly with Sr addition. This observation is consistent with the published data. The effects of Cu, Mg, and Mn are less clear. It appears that they have no measurable effect on porosity at the levels used in this study. They may, however, have an effect at higher concentrations. Amongst the properties measured, UTS seems to be the most affected by porosity, followed by yield strength and percent elongation.

6- It is expected that the presence of the hard sludge particles within the soft α-Al dendrites would lead to a uniform distribution of stresses throughout the alloy matrix, thereby improving alloy properties.

7- The Al_2Cu phase particles are more or less completely dissolved in the Al matrix after solution heat treatment in all the alloys studied.

8- The $Al_5Cu_2Mg_8Si_6$, α-Fe, and sludge intermetallics are insoluble, whereas the plate-like β-Fe phase dissolves partially during solution heat treatment at 495°C/8h.

9- The precipitation of the β-Fe phase in the RF4 alloy (~1 wt% Fe and 0.5 wt% Mn) provides nucleation sites for the precipitation of the Al_2Cu phase which, in turn, reduces the severity of its segregation. In this case, the formation of blocky Al_2Cu as small particles may be a contributing factor to the dissolution of Al_2Cu during the solution heat treatment.

10- The combined Sr-and-Ti melt treatment improves the mechanical properties of alloys considerably, whether in the as-cast condition or after T6 heat treatment. A combined melt treatment is thus a necessary requirement for the Al-10.8%Si near-eutectic alloy.

11- The refinement of eutectic silicon is mainly responsible for an improvement in hardness, although refinement of the α-Al dendrites also has the effect of improving hardness.

12- The higher toughness and ductility of modified alloys may be attributed to the fine fibrous morphology of the Si particles obtained through modification accompanied

by the stress-strain state in the matrix material which is associated with the refinement of eutectic Si.

13- At 0.5% Mn, the β-Fe phase forms when the Fe content is above a critical concentration (0.75%), causing a severe decline in the mechanical properties. Due to the formation of sludge, the same result is obtained when the levels of both Fe and Mn are increased beyond 0.75%.

14- For the Al-10.8%Si alloy, with the addition of different alloying elements, peak hardness is observed at 180°C/5h aging condition. The peak-aged hardness and the tensile strength increases with increasing Cu content in this alloy.

15- The impact properties of the Al-10.8%Si alloy are influenced by its microstructure which depends strongly on alloy composition. The morphology of fibrous Si in Sr-modified alloys enhances toughness because of its profound effect on crack initiation and crack propagation resistance. In alloys containing high levels of iron, such as the RF2 and RF4 alloys, the addition of iron leads to an increased precipitation of sludge or β-Fe platelets, respectively; they also act as crack initiation sites and reduce the impact properties noticeably. In alloys already containing high levels of copper, such as the RC2 and RC5 alloys, increasing the copper level lowers the impact properties significantly, in view of the fact that the fracture behaviour is now predominantly influenced by the Al_2Cu phase rather than by the Si particles.

16- The average crack speed of impact-tested samples shows a good inverse relationship with impact energy. Crack speed can thus provide a qualitative estimation of the impact energy expected for special alloy conditions.

17- Impact testing is more sensitive to variations in microstructure than tensile testing. The combined impact energy–percent elongation plots display linear relationships in all the alloys, for as-cast and heat-treated conditions, regardless of alloy composition.

Addition of Trace Elements

18- The addition of lead individually has no significant effect on the microstructure and mechanical properties of the modified grain-refined Al-10.8%Si alloy in as-cast and heat-treated conditions.

19- The addition of 0.5% bismuth to the modified grain-refined Al-10.8%Si alloy counteracts the modifying effect of Sr, leading to a noticeable coarsening of the eutectic Si particles.

20- Tin precipitates as particles of β-Sn within the Al_2Cu network when added individually to the modified grain-refined Al-10.8%Si alloy. When added in combination with indium, it precipitates mainly in the form of irregular In_3Sn phase particles. Tin, when added individually, causes a decrease in the UTS and hardness of the alloy in the as-cast and artificially-aged conditions. The addition of Sn causes an increase in elongation, however, only in the as-cast condition.

21- No marked difference in the yield strength of the as-cast samples is to be observed as a result of adding Pb, Bi, and Sn, whether individually or in combination.

22- In the case of the modified grain-refined Al-10.8%Si alloy with the addition of Pb, Bi, and Sn, whether individually or in combination, peak hardness is observed at the 180°C/5 h aging condition.

23- The combined addition of Pb and Bi to the modified grain-refined Al-10.8%Si alloy provides better mechanical properties in the as-cast and aged conditions than is provided by a combined addition of Bi and Sn.

24- The mechanical properties regarding the T6-condition display similar trends for all the alloys studied.

25- As regards the B319.2 alloy, Sn precipitates in the form of β-Sn particles within the Al_2Cu network and in the form of tiny (300-500 nm) Mg_2Sn particles on the eutectic Si particles. In the A356.2 alloy, however, Sn precipitates mainly as Mg_2Sn in the form of Chinese script-like particles.

26- In the as-cast B319.2 and A365.2 alloys, increasing the Sn content from 0 to 0.15% lowers the YS, UTS, and hardness by 3.5% and 4%, and raises the ductility by 7% and 17%, respectively.

27- With the addition of Sn to the A356.2 alloy, a large proportion of the Si in the Mg_2Si phase is replaced by Sn, which thus changes its composition to $Mg_2Si_{0.2}Sn_{0.8}$.

28- The mechanical properties of heat-treated B319.2 and A356.2 alloys decrease with increasing Sn content.

29- The Al-7% Si-0.35% Mg alloy containing 0.05 wt% Sn displays optimum mechanical properties compared to the alloys containing higher or lower levels of tin

Application of Statistical Design

Valuable information was obtained on the interrelationships of four independent variables by using an experimental design with only eight experiments and the resulting polynomial equations. These four variables involved the elemental content in Cu, Mg, Fe, and Mn of an experimental T6-treated Al-10.8%Si alloy which was examined from the point of view of its mechanical properties. From the results of this study, the following conclusions may be drawn.

30- Copper is the most effective strengthener under T6 conditions (180°C) for the Al-10.8% Si alloy studied. Magnesium and manganese also contribute to strength properties in the range studied, although the effect is relatively less intense. Iron, on the other hand, has a deleterious effect on the strength properties of the alloy.

31- Statistical analysis shows that the variation in Cu content has a more pronounced effect on the mechanical properties than does the variation in other alloying elements.

32- The different interactions provide a range of insights into the mechanism of strengthening.

33- Percent elongation and toughness of the alloys are affected by all four elements, of which Cu has the greatest effect and Mg the least.

34- Three-dimensional response surfaces were constructed using the respective regression models for different mechanical properties to help distinguish between the variations in response and the variations in alloy composition. Superimposition

of these response surfaces reveals the region of alloying element additions for obtaining an optimum combination of properties.

35- The validity of the equations was confirmed and they were found to be accurate over the range of variables considered, in other words, the predicted values of the mechanical properties compared well with the experimentally obtained values.

7.2 SUGGESTIONS FOR FUTURE WORK

The results of this investigation show how the microstructure and mechanical properties of a cast Al-10.8%Si near-eutectic alloy can be significantly affected by the addition of alloying and trace elements. Before these results can be adapted to foundry practice and commercial exploitation, however, several areas are to be recommended for further research, as follows.

1- Mechanical properties could be extended to include a study of the fatigue properties of these alloys, thus providing useful information in regard to the use of this alloy for critical applications. Such studies could also be further extended to include machinability characteristics.

2- The impact properties could be extended to include a study of the fracture surfaces in order to examine the fracture features and to relate them to the causes and basic mechanisms of fracture.

3- The impact strength study should be extended to include an experimental Al-10.8%Si alloy for investigation with regard to trace elements. It is believed that the

larger microstructural changes occurring with such structures would be reflected conspicuously in the total impact energy, crack initiation, and ductility index.

REFERENCES

REFERENCES

[1] C.M. Sonsino, J. Ziese, "Fatigue Strength and Application of Cast Aluminum Alloys with Different Degrees of Porosity", *International Journal of Fatigue*, 1993, vol. 15(2), pp. 75-84.

[2] H. Liao, G. Sun, "Mutual Poisoning Effect between Sr and B in Al-Si Casting Alloys", *Scripta Materialia*, 2003, vol. 48, pp. 1035-1039.

[3] G.K. Sigworth, "Theoretical and Practical Aspects of the Modification of Al-Si Alloys", *AFS Transactions*, 1983, vol. 91, pp. 7-16.

[4] H. Liao, Y. Sun, G. Sun, "Effect of Al-5Ti-1B on the Microstructure of Near-Eutectic Al-13.0% Si Alloys Casting Alloys", *Journal of Materials Science*, 2002, vol. 37, pp. 3489-3495.

[5] M.M. Haque, "Effect of Strontium on the Structure and Properties of Al-Si Alloys", *Journal of Materials Processing Technology*, 1995, vol. 55, pp. 193-198.

[6] H. Liao, Y. Sun, G. Sun, "Restraining Effect of Strontium on the Crystallization of Mg_2Si Phase during Solidification in Al-Si-Mg Casting Alloys and Mechanisms", *Materials Science and Engineering*, 2003, vol. A358, pp. 164-170.

[7] H. Liao, G. Sun, "Influence of Boron on the Microstructure and Mechanical Properties of Al-11.6%Si-0.4%Mg Casting Alloy Modified with Sr", *Materials Science and Technology*, 2004, vol. 20, pp. 521-527.

[8] K. Venkateswarlu, M. Chakraborty, B. Murty, "Influence of Thermo-Mechanical Processing of Al-5Ti-1B Master Alloy on Its Grain Refining Efficiency", *Materials Science and Engineering A*, 2004, vol. 364, pp. 75-83.

[9] L. Pio, S. Sulaiman, A. Hamouda, M. Ahmad, "Grain Refinement of LM6 Al-Si Alloy Sand Castings to Enhance Mechanical Properties", *Journal of Materials Processing Technology*, 2005, vols 162-163, pp. 435-441.

[10] J. Grobner, D. Mirkovi, R. Fetzer, "Thermodynamic Aspects of Grain Refinement of Al-Si Alloys Using Ti and B", *Materials Science and Engineering A*, 2005, vol. 395, pp. 10-21.

[11] A.M. Samuel, J. Gauthier, F.H. Samuel, "Microstructural Aspects of the Dissolution and Melting of Al_2Cu Phase in Al-Si Alloys during Solution Heat Treatment", *Metallurgical and Materials Transactions A*, 1996, vol. 27A, pp. 1785-1798.

[12] M. Kral, H. McIntyre, M. Smillie, "Identification of Intermetallic Phases in a Eutectic Al-Si Casting Alloy Using Electron Backscatter Diffraction Pattern Analysis", *Scripta Materialia*, 2004, vol. 51, pp. 215-219.

[13] G. Pucella, A.M. Samuel, F.H. Samuel, H. Doty, S. Valtierra, "Sludge Formation in Sr-Modified Al-11.5 wt% Si Die-Casting Alloys", *AFS Transactions*, 1999, vol. 24, pp. 117-125.

[14] K. Radhakrishna, S. Seshan, M. Seshardi, "Effect of Porosity on Mechanical Properties of Aluminum Alloy Castings", *Transactions of the Indian Institute of Metals*, 1981, vol. 34(2), pp. 169-171.

[15] D. Montogomery, *Design and Analysis of Experiments*, 3rd ed., John Wiley & Sons, New York, 1991, pp. 270-569.

[16] Berthouex, L. Brown, *Statistics for Environmental Engineers*, 2nd ed., Lewis Publishers, New York, 2002, pp. 185-276.

[17] B. Irving, "Interest in Welded Aluminum Automobiles Gathers Momentum Worldwide", *Welding Journal*, 1998, vol. 77(6), pp. 31-35.

[18] K.H. Kirgin, "The AFS Metalcasting Forecast and Trends Report", *Modern Casting*, 1999, vol. 89 (11), pp. 34-38.

[19] J.L. Jorstad, "The Aluminum Casting Market a Technical Perspective", *Modern Casting*, 1988, pp. 39-41.

[20] J.E. Hatch, *Aluminum: Properties and Physical Metallurgy*, American Society for Metals, Metals Park, OH, 1984, pp. 50-51.

[21] I.J. Polmear, *Metallurgy of the Light Metals*, E. Arnold, New York, 1989.

[22] J.E. Gruzleski, B.M. Closset, *The Treatment of Liquid Aluminum-Silicon Alloys*, American Foundrymen's Society, Inc., Des Plaines, IL, USA, 1990. pp. 16; 25-55.

[23] L.F. Mondolfo, *Aluminum Alloys: Structure and Properties*, Butterworths, London, Boston, 1976.

[24] O. Madelaine-Dupuich, J. Stolarz, "Fatigue of Eutectic Al-Si Alloys", *Materials Science Forum*, 1996,vols 217-222, pp. 1343-1348.

[25] *Metals Handbook*, vol. 8th Edition, American Society for Metals, Materials Park, Ohio, 1973.

[26] S.C. Hansen, "Antimony Modification of Aluminum-Silicon Alloys", Ph.D Thesis, University of Wisconsin-Madison, 2000.

[27] L.F. Mondolfo, *Metallography of Aluminum Alloys*, Wiley, New York, 1943.

[28] E.L. Roy, *ASM Handbook, Castings*, 9th Edition, ASM International, Materials Park, OH, 1992, vol. 15, pp. 743-769.

[29] M. Moustafa, F.H. Samuel, H.W. Doty, S. Valtierra, "Effect of Mg and Cu Additions on the Microstructural Characteristics and Tensile Properties of Sr-modified Al-Si Eutectic Alloys", *International Journal of Cast Metals Research*, 2002, vol. 14, pp. 235-253.

[30] J. Hatch, (Ed.), *Aluminum: Properties and Physical Metallurgy*, American Society for Metals, Metals Park, OH, 1993, pp. 232-233.

[31] Z. Li, A.M. Samuel, F.H. Samuel, C. Ravindran, S. Valtierra "Effect of Alloying Elements on the Segregation and Dissolution of $CuAl_2$ Phase in Al-Si-Cu 319 Alloys", *Journal of Materials Science*, 2003, vol. 38, pp. 1203-1218.

[32] F.H. Samuel, A.M. Samuel, "Effect of Heat Treatment on the Microstructure, Tensile Properties, and Fracture Behavior of Permanent Mold Al-10wt% Si-0.6wt%Mg/SiC/10_p Composite Castings", *Metallurgical and Materials Transactions A*, 1994, vol. 25A, pp. 2247-63.

[33] ASM, *Properties and Selection: Nonferrous Alloys and Special-Purpose Materials*, Metals Handbooks, 10th Edition, 1990, vol. 2, pp. 52-53.

[34] A. Joenoes, J. Gruzleski, "Magnesium Effects on the Microstructure of Unmodified and Modified Al-Si Alloys", *Cast Metals*, 1991, vol. 4(2), pp. 62-71.

[35] R. Dunn, W. Dickert, "Magnesium Effect on the Strength of A380.0 and 383.0 Aluminum Die Casting Alloys", *Die Casting Engineer*, 1975, vol. 19, pp. 12-20.

[36] I.J Polmear, *Light Alloys Metallurgy of Light Metals*, Edward Arnold Ltd and American Society for Metals, 1981, vol. 58-63, pp. 82-83.

[37] F. King, *Aluminum and its Alloys*, Ellis Howood Limited, 1987, pp. 112-117.

[38] M.M. Makhlouf, H.V. Guthy, "The Aluminum-Silicon Eutectic Reaction: Mechanisms and Crystallography", *Journal of Light Metals*, 2001, vol. 1, pp. 199-218.

[39] A.D. Tronche, J.E Gruzleski, "A General Grain Size determination Technique for Al-Si Casting Alloys", *Int. J. Cast Metals Res.*, 1999, vol. 11, pp. 211-218.

---

[40] J.M. Boileau, "The Effect of Solidification Time on the Mechanical Properties of a Cast 319 Aluminum Alloy", *Ph.D Dissertation*, Wayne State University, 2000.

[41] M.C. Flemings, T.Z. Kattamis, B.P. Bardes, "Dendrite Arm Spacing in Aluminum Alloys", *AFS Transactions*, 1996, vol. 91, pp. 501-506.

[42] M. Tsukuda, S. Koike, "The Heat Treatment of Al-7%Si-0.3%Mg Alloy", *J Jpn. Inst. Light Met.*, 1978, vol. 28(3), pp.109-115.

[43] O. Vorren, J.E. Evensen, T.B. Pederson, "Microstructure and Mechanical Properties of AlSi(Mg) Casting Alloys", *AFS Transactions*, 1984, vol. 93, pp. 459-466.

[44] J. Espinoza-Cuadra, G. Garcia-Garcia, H. Mancha-Molinar, "Influence of Defects on Strength of Industrial Aluminum Alloy Al-Si-Cu 319", *Materials and Design*, 2007, vol. 28, pp. 1038-1044.

[45] B. Closset, J.E. Gruzleski, "Structure and Properties of Hypoeutectic Al-Si-Mg Alloys Modified with Pure Strontium", *Metallurgical Transactions A.*, 1982, vol. 13, pp. 945-951.

[46] B. Closset, J.E. Gruzleski, "A Study on the Use of Pure Metallic Strontium in the Modification of Al-Si Alloys", *AFS Transactions*, 1981, vol. 89, pp. 801-808.

[47] N. Roy, A.M. Samuel, F.H. Samuel, "Porosity Formation in Al-9%Si-3%Cu Alloy Systems: Metallographic Observations", *Metallurgical and Material Transactions A*, 1996, vol. 27, pp. 415-429.

[48] N. Roy, L. Zhang, P.R. Louchez, F.H. Samuel, "Porosity Formation in Al-9%Si-3%Cu-X Alloy systems: Measurements of Porosity", *J. Materials Science*, 1996, vol. 31, pp. 1243-1254.

[49] Y. Awano, Y. Shimizu, "Non-equilibrium Crystallization of AlFeSi Compound in Melt-Superheated Al-Si Alloy Castings", *AFS Transactions*, 1990, vol. 98, pp. 889-895.

[50] M.M. Haque, "Strontium Modification of Aluminum-Silicon Eutectic Alloy and the Factors Affecting It", *Metal Forum*, 1983, vol. 6(1), pp. 54-56.

[51] M. Garat, R. Scalliet, "A Review of Recent French Casting Alloy Developments" *AFS Transactions*, 1978, vol. 86, pp. 549-62.

[52] G. Kumar, S. Hegde, K.N. Prabhu, "Heat Transfer and Solidification Behaviour of Modified A357 Alloy", *Journal of Materials Processing Technology*, 2007, vol. 182, pp. 152-56

[53] S. Shivkumar, S. Ricci, D. Apelian, "Influence of Solution Parameters and Simplified Supersaturation Treatments on Tensile Properties of A356 Alloy", *AFS Transactions*, 1990, vol. 98, pp. 913-922.

[54] R.X. Li, R.D. Li, Y.H. Zhao, L.Z. He, Li, H. Guan, Z. Hu, "Age-Hardening Behavior of Cast Al-Si Base Alloy", *Materials Letters*, 2004, vol. 58, pp. 2096-2101.

[55] http://www.wargamer.org/GvA/background/hardness1.html

[56] http://www.bikepro.com/products/metals/hardness.html

[57] American Society of Testing and Materials, Standard Methods of Tension Testing of Metallic Materials, ASTM B557-84, ASTM, Philadelphia, 1986.

[58] American Society of Testing and Materials, Standard Methods for Notched Bar Impact Testing of Metallic Materials, ASTM E23-96, ASTM, Philadelphia, 1986.

[59] M. Drouzy, "Interpretation of Tensile Test Results Using Quality Index and Probable Elastic Limit-Applications to Cast Al-Si-Mg Alloys", *Revue de Métallurgie* 1978, vol. 75(1), pp. 51-59.

[60] C.H. Cáceres, "Microstructure Design and Heat Treatment Selection for Casting Alloys Using the Quality Index", *Journal of Materials Engineering and Performance*, 2000, vol. 9(2), pp. 215-221.

[61] T. Din, "High Strength Aerospace Casting Alloys: Quality Factor Assessment", *Materials Science and Technology*, 1996, vol. 12, pp. 269-273.

[62] C.H. Cáceres, "A Phenomenological Approach to the Quality Index of Al-Si-Mg Casting Alloys", *International Journal of Cast Metals Research*, 2000, vol. 12, pp. 367-375.

[63] A.M. Samuel, F.H. Samuel, "Relevance of the Use of the Quality Index Concept in Cast SiCp-Reinforced Al-Si-Mg Composites", *Journal of Materials Science*, 1995, vol. 30, pp. 568-572

[64] C.H. Cáceres, J.A. Taylor, "Enhanced Ductility in Al-Si-Cu-Mg Casting Alloys with High Si Content", *Shape Casting: The John Campbell Symposium,* Murat Tiryakioglu

and Paul N. Crepeau (Eds), The Minerals, Metals, and Materials Society, Warrendale, PA, 2005, pp. 245-254.

[65] C.H. Cáceres, B. Johannesson, J.A. Taylor, A. Canales-Nuñez, M. Cardoso, J. Talamantes, "The Effect of Si Content on the Size and Morphology of Fe-Rich and Cu-Rich Intermetallics in Al-Si-Cu-Mg Alloys", *Shape Casting: 2nd International Symposium* Paul N. Crepeau, Murat Tiryakioglu, John Campbell (Eds) The Minerals, Metals, and Materials Society, Warrendale, PA, 2007, pp. 1-7.

[66] H. Westengen, O. Holta, "Low Pressure Permanent Mould Casting of Magnesium-Recent Developments", *International Congress and Exposition*, Detroit MI (Paper # 880509), Publisher: SAE, Warrrendale, PA, 1988.

[67] T. Din, A.K. Rashid, J. Campbell, "High Strength Aerospace Casting Alloys: Quality Factor Assessment", *Materials Science and Technology*, 1996, vol. 12(3), pp. 269-273.

[68] J. Gauthier, P.R. Louchez, F.H. Samuel, "Heat Treatment of 319.2 Aluminum Automotive Alloy: II. Aging Behavior", *Cast Metals*, 1995, vol. 8(2), pp. 107-114.

[69] C.H. Cáceres, "A Rationale for the Quality Index of Al-Si-Mg Casting Alloy", *International Journal of Cast Metals Research*, 1998, vol. 10(5), pp. 293-299.

[70] N. Komatsu, M. Nakamura, Y. Yamamoto, "Relationship between Si Crystallized form and Impact Strength of Al-Si Alloys Observations of Impact Strength of Al-Si Alloys", *Japanese Journal of Light Metals*, 1997/98, vol. 43, pp. 398-408.

[71] S. Khan, R. Elliot, "Solidification Kinetics of the Unmodified Aluminum-Silicon Flake Structure", *Acta Metallurgica et Materialia*, 1993, vol. 41(8), pp. 2433-2439.

[72] L. Lu, K. Nogito, A. Dahle, "Combining Sr and Na Additions in Hypoeutectic Al-Si Foundry Alloys", *Materials Science and Engineering A*, 2005, vol. 339, pp. 244-253.

[73] V. Davies, J. M. West, "Factors Affecting the Modification of the Aluminum-Silicon Eutectic", *Journal of the Institute of Metals*, 1992, vols 175-180, pp.1963-64.

[74] D. Emadi, "Porosity Formation in Sr-Modified Al-Si Alloys", Ph.D. Thesis, McGill University, Montreal, QC, Canada, 1995.

[75] J.E. Gruzleski, "The Art and Science of Modification 25 Years of Progress", *AFS Transactions*, 1992, vol. 100, pp. 673-683.

[76] A. Dahle, K. Nogita, S. McDonald, C. Dinnis, L. Lu, "Eutectic Modification and Microstructure Development in Al-Si Alloys", *Materials Science and Engineering A*, 2005, vol. 413-414, pp. 243-248.

[77] J. Asensio-Lozano, B. Suárez-Peña, "Effect of the Addition of Refiners and/ or Modifiers on the Microstructure of Die Cast Al-12Si Alloys", *Scripta Materialia*, 2006, vol. 54, pp. 943-947.

[78] L. Bäckerud, G. Chai, J. Tamminen, *Solidification Characteristics of Aluminum Alloys, Volume 2: Foundry Alloys*, AFS/SKANALUMINUM, Des Plains, IL, 1990.

[79] G. Nagel, R. Portalier, "Structural Modification of Aluminum-Silicon Alloys by Antimony Treatment", *International Cast Metals Journal*, 1980, vol. 5(4), pp. 2-6

[80] Shu-Zu Lu, A. Hellawell, "Modification of Al-Si Alloys: Microstructure, Thermal Analysis, and Mechanisms", *JOM*, Feb 1995, pp. 38-40.

[81] Shu-Zu Lu, A. Hellawell, "The Mechanism of Silicon Modification in Aluminum-Silicon Alloys: Impurity Induced Twinning" *Metallurgical Transactions A*, 1987, vol. 18, pp.1721-33.

[82] S.C. Flood, J.D. Hunt, "Modification of Al-Si Eutectic Alloys with Na", *Metal Science*, July 1981 vol. 15, pp. 287-294,

[83] M.D. Hanna, Shu-Zu Lu, A. Hellawell, "Modification in the Aluminum Silicon System", *Metallurgical Transactions A*, 1984, vol. 15, pp. 459-469.

[84] M.D. Hanna, Shu-Zu Lu, A. Hellawell, "Modification of Al-Si Microstructure – the Al-Si-Sr Phase Diagram from 0-20wt% Si and 0-5wt% Sr" in L. H. Bennett, T. B. Massalski, B. C. Giessen, (Eds), *Alloy Phase Diagrams*, Elsevier Science Publishing Co., Inc., 1983, pp. 411-416.

[85] S.M. Glenister, R. Elliot, "Strontium Modification of Al-12.7wt%Si Alloys", *Metal Science*, April 1981, pp. 181-84.

[86] W. Griffiths, M. Jolly, W. Kattilz, *Light Metals 1991*, The Minerals, Metals and Materials Society, Warrendale, PA, USA, 1991, pp. 1047-1055.

[87] J.W. Rutter, "Modification of Eutectic Morphology", *J. Crystal Growth*, 1977, vol. 42, pp. 515-525.

[88] H. Liao, Y. Sun, G. Sun, "Correlation Between Mechanical Properties and Amount of Dendritic α-Al Phase in As-Cast Near-Eutectic Al-11.6% Si Alloys Modified with Strontium", *Materials Science and Engineering A*, 2002, vol. 335, pp. 62-66.

[89] M. Djurdjevic, T. Stockwell, J. Sokolowski, "The Effect of Strontium on the Microstructure of the Aluminum-Silicon and Aluminum-Copper Eutectics in the 319

Aluminum Alloys", *International Journal of Cast Metals Research*, 1999, vol. 12, pp. 67-73.

[90] J. Gruzleski, F. Paray, S. Shabestari, "Applications of Strontium in Cast and Wrought Aluminum Alloys", *le Magazine de l'Aluminium*, 1996, vol. 2(1), pp. 23-33.

[91] J.L. Jorstad, W.M. Rasmussen, *Aluminum Casting Technology*, 2nd Edition, American Foundrymen's Society, Des Plaines, IL, 1993.

[92] I. Huang, "Nonferrous Cast Alloys and Their Melting", National Industry Publishers, Beijing, P.R. China, 1980, pp. 9-29.

[93] K. Alker, U. Hielscher, "Experience with Permanent Modification of Aluminum-Silicon cast Alloys", *Aluminum*, 1972, vol. 48(5), pp. 362-367.

[94] W. Meyer, "Comparison of the Effects of Strontium, Antimony or Sodium on the Aluminum-Silicon Eutectic in Dependence on the Rate of Cooling", *Aluminum,* 1974, vol. 50(11), pp. 699-703.

[95] M. Pekguleryuz, "Strontium Dissolution in Liquid Aluminum and A356 Alloy", Ph.D. Thesis, McGill University, 1987.

[96] M. Hafiz, T. Kobayashi, "Mechanical Properties of Modified and Nonmodified Eutectic Al-Si Alloys", *Journal of Japan Institute of Light Metals*, 1994, vol. 44(1), pp. 28-34.

[97] N. Fat-Halla, "Structural Modification of Al-Si Eutectic Alloy by Sr and Its Effect on Tensile and Fracture Characteristics", *Journal of Materials Science*, 1989, vol. 24, pp. 2488-2490.

[98] B. Kulunk, D. Zuliani, "Application for the Strontium Treatment of Wrought and Die-Cast Al", *JOM*, January 1996, pp. 60-63.

[99] B.M. Closset, "Modification and Quality of Low Pressure Aluminum Castings", *AFS Transactions*, 1988, vol. 96, pp. 249-260.

[100] Q.T. Fang, D.A. Granger, "Porosity Formation in Modified and Unmodified A356 Alloy Castings", *AFS Transactions*, 1989, vol. 97, pp. 989-1000.

[101] J.R. Denton, J.A. Spittle, "Solidification and Susceptibility to Hydrogen Absorption of Al-Si Alloys Containing Strontium", *Materials Science Technology*, 1985, vol. 1, pp. 305-11.

[102] H. Iwahori, K. Yonkura, Y. Yamamoto, M. Nakamura, "Occurring Behaviour of Porosity and Feeding Capabilities of Sodium and Strontium Modified Al-Si Alloys", *AFS Transactions*, 1989, vol. 97, pp. 989-1000.

---

[103] D. Argo, J.E. Gruzleski, "Porosity in Modified Aluminum Alloy Castings", *AFS Transactions*, 1988, vol. 96, pp. 65-74.

[104] G. Laslaz, P. Laty, "Gas Porosity and Metal Cleanliness in Aluminum Casting Alloys", *AFS Transactions*, 1991, vol. 99, pp. 83-90.

[105] D.R. Poirier, K. Yeum, A.L. Maples, "A Thermodynamic Prediction for Microporosity Formation in Aluminum-Rich Al-Cu Alloys", *Metallurgical and Materials Transactions A*, 1987, vol. 18, pp. 1979-87.

[106] R.J. Kissling, J.F. Wallace, "Grain Refinement of Aluminum Castings", *Foundry*, June 1963, pp. 78-82.

[107] G.K. Sigworth, M.M. Guzowski, "Grain Refining of Hypoeutectic Al-Si Alloys", *AFS Transactions*, 1985, vol. 93, pp. 907-912.

[108] G.K. Sigworth, "Fundamentals of Grain Refining in Aluminum Alloy Castings", *Proc. AFS International Conference on Molten Metals Processing*, City of Industry, CA, 1986, pp. 75-99.

[109] F.A. Crossley, L.F. Mondolfo, "Mechanism of Grain Refinement in Aluminum Alloys", Transactions AIME, *Journal of Metals*, 1951, vol. 3, pp. 1143-1148.

[110] P.S. Mohanty, R.L. Guthrie, J.E. Gruzleski, "Studies on the Fading Behavior of Al-Ti-B Master Alloys and Grain Refinement Mechanism Using LiMCA", *Light Metals*, 1995, pp. 859-868.

[111] H.T. Lu, L.C. Wang, S.K. Kung, "Grain Refining of Hypoeutectic Al-Si Alloys", *Journal of Chinese Foundryman's Association*, 1981, vol. 29, pp. 10-18.

[112] P.A. Tondel, G. Halvorsen, L. Arnberg, "Grain Refinement of Hypoeutectic Al-Si Foundry Alloys by Addition of Boron Containing Silicon Metal", in *Light Metals*, ed. S.K. Das, TMS, Denver, CO, 1993, pp. 783-790.

[113] J.E. Gruzleski, "Microstructure Development during Metalcasting", *American Foundrymen's Society Publication*, Des Plaines, IL, 2000.

[114] P.S. Mohanty, J.E. Gruzleski, "Grain Refinement Mechanisms of Hypoeutectic Al-Si Alloys" *Acta Materialia,* 1996, vol. 44, No. 9, pp. 3749-3760.

[115] L.F. Mondolfo, S. Farooq, T. Chikai, "Grain Refinement of Aluminum Alloys by Titanium and Boron", *Solidification Technology in the Foundry and Cast House*, London, the Metals Society, 1983, pp. 133-136.

[116] R. Kiusalaas, L. Bäckerud, "Influence of Production Parameters on Performance of Al-Ti-B Master Alloys", *Solidification Processing,* The Institute of Metals, London, 1987, pp. 137-140.

[117] L. Bäckerud, P. Gustafson, M. Johnsson, "Grain Refining Mechanisms in Aluminum as a Result of Additions of Titanium and Boron, Part II", *ALUMINUM 67*, 1991, pp. 910-915.

[118] M.E. Birch, P. Fisher, "Mechanism of Fade in Grain Refining of Aluminum with Titanium Boron Aluminum", *Solidification Processing*, The Institute of Metals, London, 1987, pp. 500-502.

[119] A. Cibula, "The Grain Refinement of Al Alloy Castings by Additions of Ti and B", *Journal of the Institute of Metals*, 1951-52, vol. 90, pp. 1-16.

[120] K. Barbara, "Thermal Analysis: Metallurgical Thumbprinting", *Modern Casting*, March 1985, pp. 21-25.

[121] P.S. Mohanty, J.E. Gruzleski, "Mechanism of Grain Refinement in Al", *Modern Casting*, March 1985, pp. 21-25.

[122] F. Mollard, W. Lidman, "Systematic Selection of the Optimum Grain Refiner in the Aluminum Cast Shop", *Light Metals* 1987, TMS, pp. 749-754.

[123] S. Kori, B. Murty, M. Chakraborty, "Development of an Efficient Grain Refiner for Al-7Si Alloy and Its Modification with Strontium", *Materials Science and Engineering A*, 2000, vol. A283, pp. 94-104.

[124] R. Kowatschewa, R. Dafinowa, Z. Kamenowa, "Metallographic Determination of Intermetallic Compounds in Al Alloys" *Praktische Metallographie*, 1973, vol. 10, pp. 131-143.

[125] G. Drossel, R. Mai, O. Liesenberg, "Influence of Treatment on the Density of Castings Made from Al-Si Alloy", *Giessereitechnik*, 1981, vol. 27, pp. 167-180.

[126] W. LaOrchan, J.E. Gruzleski, "Grain Refinement, Modification and Melt Hydrogen - Their Effects on Microporosity, Shrinkage and Impact Properties in A356 Alloy", *AFS Transactions*, 1992, vol. 100, pp. 415-424

[127] G.K. Sigworth, "A Scientific Basis for the Degassing of Aluminum", *AFS Transactions*, 1987, vol. 95, pp. 73-78.

[128] S. Shivkumar, L. Wang, D. Apelian, "Molten Metal Processing of Advanced Cast Aluminum Alloys", *Journal of Metals*, 1991, pp. 26-32.

[129] D. Qiu, J.A. Taylor, M.X. Zhang, P.M. Kelly, "A Mechanism for the Poisoning Effect of Silicon on the Grain Refinement of Al-Si Alloys", *Acta Materialia*, 2007, vol. 55, pp. 1447-1456.

[130] H. Liao, Y. Sun, G. Sun, C, Tang, "Effect of Al-5%Ti-1%B on the Microstructure of Al-13%Si Alloys Modified with Sr", *Foundry*, 2000, vol. 49(5), pp. 251-256.

[131] J.R. Davis, *ASM Specialty Handbook: Aluminum and Aluminum Alloys*, ASM International, Materials Park, Ohio, 1993.

[132] C.H. Cáceres, M.B. Djurdjevic. T.J. Stockwell, J.H. Sokolowski, "The Effect of Cu Content on the Level of Microstructure on Al-Si-Cu-Mg Casting Alloys", *Scripta Materialia*, 1999, vol. 40(5), pp. 631-637

[133] C.H. Cáceres, I. Svensson, J. Taylor, "Strength-Ductility Behavior of Al-Si-Cu-Mg Casting Alloys in T6 Temper", *International Journal of Cast Metals Research*, 2003, vol. 15, pp. 721-726.

[134] S.G. Shabestari, M. Mahmudi, M. Emami, J. Campbell, "Effect of Mn and Sr on Intermetallics in Fe-rich Eutectic Al-Si Alloy", *International Journal of Cast Metals Research*, 2002, vol. 15(1), pp. 17-24.

[135] H.W. Phillips, *Annotated Equilibrium Diagrams of Some Aluminum Alloy Systems*, Institute of Metals, London, 1959, pp. 8-10.

[136] F.H. Samuel, P. Ouellet, A.M. Samuel, H.W. Doty, "Effect of Mg and Sr Additions on the Formation of Intermetallics in Al-6 Wt Pct Si-3.5 Wt Pct Cu-(0.45) to (0.8) Wt Pct Fe 319-Type Alloys" *Metallurgical and Materials Transactions A*, 1998, vol. 29A, pp. 2871-2884.

[137] C.M. Dinnis, J.A. Taylor, A.K. Dahle, "As-Cast Morphology of Iron-Intermetallics in Al-Si Foundry Alloys", *Scripta Materialia*, vol. 53, 2005, pp. 955-958.

[138] M.K. Kral, "A Crystallographic Identification of Intermetallic Phases in Al-Si Alloys", *Materials Letters*, 2005, vol. 59, pp. 2271-2276.

[139] B. Xiufang, C. Guohua, M. Jiaji, "The Spheroidisation of Needle-Form Iron Compounds in an Al-Si alloy", *Cast Metals*, 1992, vol. 5(1), pp. 39-42.

[140] M.H. Mulazimoglu, A. Zaluska, J.E. Gruzleski, F. Paray, "Electron Microscope Study of Al-Fe-Si Intermetallics in 6xxx Series Aluminum Alloys", *Metallurgical and Materials Transactions A*, 1996, vol. 27A, pp. 929-936.

[141] S. Shivkumar, L. Wang, D. Apelian, "Molten Metal Processing of Advanced Cast Aluminum Alloys", *AFS Transactions*, 1989, vol. 97, pp. 285-293.

[142] A. Couture, "Iron in Aluminum Casting Alloys", *AFS International Cast Metals Journal*, 1984, vol. 6(6), pp. 9-17.

[143] G. Vorobev, R. Golshtein, I. Maurits, "Effect of Impurities on the Main Properties of Silumin", *Metallurgical Abstracts*, 1964, vol. 32, pp. 960-961.

[144] L.F. Mondolfo, *Manganese in Aluminium Alloys*, The Manganese Centre, France, 1990, pp. 1-35.

[145] S. Murali, K. Raman, K. Murthy, "The Formation of β-$FeSiAl_5$ and Be-Fe Phases in Al-7Si-0.3Mg Alloy Containing Be", *Materials Science and Engineering A*, 1995, vol. 190, pp. 165-172.

[146] W. Bonsack, "Discussion on the Effect of Minor Alloying Elements on Aluminum Casting Alloys", *ASTM Bulletin*, 1942, pp. 45-51.

[147] S. Hajas, "Effect of Iron Contamination on the Mechanical Properties of Aluminium Casting Alloys", *Chemical Abstracts*, 1970, vol. 73, No. 133571.

[148] Y. Komiyama, K. Uchida, M. Gunshi, "Effect of Fe, Mn, Zn, and Ti on Mechanical Properties and Microstructures of Al-Si-Cu-Mg Casting Alloy", *Journal of the Japan Institute of Light Metals*, 1976, Vol. 26(7), pp. 311-319.

[149] P.N. Crepeau, "Effect of Iron in Al-Si Alloys: A Critical Review", *AFS Transactions*, 1995, vol. 103, pp. 361-366.

[150] K.H. Kirgin, "1996 Slowdown Sets Stage For 1997 Resurgence", *Modern Casting*, January 1996, pp. 27-30.

[151] S.G. Shabestari, J.E. Gruzleski, "Gravity Segregation of Complex Intermetallic Compounds in Liquid Aluminum Silicon Alloys", *Metallurgical Transactions A*, 1995, vol. 26A, pp. 999-1006.

[152] S.G. Shabestari, J.E. Gruzleski, "Modification of Iron Intermetallics by Strontium in 413 Alloys", *AFS Transactions*, 1995, vol. 103, pp. 285-293.

[153] S. Yaneva, N. Stoichez, Z. Kamenova, S. Budurov, "Quaternary Iron-containing Phases in Al-Si Cast Alloys", *Zeitschrift für Metallkunde*, 1984, vol. 75, pp. 395-398.

[154] ASM Handbook, Volume 2: *Properties and Selection: Nonferrous Alloys and Special Purpose Materials*, ASM International, Materials Park, Ohio, USA, 1990.

[155] D. Colwell, R. Kissling, "Die and Permanent Mold Casting Aluminum Alloy Minor Elements", *AFS Transactions*, 1961, vol. 69, pp. 610-616.

[156] J. Gobrecht, "Ségrégation par Gravite du Fer, du Manganèse et du Chrome dans les Alliages Al-Si de Fonderie", *Fonderie*, 1977, vol. 367, pp. 171-173.

[157] A. Lakshmanan, S. Shabestari, J. Gruzleski, *Zeitschrift für Metallkunde*, 1995, vol. 86, pp. 457-464.

[158] R. Dunn, "Aluminium Melting Problems and Their Influence on Furnace Selection", *Die Casting Engineer*, September 1965, pp. 8-16.

[159] S.G. Shabestari, J.E. Gruzleski, "The Effect of Solidification Condition and Chemistry on the Formation and Morphology of Complex Intermetallic Compounds in Aluminum-Silicon Alloys", *Cast Metals*, 1994, vol. 6, pp. 217-24.

[160] S.G. Shabestari, "The Effect of Iron and Manganese on the formation of intermetallic Compounds in Aluminum-Silicon alloys", *Materials Science and Engineering A*, 2004, vol. 383, pp. 289-298.

[161] V.G. Rivlin, G.V. Raynor, "Critical Evaluation of Constitution of Aluminum-Iron-Silicon System", *International Metals Reviews*, 1981, vol. 3, pp. 133-35.

[162] J. Barresi, M.J. Kerr, H. Wang, M.J. Couper, "Effect of Magnesium, Iron, and Cooling Rate on Mechanical Properties of Al-7Si-Mg Foundry Alloys", *AFS Transactions*, 2000, pp. 563-70.

[163] J. Gauthier, P. Louchez, F.H. Samuel, "Heat Treatment of 319.2 Al Automotive Alloy: Part 1, Solution Heat Treatment", *Cast Metals*, 1995, vol. 8(1), pp. 91-106.

[164] F. Paray, J. Gruzleski, "Modification - A Parameter to Consider in the Heat Treatment of Al-Si Alloys", *Cast Metals*, 1993, vol. 5(4), pp. 187-198.

[165] M. Tiryakioglu, "The Effect of Solution Treatment and Artificial Aging on the Work Hardening Characteristics of a Cast Al-7%Si-0.6%Mg Alloy", *Materials Science and Engineering A*, 2006, vol. 427, pp. 154-159.

[166] P. Ouellet, F.H. Samuel, "Effect of Mg on the Ageing Behavior of Al-Si-Cu 319 Type Aluminum Casting Alloys " *Journal of Materials Science*, 1999, vol. 34(19), pp. 4671-4697.

[167] G. Wang, X. Bain, W. Wang, J. Zhang, "Influence of Cu and Minor Elements on Solution Treatment of Al-Si-Mg-Cu Cast Alloys", *Materials Letters*, 2003, vol. 57, pp. 4083-4087.

[168] L. Lasa, J. Ibabe, "Characterization of the Dissolution of the Al_2Cu Phase in Two Al-Si-Cu-Mg Casting Alloys Using Calorimetry", *Materials Characterization*, 2002, vol. 48, pp. 371-378.

[169] J.H. Sokolowski, X.C. Sun, G. Byczynski, D.O. Northwood, D.E. Penord, R. Thomas, A. Esseltine, "A Metallurgical Study of the Heat Treatment of Aluminum Alloy 319 (Al-6Si-3.5Cu) Castings", *Journal of Materials Processing Technology*, 1995, vol. 53(1-2), pp. 385-392.

[170] N. Crowell, S. Shivkumar, "Solution Treatment Effects in Cast Al-Si-Cu Alloys", *AFS Transactions*, 1995, vol. 103, pp. 721-726.

[171] K.A. Yoshida, R.M. Arrowood, "Microstructure and Mechanical Properties of A356 Aluminum Castings as Related to Various T6-Type Heat Treatment", in *Light Weight Alloys for Aerospace Applications* III, 1995, The Minerals, Metals, and Materials Society, Warrendale, PA, pp. 77-87.

[172] D. Apelian, S. Shivkumar, G. Sigworth, "Fundamental Aspects of Heat Treatment of Cast Al-Si-Mg Alloys", *AFS Transactions*, 1989, vol. 97, pp. 727-742.

[173] D.L. Zhang and L. Zheng, "The Quench Sensitivity of Cast Al-7 Wt Pct Si-0.4 Wt Pct Mg Alloy", *Metallurgical and Materials Transactions A*, 1996, vol. 27A, pp. 3983-3991.

[174] D. Emadi, "Optimal Heat Treatment of A356.2 Alloy", *Light Metals*, The Minerals, Metals, and Materials Society, Warrendale, PA, 2003, pp. 983-989.

[175] T. Croucher, B. Butler, "Polymer Quenching of Aluminum Castings", *26th National SAMPE Symposium*, 1981, pp. 527-535.

[176] G.E. Totten and D.S. Mackenzie, "Aluminum Quenching Technology: A Review", *Materials Science Forum*, 2000, vols 331-337, pp. 589-594.

[177] A.V. Sverdlin, G.E. Totten, G.M. Vebster, "Polyalkyleneglycol Base Quenching Media for Heat Treatment of Aluminum Alloys" *Metallovedenie Termicheskaya Obrabotka Metallov*, 1996, vol. 6, pp. 17-19.

[178] O.G. Senatorova, "Low Distortion Quenching of Aluminum Alloys in Polymer Medium", *Materials Science Forum*, 2002, vols 396-402, pp. 1659-1664.

[179] H. Beitz, "None-Combustible Water-Based Quenchants in Forging Shops for Automotive Parts- Latest Development", *The 1st International Automotive Heat Treating Conference*, Puerto Vallerta, Mexico, 1998, pp. 106-109.

[180] H.M. Kandil, "Recent Development in Age Hardening Behaviour of Aluminum Alloys- A Review Article", *In Heat Treating: Proceeding of the 21st Conference,* Indianapolis, Indiana: ASM International, 2001, pp. 343-351.

[181] *ASM Handbook*, Materials Park, OH, 1995, pp. 823-873.

[182] A.J. Ardel, "Precipitation Hardening", *Metallurgical Transactions A*, 1985, vol. 16A, pp. 2132-65.

[183] A. Zanada, G. Riontino, "A Comparative Study of the Precipitation Sequences in Two AlSi7Mg Casting Alloys and their Composites Reinforced by 20% Al_2O_3 Discontinuous Fibers", *Materials Science Forum*, 2000, vols 331-337, pp. 229-234.

[184] S. Kumai, "Hardness Characteristics in Aged Particulate", *Scripta Metallurgica et Materialia*, 1992, vol. 27, pp. 107-110.

[185] R.X. Li, "Age-Hardening Behavior of Cast Al-Si Base Alloy", *Materials Letters*, 2004, vol. 58, pp. 2096-2101.

[186] D.S. Jiang, L.H. Chen, T.S. Liu, "Effect of Aging on the Crack Propagation Behaviour of A356", *Materials Transactions*, JIM, 2000, vol. 41(4), pp. 499-506.

[187] S.W. Han, "Effects of Solidification Structure and Aging Condition on Cyclic Stress-Strain Response in Al-7%Si-0.4%Mg Cast Alloys", *Materials Science and Engineering A*, 2002, vol. 337, pp. 170-178.

[188] A.D. Porter, K.E. Easterling, *Phase Transformations in Metals and Alloys*, Van Nostrand Reinhold, Berkshire, England, 1981.

[189] J.D. Verhoeven, *Fundamentals of Physical Metallurgy*, J. Wiley and Sons, New York, N.Y., 1975.

[190] W.F. Smith, *Structure and Properties of Engineering Alloys*, McGraw-Hill, New York, N.Y., 1981.

[191] F.H. Samuel, A.M. Samuel, H. Liu, "Effect of Magnesium Content on the Aging Behaviour of Water-Chilled Al-Si-Cu-Mg-Fe-Mn (380) Alloy Castings", *Journal of Materials Science*, 1995, vol. 30, pp. 1-10.

[192] D. Gloria, F. Hernandez, S. Valtierra, "Dimensional Changes During Heat Treating of an Automotive 319 Alloy", *20th ASM Heat Treating Society Conference Proceedings*, 9-12 October 2000, St. Louis, MO, ASM International Materials Park, OH, 2000, pp. 674-679.

[193] S. Shivkumar, C. Keller, D. Apelian, "Aging Behaviour in Cast Al-Si-Mg Alloys", *AFS Transactions*, 1990, vol. 98, pp. 905-911.

[194] I.J. Polmear, "Role of Trace Elements in Aged Aluminum Alloys", *Materials Science Forum*, 1987, vols 12-14, pp. 195-214.

[195] R.F. Pierret, *Semiconductor Device Fundamentals*, Addison-Wesley Publishing Company, New York, 1996.

[196] C.T. Sims, N.S. Stoloff, W.C. Hagel, *Superalloys II*, J. Wiley and Sons, New York, 1987.

[197] J.R. Terrill, C.N Cochran, J.J. Stokes, W.E. Haupian, "Understanding the Mechanisms of Aluminum Brazing Can Improve Results in Production Operations", *Welding Journal*, 1971, vol. 50, pp. 833-838.

[198] W.L. Winterbottom, "Process Control Criteria for Brazing Aluminum under Vacuum", *Welding Journal*, 1984, vol. 63, pp. 33-39.

[199] H. Schoer, W. Schultze, W., "Development of a Process for Flux-free Brazing of Aluminum under an Inert Gas Atmosphere", *Zeitschrift für Metallkunde*, 1972, vol. 63, pp. 755-781.

[200] F. Porter, *Zinc Handbook*, Marcel Dekker, 1991.

[201] B.L. Davidson, I.J. Polmear I.R. Dover, "Effect of Lead Impurities on the Hot Tensile Properties of 3004 Aluminum Castings", *Journal of Materials Science Letters*, 1987, vol. 6, pp. 381-382.

[202] *ASM Metals Handbook, Volume 3: Alloy Phase Diagrams*, ASM International, Materials Park, OH, 1992.

[203] O. Melikhova, J. Čížek, J. Kuriplach, J. Faltus, I. Stulikova, "Positron-Lifetime Investigation of Precipitation Effects in Al-Cu Alloy", *Materials Structure*, 2001, vol. 8(2), pp. 61-67.

[204] J. Faltus, K. Plaček, in *Proceedings of 6th International Metallurgic Symposium METAL 97*, edited by T. Prnka, 1997, vol. 3, p. 131.

[205] H. Torabin, J.P. Pathak, S.N. Tiwari, "On Wear Characteristics of Leaded Aluminum-Silicon Alloys," *Wear*, 1994, vol. 177(1), pp. 47-54.

[206] A. Smolej, V. Dragojevic, E. Slacek, T. Smolar, U.S. Patent No. 6,248,188B1 2001.

[207] S. Subhasich, U.S. Patent No. 5,587,092 1996.

[208] S.V. Inkin, E.V. Klyanina, A.V. Kurdyumov, V.S. Chulkov, "Effect of Lead and Tin Impurities on the Technological Properties of Aluminum Alloys," *Tsvetnye Metally/Nonferrous Metals*, 1989, pp. 80-81.

[209] H. Zoller, G. Enzier, J.C. Fornerod, "The Machinability of Aluminium Alloys", *Aluminum*, 1969, vol. 45(1), pp. 49-54.

[210] J.M. Silcock, T.J. Heal, H.K. Hardy, "The Structural Aging Characteristics of Ternary Al-Cu Alloys with Cd, In, or Sn", *Journal of the Institute of Metals*, 1955, vol. 84(1), pp. 23-31.

[211] H. Hardy, "The Aging Characteristics of Ternary Aluminum-Copper Alloys with Cadmium, Indium, or Tin", *Journal of the Institute of Metals*, 1951-52, vol. 80, pp. 483-92.

[212] J.M. Silcock, H.M., Flower, "Comments on a Comparison of Early and Recent Work on the Effect of Trace Additions of Cd, In, or Sn on Nucleation and Growth of θ′ in Al-Cu Alloys", *Scripta Materialia*, 2002, vol. 46, pp. 389-94.

[213] J. Čížek, O. Melikhovo, I. Prochazka, J. Kuriplach, I. Stulikova, P. Vostry, "Annealing Process in Quenched Al-Sn Alloys: A Positron Annihilation Study", *Physical Review B*, 2005, vol. 71, pp. 1-13.

[214] S.P. Ringer, K. Hono, T. Sakurai, "The Effect of Trace Additions of Sn on Precipitation in Al-Cu Alloys: An Atom Probe Field Ion Microscopy Study," *Metallurgical and Materials Transactions A*, 1995, vol. 26A, pp. 2207-17.

[215] L. Bourgeois, J.F. Nie, B.C. Muddle "Assisted Nucleation of θ′ Phase in Al-Cu-Sn: The Modified Crystallography of Tin Precipitates," *Philosophical Magazine*, 2005, vol. 85, pp. 3487-3509.

[216] S. Murali, K.T. Kashyap, K.S. Ramen, K.S.S. Murthy, "Inhibition of Delayed Aging by Trace Additions in Al-7% Si-0.3% Mg Cast Alloy," *Scripta Metallurgica et Materialia*, 1993, vol. 29, pp. 1421-26.

[217] V.S. Grebenkin, T.V. Sil'chenko, A.A. Gorshkov, Y. Dzykovich, "Effect of Magnesium on the Distribution of Tin and Lead in Al-Si Alloys", *Metal Science and Heat Treatment*, 1972, vol. 3, pp. 50-54.

[218] S. Sircar, "X6030, A New Lead-Free Machining Alloy", *Materials Science Forum*, 1996, vols 217-222, pp. 1795-1800.

[219] H. Baker, *Alloy Phase Diagrams*, ASM International, Materials Park, Ohio, 1992.

[220] T.B. Massalski, *Binary Alloy Phase Diagrams*, 2nd ed., H. Okamoto L. Kacprzak, (Eds), American Society for Metals, 1990.

[221] R.C. Harris, S. Lipson, H. Rosenthal, "Tensile Properties of Al-Si-Mg Alloys and the Effects of Sodium Modification", *AFS Transactions*, 1965, vol. 64, pp. 470-481.

[222] A.M. Samuel, F.H. Samuel, H.W. Doty, "Observation on the Formation of β-AlFeSi Phase in 319 Type Al-Si Alloys", *Journal of Materials Science*, 1996, vol. 31, pp. 5529-5539.

[223] P.Y. Zhu, Q.Y. Liu, "Kinetics of Granulation of Discontinuous Phase in Eutectic Structures", *Materials Science and Technology*, 1986, vol. 2, pp. 500-507.

[224] H. Rosenbaum, D. Turnbull, "Metallographic Investigation of Precipitation of Silicon from Aluminum", *Acta Metallurgica*, 1959, vol. 7, pp. 664-674.

[225] J.V. Suchtelen, "Coarsening of Eutectic Structures during and after Unidirectional Growth", *Journal of Crystal Growth*, 1978, vol. 43, pp. 28-46.

[226] C.W. Meyers, "Solution Heat Treatment Effects in A357 Alloys", *AFS Transactions*, 1985, vol. 93, pp. 741-750.

[227] P. Zhu, Q. Liu, T. Hou, "Spheroidization of Eutectic Silicon in Al-Si Alloys", *AFS Transactions*, 1985, vol. 93, pp. 609-614.

[228] M.H. Mulazimoglu, "Electrical Conductivity Studies of Cast Al-Si and Al-Si-Mg Alloys", Ph.D Thesis, McGill University, Montreal, Canada, 1988.

[229] C.M. Adams, D.C. Jenkinson, " The Stability of Silicon Fibres in Al-Si Alloys and Their Influence on Mechanical Properties", *Proceedings 27th Annual Congress, Australian Institute of Metals*, Christ Church, New Zealand, 1974, pp. 58-63.

[230] J.E. Hutt, M, Easton, L.M. Hogan, D. StJohn, "Effect of Nucleant Particles and Alloy Chemistry on the Grain Structure of Aluminum Castings", *In 4th International Conference on Solidification Processing (SP97)*, Sheffield, UK, 1997, pp. 268-272.

[231] C. Villeneuve, F.H. Samuel, "Fragmentation and Dissolution of β-Al_5FeSi Phase during Solution Heat Treatment of Al-13% Si-Fe Alloys", *International Journal of Cast Metals Research*, 1999, vol. 12, pp. 145-160.

[232] F.H. Samuel, A.M. Samuel, H.W. Doty, "Factors Controlling the Type and Morphology of Cu-Containing Phases in 319 Al Alloy", *AFS Transactions*, 1996, vol. 104, 1996, pp. 893-901.

[233] G.A. Edwards, G.K. Sigworth, C.H. Cáceres, H.D. StJohn, J. Barresi, "Microporosity Formation in Al-Si-Cu-Mg Casting Alloys", *AFS Transactions*, 1997, vol. 105, pp. 809-815.

[234] P.N. Anyalebechi, "Analysis of the Effects of Alloying Elements on Hydrogen Solubility in Liquid Aluminum Alloys", *Scripta Metallurgica et Materialia*, 1995, vol. 33(8), pp. 1209-1216.

[235] M. Moustafa, F.H. Samuel, H.W. Doty, "Effect of Solution Heat Treatment and Additives on the Microstructure of Al-Si (A413.1) Automotive Alloys", *Journal of Materials Science*, 2003, vol. 38, pp. 4507-4522.

[236] J. Barresi, "Casting of Aluminum Alloy Component", *Materials Forum*, 1996, vol. 20, pp. 53-70.

[237] R. Singh, R. Ganguly, B. Dhindaw, "Application of Statistical Design of Experiments for Quantitatively Studying the Strengthening Characteristics of Cast Al-Si-Cu-Mg Alloys", *Foundryman*, 1984, vol. 77 (8), pp. 436-440.

[238] W. Reif, J. Dutkiewicz, R. Ciach, S. Yu, J. Król, "Effect of Aging on the Evolution of Precipitate in AlSiCuMg Alloys", *Materials Science and Engineering A*, 1997, vols 224-236, pp. 165-168.

[239] C. Meyers, K. Hinton, J. Chou, "Toward the Optimization of Heat Treatment in Aluminium Alloys", *Materials Science Forum*, 1992, vols 102-104, pp. 75-84.

[240] A. Saigal, J. Berry, "Study of the Effects of Volume Fraction, Size and Shape of Silicon Particles on Mechanical Properties in Al-Si Alloys Using Finite Element Method", *AFS Transactions*, 1985, vol. 93, pp. 699-704.

[241] G.E. Dieter, *Deformation of Two-Phase Aggregates, Mechanical Metallurgy*, London, UK: McGraw Hill, 1988, pp. 208-212.

[242] M.F. Ashby, D. Jones, *Yield Strength, Tensile Strength, Hardness and Ductility*, Engineering Materials, 2nd edition, vol. 1, Oxford, UK: Pergamon, 1996, pp. 77-92.

[243] M.F. Ashby, D. Jones, *Fast Fracture, Toughness and Fatigue*, Engineering Materials, 2nd edition, vol. 1, Pergamon Press, Oxford, UK, 1996, pp. 131-154.

[244] R.E. Stoltz, R.M. Pelloux, "The Bauschinger Effect in Precipitation Strengthed Aluminum Alloys", *Metallurgical Transactions A*, 1976, vol. 7A, pp. 1295-1306.

[245] G.K. Sigworth, G. Shivkumar, D. Apelian, "The Influence of Molten Metal Processing on Mechanical Properties of Cast Al-Si-Mg Alloys", *AFS Transactions*, 1989, vol. 97, pp. 811-824.

[246] A.K. Gupta, M.C. Chaturvedi, A.K. Jena, "Effect of Silicon on Aging Behaviour of Al-1.52Cu-0.75Mg Alloy", *Materials Science and Technology*, 1989, vol. 5(1), pp. 52-55.

[247] H. Suzuki, I. Araki, M. Kanno, K. Itoi, "Effect of Si Additions on the Aging Behaviour of an Al-2%Cu-0.9%Mg Alloy", *Transactions of the Japan Institution of Light Metals*, 1977, vol. 27(5), pp. 239-245.

[248] K. Hono, N. Sano, S. Babu, "Atom Probe Study of the Precipitation Process in Al-Cu-Mg-Ag Alloys", *Acta Metallurgica et Materialia*, 1993, vol. 41, pp. 829-838.

[249] C. Cárceres, J. Griffiths, "Damage by the Cracking of Silicon Particles in an Al-7Si-0.4Mg Casting Alloy", *Acta Materialia*, 1996, vol. 44, pp. 25-33.

[250] T. Kobayashi, M. Niinomi, "Fracture Toughness and Fatigue Characteristics of Aluminum Casting Alloy", *Journal of Japan Institute of Light Metals*, 1991, vol. 41(6), pp. 398-405.

[251] M. Tsukuda, "Problem on Modification of Al-7% Si-0.8% Mg Alloy by Sb", *Journal of Japan Institute of Light Metals*, 1980, vol. 30, pp. 65-71.

[252] N. Komatsu, M. Nakamura, Y. Yamamoto, "Metallurgical Structure and Impact Strength of Al-Si Alloys", *Technical Report of Toyota R&D Center*, TR-11, 1975, pp. 1-46 (in Japanese).

[253] M. Richard, "Impact Strength of Aluminum Alloy Castings", *Fonderie*, 1980, vol. 35(404), pp. 397-400.

[254] F. Paray, B. Kulunk, J.E. Gruzleski, "Impact Properties of Al-Si Foundry Alloys", *International Journal of Cast Metals Research*, 2000, vol. 13, pp. 17-37.

[255] L. Grand, "Influence of Some Impurities on the Quality of Aluminum Alloys", *Fonderie*, 1964, vol. 217, pp. 95-100

[256] J. Carr, E. McCracken, "Statistical Program Plaining and Process Development", *Chemical Engineering*, 1960, vol. 56(11), pp. 56-61.

[257] J. Major, A. McLeod, J. Rutter, "Designed Experimentation: Microstructural Optimization of Al AA512 for the PM Process and Its Possible Use as a Structural Diecasting", *AFS Transactions,* Pittsburgh, PA, USA, 2000, vol. 108, pp. 287-296.

[258] E. Carranza-Barraza, M. Castro, M. Herrera-Trejo, M. Stapleton: *Proceedings of 2nd International Aluminum Casting Technology Symposium,* October, ASM International, Columbus, OH, 2002.

[259] R. Ganguly, B. Dhindaw, P. Dhar, "Study and Control of Properties and Behaviour of Al-Mg-Si Alloys by Application of Statistical Design of Experiments", *Transactions of the Japan Institute of Metals*, 1977, vol. 18(7), pp. 511-519.

[260] J.I. Cho, J. Loper, "Limitation of Bismuth Residual in A356.2 Al", *AFS Transactions*, 2000, vol. 108, pp. 359-367.

[261] N. Eustathopoulos, L. Coudurier, J.C. Joud, P. Desré, "Tension Interfaciale Solide-Liquide des Systémes Al-Sn, Al-In et Al-Sn-In", *Journal of Crystal Growth*, 1976, vol. 33, pp. 105-115.

[262] S.G. Song, J.S. Vetrano, S.M. Bruemmer, "Pinning Effect of Solute Atoms on Grain Boundary Dislocation Dissociation", *Materials Science and Engineering A*, 1997, vol. 232, pp. 23-30.

[263] U. Erb, K.T. Aust, "The Effect of Non-Equilibrium Segregation on the Microstructure of a Dilute Al-Sn Alloy" *Scripta Metallurgica*, 1984, vol. 18 (11), pp.1263-1266.

[264] J. Roset, J.A. Saeter, T. Ustad, O. Reiso, "Effects of Sn Addition on Microstructure, Extrudability, Mechanical Properties and Machinability of a 6082 Alloy", *Materials Science Forum*, 2002, vols 396-402, pp. 1205-1210.

[265] Aric A. Brandes, *Smithells Metals Reference Book*, New York, 1983, pp. 434-440.

[266] M.H. Mulazimoglu, N. Tenekedjiev, B.M. Closset, J.E. Gruzleski, "Studies on the Minor Reactions and Phases in Strontium-Treated Aluminum-Silicon Casting Alloys" *Journal of Cast Metals*, 1993, vol. 6, pp. 16-28.

[267] P.M. Hansen, *Constitution of Binary Alloys,* 2nd ed., McGraw-Hill Book Company, Inc., New York, 1958. pp. 918-920.